Impacts of land use change on dry season flows across the tropics

Forests as ‘sponges’ and ‘pumps’

A thesis submitted to the University of London for the degree of

Doctor of Philosophy

Submitted by

Jorge Luis Peña Arancibia

King’s College London

London, May 2013

Para ti, mamita...

Acknowledgements

I am very thankful to my supervisor at King's College London, Dr Mark Mulligan, and my supervisor at VU University, Prof Dr Sampurno Bruijnzeel. I would venture to say I got the best of both worlds in hydrology a PhD student could wish for. Mark opened his door without knowing me very well and gave strong support along the way for me to complete this thesis. He taught me valuable lessons in hydrology and how to model hydrologic systems. He also provided the first opportunity I had to be a teaching assistant in one of his modelling courses. I learnt a lot from this experience, from him and other PhD students teaching at that time. Since graduate school, Sampurno instigated in me a profound interest in hydrology as a whole. Besides being grabbed by his lectures on ecohydrology, I learnt that producing scientific evidence is only a stage of several more before an environmental problem can be tackled. I am inspired by his long-time advocacy for better management of natural resources in developing countries. My aim is to surpass this scientific stage and make a contribution that also makes a difference on peoples' lives.

Back in 2007, I was doing an internship in Canberra with CSIRO Land and Water. It was the beginning of the peak of the 'Big Dry', the last ravaging drought to affect Australia. I was working on salinity issues with Prof Dr Albert van Dijk as my supervisor. I did not know at the time how fortunate I was to be taught by him nor how influential he was going to be in many of my future life and life decisions. I am very grateful he encouraged and put me in the right track to pursue this PhD, and even more grateful he assumed as a 'voluntary' supervisor. This thesis could not have been written without his kindness, time, support and encouragement. Many times he went 'beyond and above the call of duty'.

I am also grateful to Dr Hannah Cloke, my second supervisor at King's. Since you were not involved in the nitty-gritty details, you had the big picture in mind and always gave sound advice in the formal meetings we had.

Special thanks go to both examiners, Dr Wouter Buytaert and Dr Nick Chappell, who provided insightful and constructive comments and made the *viva voce* an enjoyable experience.

Microsoft Research provided the scholarship for the PhD position in the Department of Geography at King's College London. CSIRO Land and Water, Conservation International, and the Basin Focal project Andes, a project of the CGIAR Challenge Program on Water and Food, generously provided additional funds without which this thesis wound not have been possible.

Special thanks to Dr Tim McVicar, I truly admire your ways and work. I'm lucky to have you as a mentor in the post-doc program.

During the past five years or so, several colleagues and friends supported me in different ways to complete this thesis: Shatish Kundaiker, Elena Tarnavsky, Juan Carlos Verhelst, Arnout van Soesbergen, Sam Sperling, Leo Zurita, Kate Parks, Liu Yi, Jaap Schellekens, Richard de Jeu, Hylke Beck, Niels Andela, Ellen Kwantes, Carolina Sardella, Chuwah Clifford, Eva Ampe, Evelyn Aparicio, Randall Donohue, Lingtao Li, Marta Yebra, Juan Pablo Guerschman, Ben Gouweleeuw, Yongqiang Zhang, Julien Lerat, Zahra Paydar, Jai Vaze, Kerry Tomkins, Jessica van Dijk, Consuelo Wolfhard, Sara de Rezzonico, Marcelo Pino, Luis Lugones, Juan Pablo Cáceres, Carla García, Beatriz, Arturo, Claudia, Cecilia y Toto Arancibia and the DEH grads and partners in Canberra.

My current supervisor, Francis Chiew, provided a lot of encouragement and support in this final stage.

I would not be here if it weren't for my parents, Jorge and Isabel, and my two beautiful sisters, Ximena and Carolina. My dad embarked me into the world of hydrology since I was very little. He took me on his field trips to rural Bolivia, in which I developed a keen interest in water management and how it affects people's lives. Many, many thanks dad for your time and love.

I'm also grateful to the Lai family, my foster family in Australia. I cannot be more fortunate to have such a beautiful family, both in Bolivia and Australia. Thanks heaps for all the love and support!

Judy, my partner of nine wonderful years, you have supported me wholeheartedly, in good and bad times. You are truly awesome, all my love to you.

It was a long and winding road, but all the efforts were worth it.

Table of contents

* Page numbering in italics (Chapters 2 and 4) corresponds to the numbering assigned by the respective journals in which the chapters were published.

Abstract

In the last few decades, pan-tropical land use and land cover change (LUCC) has led to increased disturbance and fragmentation of forested lands, with consequent impacts on hydrology. Most of the evidence, gathered from controlled site and small catchment studies, suggests that forest removal leads to increases in total annual water yield because of their greater water use (the 'pump' effect) compared to short vegetation. However, these controlled experiments cannot be considered representative of ongoing LUCC in many tropical landscapes, where more intensive farming practices have triggered new land degradation processes at large scales that may have a strong impact on soil infiltration (the 'sponge' effect).

This thesis examines the potential and likely impact of LUCC on streamflow, particularly dry season flows, for the entire tropics ('pan-tropically') through a combination of hydrological analysis of flow datasets and modelling experiments of the tradeoff between changes to the sponge and pump effects with land use change. It is hypothesised that if soil infiltration capacity is severely diminished due to LUCC, and if prevailing rainfall intensities are (frequently) greater than surface infiltration capacity, then a net reduction of infiltration amounts may reduce soil profile moisture storage and enhance storm flows. This will serve to diminish baseflows due to the corresponding reduction in groundwater recharge. In catchments dominated by a seasonal precipitation regime (wet-dry cycles), dry season flows (generally composed mostly of baseflows) can be thus diminished. This can be crucial if dry season flows are used for productive activities and/or to maintain ecosystems. The main aims of this thesis are thus to: (*i*) evaluate where tropical LUCC can be expected to have the greatest impacts on dry season flows; and, on the basis of the resulting changes in evapotranspiration and infiltration (*ii*) to assess potential areas for rehabilitation and regeneration of hydrological services in degraded areas through reforestation.

Hydrological analysis in two large Australian catchments (>10,000 km^2) demonstrated that deforestation enhanced storm flow of all magnitudes and somewhat decreased slower flows, possibly as a consequence of reduced infiltration (*i.e.*, a reduction of the 'sponge' effect). This finding showcases that, depending on the degree of soil disturbance, trade-offs in the 'pump' and 'sponge' effects may cause reductions in dry season flows for this landscape or elsewhere.

The model used for the current pan-tropical impact experiments, the "World-Wide Water Resources Assessment system - Land Use Model" (W3RA-LUM), was tailored to incorporate not only changes in LUCC that directly affect evapotranspiration, but also those that affect the partitioning of infiltration and surface runoff. Model evaluation showed that the model had a reasonable performance compared to streamflow observations for 1461 tropical catchments and outputs obtained with various other hydrological models. It was also able to replicate the patterns of the response to LUCC at four tropical sites (although not replicating the observed magnitudes), three of which with documented negative impacts of LUCC on dry season flows.

Pan-tropical sensitivity analyses, performed for scenarios with or without full forest cover and/or good or poor surface infiltration conditions showed an increase in mean annual streamflow of 18% if only vegetation changes were taken into account. Streamflow increased by 26% if there were concurrent changes in soil surface conditions from good to poor. Much of the increase in mean annual streamflow occurred in more water-limited and seasonal environments. In some of these areas there was a reduction of dry season flows, at least for some of the driest months. Besides locating these sensitive areas, statistical analysis of the outputs suggested that current forested landscapes with the largest potential impact of LUCC on dry season flows would have the following biophysical and climate characteristics: (*i*) there is sufficient rainfall in excess of potential evapotranspiration during the wet season to recharge deeper soil profiles and/or the groundwater system; (*ii*) the surface infiltration capacity can accommodate prevailing rainfall intensities during the wet season; (*iii*) there is sufficient soil water storage to ‘carry over' rainfall infiltrated during the wet season; (*iv*) a sufficiently long ‘buffer time' (in terms of groundwater recession coefficient) modulates the release of water stored in the deep soil profile or saturated zone as baseflow. Modelling outputs obtained from comparing scenarios of current and pre-agricultural tree cover highlighted areas in which soil rehabilitation and regeneration through forestation can boost dry season flows in degraded areas. Some of these areas coincided with areas targeted by ongoing reforestation and restoration efforts, suggesting that these may (ultimately) have a positive effect on baseflow.

Chapter 1 Research context, aims and objectives

Contents

1.1 Hydrological impacts of tropical land use and land cover change (LUCC)

Tropical landscapes are undergoing rapid land use and land cover change (LUCC[1]). In the last few decades, vast areas of tropical forests have been replaced at unprecedented rates. The Forest Resource Assessment (FRA) completed by the FAO in 2005 and preliminary results of FRA 2010 indicate that on a global scale the total forest area continues to decrease (FAO, 2006; FAO, 2010). It is across the tropics that deforestation continues at the highest rates, and FRA estimates for 1990–2005 suggest annual rates of deforestation of 0.9% in South Asia and Southeast Asia, 1.2% in Central America, 0.45% in South America and 0.62% in Africa. This means that, on average, each year from 1990 to 2005, an area of 116,000 km^2 of tropical forest was lost, roughly thrice the area of Denmark.

Many tropical landscapes have experienced expansion and intensification of agricultural practices. Often, these new practices have triggered widespread land degradation processes which may have an important impact on hydrological processes, particularly through adverse changes in soil physical properties, that reduce surface soil infiltration capacity and enhance the intensity and frequency of infiltration-excess overland flow and surface erosion (Loker, 1994; Eswaran *et al.*, 2002; Lamb *et al.*, 2005; Turkelboom *et al.*, 2008; Ziegler *et al.*, 2009).

In a hydrological context, any forest type can be metaphorically compared both to a 'pump' and a 'sponge'[2]. Forests act as 'pumps' through plant evaporation. Forests also act as 'sponges' by enhancing infiltration rates and moisture retention due to the effects of organic matter and the root network on soil physical properties. Water that is not evaporated or lost to streams as

[1] Land use and land cover change (LUCC) is a general term for the human modification of the Earth's terrestrial surface (Ellis and Pontius, 2011). Land cover refers to the physical and biological cover over the surface of land, whereas the human activities that alter the land surface processes (*e.g.,* agriculture, forestry and construction) refer to land uses (Ellis and Pontius, 2011). The LUCC that pertains to the removal of natural forest referred herein as deforestation. Both LUCC that pertains to reforestation, either by natural regeneration or by plantation forestry, or to the establishment of new forest in areas where there were none before (afforestation), are referred herein as forestation (Scott *et al.*, 2005). Either afforestation or reforestation will be used to define LUCC in cases were these cannot be used interchangeably.

[2] Bruijnzeel (2004) provides an insightful discussion of how these two interpretations of the hydrological role of forest during the 1920s and 1930s were taken by Dutch researchers in the former Dutch East Indies (now Indonesia) to a great extent as mutually exclusive and how the debate continued until very recently, when new scientific research led to a view of forests both acting as 'sponges' *and* 'pumps'. Nevertheless, both arguments are still used in the public arena to favour or undermine policies that aim at conservation and/or establishment of forests. Nowadays, not only elucidating the hydrological role of forests, but also conveying the science to stakeholders, is of key importance for proper resource management.

overland flow and/or subsurface flow, infiltrates to deeper layers and is stored in the soil or the groundwater system and ultimately released as baseflow. These two concepts occur together at any one time and LUCC will have effects on both the 'sponge' and 'pump' characteristics of forests.

The impacts on hydrology of (mainly temperate) forest conversion to a different land use generally consist of increases in total annual water yield, infiltration and ground water recharge commensurate with the percentage of forest removed (Bosch and Hewlett, 1982; Stednick, 1996; Brown *et al.*, 2005). The increase in flows occurs mainly because dense forests have both greater water use and interception losses than grasses and crops (Van Dijk and Keenan, 2007; Van Dijk and Bruijnzeel, 2001), and in this context forests act more like 'pumps' than the alternative land use (*e.g.,* grazed pastures, cropped fields). The bulk of the annual increase in flows typically occurs during conditions of baseflow as long as surface soil infiltration characteristics are reasonably maintained following forest conversion (Bruijnzeel, 2004; Brown *et al.*, 2005). There are two known probable exceptions where the loss of forests can lead to a *reduction* in total annual water yield (irrespective of the gains from reduced water use by the new vegetation): (*i*) in montane cloud forests where fog deposition or 'cloud stripping' may amount to 5–20 % of incident rainfall (or exceed rainfall during the dry season) and in excess of interception evaporative losses (Bruijnzeel and Proctor, 1995; McJannet *et al.*, 2007; Mulligan *et al.*, 2010; Bruijnzeel *et al.*, 2011); and (*ii*) in some types of old-growth forests, where the water use of the replacing vigorous regrowth having a much higher stomatal conductance (*e.g.,* Juhrbandt *et al.*, 2004) may exceed the evapotranspiration of the former forest (*e.g.,* Langford, 1976 for temperate mountain ash forest; Giambelluca, 2002; Hoelscher *et al.* 2005 for tropical forest types).

The evidence to support the previous findings has mostly been gathered through controlled experiments. These include direct observational means (*e.g.,* sap flow measurements), site water balance or atmospheric water balance studies, and small, controlled paired catchment studies (*i.e.,* <1 km^2) (*cf.* Van Dijk and Keenan, 2007; Bruijnzeel, 1990; Grip *et al.*, 2004). Under such controlled experimental conditions, measurements often lasted for a few years after forest clearing and surface disturbance was limited in most cases (Grip *et al.*, 2004; Malmer *et al.,*

2010). Conversely, post-forest conditions where productive activities have taken place for decades frequently may show severe soil degradation and reduction in porosity and infiltration. This may be caused by soil compaction through overgrazing, logging and/or mechanized agriculture (Martinez and Zinck, 2004; Ziegler *et al.*, 2006, Mehta *et al.*, 2008, Germer *et al.*, 2009), raindrop-impact soil compaction (Lal, 1987, 1996; Moss, 1991), an increase of compacted and/or sealed rural roads, trail and yard surfaces (Wemple and Jones, 2003; Ziegler *et al.*, 2004; Rijsdijk *et al.*, 2007; Negishi *et al.*, 2008), and the reduction in soil bioporosity (Lal, 1987; Chappell, 2010). In such cases, the net effect translates into a reduction of the 'sponge' characteristics of the former forest soil (Bruijnzeel, 2004).

In landscapes where soil degradation has reduced the 'sponge' characteristics of the soil and diminished infiltration opportunities, rainfall intensities are likely to exceed more frequently the soil's infiltration capacity, thus enhancing overland flow occurrence (*e.g.,* Zimmermann *et al.*, 2010; Bonell *et al.*, 2010). This assumes additional importance in catchments dominated by seasonal rainfall, where infiltration and subsequent percolation ultimately replenish a slow groundwater system that sustains streamflow during the dry season. In such catchments, the distribution of streamflow throughout the year may be more important than total annual water yield (Bruijnzeel, 2004; Chandler, 2006). In severely degraded catchments with the aforementioned characteristics, the reduced recharge and storage of groundwater may in turn reduce dry season flows; irrespective of the increases in total flows due to reduced the forest water use (see examples in Bruijnzeel, 2004).

Evidence of reduced dry season flows after LUCC has been showcased in the literature for different tropical environments. In monsoonal Sri Lanka, a decrease in dry season flows was observed in the 1,100 km^2 upper Mahaweli catchment, which was ascribed to conversion of tea plantations to annual cropping and home gardens without appropriate soil conservation measures (Madduma-Bandara and Kuruppuruarachchi, 1988; Bruijnzeel, 2004). Rainfall and streamflow time-series for the 1940–1980 period showed that, although the observed negative trend in rainfall was not significant, there was an overall increase in wet season flows and a slight decrease in dry season flows (Figure 1.1). A gradual reduction over 50 years since 1940 of forest area from 50% to 15% and the early establishment of tea plantations and home

gardens in the Nilwala catchment (1,073 km^2), elsewhere in Sri Lanka; also resulted in a change in seasonal streamflow regime, with reduced dry season flows and wet season flows peaks occurring earlier in the year (Elkaduwa and Sakthivadivel, 1998). The changes in flow regime were attributed to a loss of infiltration opportunities associated with the new land uses; however, the role of climate variability was not fully addressed by the authors.

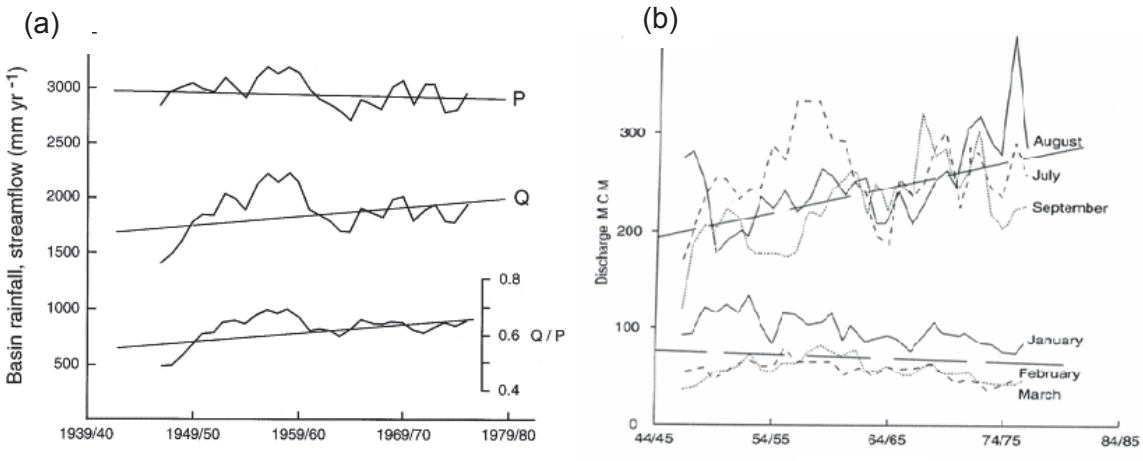

Figure 1.1 (a) Five-year moving averages of annual rainfall, streamflow and runoff ratios for the upper Mahaweli basin above Peradeniya, Sri Lanka. (b) Streamflow volume (in millions of m^3 per month) for the wet season (August–September) and the dry season (January–March) (after Bruijnzeel, 2004).

In the upper Konto catchment in East Java (Indonesia), the clearing of 33% of forest and its replacement by rainfed cropping with poor conservation measures, plus an increase in sealed surfaces such as roads and settlements reduced infiltration opportunities (Rijsdijk and Bruijnzeel, 1991; Rijsdijk *et al.*, 2007). The excess water associated with reduced evapotranspiration following forest clearing, did not compensate for the loss of soil-water and groundwater recharge due to the diminished infiltration, thereby changing the seasonal distribution of streamflow and reducing dry season flows (Figure 1.2).

Sandström (1995) established that a reduction in dry season flows in northern semi-arid Tanzania since the mid-1940s was caused by accelerated forest clearing and subsequent land degradation due to grazing and not climatic change (or variability). The loss of soil macropore

networks (or bioporosity) due to rainfall and human induced compaction was deemed key to the reduced surface infiltration rates, especially on steeper slopes with fine-textured soils.

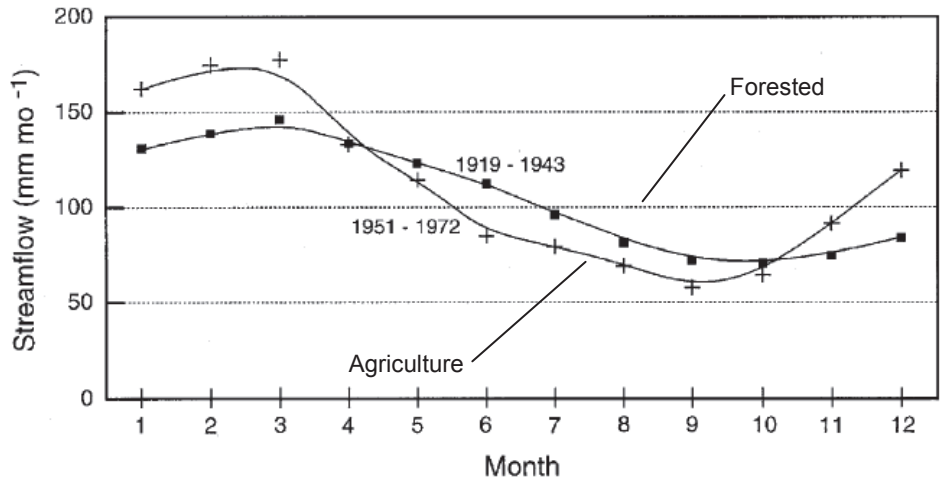

Figure 1.2 Change in seasonal distribution of streamflow depth (mm mo^{-1}) at Selorejo, upper Konto catchment, East Java, Indonesia, following the replacement of 33% of forest by rainfed cropland and settlements (after Bruijnzeel, 2004).

Several studies showed that the saturated hydraulic conductivity (K_{sat}) or infiltration rates (I) in disturbed soils can be up to several orders of magnitude lower in extreme cases than in nearby undisturbed forests. Table 1 presents a summary of studies conducted in the tropics that compare K_{sat} or I before and after LUCC. The extent of disturbance and soil type will often dictate the impact. For example, low impact cropping such as swidden cultivation in Northern Vietnam (Ziegler *et al.*, 2004) has relatively lower and less lasting effects on soil infiltrability than repeated surface disturbance (in the form of litter removal and fuel-wood collection) in degraded forests in the Indian Western Ghats (Bonell *et al.*, 2010).

Few studies have examined the impacts of forestation or natural regrowth on the recovery of soil infiltration characteristics and how this in turn affects dry season flows in degraded tropical areas. Forestation or natural regrowth generally increases infiltrability in tropical soils (Ilstedt *et al.*, 2007) but it may well take two or more decades of uninterrupted soil recovery to bring the infiltration characteristics of severely disturbed soils back to their former values (Ziegler *et al.*, 2004; Bonell *et al.* 2010; Hassler *et al.*, 2011; Ghimire *et al.*, 2013). Ziegler *et al.* (2004)

reported that K_{sat} had a slow recovery in abandoned swidden fields in northern Vietnam, with 15–25 years needed before K_{sat} values resembled those of natural forest. In the Western Ghats of India, Bonell *et al.* (2010) reported only a small increase in K_{sat} after 10 years of forestation of previously degraded land. Hassler *et al.* (2011) concluded that recovery of K_{sat} may take more than 8 years in grazing lands in two catchments of central Panama.

Table 1-1 Changes in soil hydraulic properties after LUCC in terms of: (a) infiltration rate (I) or (b) near soil surface field saturated hydraulic conductivity (K_{sat}). K_{sat} measured in the field can be half of that estimated in laboratory (Bonell *et al.*, 2010).

Site	Metric	Land cover pre-LUCC	mm h^{-1}	Land cover post-LUCC	mm h^{-1}	% change	Source
Brazilian Amazonia	K_{sat}	pasture	200	grazed pasture	50	-75	Zimmermann *et al.* (2010)
Brazilian Amazonia	K_{sat}	forest	260	abandoned pasture	30	-88	Godsey and Elsenbeer (2002)
Brazilian Amazonia	K_{sat}	forest	230	pasture	4	-98	de Moraes *et al.* (2006)
Colombian Amazonia	I	forest	150	grazed pasture	10	-93	Martinez and Zinck (2004)
Costa Rica	I	forest	2462	grazed pasture	29	-99	Deuchars *et al.* (1999)
Northern Australia	K_{sat}	Eucalypt woodland	290	bare	65	-78	Bonell and Williams (2009)
Northern Australia	K_{sat}	Eucalypt woodland	720	grazed pasture*	186	-74	Bridge *et al.* (1983)
Northern Mexico	K_{sat}	pasture	29	compacted pasture	13	-55	Viramontes and Descroix (2003)
Northern Vietnam	K_{sat}	forest	154	crops	103	-33	Ziegler *et al.* (2004)
Peruvian Amazonia	K_{sat}	secondary forest	998	crops	185	-81	Alegre and Cassel (1996)
Western Ghats, India	K_{sat}	forest	60	degraded forest	15	-75	Bonell *et al.* (2010)

* Treated to simulate overgrazing

In the Philippines, Chandler and Walter (1998) compared two hillslope plots on Leyte Island, one covered with 20-year-old regrowth and the other under severely degraded grassland. A massive reduction in both overland flow and shallow subsurface flows was observed for the

forested plot compared to the degraded hillslope. Interestingly, the amount of reduction was more than sufficient to compensate for the likely increase in evapotranspiration associated with the forested plot although this could not be demonstrated in the form of increased streamflows due to the absence of surface flow channels in this karstic terrain (Chandler, 2006). Nevertheless, according to villagers in both southern and northern Leyte (i.e. in the vicinity of the Chandler and Walter study), spring discharges had increased some 15–20 years after forestation of degraded grasslands, with flows continuing during ENSO-induced drought periods where formerly the springs would dry up (L. A. Bruijnzeel, pers. comm.).

There is scant information on the hydrological impacts of forestation of degraded tropical lands at the meso-scale catchment or river basin scale. At the regional scale, the work of Zhou *et al.* (2010) demonstrated through analysis of 50 years of hydrometric data, that the occurrence of higher dry season flows after large-scale reforestation in several rivers in Guandong Province (Southern China) was not related to climatic variability or human activities (*e.g.,* redistribution of seasonality of flows through reservoirs). The observed increase in baseflows was attributed to an increase in infiltrability under forest cover, although no direct evidence for this was provided. Nevertheless, various small-scale studies in the same 'Red Soils' region of Southern China have shown major reductions in storm flow production following forestation of highly degraded lands, often within a decade after planting (*e.g.,* Zhou *et al.*, 2002; Zhang *et al.*, 2004; Zheng *et al.*, 2008). Evidence elsewhere has also shown that reforested sites have higher bioporosity than pastures and thus their infiltrability can be expected to increase with time after forestation (*cf.* Gilmour *et al.*, 1987; Zou and Gonzalez, 1997; Collof *et al.*, 2010).

The study by Zhou *et al.* (2010) is the only known to the author that showcases seasonal redistribution of flows at the regional scale (>175,000 km^2) after forestation in the tropics. This is all the more remarkable because there are several scale-related factors that may preclude the direct demonstration in larger catchments (say, >500 km^2) of the kind of results obtained in small experimental catchments; these include: (*i*) climatic and vegetation gradients in relation to the distribution of forests; (*ii*) the variety of land uses typically found in larger catchments; (*iii*) the typically limited spatial extent of convective rainfall cells in the tropics; (*iv*) spatially variable

soils and geology across the catchment (Blöschl *et al.*, 2007; Donohue *et al.*, 2010; Mulligan *et al.*, 2010; Peña-Arancibia *et al.*, 2012; Beck *et al.*, 2013).

The case studies discussed above illustrate the fact that changes in dry season flows after LUCC are catchment-specific and depend on (*i*) the competing processes that govern how rainfall is partitioned between evapotranspiration, storm runoff and soil water recharge; and (*ii*) the nature of the prevailing groundwater system (Calder *et al.*, 2002). These processes are driven by climatic and biophysical characteristics of the system, including rainfall characteristics (and their variability), land cover, soil type and surface condition, topography and the groundwater outflow system (determined, in turn, largely by geology and topography).

As discussed previously, both climate and land use are important drivers of changes in catchment hydrology, yet their relative effects are difficult to separate empirically (Tomer and Schilling, 2008). Rodriguez *et al*. (2010) summarised a number of studies that have concluded that many of the trends observed in Amazonian tributaries along the 'deforestation arc' (*cf.* Morton et al., 2006) were attributed to climatic changes and not to LUCC effects. Several techniques have been used to attempt separating the effects of LUCC and climatic variability in large catchments including time-series analysis and hydrological modelling. A third approach makes use of metrics obtained from streamflow time-series, and, by relating these to concurrent LUCC, it may be possible to explore changes in hydrological processes dynamics. For example, techniques for streamflow partitioning into storm flow and baseflow may provide straightforward evidence to assess the trade-off between the 'sponge' and 'pump' effects. A number of studies in the (sub)tropics have used these types of metrics to this end (*e.g.*, Viramontes and Descroix, 2003; Germer *et al.*, 2009; Rodriguez *et al*., 2010; Recha *et al*., 2012; Shu *et al*., 2012).

Besides changes in vegetation type, land use exerts a major influence on surface soil condition. From a modelling perspective, the framework for translating the impacts of LUCC on hydrology can be summarised by the four situations presented in Figure 1.3.

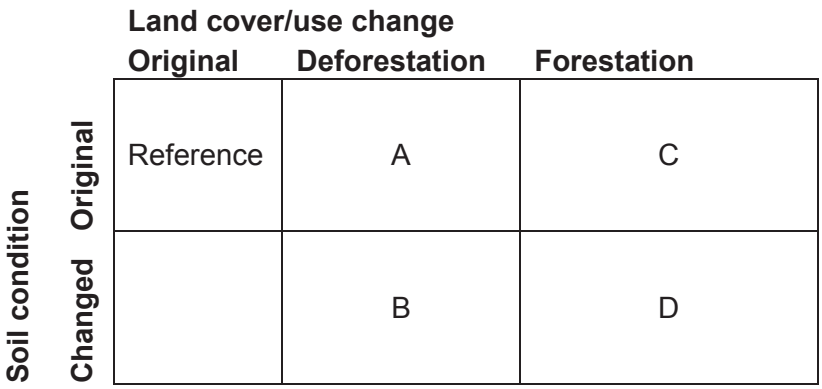

Figure 1.3 Situations for impacts of LUCC on dry season flows. Situation A corresponds to deforestation in which the soil condition is (largely) maintained. In situation B, soil conditions are changed negatively, leading to decreased infiltration opportunities. Idem for situations C (forestation with little change in surface soil condition) and D (forestation with major positive changes in soil condition).

The four situations illustrated in Figure 1.3 enable the formulation of the following research hypotheses:

(A) In situation A, deforestation associated with small or no changes in surface infiltration characteristics (in the case of low impact logging, soil conservation measures, low rainfall erosivity, stable soil aggregates or a combination thereof; *cf.* Edwards, 1979) will invariably lead to an increase of dry season flows, due to the smaller water use and interception of the grasses and crops replacing the forest.

(B) In situation B, deforestation (loss of the 'pump' effect) associated with negative changes in surface infiltration characteristics (loss of the 'sponge' effect due to soil compaction, logging and/or mechanized agriculture or a combination thereof) can either decrease or increase dry season flows, depending on the trade-off between the associated changes in vegetation water use and infiltration, respectively.

(C) In situation C, forestation accompanied by little changes in surface infiltration characteristics will invariably lead to a decrease of dry season flows, due to the larger water use and interception of the forests replacing grasses and crops.

(D) In situation D, forestation associated with negative changes in surface infiltration characteristics (*e.g.*, due to the poor soil building capacity of the planted species or repeated surface disturbance during forest maturation in the form of litter removal, understory harvesting, or grazing; *cf.* Ghimire *et al*., 2013) will invariably lead to a decrease in dry season low flows due to the higher water use and rainfall interception losses of the forest vegetation, *i.e.,* the forest acts predominantly as a 'pump'. Conversely, if surface infiltration characteristics are positive (*e.g.*, the development over time of a layer of organic matter that enhances moisture retention and a root network that enhances infiltration; *cf.* Ghimire *et al*., 2013), dry season flows can either decrease or increase again depending on the trade-off between the associated changes in vegetation water use and infiltration, respectively.

Hypotheses A and C have been generally supported with numerous small-scale catchment experiments, although direct verification at larger scales has not always been successful (Blöschl *et al*., 2007; Donohue *et al.*, 2010; Peña-Arancibia *et al.*, 2012). Bruijnzeel (1989, 2004) has provided a rationale for the investigation of hypotheses B and D. In hypotheses B, dry season flows will only decrease after deforestation if large-scale soil degradation causes a sufficiently large overall reduction in surface infiltration (with resulting increases in storm flow volumes) to counteract the increases in flows due to the lower evapotranspiration of the post-forest land cover. The associated diminished soil and groundwater recharge reduces groundwater outflows and thus dry season flows. In other words, soil degradation causes a net loss of the former forest's 'sponge' effect. Likewise, in hypothesis D, dry season flows will only increase after reforestation if the extra water use by the new trees is more than compensated by improved infiltration. A positive effect on dry season flows thus requires that the increase in infiltration is greater than the increase in evapotranspiration. In addition, it requires sufficient soil depth (for soil profile water storage during the dry season) and a sufficiently degraded starting situation to allow the soil's infiltrability to be improved sufficiently after planting. The net effect in this case is the return of the forest 'sponge' effect. The above 'pre-requisites' may also become more influential if the rainfall regime is dominated by marked wet and dry cycles (*i.e.,* if there is

a clear dry season) and slow groundwater discharge buffers streamflow variability during the dry cycles.

1.2 Aims and objectives

The aim of this thesis is to assess the potential and likely impact of LUCC on dry season flows for the entire tropics (pan-tropically) through a combination of hydrological analysis and modelling. This aim incorporates the following specific objectives: (*i*) to define reference hydrological conditions under natural forest conditions; (*ii*) to evaluate where tropical LUCC can be expected to have the greatest impacts on dry season flows; and on the basis of changes in evapotranspiration and infiltration (*iii*) to assess potential areas for rehabilitation and regeneration of hydrological services in degraded areas through reforestation.

The aim of predicting the impacts of LUCC on the water balance through modelling requires the simulation of processes involving vegetation and soil dynamics critical to the partition of rainfall into evapotranspiration and runoff. Several hydrological models applied globally where developed in principle to estimate runoff, floods and for water resources assessments (*e.g.* Vörösmarty *et al.*, 1989; Arnell, 1999; Döll *et al.*, 2003; Widen-Nilsson *et al.*, 2007). The focus was mainly to capture the distribution and timing of water movement along drainage networks; hence many of the processes that describe soil and vegetation interactions did not provide enough information to make them amenable to simulating impacts of LUCC. On the other hand, so-called land surface models (LSMs) can capture the effects of LUCC on the water and energy balance using sophisticated descriptions of vegetation and root-zone dynamics through soil-vegetation-atmosphere transfer schemes (SVATS) (*e.g.* Essery *et al.*, 2003; Krinner *et al.*, 2005). These were primarily developed as part of general circulation models (GCMs) used to simulate climate change (Pitman, 2003). LSMs have rarely interaction of lateral surface and subsurface flows as in hydrologic models (Overgaard *et al.*, 2006), although more recent spatially distributed LSMs combine features of hydrological models that permit such interactions (*e.g.* Hasanaki, 2007; Rost *et al.*, 2008; Dadson *et al.*, 2011). For example, the LSMs ORCHIDEE (de Rosnay *et al.*, 2003), LPJ (Sitch *et al.*, 2003), JULES (Best *et al.*, 2011) and the

GLDAS suite of models (Rodell *et al*., 2004) can be coupled to routing schemes to simulate lateral transport.

The model that is used here to simulate the hydrological impacts of LUCC and test the respective hypotheses summarised in Figure 1.3 is a global variant of the Australian Water Resources Assessment system Landscape hydrology (AWRA-L, version 0.5) model (Van Dijk, 2010a, Van Dijk and Renzullo, 2011) referred to here as the 'World-Wide Water Resources Assessment system' (W3RA) (Peña-Arancibia *et al.*, 2011; Van Dijk *et al.*, 2013). The variant of W3RA used here, which uses a structure amenable to LUCC scenario modelling is referred to as the W3RA Land use Model (W3RA-LUM). W3RA-LUM can be considered a hybrid between a simplified grid-based land surface model and a lumped catchment model applied to individual grid cells. Where possible, process equations were selected using a downward approach through evaluation against a range of Australian hydrometric and climatic data as part of the model's development (Van Dijk, 2010b; Van Dijk, 2010c) or sourced from published literature. The version of the model used here represents subgrid variation in vegetation cover by considering two 'hydrological response units' (HRUs):

- Deep-rooted tall vegetation ('forest') which can use water from shallow and deep soil layers.
- Shallow-rooted short vegetation ('herbaceous') which can only use water from shallow soil layers.

W3RA-LUM will be run at 1° grid resolution and at a daily time-step, commensurate with the resolution of high-quality long-term climatic data (discussed in Chapter 3). Model outputs at this temporal scale are considered applicable to catchments with sizes up to around the model's grid resolution (10,000 km2). The version of the model used here does not include a representation of river routing, although aggregation for larger catchments over monthly periods might not be greatly affected by the lack of routing *per se*. In addition, there is no representation of lateral redistribution of water between grid cells. The model does not account either for sources of losses and withdrawals, which may be of importance, particularly in drier areas and/or seasons. In addition, river management such as regulation, reservoir operation and extraction and transmission losses are not represented in this version of the model. Under these

assumptions and model structural simplifications, the implications for the appropriate interpretation of model outputs will be discussed in Chapter 5.

AWRA-L was extensively evaluated against a range of *in situ* and satellite observations in Australia, representing several climatic and biophysical environments also including tropical environments (Van Dijk and Warren 2010; Van Dijk and Renzullo, 2011; Van Dijk *et al.*, 2013). Full technical details of the model can be found elsewhere (Van Dijk, 2010a). Technical details pertaining to the application of the model in this thesis are covered in Chapters 5 and 6 (see Thesis outline below).

Feedbacks of LUCC on rainfall generation are not considered in W3RA-LUM. Although it has been claimed that the rain forests of the Amazon and Congo maintain their own climate through 'rainfall recycling', and that clearing of large tracts of forest may cause a major reduction in rainfall (Makarieva and Groshkov, 2007; Sheil and Murdiyarso, 2009), the physical foundations of this hypothesis have been severely criticised (Meesters *et al.*, 2009). More importantly, no physical evidence of a reduction in rainfall was found by Angelini *et al.* (2011) after major reductions in the amount of vegetation in Amazonia. Similarly, no statistically significant rainfall changes directly attributable to large scale LUCC have yet been observed (Wilk *et al.*, 2001; Costa *et al.*, 2003).

1.3 Thesis outline

Some of the chapters that make up this thesis were originally written as research articles, most of which have been published in the meantime. Following this introductory chapter, Chapters 2 and 4 are self-contained studies that are presented here in the original format of the respective journals. Chapter 2 describes and presents results of several inference methods to assess the hydrological impacts of LUCC on two large catchments (>10,000 km^2) in the seasonal tropics of Australia. Chapter 3 is based on an unpublished report, a journal article and a peer-reviewed conference article. The conference and journal articles can be found in the corresponding appendix section. In this chapter, several climate datasets are assessed (through a literature review and/or evaluation against observations) for their strengths and weaknesses. Results of

the assessment provide the rationale for the choice of data used in the subsequent modelling experiments. In Chapter 4, statistical methods are used to parameterise the groundwater hydrology module of W3RA-LUM. Chapter 5 describes the model's structure, pan-tropical parameterisation and model evaluation whereas scenario modelling and analysis of results are presented in Chapter 6. Finally Chapter 7 presents the conclusion and recommendations. In addition, Appendix A contains a glossary (adapted from the UNESCO International Glossary of Hydrology and from Wikipedia) of the main hydrologic terms used herein (UNESCO, 2013).

A summary of each chapter, the underlying publications and the interrelation between these are presented below and summarised in Figure 1.4.

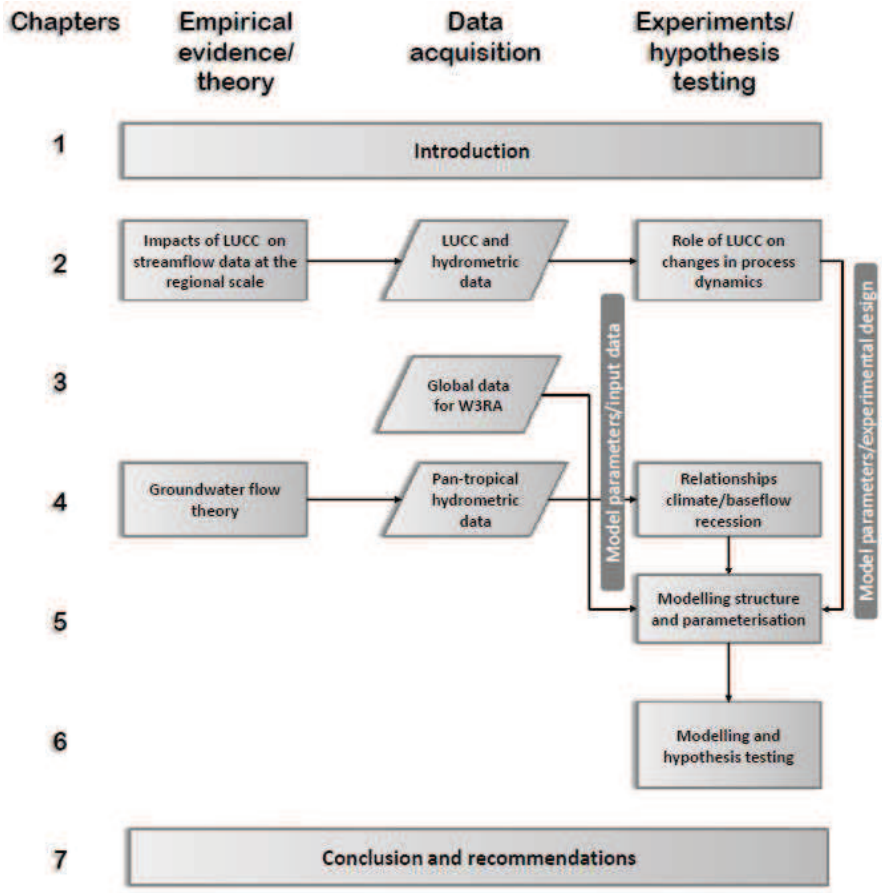

Figure 1.4 Diagram of the thesis structure highlighting the studies conducted, the corresponding chapters and their interrelations.

Chapter 2 Identifying hydrological impacts of LUCC on streamflow metrics at the regional scale

Peña-Arancibia, J. L., A. I. J. M. van Dijk, J. P. Guerschman, M. Mulligan, L. A. Bruijnzeel, and T. R. McVicar (2012), Detecting changes in streamflow after partial woodland clearing in two large catchments in the seasonal tropics, **Journal of Hydrology**, 416/417, 60-71.

This article presents a summary of the body of hydrological literature dealing with the impacts of LUCC on the hydrology of large (sub)tropical catchments. Two large catchments (>10,000 km^2) in the seasonal tropics of Australia and several published inference methods are used to discriminate between climate and LUCC (in this case clearing of *Acacia* and *Eucalyptus* woodlands for cattle ranching) as drivers of hydrological change. In the first catchment (the Comet river basin), two periods before and after LUCC separated by a number of years (to permit the establishment of a new hydrological equilibrium) were used to assess the role of LUCC in the shifts in dynamics of hydrological processes, independently of climate. In the second catchment (the Upper Burdekin river basin), detailed temporal information on LUCC permitted the assessment of transitional shifts in dynamics of hydrological processes that could be related to LUCC.

It is postulated that, although concurrent climate variability is the main driver of hydrological change, some changes in catchment dynamics were attributable to LUCC. In particular, it was observed that for both catchments, changes in LUCC resulted in enhanced storm flow of all magnitudes and a decrease in slower flows, *possibly* as a result of a decrease in infiltration opportunities.

The findings in this article were used as rationale to modify model parameters and tailor scenarios to test hypothesis B.

Further discussion about the apparent weak influence of LUCC on the water balance in the Comet catchment and published evidence about the weak influence of vegetation type *in general* in larger catchments with mixed land cover (*e.g.,* Oudin *et al.*, 2008); prompted further analysis using synthetic experiments and AWRA-L to determine methodological limitations and physical processes that may preclude a stronger land cover signals. The results were summarised in:

Van Dijk, A. I. J. M., **J.L. Peña-Arancibia** and L. A. Bruijnzeel (2012), Land cover and water yield: inference problems when comparing catchments with mixed land cover. **Hydrology and Earth System Sciences,** 16*,* 3461-3473.

This study is discussed further in Chapter 5 and is reproduced in Appendix F.

Chapter 3 Availability and quality assessment of data for pan-tropical scale modelling of surface hydrology

Peña-Arancibia, J. L., A. I. J. M. van Dijk, M. P. Stenson, and N. R. Viney (2011) Opportunities to evaluate a landscape hydrological model (AWRA-L) using global data sets, **MODSIM 2011**, 19th International Congress on Modelling and Simulation Modelling and Simulation Society of Australia and New Zealand, December 2011, 4071-4077 pp.

Peña-Arancibia, J. L., A. I. J. M. van Dijk, M. P. Stenson, and N. R. Viney (Unpublished) Data sets for the implementation of a global version of AWRA-L: Opportunities for further model evaluation. CSIRO: Water for a Healthy Country National Research Flagship, pp.32.

Peña-Arancibia, J. L., A. I. J. M. van Dijk L.J. Renzullo, and M. Mulligan (2013), Evaluation of precipitation estimation accuracy in reanalyses, satellite products and an ensemble method for regions in Australia and in South and East Asia, **Journal of Hydrometeorology**, 14, 1323-1333.

The report, the peer reviewed conference article are amalgamated and presented as a Thesis chapter. Methods for rainfall evaluation are drawn from the journal article. The chapter describes and assesses the strengths and weaknesses of meteorological forcing data required to implement W3RA-LUM, particularly in terms of daily rainfall, radiation, and temperature.

Chapter 4 Parameterising pan-tropical scale models of groundwater hydrology and baseflow generation

Peña-Arancibia, J. L., A. I. J. M. van Dijk, M. Mulligan, and L. A. Bruijnzeel (2010), The role of climatic and terrain attributes in estimating baseflow recession in tropical catchments, **Hydrology and Earth System Sciences**, 14(11), 2193-2205.

The values for most biophysical parameters in W3RA-LUM can be readily obtained or inferred from global datasets, or derived through model testing as was done in the Australian implementation of AWRA-L (Van Dijk, 2010a). Often this is not the case with model parameters describing the groundwater system. Since there is a dearth of hydrogeological data at the global scale, modelling of groundwater flow might be more amenable to application of empirical conceptual storage-discharge models that relate catchment climate, geology and morphology to the shape of the recession hydrograph. W3RA-LUM represents groundwater flow using a linear reservoir whose drainage characteristics are represented by the baseflow recession constant k_{bf} and were estimated from analysis of streamflow data for several hundred small upland

catchments in Australia. The aim of this article was to obtain an empirical relation between k_{bf} and selected variables describing climatic and physical catchment characteristics to spatially estimate k_{bf} from readily available climatic and physical datasets at the pan-tropical scale.

Groundwater flow theory, streamflow separation analysis and statistical regression techniques in 167 tropical and sub-tropical catchments were used to determine the best predictors for $k_{bf.}$ The latter proved to be related primarily to climatic characteristics at the catchment scale, such as catchment aridity and mean annual rainfall, whereas catchment physical characteristics were of secondary importance. This finding was partly considered as a justification for the use of the grid cell as the spatial modelling unit and the simplified representation of a 'catchment', thereby avoiding complex grid and vector model hybrids to emulate catchment boundaries.

Chapter 5 Model description, pan-tropical parameterisation and evaluation

This chapter provides a condensed description of the W3RA-LUM model including modelling philosophy, the hydrological processes modelled and their corresponding equations, spatial representation, data requirements and previous applications. It describes the structural modifications to model the effects of LUCC on partition of infiltration and runoff according to the U.S. Soil Conservation Service Curve Number Method (SCS-CN; USDA, 1986). The SCS-CN method is currently the only method for global application of these scenarios that has a strong empirical basis and is responsive to soil type and degradation (or improvement) scenarios. Soil condition is considered in the SCS-CN method by including the effects of cover type and soil treatment (*e.g.*, tillage) on infiltration and runoff. Soil condition is typified as good, fair or poor hydrologic condition, implying a low, moderate or high runoff potential respectively. To characterise soil hydrologic condition pan-tropically, rainfall corrected negative trends of satellite-derived Normalized Vegetation Index (NDVI) over the period 1981–2003 are used as a proxy to identify areas with severe land degradation (Bai *et al.*, 2008). The chapter also includes the evaluation of W3RA-LUM outputs using streamflow observed in catchments with a drainage area <10,000 km^2 (*i.e.,* commensurate with the modelling grid scale) and streamflow observed in large basins.

Chapter 6 Modelling the pan-tropical impact of LUCC and surface degradation on dry season flows and comparison with empirical observations at sites across the tropics

Peña-Arancibia, J. L., M. Mulligan, L. A. Bruijnzeel and A.I.J.M van Dijk (in prep.), Pan tropical modelling of the effects of land use and land cover change on dry season flows. **Agriculture Ecosystems & Environment,** manuscript in preparation.

The hypotheses regarding the streamflow impacts of deforestation or forestation including impacts on surface soil condition are tested in this chapter. The scenario modelling approach is described in detail. For situations B and D depicting changes in soil condition, surface runoff related model parameters are modified following a Soil Conservation Service Curve Number (SCS-CN) method, tailored for tropical soils as typified by the FAO. Two types of analyses are conducted: (*i*) soil and vegetation changes are used in a sensitivity analysis to determine the impacts of LUCC pan-tropically and in locations for which there is published observational evidence of the hydrological impacts of LUCC and (*ii*) 'what if' scenarios are used to test the respective hypotheses for different forest cover realisations.

Spatial maps of streamflow metrics are derived to identify 'hotspots' in which LUCC may produce important dry season flow regime alterations. Results from pan-tropical modelling using both current forest cover and future forest cover maps showed areas with reduction in streamflow for some of the driest months after forest removal and advanced soil degradation, despite the corresponding decreases in evapotranspiration due to deforestation. These areas included: Central America, northern South America, the Andes, Bolivia, Brazil, the Caribbean, Congo, Gabon, Tanzania, Ethiopia, South Africa, Madagascar, India, Bangladesh, and several countries in Southeast Asia. Similarly, but using modelling results from pre-agricultural forest cover and current forest cover maps, areas with similar climatic and biophysical characteristics but deforested and/or degraded according to Bai *et al.* (2008) were then identified for forestation with associated potential for recovery of infiltration. Some of the areas coincided with areas targeted by ongoing reforestation and restoration initiatives (*cf.*Minnemeyer *et al*., 2011; http://www.wri.org/project/forest-landscape-restoration) and the map of Lepers *et al.* (2005) showing the main areas of rapid forest cover changes over the period 1980–2000.

Chapter 2 Identifying hydrological impact of LUCC on streamflow data at the regional scale

Contents

Journal of Hydrology 416–417 (2012) 60–71

Contents lists available at SciVerse ScienceDirect

Journal of Hydrology

journal homepage: www.elsevier.com/locate/jhydrol

Detecting changes in streamflow after partial woodland clearing in two large catchments in the seasonal tropics

Jorge L. Peña-Arancibia [a,b,c,*], Albert I.J.M. van Dijk [a], Juan P. Guerschman [a], Mark Mulligan [b], L. Adrian (Sampurno) Bruijnzeel [c], Tim R. McVicar [a]

[a] CSIRO Land and Water, GPO Box 1666, Black Mountain, Canberra ACT 2601, Australia
[b] Environmental Monitoring and Modelling Research Group, Department of Geography, King's College London, Strand, London WC2R 2LS, UK
[c] Faculty of Earth and Life Sciences, VU University Amsterdam, De Boelelaan 1085-1087, 1081 HV Amsterdam, The Netherlands

ARTICLE INFO

Article history:
Received 1 September 2011
Received in revised form 14 November 2011
Accepted 16 November 2011
Available online 25 November 2011
This manuscript was handled by Geoff Syme, Editor-in-Chief

Keywords:
Deforestation
Tropical hydrology
Hydrological processes
Hydrological models
Streamflow
Land use change

SUMMARY

We used daily rainfall and streamflow time series from two large catchments in the seasonal tropics of Queensland, Australia to investigate the hydrological impacts of woodland clearing. The Comet catchment (16,440 km^2) had 45% of the native woodland cleared during the mid-1960s. In the Upper Burdekin catchment (17,299 km^2) clearing decreased native woodland extent from 83% to 58% between 1998 and 2009. An earlier modelling study concluded that clearing in the Comet catchment increased annual streamflow by more than 40%. Here, several published inference methods to separate land use effects from climate variability were applied. Trend analysis of daily rainfall and streamflow data showed that interannual changes in mean streamflow in the Comet catchment were mostly due to changes in rainfall. In particular, a series of La Niña events after clearing led to an unusual lack of dry periods and an apparently associated temporary increase in runoff coefficient. The overriding importance of climate variability was further confirmed using a conceptual framework that was used to interpret changes in the long-term coupled water–energy budget. Even so, there was some evidence for a slight increase in streamflow for the first few years after clearing. Fitting a Budyko-type model for two climatically similar pre- and post-clearing periods (1920–1953 and 1979–2007) did not suggest a considerable change in the catchment water balance after clearing. Analysis of daily streamflow metrics did reveal some changes however, with enhanced peak flows and reduced low flows. In the Upper Burdekin catchment, trend analysis revealed a change in baseflow dynamics after clearing, while event storm flow for large rainfall events increased. In summary, woodland clearing in northern Queensland appears to have had a smaller impact on mean and interannual streamflow than might be expected from studies at sites and in small experimental catchments, but changes in daily streamflow patterns do suggest a modest change in catchment dynamics.

1. Introduction

There is an extensive body of hydrological literature dealing with impacts of land use and land cover change (LUCC) on small (i.e. <1 km^2), mainly temperate experimental catchments (Bonell and Bruijnzeel, 2005; Brown et al., 2005; Peel, 2009). In such controlled conditions, total annual water yield, infiltration and groundwater recharge appeared to increase proportionally to the area of forest removed (e.g. Brown et al., 2005; Van Dijk and Keenan, 2007). Most of the increase occurred as baseflow, as long as surface infiltration characteristics were maintained during and after forest conversion (Bruijnzeel, 1990, 2004).

There are several scale related differences that may preclude the direct verification in larger catchments (>500 km^2) of results in small experimental, these include: (*i*) climate gradients; (*ii*) the mosaic of land uses; (*iii*) vegetation types and (*iv*) spatially variable soils and geology across the catchment, among others (Blöschl et al., 2007; Donohue et al., 2010).

There are few studies of LUCC impacts on streamflow (Q) in large tropical catchments (>10,000 km^2), their results often contrast those observed in small catchments in that not all show increased streamflow after forest clearing (Table 1). In some of the studies, the increase in streamflow was not attributed primarily to changes in vegetation. For example, Bruijnzeel (2004) argued that most of the observed 11% water yield increase in the Citarum River catchment in Java, Indonesia from 1979 to 1986 (Van der Weert, 1994) could be ascribed to a concurrent considerable increase in compacted roads and settlements (cf. Sidle et al., 2004; Ziegler et al., 2001, 2007; Negishi et al., 2008), instead of changes

* Corresponding author at: CSIRO Land and Water, GPO Box 1666, Canberra ACT 2601, Australia. Tel.: +61 (2)6246 5711; fax: +61 (2)6246 5800.
E-mail address: jorge.penaarancibia@csiro.au (J.L. Peña-Arancibia).

0022-1694/$ - see front matter
doi:10.1016/j.jhydrol.2011.11.036

Table 1
Studies and methodologies implemented to investigate the effects of land use/land cover change (LUCC) on streamflow in large (>10,000 km^2) tropical catchments. Methods refer to: TSA, time-series analysis; MOD, modelling.

Catchment (Country)	Area (km^2)	Forest cover change (%)	Period pre- and post-LUCC	Method(s)	Effects on streamflow (% change)	Reference
Pasak River (northern Thailand)	14,500	−50	1955–1980[a]	TSA	No change	Dyhr-Nielsen (1986)
Citarum River (west Java, Indonesia)	4133	−50	1922–1929 1979–1986	TSA, MOD	Increase (11%)	Van der Weert (1994)
Tocantins River (central Brazil)	767,000	−19	1949–1968 1979–1998	TSA, MOD	Increase (24%)	Costa et al. (2003)
Nam Pong River (north-eastern Thailand)	12,100	−63	1957–1965 1969–1995	TSA, MOD	No change	Wilk et al. (2001)
Comet River (central Queensland, Australia)	16,440	−45	1920–1949 1970–2000	TSA, MOD	Increase (40%)	Siriwardena et al. (2006)
Ji-Paraná (southwestern Amazonia, Brazil)	33,012	−50	1978–2000[b]	TSA	No change	Linhares (2005) and Rodriguez et al. (2010)
Pearl river and East, North and West Rivers (Guandong Province, China)	179,752	+37	1965–1986 1993–2006	TSA	No change	Zhou et al. (2010)

[a] No distinctive pre- and post-LUCC periods.
[b] No distinctive pre- and post-LUCC periods but transitory changes of LUCC and streamflow.

in evapotranspiration (*ET*) due to forest conversion into irrigated rice fields (which may have similar or higher water consumption than forest). Large-scale weather patterns may be a cause of the 24% increase in streamflow from 1979 to 1998 in the Tocantins basin after LUCC (Costa et al., 2003; Linhares, 2005). Although periods pre- and post-LUCC were climatically similar, Garcia and Mechoso (2005) observed an increase in mean annual streamflow in all major rivers in South America (including the Tocantins) associated to changes in the intensity of the South American monsoon system, this increase coincided in the Tocantins with increases in streamflow after LUCC. Trancoso (2006) also attributed the trends in observed streamflow in Amazon tributaries in the area known as the 'deforestation arc' (cf. Morton et al., 2006) to climatic changes and not to LUCC effects. Wilk et al. (2001) and Linhares (2005) did not find changes in mean annual streamflow in the Nam Pong catchment (Thailand, 1969–1995) and the Ji-Paraná catchment (south-western Amazonia, Brasil, 1978–2000) after 63% and 50% of the original forest coverage was removed respectively. Conversely, Zhou et al. (2010) found that 37% afforestation in Guandong Province in China did not reduce streamflow (1993–2006) as would have been inferred from small catchment experiments.

In recent decades, clearing rates in the seasonal tropics (i.e. areas in the tropics with marked rainfall seasonality, Peel et al., 2007) have been comparable to those observed for humid tropical forests (FAO, 1993; Lepers et al., 2005). According to UNESCO (2009) most population growth will occur in the tropics. Hence, the proximity of seasonal tropical forests to densely populated areas, extraction pressures and their often rich agricultural soils make them more vulnerable to deforestation than their humid counterparts (e.g. Songer et al., 2009). Understanding of the LUCC effects on catchment streamflow is vital to inform water and land use management (e.g. Calder, 2007; McVicar et al., 2007). In the seasonal tropics, the distribution of streamflow is more important than total annual water yield for sustaining aquatic and riparian ecosystems, and agricultural and industrial activities (e.g. Bruijnzeel, 2004; Foley et al., 2005). Rapid agricultural development may lead to changes in hydrological process dynamics. In catchments where human productive activities have taken place for decades, soils may have become disturbed to the extent that topsoil porosity and infiltration capacity are critically reduced (Alegre and Cassel, 1996; Negishi et al., 2008), leading to enhanced overland flow occurrence and possibly decreased groundwater recharge (Ziegler et al., 2006). If continued over a sufficiently long period, as happens in many agricultural areas (e.g. Bruun et al., 2009; Ziegler et al., 2009), this topsoil degradation, in addition to intensification of agricultural activities, may produce a shift in streamflow regime, with increased peaks during the rainy season and decreased flows during the dry season (Madduma Bandara and Kuruppuarachchi, 1988; Bruijnzeel, 1990, 2004; Viramontes and Descroix, 2003; Rodriguez et al., 2010).

Clearing of seasonal tropical woodlands in Queensland (Australia) has proceeded at a fairly steady rate of around 1% annually for the last 41 years, and has exceeded or at least sustained these rates in the two last decades (Fensham and Fairfax, 2003). Several plot or small catchment studies in the Australian seasonal tropics support the notion of increased streamflow after clearing of native vegetation (e.g. Tullberg et al., 2001; Rohde, 2005; Bonell and Williams, 2009). In particular, a paired catchment experiment conducted from 1965 to 2004 in small catchments (~15 ha) of the Fitzroy River Basin showed that streamflow from two catchments increased by 9–11% after clearing (Thornton et al., 2007).

Siriwardena et al. (2006) investigated the effects of deforestation in a large catchment in central Queensland. The Comet catchment (16,440 km^2) had 45% of the native woodland cleared during the mid-1960s. Rainfall (*P*) and streamflow for periods pre (1920–1949) and post-deforestation (1970–1999) were compared using statistics on mean annual averages and daily flow duration curves. Results indicated that the post-clearing period had a statistically significant (5% level) increase of 78% in mean annual streamflow, although some proportion could be explained by a concurrent 8.4% increase in rainfall. Without going into detail with respect to the models, two modelling approaches were used to separate climate variability from LUCC effects (see Siriwardena et al., 2006 for details). An annual rainfall–runoff relationship and a daily conceptual model were calibrated to simulate annual or daily streamflow over the period pre-LUCC and then simulations were conducted for the period post-LUCC, with a 40–58% increase in observed mean annual streamflow in the second period being attributed to LUCC. The authors noted that only 1 year with much higher than average rainfall occurred in the calibration period pre-LUCC and consequently both models simulated streamflow poorly in 'wet' periods (Siriwardena et al., 2006). The period after deforestation, which was used to establish differences in streamflow attributed to LUCC, had very high rainfall in northeast Queensland linked to La Niña conditions from 1973 to 1976 (BOM, 2010; Fu et al., 2010). As a result, climatic conditions in this period may have

caused most of the observed increase in streamflow after deforestation.

In this study, we aim to isolate LUCC effects on streamflow by using several approaches for two large catchments in the seasonal tropics of Queensland Australia, i.e. the Comet catchment and the Upper Burdekin catchment (17,299 km^2). Multiple approaches may well provide corroborating evidence that can be used to differentiate LUCC effects from climate variability in observed changes of streamflow. The Comet catchment is revisited to further investigate the effect of the 'wet' period in the 1970s on the observed increase in streamflow and the subsequent role of LUCC.

Section 2 of this paper provides a description of catchments, data and associated LUCC. The next section describes the methodology used (Section 3). Results are presented and analysed (Section 4), the findings are discussed in the international scientific context (Section 5) and finally conclusions are drawn (Section 6).

2. Catchment description and data

2.1. The Comet catchment

The Comet River (drainage area 16,440 km^2) is a tributary of the Fitzroy River in central Queensland (Fig. 1a). Elevation ranges from 150 to 1223 m a.s.l. Soils in the lowlands and floodplains consist mainly of cracking clayey vertisols (FAO soil classification, IUSS Working Group WRB, 2006). The uplands have mainly duplex Luvisols. Climate is dry sub-humid with summer rainfall dominance (Köppen-Geiger type Cfa/BSh) (Peel et al., 2007). Mean annual rainfall over 1920–2007 was 650 mm y^{-1}, with 60% of the rain occurring between December and March. Rainfall varies across the catchment from 520 to 900 mm y^{-1} and there is a marked interannual variability. Mean annual Morton-type potential evaportranspiration (*PET*) is 1680 mm y^{-1} and is in phase with rainfall. Catchment averaged actual evapotranspiration estimated from remote sensing (Guerschman et al., 2009) for 2002–2008 was 620 mm y^{-1}. Streamflow is ephemeral, occurring generally from December to April and peaking in February. The mean annual average streamflow in 1920–2007 was 22.1 mm y^{-1} at gauging station 130504B (Fig. 1a).

LUCC have been described in detail by Siriwardena et al. (2006). In summary, removal of 45% of the native woodland vegetation (Acacia and Eucalypt open woodlands) for cattle ranching and cropping occurred over a short period in the mid-1960s and clearing of regrowth has continued to present. Sequential maps of forest cover classification from the National Carbon Accounting System (considered forest if a 0.2 ha has >20% and 2 m height forest cover; Furby, 2002) show that an additional 10% of native vegetation or plantation forest was cleared between 1980 and 2009 (Fig. 2). The majority of forest clearing was performed using conventional methods (bulldozers and chain). Fire, re-clearing and/or blade-ploughing is generally applied to control the vigorous regrowth after the initial clearing (Scanlan and Anderson, 1981).

Water extractions for irrigation purposes from the Comet River are considered to have very small impact on streamflow throughout the study period (see Siriwardena et al., 2006). However, there was an increase in farm dam construction in the post-clearing period and thus an increase in the catchment storage capacity. The implications of combined impact of farm dam expansion and increase in water demand for irrigation are discussed in Section 5.

Daily rainfall data for 1920–2007 were obtained from the interpolated 0.05° resolution gridded rainfall data set known as 'SILO' (Jeffrey et al., 2001). Morton-type areal *PET* values (Morton, 1983; Chiew and McMahon, 1991) for 1957–2007 were derived using climate variables from SILO and prior to 1957 from Rayner et al. (2004). This formulation of *PET* was selected over physically

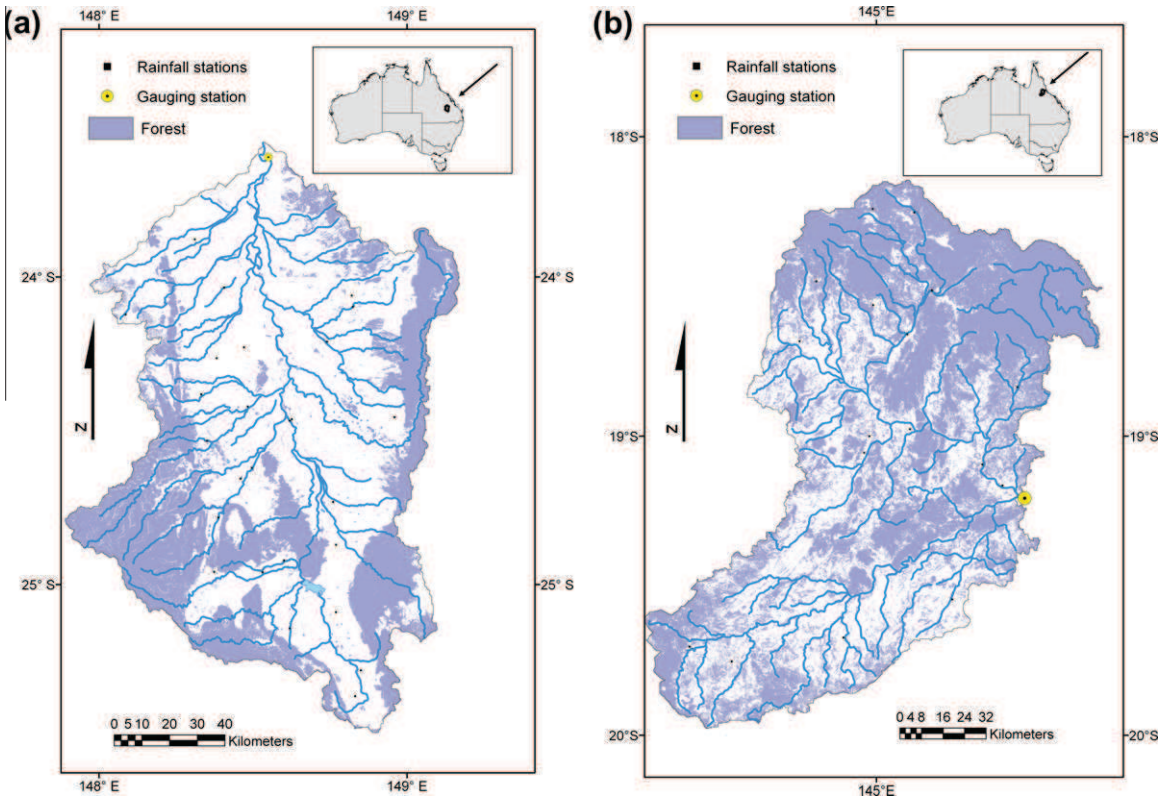

Fig. 1. (a) The Comet River catchment, active rainfall stations and streamflow gauge 130504B. (b) Idem for the Upper Burdekin catchment with streamflow gauge 120110A. Forested areas correspond to 2009. Note the different scale bars.

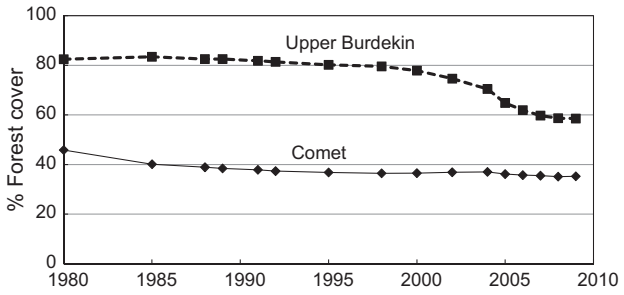

Fig. 2. Time-series of percentage forest cover for the Comet and Upper Burdekin catchments. Forest cover percentages estimated from the NCAS dataset (Furby, 2002). Markers indicate years with available forest cover maps.

based formulations as all input data (specifically wind speed; McVicar et al., 2008) forcing are not available for the time series in the Comet catchment.

Streamflow (Q) data were provided by the Queensland Department of Environment and Resource Management (DERM). In summary, discontinuous records from three gauging stations were used to construct a continuous daily streamflow time series for the period 1920–2007; the records begin with the daily-read gauge 130501A (operational from August 1919 to October 1973). In 1971 the station was moved 6.4 km upstream and the record continued as 130504A (operational from August 1971 to January 2004); in 2004 the station was relocated back to its original location and the record continued as 130504B. Siriwardena et al. (2006) checked the influence of gauge relocation from station 130501A to 130504A for a period (February 1972 to May 1973) in which both gauges were operational by visually comparing daily streamflow time series and concluded that this did not affect the consistency of the record. Following this procedure, the same was concluded by the present study for stations 130501A and 130504B for daily streamflow time series from February 2003 to January 2004. Siriwardena et al. (2006) noted that the records for the unusually wet period between 1950 and 1956 were unreliable because the very high daily flow rates recorded during that time exceeded up to six times the measurements used to construct the rating curve. These data were excluded from the present analysis as well.

2.2. The Upper Burdekin catchment

The Upper Burdekin catchment comprises all the drainage area above the Burdekin Falls Dam (40,000 km^2). Here we define the Upper Burdekin catchment as the area above gauging station 120110A (17,299 km^2, Fig. 1b). Elevation ranges from 350 to 900 m a.s.l. Soils vary considerably, with duplex Luvisols and Solonetz dominating the lowlands and Ferralsols and Acrisols the uplands. Climate ranges from tropical sub-humid closer to the Great Dividing Range (Köppen-Geiger type Cwa), to semi-arid in the far west of the interior (Köppen-Geiger type BSh) (Peel et al., 2007). Mean annual rainfallover 1966–2009 was 690 mm y^{-1}, with 70% occurring between December and March. Rainfall varies across the catchment from 560 to 1000 mm y^{-1} and shows marked interannual variability, occurring mostly as cyclonic or monsoon-driven events followed by extensive dry periods (Roth et al., 2002). Mean annual Morton-type areal *PET* is 1930 mm y^{-1} and exhibits seasonality in phase with rainfall. Remotely sensed actual evapotranspiration (Guerschman et al., 2009) for 2002–2008 was 550 mm y^{-1}. Streamflow occurs from December to April, peaking in February. Although flows from May to November are low, the Upper Burdekin only ceases to flow in very dry years. The mean annual average streamflow between 1966 and 2009 was 99 mm y^{-1} at gauging station 120110A (Fig. 1b).

The Upper Burdekin catchment had 83% forest cover in 1980. From 1999 to 2009 the catchment experienced an average annual clearing rate of 1.9%, decreasing the forest cover to 58% (Fig. 2). Clearing has been undertaken to support grazing, although managing regrowth has proven to be a challenge (Roth et al., 2002). Cattle numbers vary greatly across the catchment, with an average stocking density of 0.09 head ha^{-1}.Gridded daily rainfall and Morton-type *PET* were derived from the same SILO data set mentioned before. Continuous daily streamflow records from station 120110A were sourced from the Queensland Department of Environment and Resource Management (DERM).

3. Methods

Different published methods to separate land use effects from climate variability were applied by considering the length of hydroclimatic time series in both catchments. The length of time series in the Comet catchment (1920–2007) permitted the investigation of changes in mean annual streamflow (Q) in pre- and post-LUCC periods. On the other hand, shorter records (1966–2009) but detailed land cover mapping enabled the assessment of changes in daily Q descriptors from daily data and their relationship with transitional LUCC.

To discriminate between fast and slow runoff generating processes, Q was separated into storm flow (Q_{SF}) and baseflow (Q_{BF}) using a non-linear reservoir model, combining forward and backward recursive filters (Wittenberg, 1999; Van Dijk, 2010a). Daily records of Q, rainfall (P) and *PET* (all in mm d^{-1}) were summed to give annual totals per water year (1 October to 30 September). We performed the following analyses in the Comet for periods pre- and post-LUCC : (*i*) double mass curves and time series analysis of P and Q (Section 3.1); (*ii*) a conceptual framework based on the long-term coupled water–energy budget at interannual scales (Tomer and Schilling, 2009) (Section 3.2); (*iii*) a top-down Budyko-type modelling approach (Zhang et al., 2008) (Section 3.3); (*iv*) comparison of metrics of daily Q (Yilmaz et al., 2008; Rodriguez et al., 2010) (Section 3.4) and; (*v*) comparison of event storm flow (Van Dijk, 2010b) (Section 3.5). Due to the shorter hydroclimatic time series available (i.e. 1966–2009) only methods (*iv*) and (*v*) could be used in the Upper Burdekin. In method (*v*), detailed land cover mapping available for several years (Fig. 2) permitted analysis of temporal correlations between woodland cover extent, climate descriptors and metrics of daily Q.

3.1. Double mass curve analysis and trend analysis

Streamflow changes in the Comet catchment were investigated by constructing double mass curves of annual rainfall (P) vs. streamflow (Q). Assuming that P data is consistent over the analysis period, changes in the slope of the double mass curve can indicate (Siriwardena et al., 2006): (*i*) change in gauging station and/or rating curve, (*ii*) errors in the data, and/or (*iii*) changes in catchment conditions and/or (*iv*) climate that affect the rainfall–runoff relationship. Break points in slope were found using the methodology of Ryan and Porth (2007). The seasonal non-parametric Mann–Kendall test (10%, 5% and 2.5% significance levels; Hirsch et al., 1982) was used to detect monotonal trends in P and Q for periods in which a change in slope was observed. The seasonal version of the test was chosen instead of the annual time step in order to eliminate serial correlation due to the high seasonality of both P and Q (cf. Yue et al., 2002; Yue and Wang, 2004). The rate of change was estimated using the Sen-slope method (Sen, 1968).

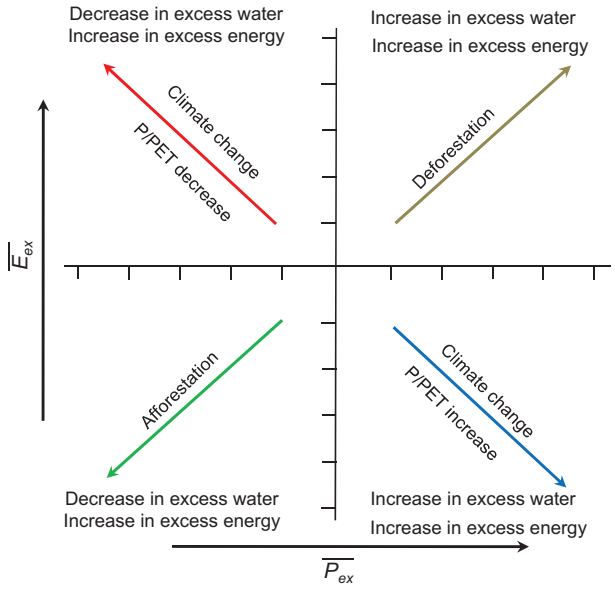

Fig. 3. Conceptual model based on the long-term coupled water–energy budget at interannual scales associated with changes in climate and land use (adapted from Tomer and Schilling, 2009). *P* refers to rainfall, areal *PET* to potential evapotranspiration, $\overline{P_{ex}}$ and $\overline{E_{ex}}$ .refer to excess amounts of water and energy respectively. Other types of land management which increase (e.g. conservation tillage, removal of perennials) or decrease *ET* (e.g. conservation cover, increased forages) are encompassed by deforestation or afforestation, respectively (Tomer and Schilling, 2009).

3.2. Tomer–Schilling framework

Tomer and Schilling (2009) developed an elegant coupled water–energy balance framework that requires long-term time series of rainfall (*P*), streamflow (*Q*), and *PET* to assess if unused available energy and water were related to climate and/or to land management in agricultural catchments for the mid-Western US. Results were used to advance a conceptual framework that qualitatively discriminates whether the dominant drivers of observed changes are related to LUCC and/or climate. The framework relating changes in LUCC and/or climate to the observed changes in the excess amounts of water (P_{ex}) and excess amounts of energy (E_{ex}) as fractions is illustrated in Fig. 3. The catchment water balance can be written as:

$$\Delta S = P - ET - Q. \tag{1}$$

Assuming that there is a 'steady state' water balance in the long-term, i.e. when catchment storage change ΔS (mm) can be neglected, long-term mean evapotranspiration $\overline{ET}$ (mm) can be estimated from long-term mean rainfall $\overline{P}$ (mm) and streamflow $\overline{Q}$ (mm) as:

$$\overline{ET} = \overline{P} - \overline{Q}. \tag{2}$$

Interannual intervals in which catchment storage ΔS may be considered minimal were selected from the baseflow time series by choosing periods that began and ended with very low baseflow. Further, excess amounts of $overline{P_{ex}}$ and $\overline{E_{ex}}$ in each interval are defined as (Tomer and Schilling, 2009):

$$\overline{P_{ex}} = \frac{(\overline{P} - \overline{ET})}{\overline{P}}, \text{ and} \tag{3}$$

$$\overline{E_{ex}} = \frac{(\overline{PET} - \overline{ET})}{\overline{PET}}. \tag{4}$$

The Tomer–Schilling framework assumes that LUCC will affect $\overline{ET}$ but not $\overline{P}$ or $\overline{PET}$, acknowledging that effects on $\overline{P}$ and $\overline{PET}$ can be considered indirect at this scale and of second order when compared to changes in $\overline{ET}$ in the woodland environment of the Comet. Thus LUCC will cause ecohydrological shifts towards increased $\overline{P_{ex}}$ and $\overline{E_{ex}}$, or towards decreased $\overline{P_{ex}}$ and $\overline{E_{ex}}$. Changes in climate are required to cause increased $\overline{P_{ex}}$ and decreased $\overline{E_{ex}}$, due to the temporal increase in the $\overline{P}/\overline{PET}$ ratio and *vice versa*.

3.3. The Budyko framework

The Fu (1981) formulation of the Budyko framework (Budyko, 1974) is given as:

$$\frac{\overline{ET}}{\overline{P}} = 1 + \frac{\overline{PET}}{\overline{P}} - \left[1 + \left(\frac{\overline{PET}}{\overline{P}}\right)^{w}\right]^{\frac{1}{w}}, \tag{5}$$

and was used to interpret whether the parameter related to evapotranspiration efficiency (w) changed in each interval. Combining Eqs. (2) and (5) and with $\alpha = 1 - 1/w$ so that α varies between 0 and 1, one obtains the following expression (Zhang et al., 2008):

$$\overline{Q} = \left(\overline{P}^{\frac{1}{1-\alpha}} + \overline{PET}^{\frac{1}{1-\alpha}}\right) - \overline{PET}. \tag{6}$$

The parameter α can be interpreted as a catchment-level vegetation $\overline{ET}$ efficiency: a higher value indicates a greater ability of the catchment to retain and evaporate *P*, for example because of greater rooting depth (e.g. Zhang et al., 2004). Values of α are obtained for each interval by minimising the squared difference between observed and simulated $\overline{Q}$.

They were calculated for intervals corresponding to the intervals pre-LUCC (1920–1953) and used to simulate $\overline{Q}$ ($\overline{Q_{sim}}$) in intervals in the post-LUCC period (1970–2007) using Eq. (6). The total change in streamflow due to LUCC effects can then be estimated as:

$$\Delta\overline{Q_{LUCC}} = \sum_{i=1}^{n} \overline{Q_{obs,i}} - \sum_{i=1}^{n} \overline{Q_{sim,i}}, \tag{7}$$

where $\Delta\overline{Q_{LUCC}}$ is the change in total streamflow due to vegetation changes, $\overline{Q_{obs}}$ is the streamflow observed in each interval of the post-LUCC period, and $\overline{Q_{sim}}$ is the simulated streamflow in each interval, whereas n is the number of intervals considered in the analysis.

3.4. Yilmaz–Rodriguez daily streamflow metric analysis

Rodriguez et al. (2010) adapted the method developed by Yilmaz et al. (2008) to detect changes in streamflow regime associated with different hydrological processes resulting from LUCC. Yilmaz et al. (2008) partitioned the daily flow duration curve (FDC) in segments corresponding to: (*i*) high flows (exceedance probability EP < 0.02); (*ii*) intermediate flows ($0.2 \leqslant EP \leqslant 0.7$); and (*iii*) low flows (EP > 0.7). Daily *Q* (ML d^{-1}) were used to avoid negative values for log-transformed records <1.

Following Rodriguez et al. (2010), five streamflow (*Q*) regime summary metrics were derived by partitioning the FDC. Three of these five metrics corresponded to the respective volumes of *Q* ($VFLOW_x$ in ML) belonging to each segment of the FDC curve:

$$VFLOW_x = \sum \frac{(Q_i + Q_{i+1}) \times \Delta f}{2}, \tag{8}$$

where Q_i is the *i*th probability discharge, Δf is the frequency increment and the subscript x corresponds to high (*high*), intermediate (*int*) and low flows (*low*). High flow volume ($VFLOW_{high}$) is associated to catchment response from large rainfall events. Intermediate flow volume ($VFLOW_{int}$) is associated to the slower catchment response from moderate rainfall events and also to intermediate-term baseflow response. The low flow volume ($VFLOW_{int}$) is related to the long-term baseflow response (Yilmaz et al., 2008).

In addition, the total volume of log-transformed low flows ($LFLOW_{low}$) was computed to place more weight on lower values of low flows, thus giving a fourth metric:

$$LFLOW_{low} = \sum \frac{(\log(Q_i) + \log(Q_{i+1})) \times \Delta f}{2}. \quad (9)$$

Finally, log-transformed values were also used to calculate a fifth metric, the slope of the intermediate flows (SLO_{int}) within the FDC:

$$SLO_{\text{int}} = \frac{\log(Q_{m1}) + \log(Q_{m2})}{\Delta f}, \quad (10)$$

where Q_{m1} and Q_{m2} are the 0.2 and 0.7 exceedance probability discharge, respectively. This was used to infer changes in catchment flow recession. Higher (steeper) slope values would suggest faster catchment recession and lower slopes are associated with more sustained baseflow. Metrics were subsequently grouped for each water year, adding volumes and averaging SLO_{int}.

For the Comet catchment, long-term LUCC impacts on Q signals were compared by using probability of exceedance curves for Q signals for periods pre- and post-LUCC.

In the Upper Burdekin catchment, to assist in the interpretation of temporal changes due to LUCC impacts on Q signals, lagged non-parametric Spearman correlations were computed between signals, climate descriptors and percentage forest cover extent (*%FCE*) values. Linear regression analysis was used to interpret relations between signals, climate descriptors, and *%FCE*. The strongest predictors were combined through stepwise multiple regression equation that included *%FCE*. The following climate descriptors were computed: mean annual rainfall (*MAP*, mm y^{-1}), mean annual *PET* (*MPET*), a humidity index (*HI* = *MAP*/*MPET*) and a proxy for mean annual P intensity *MAPI* (mm y^{-1}) defined as:

$$MAPI = MAP \times \frac{RP}{TD}, \quad (11)$$

where *RP* is the sum of P for days with $P > 10$ mm each and *TD* is the sum total of days with rainfall. The threshold value of 10 mm was chosen because inspection of daily flow records showed that this amount of P usually triggered Q_{SF}. In addition standard Mann–Kendall trend analysis (2.5%, 5% and 10% significance level) was performed on signals, climate descriptors and *%FCE*.

3.5. Event storm flow for periods pre- and post-LUCC

To investigate the impact of LUCC on faster hydrological components of the hydrograph, event rainfall and storm flow for periods pre- and post-LUCC were computed following the procedure described by Van Dijk (2010b), based on Wittenberg (1999). Following linear storage theory a weighted average storm flow recession constant k_{SF} (d^{-1}) was calculated:

$$k_{SF} = -\ln\left[\frac{\sum Q_{SF}(i+1)}{\sum Q_{SF}(i)}\right]. \quad (12)$$

Total event rainfall $P_{ev}(i)$ (mm) for the event peaking on day $t = i$ was subsequently estimated as:

$$P_{eV}(i) = \sum_{t=i-2}^{i} P(i), \quad (13)$$

where t was suggested by Van Dijk (2010b) as $i - 2$ to account for antecedent P effects. Total event storm flow R_{ev}(i) (mm) was estimated as:

$$R_{eV}(i) = \sum_{t=i-2}^{t_n} Q_{SF} + S_R(t_n) = \sum_{t=i-2}^{t_n} Q_{QF} + \frac{Q_{SF}(t_n+1)}{1 - e^{(-k_{SF})}}, \quad (14)$$

where t_n is the day on which $Q_{SF}(t_n)$ is one tenth of $Q_{SF}(i)$. This was done in Eq. (14) to avoid inclusion of Q_{SF} generated by subsequent P_{ev}. The term $S_R(t_n)$ (mm) is the estimated storm runoff still in storage at the end of day t_n based on linear reservoir theory Van Dijk (2010b).

In the Comet catchment, we used daily rainfall (P) and daily streamflow (Q) from 1920 to 1949 and 1981–2007 to represent pre- and post-LUCC conditions, respectively. In the Burdekin catchment, 1980–1985 represented pre-LUCC and 2004–2009 post-LUCC respectively. *%FCE* did not experience important reductions within either period (Fig. 3). Differences in R_{ev} during the pre- and post-LUCC situations were analysed for both catchments using probability of exceedance curves.

4. Results

4.1. Double mass curve analysis and trend analysis

Double mass curves of annual rainfall vs. annual streamflow for the Comet catchment are presented in Fig. 4. The slopes for the periods 1950–1956 and 1971–1980 are markedly higher (0.13 and 0.08 respectively) than those associated with the other periods distinguished (0.023, 0.03 and 0.025 for 1920–1949, 1961–1970 and 1981–2007 respectively). Note that data for the very wet period from 1952 to 1958 were considered unreliable and were not used in any analysis (see Section 3.1). The higher streamflow (Q) production in 1971–1980 occurred after land clearing was completed in the mid-1960s. Table 2 shows the rainfall (P) and Q characteristics for 1920–1949, 1961–1970, 1971–1980 and 1981–2007. The 1970s were particularly wet, with annual rainfall 20–30% higher than the other periods. Streamflow was 60–70% higher and the annual runoff coefficient for 1971–1980 was roughly twice the value observed during other periods (Table 2). The double mass curve analysis and summary statistics in Table 2 show that 1981–2007 was climatically similar to the pre-LUCC period in contrast to 1971–2007. Therefore 1981–2007 was considered in further analysis when comparing pre- and post-LUCC (see also Section 4.5 for details on rainfall variability between pre-LUCC and 1981–2007).

Trend analysis was performed for the periods in Fig. 4. 1971–2007 was examined separately to assess the influence of the wet 1970s on temporal trends for the entire post-LUCC period. No significant (10% significance level) temporal trends in P or Q were detected for 1920–1949 whereas statistically significant negative (5% significance level, but not 2.5%) trends were detected for P for 1971–2007 and 1981–2007 and for Q for 1971–2007 period (2.5% significance level).

Given the high rainfall and streamflow seasonality, the Mann–Kendall test was performed for time series of each month separately in the periods 1971–2007 and 1981–2007 respectively to aid in the interpretation of changes during the dry and/or wet

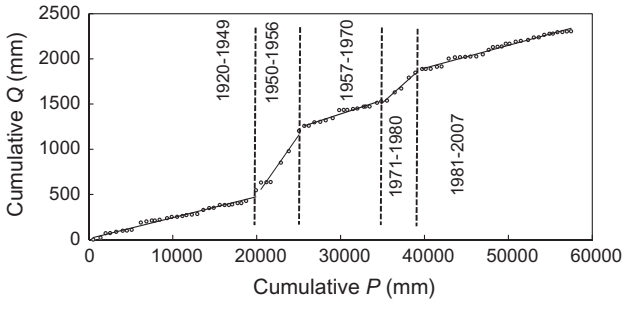

Fig. 4. Double mass curves of cumulative annual rainfall (P) vs. streamflow (Q) for the Comet catchment. Periods with a marked change in slope are delimited with dashed lines.

Table 2
Characteristics of rainfall and streamflow for the Comet River basin for four different periods, encompassing pre- and post-clearing and the period of rapid forest clearance (1961–1970).

	Hydrological years			
	Pre- clearing 1920–1949	Rapid-clearing 1961–1970	Post-clearing 1971–1980	Post-clearing 1981–2007
Rainfall				
Mean ($mm\ y^{-1}$)	624	586	783	619
Max ($mm\ y^{-1}$)	1089	837	919	877
Min ($mm\ y^{-1}$)	351	225	424	410
Coefficient of variation	0.24	0.32	0.23	0.19
Streamflow				
Mean ($mm\ y^{-1}$)	14.3	17.1	41.7	15.4
Max ($mm\ y^{-1}$)	81.9	88.4	120.7	88.4
Min ($mm\ y^{-1}$)	0.0	0.0	0.8	0.9
Baseflow ($mm\ y^{-1}$)	2.3	1.6	9.4	2.2
Quickflow ($mm\ y^{-1}$)	12.0	15.5	32.3	13.2
Runoff coefficient (%)	2.29	2.90	5.72	2.47
Baseflow index	0.16	0.09	0.22	0.14
Quickflow index	0.84	0.91	0.78	0.86
Coefficient of variation	1.23	1.57	0.93	1.24

season. For 1971–2007, negative trends (10% significance level, but not 5%) in P were detected for the wet months of December and February. In addition, negative trends in streamflow were found for December–March and July–September (10% significance level, but not 5%). However, significant trends (10% significance level) were largely absent after separating the wet 1970s from the entire post-LUCC data set. When considering 1981–2007, only the drier months of August and October presented a significant negative trend (10% significant level, but not 5%) in P and November for Q (5% significant level, but not 2.5%).

4.2. Tomer–Schilling framework

Thirteen intervals in which change of storage (ΔS) within may be considered to have been minimal impact were identified by plotting mean annual baseflow time series (not shown but can be easily identified in Fig. 5a) and choosing periods that began and ended with very low or no baseflow. These intervals are shown in the upper-x axis in Fig. 5a, as well as the streamflow (Q) time series and averages for each interval. Unused amounts of water ($\overline{P_{ex}}$) and energy ($\overline{E_{ex}}$) were estimated for each interval as shown in Fig. 5b–d.The colour coded arrows in Fig. 5b–d indicate the direction in the shifts attributed to the changes in climate and/or LUCC depicted in Fig. 3 (Tomer and Schilling, 2009). Fig. 5b indicates that changes in climate may have dominated the shifts observed in 1920–1953 (intervals 1–5), with a short wet cycle (1920–1926 to 1926–1931), a dry cycle (1926–1931 to 1938–1948) being followed by a wet cycle (1938–1948 to 1948–1953). Similarly, Fig. 5c shows that the shift observed in 1958–1964 to 1964–1967 was dominated by the occurrence of a dry cycle. The period immediately after extensive clearing of native vegetation (1964–1967 to 1967–1970) exhibited a shift consistent with LUCC, with a distinct decrease in ET (Fig. 5c). Finally, 1970–1979 to 2003–2007 showed mainly an overriding influence of climate again, with a decrease in excess water and an increase in excess energy, and therefore a decrease in the $\overline{P}/\overline{PET}$ ratio (Fig. 5d).

4.3. The Budyko framework

The influence of vegetation cover on overall catchment-wide evapotranspiration (ET) following Zhang et al. (2008) as expressed by the parameter α, which may be considered as a proxy for evapotranspiration efficiency (cf. Eq. (6)), showed a slight decrease during the post-LUCC period. Five out of the 13 intervals distinguished during the entire time series (Fig. 5a), were considered to have an average α representing equilibrium conditions prior to LUCC (1920–1953, intervals 1–5). Optimised α values for these five intervals ranged 0.698–0.736 and had a mean of 0.718. A further five intervals between 1970 and 2007 (9–13) and four between 1979 and 2007 (10–13) were considered to represent an average post-LUCC α. These intervals are similar to the years in which change was observed in the slope of the double mass curves in Section 4.1 and provided the opportunity to investigate the effect of the wet 1970s and a more climatically similar period (1981–2007). Optimised α values for 1970–2007 had a mean of 0.707 (range 0.694–0.727) and for 1979–2007 had a mean of 0.716 (range 0.694–0.727).

This decrease in α post-LUCC represented an annual average reduction in ET of 19–24 mm or 3.1–3.8% with an associated increase in streamflow (Q) due to LUCC (Eq. (6)) of 0.17 mm or 1% between 1970 and 2007 and 0.02 mm or 0.001% between 1979 and 2007.

4.4. Yilmaz–Rodriguez daily streamflow metric analysis

Yearly signals for volume of high flows ($VFLOW_{high}$), intermediate flows ($VFLOW_{int}$) and slope of intermediate flows (SLO_{int}) were computed for the Comet catchment. No data were available to compute volume of low flows ($VFLOW_{low}$) or the log-transformed low flows ($LFLOW_{low}$) because daily flow did not exceed the 0.7 probability of exceedance. Signals were compared for pre- and post-LUCC effects using exceedance curves. We used the 1981–2007 post-LUCC period which was more climatically similar to the pre-LUCC period. Slightly larger values were observed for $VFLOW_{high}$ during the post-LUCC period (Fig. 6a), whereas somewhat lower values were observed for $VFLOW_{int}$ (Fig. 6b). The lower slope SLO_{int} values (Fig. 6c) observed for the post-LUCC period indicates steeper yearly slopes and thence faster catchment recession.

For the Upper Burdekin, trends of yearly streamflow (Q) signals, climate descriptors and percentage forest cover (*%FCE*) were examined using annual time-step Mann–Kendall test (10%, 5% and 2.5% significance level). Only the signal associated with baseflow ($LFLOW_{low}$) exhibited a significant negative trend (10% significance level, but not 5%). Lagged non-parametric Spearman correlations were computed between signals and *%FCE*, for which only the years 1998–2009 were used because *%FCE* remained nearly constant from 1980 to 1998 (Fig. 3). Maximum correlations were found for a lag time of 2 years. Results are given in Table 3.

To account for climate variability, simple linear regressions were performed between signals and climate attributes. Mean annual precipitation intensity descriptor (*MAPI*) explained 79% of the variance in $VFLOW_{high}$, mean annual precipitation (*MAP*) explained 73%, 65% and 54% of $VFLOW_{int}$, $VFLOW_{low}$ and $LFLOW_{low}$, respectively. *MAP* also explained 30% of SLO_{int}. Further, these climate attributes were combined in stepwise regression with variously lagged values of *%FCE* to investigate the significance of vegetation in explaining the remaining variance in signals. Table

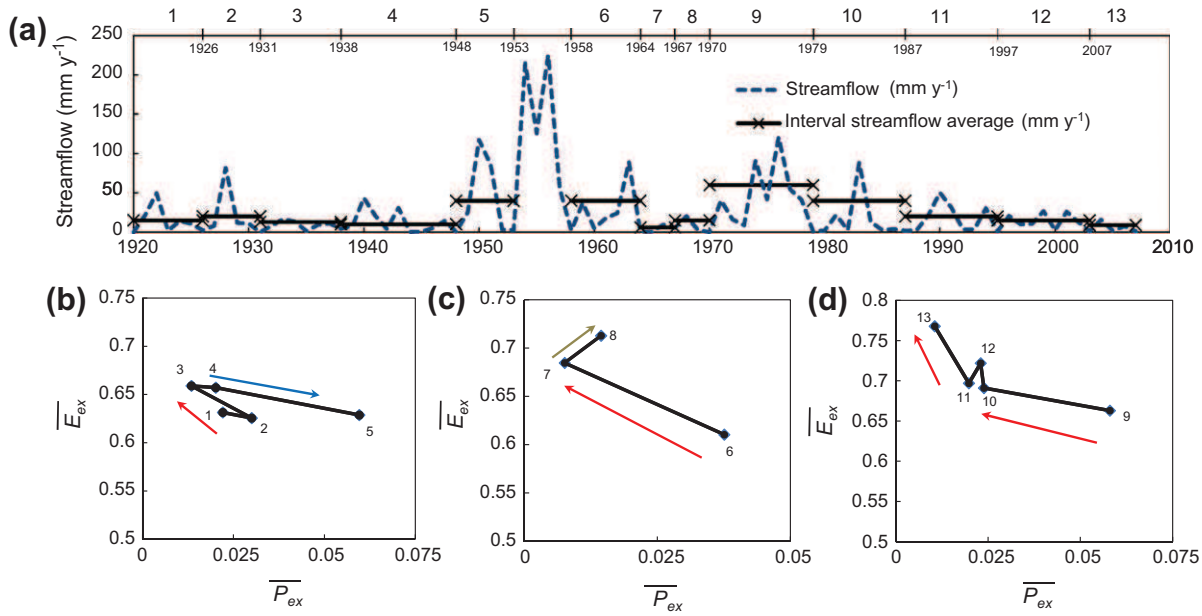

Fig. 5. (a) Annual time series of streamflow (dashed line) for the Comet catchment and interval streamflow averages (solid horizontal line) for 13 intervals in which catchment storage change (ΔS) may be considered minimal. (b) Scatter plots of long-term averages of unused amounts of water ($\overline{P_{ex}}$) and energy ($\overline{E_{ex}}$) for 1920–1953, intervals 1–5 shown on part (a); (c) idem for 1958–1970 (intervals 6–8), and (d) for 1970–2007 (intervals 9–13). The numbers at the vertices in parts (b–d) represent average conditions of the 13 intervals defined and labelled in upper *x*-axis of part (a). Colour coded arrows refer to the direction of changes associated with climate variability and/or LUCC as defined in Fig. 3. Note the different scale bars.

4 gives the resulting regression equations. For $VFLOW_{high}$ the inclusion of *%FCE* (zero lag time) improved the coefficient of determination (r^2) from 0.79 to 0.82; the negative sign associated to *%FCE* suggested a decrease in *%FCE* would increase $VFLOW_{high}$. Similarly, the value of r^2 for the relationship with $VFLOW_{int}$ improved from 0.73 to 0.90 after including *%FCE* (with a lag time of 1 year), this time with an opposite outcome (i.e. a decrease in *%FCE* would in turn decrease $VFLOW_{int}$). Using a 2 year lag time for *%FCE* improved r^2 for the relationship with $VFLOW_{low}$ from 0.65 to 0.93, again predicting a decrease in flows after decreasing *%FCE*. The addition of *%FCE* did not improve r^2 in the $LFLOW_{low}$ and SLO_{int} equations, hence these are not show in Table 4.

4.5. Event storm flow for periods pre- and post-LUCC

Rainfall (P) variability was assessed for both pre- and post-LUCC conditions in the Comet and Burdekin catchments using P frequency distribution plots (Fig. 7a and b). The largest differences in P between the two periods were observed for $P < 5$ mm d^{-1} in both catchments. The associated impact on streamflow (Q) was small, however, because generally only daily $P > 10$ mm d^{-1} initiated storm flow in either catchment.

Rainfall distributions in the Comet for the two periods were fairly similar (Fig. 7a). In terms of mean storm flow coefficient (R_{ev}/P_{ev}) there was increase post-LUCC from 1.85% to 2.5%. Fig. 7c shows higher R_{ev} post-LUCC , this increase was uniform along all runoff event regimes but the very largest, and markedly higher in lower runoff events (exceedance probability >80%).

There were more events >50 mm d^{-1} in the period post-LUCC in the Burdekin catchment, 16 events in 2004–2009 against only 6 in 1980–1985 (Fig. 7b). There was an increase in R_{ev}/P_{ev} from 5.6% to 8.4% in the Upper Burdekin catchment. R_{ev} increase was more marked in higher runoff events (exceedance probability <40%) and marginal in lower runoff events (exceedance probability >80%) (Fig. 7d).

5. Discussion

Several previous studies in the tropics that ascribed increases in streamflow (Q) primarily to LUCC in large catchments (>10,000 km^2) did not account for large-scale weather patterns including ENSO events (e.g. Richey et al., 1989; Costa et al., 2003). Richey et al. (1989) concluded that the increase in Q of the Amazon River at Iquitos was caused by climate variability instead of deforestation in the Upstream Andes. The observed increase in the Tocantins after LUCC (Costa et al., 2003, Table 1) occurred within a period with strong ENSO-related increase in P (INPE, 2004). The simultaneity in the dates of Q increase for large basins in South America (García and Mechoso, 2005) suggests large-scale interdecadal climate patterns were also important in the case of the Tocantins and that the role of LUCC should be further investigated (cf. Linhares, 2005; Espinoza Villar et al., 2009).

In the Comet catchment (16,440 km^2), the post-LUCC period (1971–1980) showed 66% more Q than the pre-LUCC period (1920–1949) (Table 2). However, 1981–2007 was not very different in terms of mean annual rainfall (P), P frequency distribution, and mean annual Q compared to the pre-LUCC period (Table 2 and Fig. 7a). 1973–1976 experienced the longest sustained period of La Niña conditions in the instrumental record; the particularly striking feature of the rainfall during this period was the complete lack of dry periods (BOM, 2010). The Tomer and Schilling (2009) coupled water–energy balance framework indicated that climate exerted an overriding effect on Q by increasing the P/PET ratio, with P_{ex} increasing from 0.014 to 0.058 from 1967–1970 to 1970–1979 (Fig. 5c and d). On the other hand, the framework also suggested that a decrease in ET occurred in 1964–1967 to 1967–1970 (Fig. 5c) which could be linked to large scale clearing.

The pre-LUCC for the Budyko-type model did not encompass the range of climate variability experienced in the 1970s. As a result, the Budyko-type model underestimated flows during intervals of (very) high Q and overestimated flows during drier years. This issue was also reported in Siriwardena et al. (2006); both

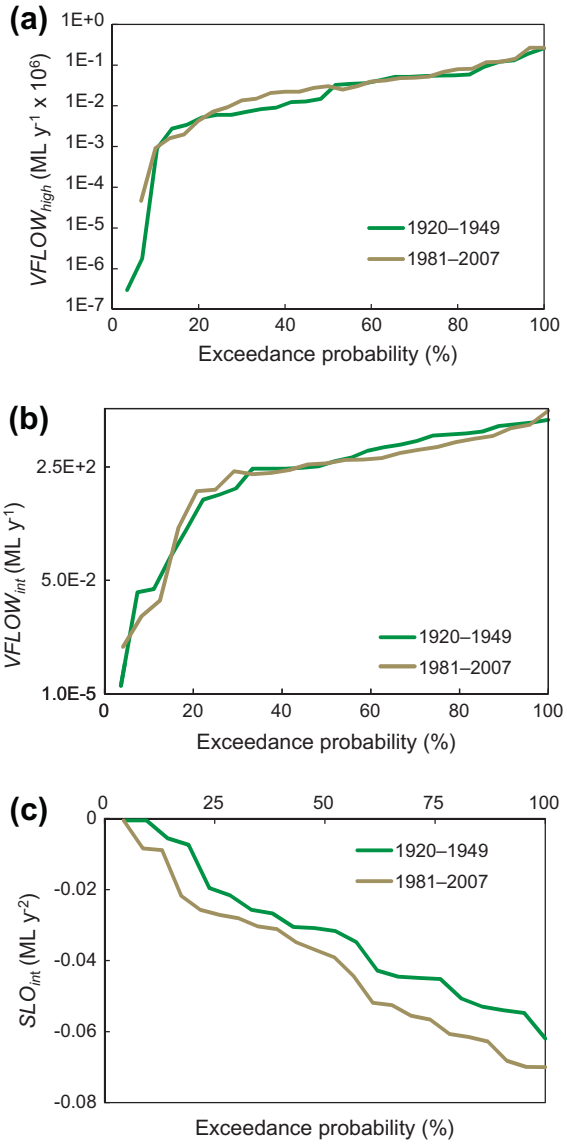

Fig. 6. Probability of exceedance curves of streamflow signals in the Comet catchment for pre-LUCC (1920–1949) and post-LUCC (1981–2007); shown are: (a) volumes of high flows ($VFLOW_{high}$); (b) intermediate flows ($VFLOW_{int}$) and (c) slope of the intermediate flows SLO_{int}. Note the log *y*-axis for (a and b).

Table 3
Lags for maximum values of Spearman non-parametric correlations between signals and forest cover extent in the Upper Burdekin. Maximum correlations were found for a lag time of 2 years.

%FCE	lag $t = 0$	lag $t = 1$	lag $t = 2$
$VFLOW_{high}$	0.10	0.17	0.38
$VFLOW_{int}$	0.26	0.49	0.57[a]
$VFLOW_{low}$	0.23	0.40	0.42
$LFLOW_{low}$	0.18	0.46	0.56[a]
SLO_{int}	0.11	0.045	−0.27

$VFLOW_x$ refers to volume flow and the subscript x corresponds to high (high), intermediate (int) and low flows (low), $LFLOW_{low}$ to log transformed values of low flows and SLO_{int} to the slope of the intermediate flows (see Section 3.4 for details).
[a] Correlations significant at 10% significance level.

models used to quantify changes associated to LUCC simulated *Q* poorly in 'wet' periods (cf. Vaze et al., 2010). In a study that used a similar modelling approach to separate climate variability and LUCC effects in the Nam Pong River in Thailand (12,100 km^2), Wilk et al. (2001) reported an increase in mean annual *Q* of 15% after deforestation. However, this increase could not be detected when one single year with a very low runoff coefficient was removed from the pre-clearing calibration period.

Table 4
Summary of results, including r^2, r^2 if percentage forest cover extent (*%FCE*) is not included (in brackets), and standard error of estimate (SEE) for linear regression equations linking *%FCE* with climate attributes for the (1998–2009) period in the Upper Burdekin.

Equation	r^2	SEE (ML)
$VFLOW_{high} = (10311.6 \times MAPI) - (7907.4 \times \%FCE)$	0.82 (0.79)	0.18×10^6
$VFLOW_{mid} = (120.4 \times MAP) + (1604.7 \times \%FCE) - 168896343$	0.90 (0.73)	10,247
$VFLOW_{low} = (8.22 \times MAP) + (148.4 \times \%FCE) - 14067.8$	0.933 (0.65)	589

$VFLOW_x$ refers to volume flow and the subscript x corresponds to high (high), intermediate (int) and low flows (low), $LFLOW_{low}$ to log transformed values of low flows and SLO_{int} to the slope of the intermediate flows. *MAP* and *MAPI* refer to mean annual precipitation and mean annual precipitation intensity respectively (see Section 3.4 for details).

Based on such considerations, 1979–2007 was deemed more suitable for use in a predictive modelling exercise for the Comet basin. Rainfall frequency distributions for the calibration and prediction periods were very similar (Fig. 7a), and although a decreasing trend was detected for rainfall (*P*) after 1981 by the seasonal Mann–Kendall test, a similar test of monthly *P* trends revealed that the decreasing trend in *P* was considered significant in the dry season month of August and October only (10% significance level, but not 5%). It is hypothesised that *P* in these months will make a small contribution to *Q* only.

The results of the Budyko framework to estimate total change in streamflow (*Q*) due to LUCC effects (Eq. (7)) showed a very small increase in *Q* (0.001%) in the Comet basin. Likely causes for the small estimated effect may be: (*i*) measurement noise, (*ii*) spatio-temporal terrain and climate factors other than *P* and *PET* which are not taken into account in Budyko theory (Donohue et al., 2007, 2010; Van Dijk et al., 2011) and (*iii*) expansion of farm dams and increase in irrigation water use that would offset increases in *Q*. The effects of LUCC at smaller scales may well be markedly higher, but the lack of data prevented a similar analysis at the sub-catchment scale. Nevertheless, results obtained in nearby small catchments showed a marked increase in runoff after LUCC (Thornton et al., 2007).

Results from the Yilmaz–Rodriguez analysis and storm flow for the Comet catchment reinforced the notion that the catchment has experienced a change in dynamics (Figs. 6 and 7c). In general, clearing of Acacia and Eucalypt woodlands enhanced storm flows of all magnitudes (Fig. 7c) but somewhat decreased slower flows (Fig. 6b). The decrease in slow flows may be related to a reduction in catchment soil water storage because of a combination of reduced infiltrability and soil compaction in riparian areas and in perched aquifers during the wet season (Tullberg et al., 2001).

The Yilmaz–Rodriguez analysis suggested a potential change in dynamics for the Upper Burdekin catchment as well (Table 3), but the time series was too short to make any firm inferences. The Mann–Kendall test suggested a significant negative trend for the baseflow signal (10% significance level, but no 5%). The inclusion of forest cover extent in various multiple regression equations (Table 4), after correcting for climate variability, showed that deforestation may be one factor influencing hydrological shifts. The fact that better results were obtained using lagged parameters in the regressions suggests that the impact of deforestation at these large scales may take some time to realise (cf. Rodriguez et al., 2010). The equations linking streamflow (*Q*) and forest cover

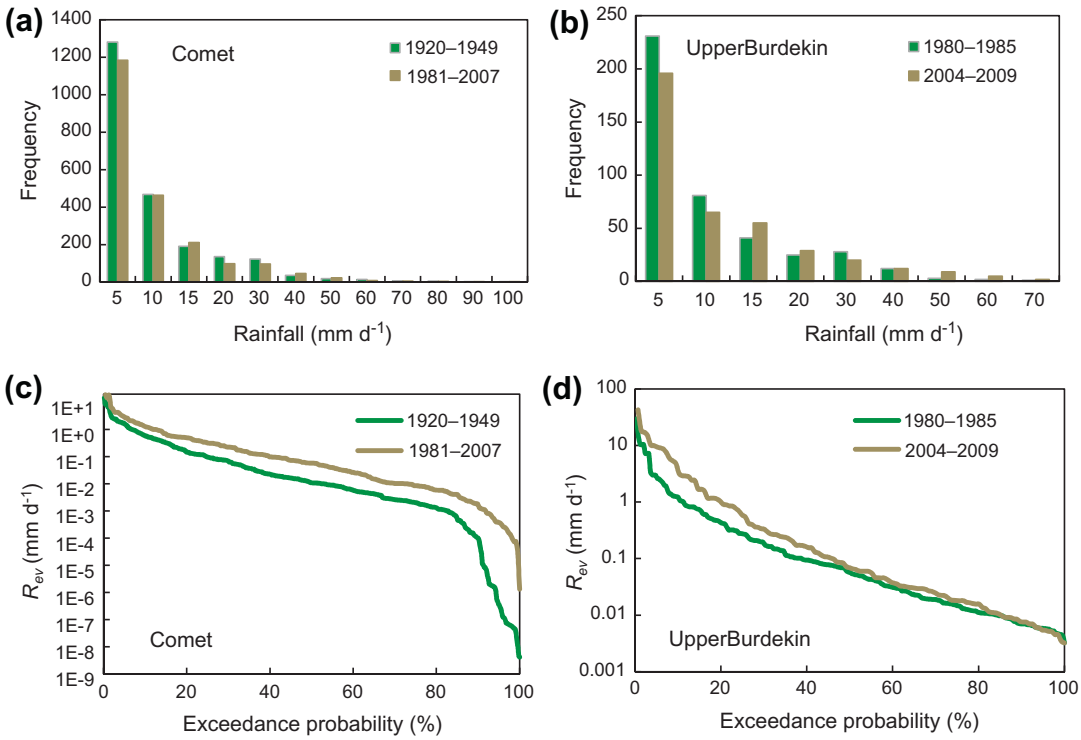

Fig. 7. Frequency distributions of daily rainfall during pre- and post-LUCC conditions for (a) the Comet catchment and (b) the Upper Burdekin catchment. Probability of exceedance of event storm flow (R_{ev}) for pre- and post-LUCC conditions for (c) the Comet catchment and (d) the Upper Burdekin catchment.

(Table 4) suggested increasing high flows and decreasing low flows to be associated with increasing deforestation in the Upper Burdekin catchment. The inclusion of vegetation information in the regression may be interpreted in terms of changes in soil water use (higher for forest) but on the other hand the removal of forest vegetation is related to changes in infiltration rates (typically reduced due to soil compaction) (e.g. Ziegler et al., 2004). For example, Zhou et al. (2010) reported that the effects of large-scale forest recovery on Q in several gauging stations in Guandong Province, China (179,752 km^2) reduced variability by redistributing water from the wet season to the dry season by promoting infiltration and recharge due to recovery of soil hydraulic characteristics.

Changes in soil water use, and their effect of decreasing low flows, may be also related to vigorous vegetation regrowth and pasture water use during the growing season. Rapid growth of secondary vegetation in seasonal Amazonia and northern Thailand has been linked to high evaporation rates after 2–3 years (Hölscher et al., 1997; Giambelluca et al., 2000). Vigorous regrowth is also a feature of Acacia and Eucalypt dominated woodlands in the Upper Burdekin area and elsewhere in Australia (Cornish and Vertessy, 2001; Roth et al., 2002; Fensham et al., 2005). In addition, the active growing season of perennial pasture occurs between mid-spring to the following mid-autumn (Hacker and Waite, 2001).

On the other hand, infiltration rates have been shown to decline after conversion to grazing land as a result of hoof impact (e.g. Daniel et al., 2002). Bonell and Williams (2009) concluded that soils in this region have a delicate fabric that is easily disturbed, leading to a reduction in infiltration capacity and increased occurrence and magnitude of overland flow. In similar soils in northern Australia, high stocking rates resulted in soil compaction whereas hillside runoff made up a large proportion of incident rainfall (Ive et al., 1976). Burning after clearing is common and may also have contributed to a further reduction in infiltration capacity (Valzano et al., 1997; Mills and Fey, 2004).

6. Conclusion

The impact of broad-scale deforestation on hydrology was investigated in two large catchments (>10,000 km^2) in the Australian seasonal tropics. Several published methods were tested to separate climate variability from land use and land cover change (LUCC) effects. The Comet catchment (16,440 km^2) had 45% of the native woodland cleared during the mid-1960s. In the Upper Burdekin (17,299 km^2), clearing reduced native woodland extent from 83% in 1989 to 58% in 2009.

In the Comet catchment, findings from a simple coupled water–energy balance framework suggested that most of the observed changes in annual streamflow were related to climate variability. However, the period immediately after clearing showed an increase in interannual streamflow that suggested a decrease in interannual evapotranspiration associated with LUCC. An overall increase in annual streamflow in the post-LUCC period (1971–2007) was mainly attributed to higher than average rainfall linked to La Niña conditions in the wet 1970s. Results from applying a Budyko-type model to assess changes in evapotranspiration efficiency for pre- (1920–1953) and a climatically similar post-LUCC (1979–2007) showed a slight decrease in evapotranspiration of 3.1–3.8% with negligible (i.e. 1%) increase in streamflow. Likely causes for the small estimated effect may be measurement noise, spatio-temporal terrain and climate factors other than rainfall and potential evapotranspiration which are not taken into account in Budyko theory and expansion of farm dams and extraction of water for irrigation. Although no differences were found in interannual yields, changes pre- and post-LUCC in metrics derived from daily streamflow highlighted changes in catchment dynamics. Clearing of Acacia and Eucalypt woodlands enhanced storm flow of all magnitudes and somewhat decreased slower flows. A similar outcome was inferred from daily streamflow metrics results in the Upper Burdekin, which were linked to effects of transitional woodland clearing, although

the short analysis period (1998–2009) made attribution difficult. Changes in hydrological process dynamics like those observed in the Comet and Burdekin catchments can be realised in any one location in the seasonal tropics as a consequence of rapid LUCC and more intense agricultural practices. In these environments with seasonal streamflow, regime variability due to LUCC will result from a trade-off between changes in evapotranspiration and/or changes in soil infiltration characteristics.

Acknowledgements

The authors gratefully acknowledge funding from Microsoft Research. The Queensland Department of Environment and Resource Management (DERM) are also thanked for providing the streamflow data. The authors are also grateful to Luigi Renzullo, Randall Donohue and Lingtao Li form CSIRO Land and Water for providing data used in this study. Jai Vaze from CSIRO Land and Water and two anonymous reviewers are also thanked for providing valuable comments on the research.

References

Alegre, J.C., Cassel, D.K., 1996. Dynamics of soil physical properties under alternative systems to slash-and-burn. Agric. Ecosyst. Environ. 58 (1), 39–48.
Blöschl, G. et al., 2007. At what scales do climate variability and land cover change impact on flooding and low flows? Hydrol. Process. 21 (9), 1241–1247.
BOM, 2010. La Niña – Detailed Australian Analysis. <http://www.bom.gov.au/climate/enso/lnlist/> (accessed 19.08.11).
Bonell, M., Bruijnzeel, L.A., 2005. Forests, Water and People in the Humid Tropics. International Hydrology Series. Cambridge University Press, 40 West 20th St, New York, NY 10011 USA, 944 pp.
Bonell, M., Williams, J., 2009. A review of hydrology research within the open eucalypt woodlands of tropical semiarid Australia: a possible source of baseline information for the West African Sahel. Secheresse (Montrouge) 20 (1), 31–47.
Brown, A.E., Zhang, L., McMahon, T.A., Western, A.W., Vertessy, R.A., 2005. A review of paired catchment studies for determining changes in water yield resulting from alterations in vegetation. J. Hydrol. 310 (1–4), 28–61.
Bruijnzeel, L.A., 1990. Hydrology of Moist Tropical Forests and Effects of Conversion: A State of Knowledge Review. UNESCO International Hydrological Programme and Free University Amsterdam, 244 pp. <http://unesdoc.unesco.org/images/0009/000974/097405eo.pdf> (accessed 19.08.11).
Bruijnzeel, L.A., 2004. Hydrological functions of tropical forests: not seeing the soil for the trees? Agric. Ecosyst. Environ. 104 (1), 185–228.
Bruun, T.B., Neergaard, A.d., Lawrence, D., Ziegler, A.D., 2009. Environmental consequences of the demise in swidden cultivation in Southeast Asia: carbon storage and soil quality. Hum. Ecol. 37 (3), 375–388.
Budyko, M.I., 1974. Climate and Life. Academic Press, New York, 508 pp.
Calder, I.R., 2007. Forests and water – ensuring forest benefits outweigh water costs. For. Ecol. Manage. 251 (1–2), 110–120.
Chiew, F.H.S., McMahon, T.A., 1991. The applicability of Morton and Penman evapotranspiration estimates in rainfall–runoff modeling. Water Resour. Bull. 27 (4), 611–620.
Cornish, P.M., Vertessy, R.A., 2001. Forest age-induced changes in evapotranspiration and water yield in an eucalypt forest. J. Hydrol. 242 (1–2), 301–322.
Costa, M.H., Botta, A., Cardille, J.A., 2003. Effects of large-scale changes in land cover on the discharge of the Tocantins River, Southeastern Amazonia. J. Hydrol. 283 (1–4), 206–217.
Daniel, J.A., Potter, K., Altom, W., Aljoe, H., Stevens, R., 2002. Long-term grazing density impacts on soil compaction. Trans. ASAE 45 (6), 1911–1915.
Donohue, R.J., Roderick, M.L., McVicar, T.R., 2007. On the importance of including vegetation dynamics in Budyko's hydrological model. Hydrol. Earth Syst. Sci. 11 (2), 983–995.
Donohue, R.J., Roderick, M.L., McVicar, T.R., 2010. Can dynamic vegetation information improve the accuracy of Budyko's model? J. Hydrol. 390 (1–2), 23–34.
Dyhr-Nielsen, M., 1986. Hydrological Effect of Deforestation in the Chao Phraya Catchment in Thailand. International Symposium on Tropical Forest Hydrology and Application, Chiangmai, Thailand, p. 12.
Espinoza Villar, J.C.E. et al., 2009. Contrasting regional discharge evolutions in the Amazon catchment (1974–2004). J. Hydrol. 375 (3–4), 297–311.
FAO, 1993. Forest Resources Assessment 1990 – Tropical Countries, Rome. <http://www.ciesin.columbia.edu/docs/002-471/002-471.html> (accessed 19.08.11).
Fensham, R.J., Fairfax, R.J., 2003. Assessing woody vegetation cover change in north-west Australian savanna using aerial photography. Int. J. Wildland Fire 12 (3–4), 359–367.
Fensham, R.J., Fairfax, R.J., Archer, S.R., 2005. Rainfall, land use and woody vegetation cover change in semi-arid Australian savanna. J. Ecol. 93, 596–606.
Foley, J.A. et al., 2005. Global consequences of land use. Science 309 (5734), 570–574.
Fu, P.B., 1981. On the calculation of the evaporation from land surface. Sci. Atmos. Sin., 22–31 (in Chinese).
Fu, G.B., Viney, N.R., Charles, S.P., Liu, J.R., 2010. Long-term temporal variation of extreme rainfall events in Australia: 1910–2006. J. Hydrometeorol. 11 (4), 950–965.
Furby, S., 2002. Land Cover Change: Specification for Remote Sensing Analysis, National Carbon Accounting System Technical Report No. 9, Australian Greenhouse Office, Canberra.
Garcia, N.O., Mechoso, C.R., 2005. Variability in the discharge of South American rivers and in climate. J. Hydrol. Sci. 50 (3), 459–478.
Giambelluca, T.W., Nullet, M.A., Ziegler, A.D., Tran, L., 2000. Latent and sensible energy flux over deforested land surfaces in the eastern Amazon and northern Thailand. Singapore J. Trop. Geogr. 21 (2), 107–130.
Guerschman, J.P., Van Dijk, A.I.J.M., Mattersdorf, G., Beringer, J., Hutley, L.B., Leuning, R., Pipunic, R.C., Sherman, B.S., 2009. Scaling of potential evapotranspiration with MODIS data reproduces flux observations and catchment water balance observations across Australia. J. Hydrol. 369 (1–2), 107–119.
Hacker, J.B., Waite, R.B., 2001. Selecting buffel grass (*Cenchrus ciliaris*) with improved spring yield in subtropical Australia. Trop. Grasslands 35 (4), 205–210.
Hirsch, R.M., Slack, J.R., Smith, R.A., 1982. Techniques of trend analysis for monthly water-quality data. Water Resour. Res. 18 (1), 107–121.
Hölscher, D., Sa, T.D.A., Bastos, T.X., Denich, M., 1997. Evaporation from young secondary vegetation in eastern Amazonia. J. Hydrol. 193 (1–4), 293–305.
IUSS Working Group WRB, 2006. World Reference Base for Soil Resources 2006, second ed. World Soil Resources Reports No. 103, FAO, Rome. <http://www.fao.org/ag/Agl/agll/wrb/doc/wrb2006final.pdf> (accessed 19.08.11).
Ive, J.R., Rose, C.W., Wall, B.H., Torssell, B.W.R., 1976. Estimation and simulation of sheet run-off. Aust. J. Soil Res. 14 (2), 129–138.
Jeffrey, S.J., Carter, J.O., Moodie, K.B., Beswick, A.R., 2001. Using spatial interpolation to construct a comprehensive archive of Australian climate data. Environ. Modell. Softw. 16 (4), 309–330.
Lepers, E. et al., 2005. A synthesis of information on rapid land-cover change for the period 1981–2000. Bioscience 55 (2), 115–124.
Linhares, C.A., 2005. Influência do desflorestamento na dinâmica da resposta hidrológica na bacia do Rio Ji-paraná/RO (In Portuguese). Doctoral Thesis. Brazilian Institute for Space Research. INPE-13778-TDI/1052. <http://mtc-m12.sid.inpe.br/col/sid.inpe.br/MTC-m13%4080/2005/09.06.13.50/doc/publicacao.pdf> (accessed 19.08.11).
Madduma Bandara, C.M., Kuruppuarachchi, T.A., 1988. Land-use change and hydrological trends in the upper Mahaweli basin. In: Paper Presented at the Workshop on Hydrology of Natural and Man-made Forests in the Hill Country of Sri Lanka, Kandy, October 1988, 18 pp.
McVicar, T.R. et al., 2007. Developing a decision support tool for China's re-vegetation program: simulating regional impacts of afforestation on average annual streamflow in the Loess Plateau. For. Ecol. Manage. 251 (1–2), 65–81.
McVicar, T.R., Van Niel, T.G., Li, L.T., Roderick, M.L., Rayner, D.P., Ricciardulli, L., Donohue, R.J., 2008. Wind speed climatology and trends for Australia, 1975–2006: capturing the stilling phenomenon and comparison with near-surface reanalysis output. Geophys. Res. Lett. 35, L20403. doi:10.1029/2008GL035627.
Mills, A.J., Fey, M.V., 2004. Frequent fires intensify soil crusting: physicochemical feedback in the pedoderm of long-term burn experiments in South Africa. Geoderma 121 (1–2), 45–64.
Morton, F.I., 1983. Operational estimates of areal evapo-transpiration and their significance to the science and practice of hydrology. J. Hydrol. 66 (1–4), 1–76.
Morton, D.C. et al., 2006. Cropland expansion changes deforestation dynamics in the southern Brazilian Amazon. Proc. Natl. Acad. Sci. USA 103, 14637–14641.
Negishi, J.N., Sidle, R.C., Ziegler, A.D., Noguchi, S., Rahim, N.A., 2008. Contribution of intercepted subsurface flow to road runoff and sediment transport in a logging-disturbed tropical catchment. Earth Surf. Proc. Land. 33 (8), 1174–1191.
Peel, M.C., 2009. Hydrology: catchment vegetation and runoff. Prog. Phys. Geogr. 33 (6), 837–844.
Peel, M.C., Finlayson, B.L., McMahon, T.A., 2007. Updated world map of the Koppen-Geiger climate classification. Hydrol. Earth Syst. Sci. 11 (5), 1633–1644.
Rayner, D.P., Moodie, K.B., Beswick, A.R., Clarkson, N.M., Hutchinson, R.L., 2004. New Australian Daily Historical Climate Surfaces using CLIMARC. Queensland Department of Natural Resources and Mines. <http://www.longpaddock.qld.gov.au/silo/CLIMARC/AustralianHistoricalDailyClimateSufacesUsingCLIMARC_nocover.pdf>, (accessed 19.08.11).
Richey, J.E., Nobre, C., Deser, C., 1989. Amazon river discharge and climate variability – 1903 to 1985. Science 246 (4926), 101–103.
Rodriguez, D.A., Tomasella, J., Linhares, C., 2010. Is the forest conversion to pasture affecting the hydrological response of Amazonian catchments? Signals in the Ji-Parana Catchment. Hydrol. Process. 24 (10), 1254–1269.
Rohde, K., 2005. Less compaction, more cover save soil. Aust. Farm J. May, 42–43.
Roth, C.H., Lawson, G., Cavanagh, D., 2002. Overview of Key Natural Resource Management Issues in the Burdekin Catchment, with Particular Reference to Water Quality and Salinity. CSIRO Land and Water. http://www.clw.csiro.au/publications/consultancy/2003/Burdekin_Catchment_Report_Condition_Study_Phase_1-2003.pdf (accessed 19.08.11).
Ryan, S.E., Porth, L.S., 2007. A tutorial on the Piecewise Regression Approach Applied to Bedload Transport Data. Gen. Tech. Rep. RMRS-GTR-189. Fort Collins, CO, US Department of Agriculture, Forest Service, Rocky Mountain Research Station, 41 p.

Scanlan, J.C., Anderson, E.R., 1981. Use of the heavy duty blade plough for control of woody regrowth in Central Queensland. Aust. Weeds 1 (2), 10–12.
Sen, P.K., 1968. Estimates of regression coefficient based on Kendalls Tau. J. Am. Stat. Assoc. 63 (324), 1379–1389.
Sidle, R.C., Sasaki, S., Otsuki, M., Noguchi, S., Nik, A.R., 2004. Sediment pathways in a tropical forest: effects of logging roads and skid trails. Hydrol. Process. 18 (4), 703–720.
Siriwardena, L., Finlayson, B.L., McMahon, T.A., 2006. The impact of land use change on catchment hydrology in large catchments: the Comet River, Central Queensland, Australia. J. Hydrol. 326 (1–4), 199–214.
Songer, M., Aung, M., Senior, B., DeFries, R., Leimgruber, P., 2009. Spatial and temporal deforestation dynamics in protected and unprotected dry forests: a case study from Myanmar (Burma). Biodivers. Conserv. 18 (4), 1001–1018.
Thornton, C.M., Cowie, B.A., Freebairn, D.M., Playford, C.L., 2007. The Brigalow Catchment Study: II. Clearing brigalow (Acacia harpophylla) for cropping or pasture increases runoff. Aust. J. Soil Res. 45, 496–511.
Tomer, M.D., Schilling, K.E., 2009. A simple approach to distinguish land-use and climate-change effects on watershed hydrology. J. Hydrol. 376 (1–2), 24–33.
Trancoso, R., 2006. Changes in Land Cover and Alterations in the Hydrological Response of Catchments in Amazonia. INPA/UFAM, 139 pp.
Tullberg, J.N., Ziebarth, P.J., Li, Y.X., 2001. Tillage and traffic effects on runoff. Aust. J. Soil Res. 39 (2), 249–257.
UNESCO 2009. The 3rd United Nations World Water Development Report: Water in a Changing World. United Nations Educational Scientific and Cultural Organization, p. 349. <http://www.unesco.org/water/wwap/wwdr/wwdr3/pdf/WWDR3_Water_in_a_Changing_World.pdf> (accessed 15.08.11).
Valzano, F.P., Greene, R.S.B., Murphy, B.W., 1997. Direct effects of stubble burning on soil hydraulic and physical properties in a direct drill tillage system. Soil Till. Res. 42 (3), 209–219.
Van der Weert, R., 1994. Hydrological Conditions in Indonesia, Delft Hydraulics, Jakarta, Indonesia.
Van Dijk, A.I.J.M., 2010a. Climate and terrain factors explaining streamflow response and recession in Australian catchments. Hydrol. Earth Syst. Sci. 14 (1), 159–169.
Van Dijk, A.I.J.M., 2010b. Selection of an appropriately simple storm runoff model. Hydrol. Earth Syst. Sci. 14 (3), 447–458.
Van Dijk, A.I.J.M., Keenan, R.J., 2007. Planted forests and water in perspective. For. Ecol. Manage. 251 (1–2), 1–9.
Van Dijk, A.I.J.M., Peña-Arancibia, J.L., Bruijnzeel, L.A., 2011. Top-down analysis of collated streamflow data from heterogeneous catchments leads to underestimation of land cover influence. Hydrol. Earth Syst. Sci. Discuss. 8, 4121–4150.
Vaze, J., Post, D.A., Chiew, F.H.S., Perraud, J.-M., Viney, N.R., Teng, J., 2010. Climate non-stationarity – validity of calibrated rainfall–runoff models for use in climate change studies. J. Hydrol. 394 (3–4), 447–457.
Viramontes, D., Descroix, L., 2003. Changes in the surface water hydrologic characteristics of an endoreic catchment of northern Mexico from 1970 to 1998. Hydrol. Process. 17 (7), 1291–1306.
Wilk, J., Andersson, L., Plermkamon, V., 2001. Hydrological impacts of forest conversion to agriculture in a large river catchment in northeast Thailand. Hydrol. Process. 15 (14), 2729–2748.
Wittenberg, H., 1999. Baseflow recession and recharge as nonlinear storage processes. Hydrol. Process. 13 (5), 715–726.
Yilmaz, K.K., Gupta, H.V., Wagener, T., 2008. A process-based diagnostic approach to model evaluation: application to the NWS distributed hydrologic model. Water Resour. Res. 44 (9), W09417. doi:10.1029/2007WR006716.
Yue, S., Wang, C.Y., 2004. The Mann–Kendall test modified by effective sample size to detect trend in serially correlated hydrological series. Water Resour. Manage. 18 (3), 201–218.
Yue, S., Pilon, P., Cavadias, G., 2002. Power of the Mann–Kendall and Spearman's rho tests for detecting monotonic trends in hydrological series. J. Hydrol. 259 (1–4), 254–271.
Zhang, L., Hickel, K., Dawes, W.R., Chiew, F.H.S., Western, A.W., Briggs, P.R., 2004. A rational function approach for estimating mean annual evapotranspiration. Water Resour. Res. 40 (2), W02502. doi:10.1029/2003WR002710.
Zhang, L., Potter, N., Hickel, K., Zhang, Y.Q., Shao, Q.X., 2008. Water balance modeling over variable time scales based on the Budyko framework – model development and testing. J. Hydrol. 360 (1–4), 117–131.
Zhou, G., Wei, X., Luo, Y., Zhang, M., Li, Y., Qiao, Y., Liu, H., Wang, C., 2010. Forest recovery and river discharge at the regional scale of Guangdong Province, China. Water Resour. Res. 46, W09503. doi:10.1029/2009WR008829.
Ziegler, A.D., Giambelluca, T.W., Sutherland, R.A., Vana, T.T., Nullet, M.A., 2001. Contribution of Horton overland flow contribution to runoff on unpaved mountain roads in northern Thailand. Hydrol. Process. 15, 3203–3208.
Ziegler, A.D. et al., 2004. Hydrological consequences of landscape fragmentation in mountainous northern Vietnam: evidence of accelerated overland flow generation. J. Hydrol. 287 (1–4), 124–146.
Ziegler, A.D., Negishi, J., Sidle, R.C., Preechapanya, P., Sutherland, R.A., Giambelluca, T.W., Jaiaree, S., 2006. Reduction of stream sediment concentration by a riparian buffer: filtering of road runoff in disturbed headwater catchments of montane mainland Southeast Asia. J. Environ. Qual. 35 (1), 151–162.
Ziegler, A.D., Negishi, J.N., Sidle, R.C., Gomi, T., Noguchi, S., Nik, Abdul Rahim, 2007. Persistence of road runoff generation in a logged catchment in Peninsular Malaysia. Earth Surf. Proc. Land. 32, 1947–1970.
Ziegler, A.D. et al., 2009. Environmental consequences of the demise in swidden cultivation in montane mainland Southeast Asia: hydrology and geomorphology. Hum. Ecol. 37 (3), 361–373.

Chapter 3 Availability and quality assessment of meteorological forcing data for pan-tropical scale modelling of surface hydrology

Contents

3.1 Introduction

The quality of climate forcing data, precipitation in particular, required as inputs in W3RA-LUM will determine to a great extent the robustness and consistency of predictions of the impacts of LUCC on dry season flows. The aim of this chapter is to evaluate meteorological forcing data required to implement W3RA-LUM globally for later use in the modelling experiments (see Chapter 6) designed to test the hypotheses outlined in Chapter 1. This is attempted through a literature review and a comparison of commonly used rainfall data against observations. This chapter is partly based on the review of climate forcing data conducted in Peña-Arancibia et al. (2011, Appendix B). The review focused on daily meteorological forcing data required to implement W3RA-LUM globally. Drawing from published literature, strengths and weaknesses of commonly used datasets and experiences in their use in global hydrological modelling are briefly discussed. A more in-depth evaluation based on the approach by Peña-Arancibia et al. (2013, Appendix C) was performed for precipitation data which, because of its importance in the hydrologic cycle and its variability in space and time, is arguably the most crucial input. Long-term global or quasi-global precipitation datasets are quantitatively evaluated by comparing them to gauge-only precipitation analysis data.

This chapter is divided in three sections. Section 3.2 reviews meteorological forcing datasets, with emphasis on the variables needed in W3RA-LUM and includes an evaluation of precipitation datasets deemed suitable for modelling purposes. Section 3.3 provides a summary and recommendations for scenario modelling.

3.2 Meteorological forcing data

The gridded meteorological forcing data required by W3RA-LUM consist of daily precipitation (P in mm), incoming shortwave radiation (SW_{down} in Wm^{-2}) and minimum and maximum temperatures ($T_{min,max}$ in ºC). Other important radiation and atmospheric humidity variables are derived using equations in the literature or derived from the aforementioned inputs (*cf.* Van Dijk, 2010).

3.2.1 Precipitation

In the tropics, precipitation provides most of the moisture input for hydrologic processes. In hydrological modelling, the accuracy of other fluxes and stores of the water balance is heavily dependent on the accuracy of precipitation inputs (Pan *et al.*, 2010; Li and Ma, 2010). However, precipitation is highly variable both in space and time and its accurate measurement requires the use of dense gauge or radar networks. Gridded precipitation analysis based on these ground observations may not be representative in areas where these networks do not exist or are sparse, as in most of the tropics (Betts *et al.*, 2006).

Precipitation derived from satellite data or modelled through retrospective analysis (reanalysis) have provided global or quasi-global precipitation estimates with daily or finer temporal resolution independently of gauge or radar networks. In reanalyses, precipitation is modelled independently of gauge observations, by numerical weather forecasting models with fluxes constrained by a succession of satellite observations (from the 1970s onwards) and supplemented by radiosonde ascents, observations from aircraft, ocean-buoys and other surface platforms. Satellite-based precipitation is obtained from the physical relationships between infrared radiances from cloud tops with surface precipitation, or from the modulation from hydrometeors on upwelling radiation from earth in the microwave range, or using a combination of these two approaches (Todd *et al.*, 2001). Quasi-global and continuous satellite derived precipitation gridded data are only available since 1998, after the launch of the TRMM satellite mission in 1997 (Huffman *et al.*, 2007). On the other hand reanalysis data go several decades in time and therefore are a valuable source of information to understand precipitation variability (Bosilovich *et al.*, 2008).

Inter-annual and inter-decadal precipitation variability in the tropics has been widely reported in the scientific literature (Nicholson, 2000; Marengo, 2004; Gu *et al.*, 2007; Fu *et al.*, 2010). Furthermore, Chapter 2 highlighted the importance of climate variability on several tropical studies of the impacts of land use and land cover change (LUCC) on hydrology, where the role of LUCC and climate variability in hydrological changes was difficult to ascertain. Based on these important considerations, long-term precipitation data from five reanalyses routinely used

in hydrological modelling and one dataset based on reanalysis and other observational measurements are initially considered for scenario modelling purposes. Several published studies have found that both reanalysis and satellite datasets are complementary and a combination of both is likely to produce better precipitation estimates (*e.g.,* Ebert *et al.*, 2007; Peña-Arancibia *et al.*, 2013). Although satellite datasets will not be further considered for scenario modeling due to their short time-series, they are included in this review for completeness.

Table 3-1 provides details of data sources including resolution, frequency, coverage, data period and publication reference for each reanalyses and satellite precipitation data. Two reanalyses are produced by the European Centre for Medium-Range weather forecast (ECMWF): (1) ERA-40, spanning from 1957 to 2002 (Uppala *et al.*, 2005). (2) ERA-Interim, which uses a new forecasting model that has among other improvements new model physics, humidity analysis, better horizontal resolution and a new set of satellite observations (Dee *et al.*, 2011). (3) The National Center for Environmental Prediction-National Center for Atmospheric Research (NCEP-NCAR) reanalysis (Kalnay *et al.*, 1996) and (4) the NCEP-Department of Energy (NCEP-DOE); both reanalyses use the medium-range forecast NCEP global spectral model (GSM). NCEP-DOE uses an updated version of the forecasting model and include fixes to “bugs” present in NCEP-NCAR (Kanamitsu *et al.*, 2002). (5) The recently released Japanese 25 year reanalysis JRA-25 (Onogi *et al.*, 2007), produced by a collaboration between the Japan Meteorological Agency (JMA) and Central Research Institute of Electric Power Industry (CRIEPI). It incorporates new satellite and conventional data. (6) The 50-Year High-Resolution Global Dataset of Metereological Forcings for Land Surface Modelling developed by Sheffield *et al.* (2006) at Princeton University, referred here to as ‘Princeton’. Precipitation in Princeton is based on the NCEP-NCAR reanalysis and used corrections for known precipitation biases in NCEP-NCAR reanalysis and rain day statistics using monthly gauge interpolated precipitation data from the Climatic Research Unit (CRU) (New *et al.*, 2000) and TRMM precipitation respectively.

Two reanalyses which due to their relatively recent release (*e.g.,* NCEP-CFSR, Saha *et al.*, 2010; MERRA, Rienecker *et al.*, 2011) have not yet being comprehensibly evaluated are not

further considered. Four satellite-based precipitation products combining microwave and infrared observations with daily or better temporal resolutions are commonly used in hydrological applications. The tropical Rainfall Measurement Mission (TRMM) Multi-satellite Rainfall Analysis (TMPA; Huffman 2007) provides two daily products: (1) product version 3B42RT in near real time, which combines calibrated passive microwave precipitation and geosynchronous infrared inputs , and (2) version TRMM 3B42V6 which also uses monthly gauge observations to scale precipitation estimates. (3) CPC morphing (CMORPH; Joyce *et al.*, 2004) which combines multiple time-interpolated microwave and infrared-based motion precipitation. (4) The Rainfall Estimation from Remotely Sensed Information using Artificial Neural Networks (PERSIANN; Sorooshian *et al.* 2000) which establishes the infrared to rain rate relationship using artificial neural networks with parameters updated using microwave data.

Table 3-1 Main characteristics of global and quasi-global reanalyses precipitation gridded data.

Dataset	Grid resolution	Frequency	Coverage	Period	Reference
Reanalysis					
ERA-40	1.125º	6 h	Global	1957–2002	Uppala *et al.* (2005)
ERA-Interim	0.7º	6 h	Global	1979–	Dee *et al.* (2011)
NCEP-NCAR	2.5º	6 h	Global	1948–	Kalnay *et al.* (1997)
NCEP-DOE	2.5º	6 h	Global	1957–	Kanamitsu *et al.* (2002)
JRA-25	1.25º	6 h	Global	1979–2004	Onogi *et al.* (2007)
Princeton*	1°	1 day	Global	1948–2008	Sheffield *et al.* (2006)
Satellite					
TRMM-3B42RT	0.25º	3h	60ºS~60ºN	1998–	Huffman *et al.* (2007)
TRMM-3B42V6	0.25º	3h	60ºS~60ºN	2002–	Huffman *et al.* (2007)
CMORPH	0.08º~0.25º	0.5, 3h	60ºS~60ºN	2002–	Joyce *et al.* (2004)
PERSIANN	0.25º	3, 6h	50ºS~50ºN	2000–	Sorooshian *et al.* (2000)

* Not a reanalysis but a combination of reanalysis and ancillary data

Several studies mainly in Europe, the U.S. and Australia, have been conducted to evaluate different precipitation products from satellite and reanalyses by comparing them to ground observations in areas with reliable gauge or radar coverage (*e.g.,* Gottschalk *et al.*, 2005; Ebert *et al.*, 2007; Ruane and Roads, 2007; Tian *et al.*, 2009; Sapiano and Arkin, 2009; Tian and Peters-Lidard, 2010; Vila *et al.*, 2010). Other studies have assessed the quality of precipitation products through the predictive capability of state variables such as soil moisture or streamflow estimates from hydrological or land-surface models (Gottschalk *et al.*, 2005; Pan *et al.*, 2010; Stisen and Sandholt, 2010).

Findings from most studies suggest a better agreement of satellite-based precipitation with observational data for warm seasons whereas reanalysis precipitation outperformed satellite-based precipitation during cooler seasons (*e.g.,* Ebert *et al.*, 2007). It was also found that high magnitude precipitation events are better captured by satellite estimates, although magnitudes were generally overestimated (Gottschalk *et al.*, 2005; Tian *et al.*, 2009). Ebert *et al.* (2007) found that over the Australian tropics satellite-based precipitation outperformed reanalysis for heavy precipitation and that the incorporation of surface rain gauge data, such as in TRMM 3B42V6, helped to reduce total errors and improved intensities. A global map of measurement uncertainties in daily satellite-based precipitation estimates produced by Tian and Peters-Lidard (2010) showed that satellite-based estimates agreed reasonably well over areas with higher magnitude precipitation, over the tropics in particular (Figure 3.1). The performance at higher latitudes degraded considerably, especially above of 40° latitude. This was due to coverage by fewer sensors (*e.g.*, lack of TRMM coverage), light precipitation events, snowfall, and in the case of land surfaces, snow and ice on the ground which produce a signal similar to precipitation. Tian *et al.* (2009) found that daily satellite-based precipitation estimates in continental US constantly missed about 20–80% of light precipitation (<10 mm d^{-1}) and that this missed precipitation contributed up to 40% of the total errors.

Daily reanalysis precipitation from ERA-40 was considered more accurate than both NCEP in the continental US, Australia, and Western Europe and generally outperformed satellite estimates during winter (Ebert *et al.*, 2007; Ma *et al.*, 2009; Pan *et al.*, 2010). ERA-40 had some high positive biases in the tropics and a negative bias over the Amazon during the rainy season

(Betts *et al.*, 2006; Bosilovich *et al.* 2008). Precipitation from the recent reanalysis JRA-25 compared reasonably well in both the Northern Hemisphere continents and the tropics, but contained distinct variation according to the available satellite data, which improved estimates after 1990 (Bosilovich *et al.* 2008). The largest discrepancies in JRA-25 occurred in the Amazon with underestimation during the rainy season, and high frequency of rain day occurrence worldwide (Saito *et al.*, 2011). These were successfully corrected in terms of the occurrence, frequency and amount of monthly precipitation, using a stochastic model (Saito *et al.*, 2011). JRA-25 precipitation also outperformed ERA-40 and NCEP-DOE in East Asia (Sohn *et al.*, 2011).

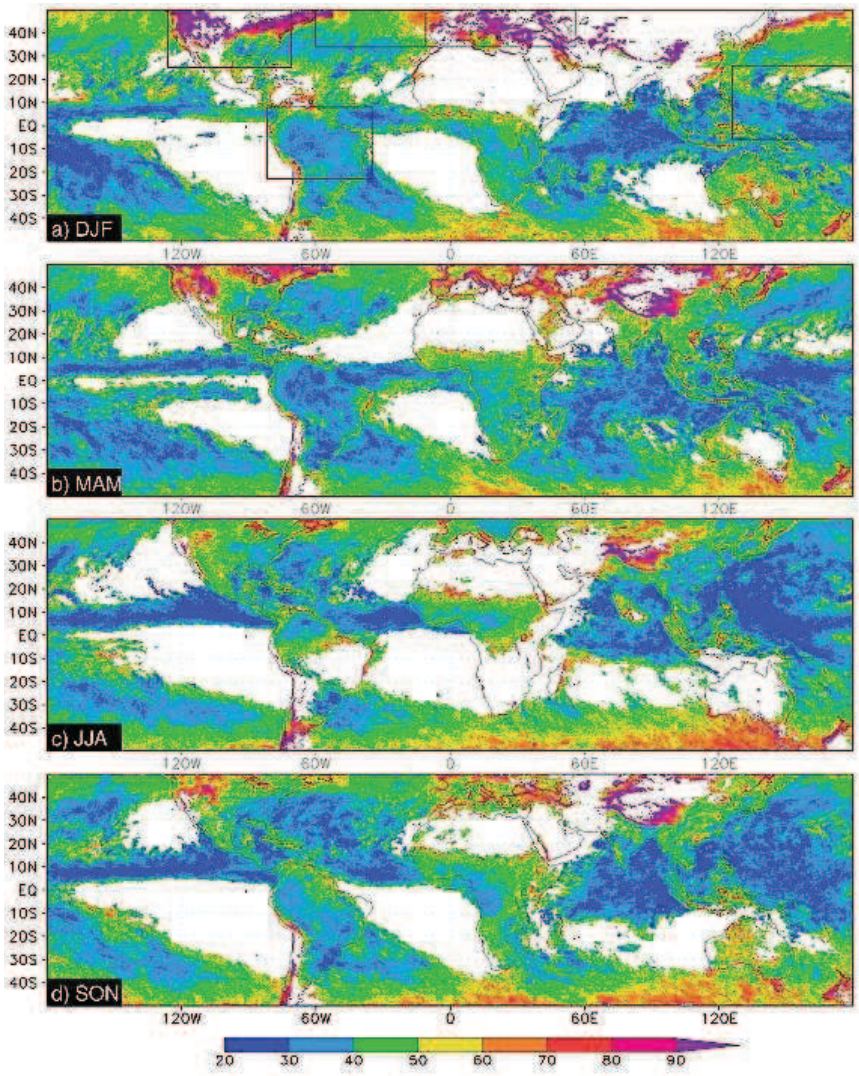

Figure 3.1 (a-d) Standard deviation from the ensemble mean, as percentage of the mean daily precipitation, averaged for the four seasons respectively. Blank areas are deemed unreliable (after Tian and Peters-Lidard, 2010).

From a reanalysis system perspective, ERA-Interim is considered far superior than its predecessor ERA-40 in several aspects; including a reduced spin-up of the precipitation in mid-latitudes, reduced drift and some improvement in the diurnal cycle of precipitation in the tropics (Betts *et al.*, 2009). Excessive precipitation in the tropics observed in ERA-40 has been largely reduced in ERA-Interim, although it still remains higher than observations (Uppala *et al.*, 2008). ERA-Interim improved the negative bias in the Amazon observed in ERA-40 (Betts *et al.*, 2009). It also performed as well as satellite-based precipitation such as TRMM 3B42RT and CMORPH and the gauge-adjusted high resolution reanalysis data NARR in continental US (Pan *et al.*, 2010).

Impacts of satellite derived and reanalyses precipitation on water balance at a basin and global scale have been researched in some detail (Fekete *et al.*, 2004; Fernandes *et al.*, 2010). Results from a global water balance simulation study showed that precipitation biases from six monthly precipitation datasets lead to errors in water balance of similar magnitude in humid areas (in terms of simulated runoff) and larger over arid and semi-arid areas (*e.g.,* Fekete *et al.*, 2004). Several studies have aimed to address reanalysis precipitation errors by correcting for biases (*e.g.,* Berg *et al.*, 2003; Betts *et al.*, 2005; Terink *et al.*, 2010) with resulting improved water balances. Bias-corrected precipitation from Princeton has been compared to NCEP-NCAR and ERA-40 in large-scale hydrological modelling to simulate soil moisture in the Yellow River Basin, showing better inter and intra-annual patterns (Li and Ma, 2010).

3.2.2 Evaluation of precipitation data

Based on the previous findings, three reanalyses (ERA-Interim, JRA-25 and NCEP-DOE) and Princeton precipitation data were chosen for further evaluation. ERA-Interim and JRA-25 showed improvements with respect to previous reanalyses and reduced notable biases, particularly in the tropics, whereas Princeton uses ancillary data to adjust monthly precipitation totals and daily statistics. Although the previous findings suggest that ERA-Interim and JRA-25 may be more accurate than both NCEP reanalyses, the more recent NCEP-DOE was also considered for completeness.

Two high resolution gauge-only daily precipitation analyses available in Australia and East Asia were used as reference to evaluate reanalyses and Princeton precipitation. The Specialised Information for Land Owners (SILO) spatial precipitation analysis (Jeffrey *et al*,. 2001) provides 0.05° grids of gauge-based spatially interpolated daily precipitation for Australia whereas 0.25° grids are provided in East Asia by the Asian Rainfall-Highly-Resolved Observational Data Integration Towards Evaluation of Water Resources (APHRODITE, Yatagai *et al.*, in press).

All data were averaged to 1° resolution as a compromise between the spatial resolutions of the different reanalyses. Only grid cells with more than 5% gauge coverage per 1° (or a density of 1 gauge per 500 km^2) are considered for use in evaluating daily and monthly time series for 1979–2007, the period in which all data overlapped.

A threshold of 1 mm d^{-1} is used to discriminate between rain and no rain in order to eliminate very light intensity 'drizzle' that would not significantly contribute to daily precipitation but may have an impact on daily precipitation intensity. To account for differences in precipitation regime, the geographical domain is divided into southern Australia (SAu), mostly dominated by synoptic system precipitation during winter; northern Australasia (NAu), mostly dominated by convective precipitation during summer; and south and east Asia (SEA), mostly dominated by monsoon precipitation (see Figure 3.2 for location of the grid cells and geographical sub-domains). Results are stratified by season to help in the interpretation of results.

The evaluation is performed at a monthly temporal scale for overall agreement in terms of correlation and root mean square differences (RMSD) and also at a daily temporal scale for agreement of precipitation intensity. Whilst it is important to evaluate monthly precipitation totals and temporal correlation, precipitation intensities are crucial for surface hydrologic processes, particularly infiltration and runoff. In general, low-intensity, large-area precipitation may tend to increase evaporation and infiltration compared to high-intensity, localised precipitation that may result in increased runoff production through infiltration excess (Sheffield *et al.*, 2006). Agreement metrics are investigated for spatial patterns by using maps of the best performing product and box-plots aggregated per geographical sub-domain. Precipitation intensity agreement is evaluated using plots of frequency of exceedance aggregated over three geographical sub domains.

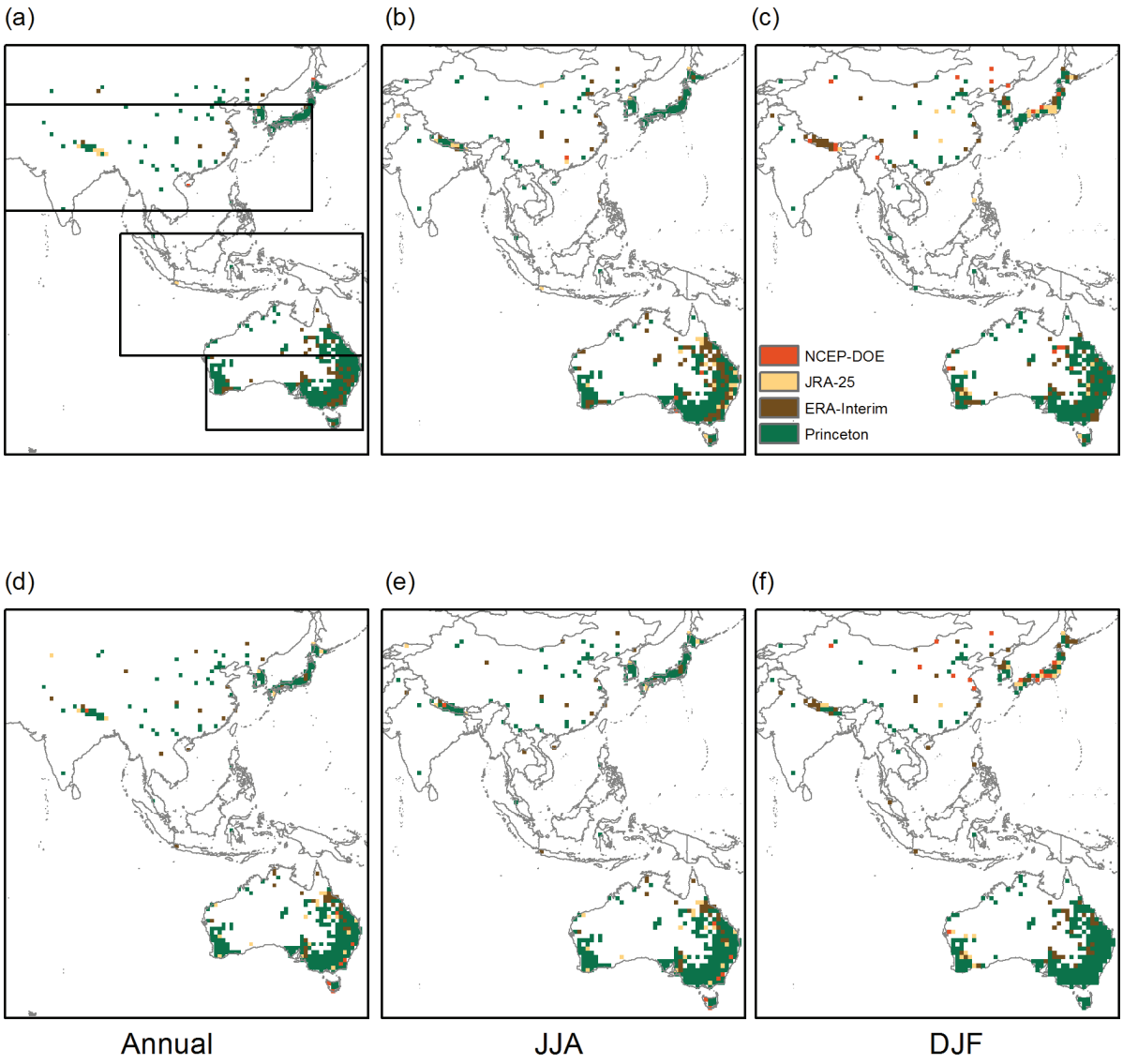

Figure 3.2 Best performing product for correlation and RMSD of monthly precipitation for 1979–2007 in each grid cell. Correlation for (a) all months, (b) for June, July and August (JJA) and (c) December, January and February (DJF), RMSD for (d) all months, (e) JJA and (c) DJF. Rectangles in (a) define the geographical extent for southern Australia (SAu), north Australasia (NAu) and south and east Asia (SEA).

Spatial results of both monthly correlation (Figure 3.2 a-c) and RMSD (Figure 3.2 d-f) show that Princeton outperforms the reanalyses in most locations for all months in the time-series, except for Nepal, parts of Japan and the Korean peninsula during December January and February (DJF) and parts of Australia during June July and August (JJA). Similar spatial patterns are observed for RMSD. Box-plots for all months show that correlation and RMSD for Princeton is

higher and has lower dispersion than the other reanalyses in all geographical sub-domains (Figure 3.3 a-b).

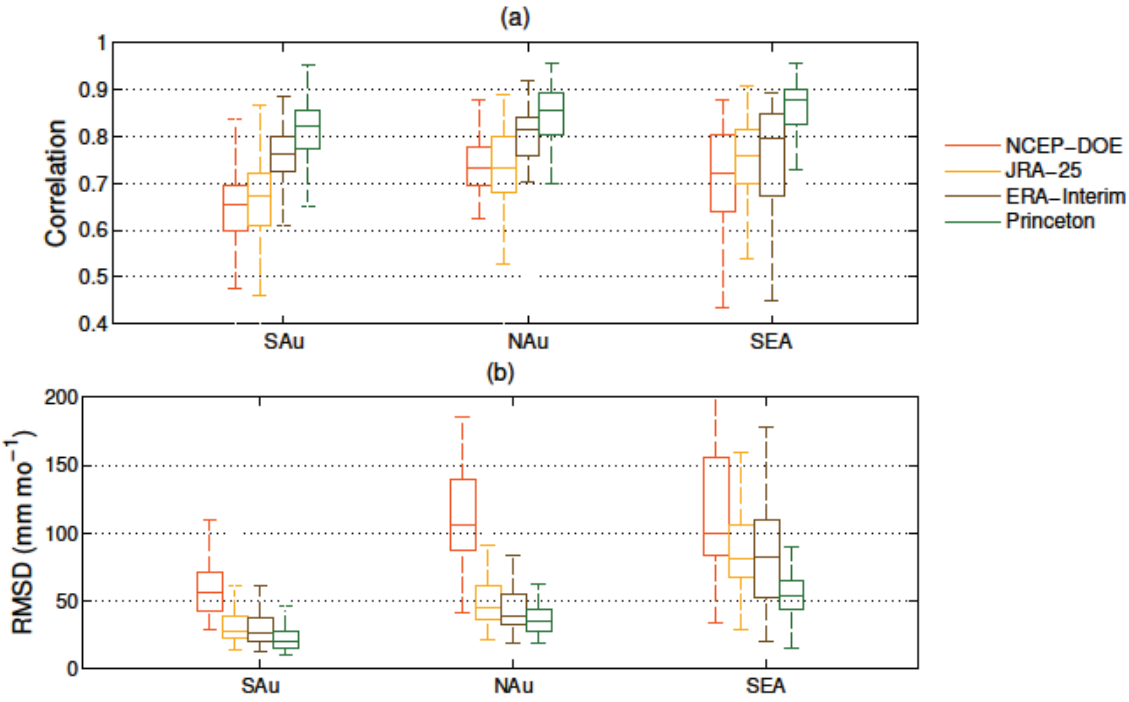

Figure 3.3 Box plots showing agreement statistics of monthly precipitation aggregated over three geographical sub domains (a) correlation (b) root mean square (RMSD). Tops and bottoms of each box are the 25th and 75th percentiles and whiskers are the 5th and 95th percentiles respectively.

Figure 3.4 shows the percentage frequency of exceedance for daily rainfall (>1 mm d^{-1}) aggregated over the three geographical sub domains, the three panels on the left use a log-scale Y axis to emphasise the mid and low intensity regimes whereas the three panels on the right limit the X axis scale to emphasise the very high intensity regimes. Princeton appears to underestimate low rainfall intensities (<2 mm d^{-1}) and overestimate high intensities (>50 mm d^{-1}) in SAu and NAu. Princeton agrees well with mid and low intensities and high intensities <50mm d^{-1} in SEA, but overestimates intensities >50 m d^{-1}. NCEP-DOE generally overestimates intensities across all regimes, and agrees well with the very high intensities in SEA. ERA-Interim and JRA-25 overestimate lower and underestimate higher rainfall intensities (>50 mm d^{-1}) respectively in all geographical domains.

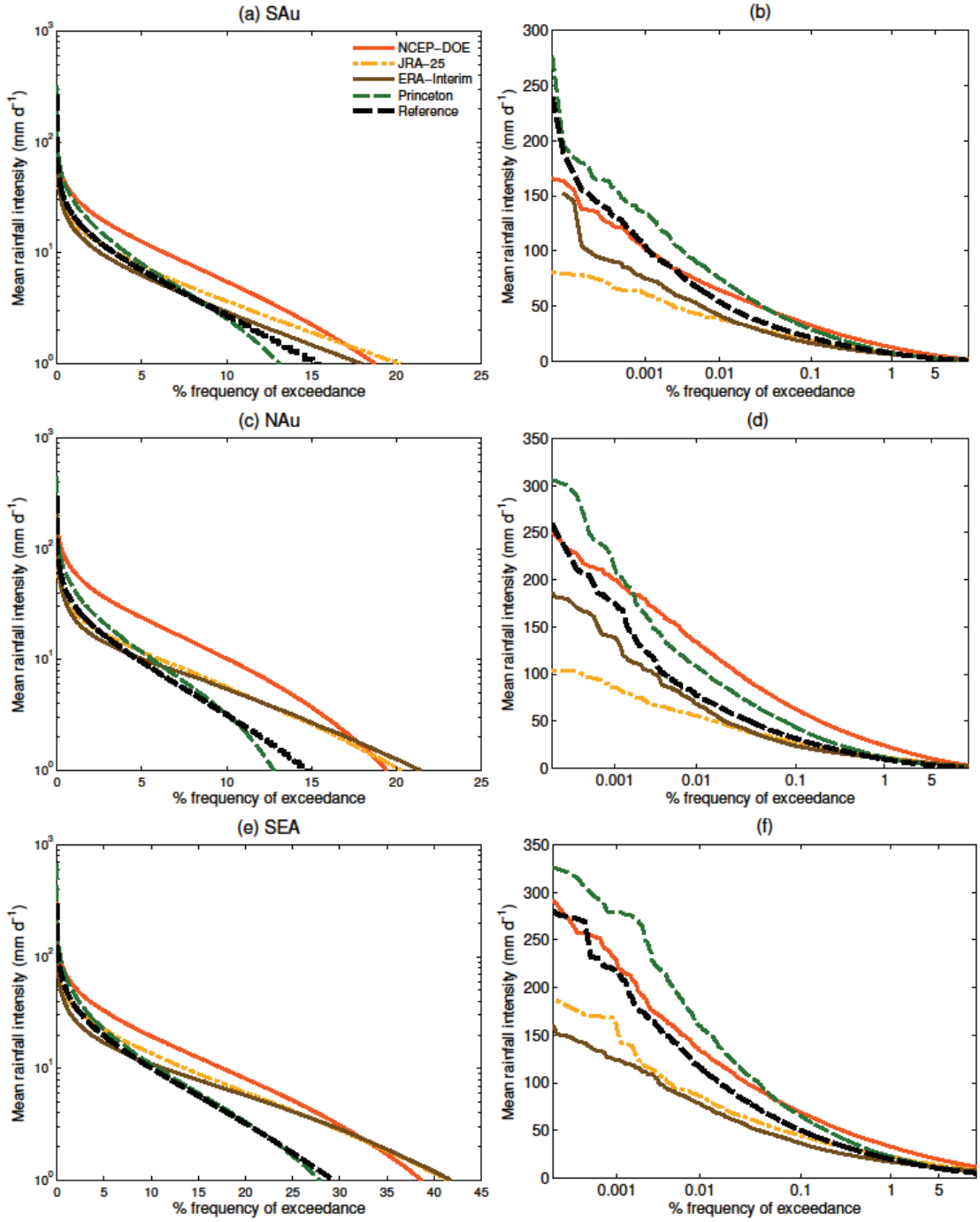

Figure 3.4 Percentage frequency of exceedance for daily rainfall (>1mm) aggregated over three geographical sub domains. (a-b) south Australia (SAu), (c-d) north Australasia (NAu), (e-f) south and east Asia (SEA).

The previous evaluation against precipitation analysis data based on interpolated rainfall gauges demonstrated that bias correction against monthly observations in Princeton precipitation resulted in better estimation in terms of correlation, RMSD and rainfall intensity

than the reanalyses. It is noted that Princeton precipitation uses interpolated gauge data to bias correct the NCEP-NCAR precipitation in which is based, thus it may not be fully independent of the analysis data used in the evaluation. The bias correction procedure brought daily low precipitation intensity events closer to observations than the reanalyses, although enhancing the very high precipitation intensity events (frequency of exceedance < 0.1%). For these very high precipitation intensities in all geographical domains no dataset appear superior to the others; with the exception of NCEP-DOE in SEA, all datasets showed higher or lower biases. Based on the previous findings, Princeton precipitation is considered for the hydrological modelling experiments conducted in Chapter 5 and 6.

3.2.3 Surface air temperature

Global gridded daily temperature data are available from satellite observations, temperature gauge observations and reanalysis. There are no global satellite datasets for air temperature as used in many land-surface models including W3RA-LUM, which is temperature measured at 2 m above the ground, or near surface air temperature (T_a). The derivation of T_a from satellite data is far from straightforward due to the large variation close to the surface layer. Nevertheless, data from several satellite sensors are used to produce T_a for different geographical regions with encouraging results (Prihodko *et al.*, 1997; Prince *et al.*, 1998; Lakshmi *et al.*, 2001; Vancutsem *et al.*, 2010).

To date, there is only one daily gridded dataset of T_a anomalies derived from daily gauge observations from GHCN and produced by the Hadley Centre for Climate Prediction and Research (HadGHCND; Caesar *et al.*, 2006). HadGHCND includes daily estimates of maximum and minimum temperatures for the period 1946–2000. The dataset was gridded onto a 2.5º×3.75º grid to facilitate comparison with the Hadley Centre GCM. The gauge density from which the surfaces were derived was relatively high in the Northern Hemisphere, but low in the Southern Hemisphere (Figure 3.4).

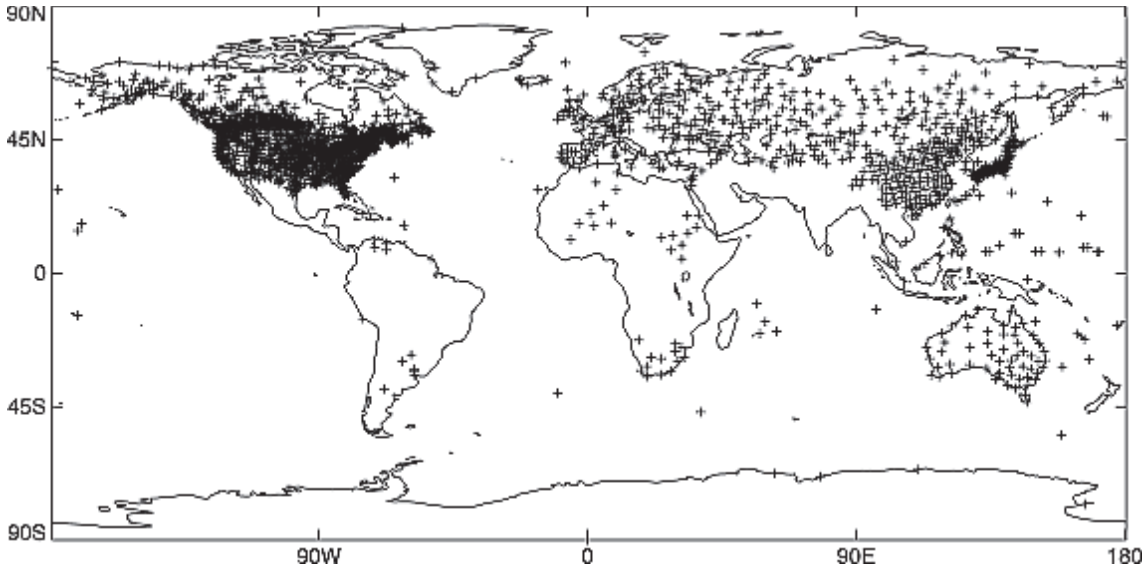

Figure 3.4 Stations selected for interpolation in HadGHCND (after Caesar *et al.*, 2006).

The only long-term time-series for global daily T_a observations are obtained from reanalysis. T_a values are derived in a similar fashion in ERA-40 and JRA-25 (Onogi *et al.*, 2007). T_a in ERA-40 was derived from 6-h background forecasts of skin temperature and temperature at the lowest model level (located at a height of 10 m) using Monin-Obukhov[1] similarity profiles consistent with the model's parameterisation of the surface layer (Monin and Obukhov, 1954). JRA-25 uses a similar approach, separating surface analysis via a two-dimensional optimum interpolation (Pitman and Perkins, 2009). The ERA reanalyses are not fully independent of the HadCRUT3 dataset, ERA-40 and ERA-Interim used assimilated data from around 8000 stations, substantially more than utilized in constructing HadCRUT3, which is based on data from around 2000 stations for recent years (Simmons *et al.*, 2010). For NCEP-NCAR, T_a values are derived from analysed atmospheric values that were constrained primarily by observations of upper air variables and surface pressure. Monthly, annual and climatological T_a anomalies from aggregated daily estimates had very similar values in most reanalysis datasets including both ERA reanalysis, JRA-25 and NCEP-NCAR; when compared to HadCRUT3 or other regional station derived datasets (Figure 3.5) (Simmons *et al.*, 2004; Onogi *et al.*, 2007; Ma *et*

[1] Monin and Obukov (1954) postulated the equations relationship describing the vertical variation of mean flow and turbulence characteristics in the surface layer as a function of height above the surface, the buoyancy flux, the kinematic stress and the temperature flux. Using these equations and the hypothesis that the fluxes in the surface layer are uniform with height, the momentum flux, sensible heat flux, and fluxes of water vapour and other gases can be determined (Huschke, 1959).

al., 2008). ERA-40 was closer to HadCRUT3 data than the NCEP-NCAR reanalysis, in all but the earliest years, reflecting the fact that surface observations were included in the ERA reanalysis (Simmons *et al.*, 2004). ERA-40 was also more accurate than both NCEP reanalyses when compared to a dense station network in China, although the three reanalyses had small negative biases related to altitude differences (Ma *et al.*, 2008).

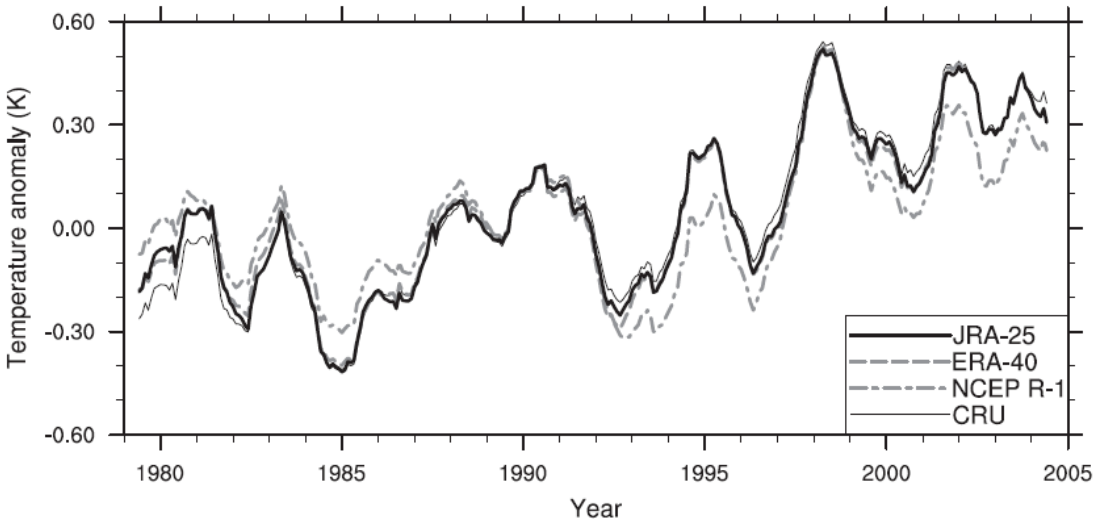

Figure 3.5 Time-series of 12-monthly running means for T_a anomalies averaged over global land areas from JRA-25, ERA-40, NCE-NCAR and CRU data (after Onogi *et al.*, 2007).

Princeton also includes T_a estimates, in which NCEP-NCAR T_a was adjusted to match an earlier version of HadCRUT3 monthly and daily averages in order to correct for known temperature biases (Sheffield *et al.*, 2006).

Although monthly estimates are useful for comparison purposes, they can hide stronger biases. At a finer temporal scale Pitman and Perkins (2009) compared daily maximum and minimum T_a probability density functions from ERA-40, JRA-25 and NCEP-DOE to regional observational data in the absence of global observational datasets. Regional data included the Mississippi, Amazon, Murray-Darling and Mackenzie Basins and the Baltic and African regions. Estimates of maximum T_a probability density functions were dissimilar in the three reanalysis with apparent large regional differences but overall no reanalysis appeared more accurate than the other two. All reanalysis failed to match observations of maximum T_a probability density functions in the

Amazon. For minimum T_a, all reanalysis showed reasonable agreement north of ~45º N, whereas ERA-40 appeared less accurate compared to the other reanalysis and to observations.

3.2.4 Surface radiation

There are several ground measurement networks for surface radiation measurements (*e.g.,* Ohmura *et al.*, 1998; Gilgen and Ohmura, 1999), including incoming shortwave radiation (SW_{down}) and longwave radiation (LW_{down}), but not yet a global gridded product (Liang *et al.*, 2010). Of these, the Global Energy Balance Archive (GEBA) (Gilgen and Omura, 1999) has ~2,000 stations worldwide with 250,000 monthly records of various surface energy balance estimates (mostly SW_{down}) since the 1950s (Lian *et al.*, 2010). Work is in progress to produce interpolated continental datasets of incoming shortwave radiation derived from GEBA (Chiacchio *et al.*, 2010).

Global gridded radiation datasets are more commonly derived from satellite sensors and reanalysis. The first global gridded dataset derived from satellite data was the World Climate Research Program-Surface Radiation Climatology Project (WCRP-SRB) (Whitlock *et al.*, 1995). It used broadband radiometer data from the Earth Radiation Budget (ERB) and the Earth Radiation Budget Experiment (ERBE). The latest version (R2) of the data has a spatial resolution of 1º×1º and 3-hourly to monthly temporal resolution for 1984–1993 and provides shortwave and longwave radiation flux data (Stackhouse *et al*, 2000). The R2 SW_{down} showed a monthly average RMSE ~25 Wm^{-2} globally. Region by region, bias differences in R2 showed a systematic decrease and are usually much less than 5% of the observed shortwave, except for biases in Central and South American sites which are ~8% (Stackhouse *et al*, 2000). Monthly biases and RMSE for LW_{down} and SW_{down} were comparable.

The International Satellite Cloud Climatology Project (ISCCP) produced a global radiative flux dataset (ISCCP-FD) on a 3-hourly, 280 km ×280 km resolution for 1983–2006. It used primarily observations from the Television and infrared Observations operational Vertical Sounder (TOVS) and other satellites to retrieve global cloud properties at diurnal, seasonal, and interannual scale. These properties were used to calculate radiative fluxes using the Goddard Institute for Space Studies (GISS) radiative transfer model (Zhang *et al.*, 2004). Comparison of

SW_{down} with the Baseline Surface Radiation Network (BSRN) data (Ohmura *et al.*, 1998) revealed a mean difference of 2 Wm^{-2} and an RMSE error of 19 Wm^{-2} (Zhang *et al.*, 2004). Evaluation was also performed against GEBA stations for 2656 SW_{down} and 62 LW_{down} samples. Mean RMSE difference is 8.8 Wm^{-2} for SW_{down} and -14.9 Wm^{-2} for LW_{down}.

More recently, the GEWEX Surface Radiation Budget (GEWEX-SRB) Project has completed a 24.5-year (July 1983 to December 2007) dataset of surface SW_{down} and LW_{down} radiative fluxes derived mainly from Geostationary Operational Environmental Satellite (GOES) data (Stackhouse *et al*, 2011). GEWEX SRB release 3.0 is produced on a 1º×1 º global grid and 3-hourly resolution using satellite-derived cloud parameters and ozone fields, reanalysis meteorology, and a few other ancillary datasets. Validation of monthly average downward SW_{down} and LW_{down} fluxes with BSRN sites mean bias for SW_{down} fluxes is ~-4 Wm^{-2} with an RMSE difference of 23 Wm^{-2}. An examination of individual sites showed that most of this underestimation arose at polar sites; especially those located on the Antarctic coast, but these were much improved over previous versions (Stackhouse *et al*, 2011). Corresponding bias for the LW_{down} fluxes were only about -0.1 Wm^{-2} with an RMSE difference of 11 Wm^{-2}.

Another satellite derived radiation dataset is the daily 1º×1 º global grid derived from the Cloud's and the Earth's Radiant Energy System Radiative Fluxes and Clouds instrument (CERES-FSW) onboard TRMM and subsequently on *Terra* and *Aqua* satellites (Wielicki *et al.*, 1996; Young *et al.*, 1998). Gupta *et al.* (2004) evaluated instantaneous-footprint of SW_{down} and LW_{down} fluxes derived from CERES/TRMM from January-August 1998 against high quality ground-based radiometric measurements from several sites of the BSRN dataset. For this instantaneous–footprint SW_{down} fluxes had significant biases in some sites, and random errors were much larger than acceptable values. The success criteria for these surface flux retrievals should be ±20 Wm^{-2} on an instantaneous-footprint basis to be truly useful in climate research studies (Suttles and Ohring, 1986). Further evaluation of the CERES *Terra* and *Aqua* products retrieved with two different models showed that SW_{down} values in clear-sky fluxes satisfied the established accuracy requirements for the global case, although with considerable scatter and biases. Significant underestimation happened in one of the models in polar and desert regions and overestimation in island situations. The second model improved estimates in polar and desert

regions but overestimation persisted over islands. LW_{down} provided very-good clear sky results in both models, whereas good cloudy-sky results occurred in only one model. Significant underestimation also occurred in areas with low vapour content.

Gui *et al.* (2010) compared 3-hourly or hourly (when available) SW_{down} measurements for 2000–2002 from ISCCP-FD, GEWEX-SRB and CERES-FSW SW_{down} against 36 stations from five different ground measurement networks. Results showed that SRB met accuracy criteria in most regions, followed by FD and FSW. Both SRB and FD underestimated SW_{down} in the Tibetan Plateau and Greenland and had large biases and overestimation in Southeast Asia. In addition, FD had slight overestimation in the Amazon. FSW had low correlations, had large biases and overestimates ground measurements in the Tibetan Plateau and Southeast Asia, as well as large overestimation in North America and the Amazon (Figure 3.6). Large biases in South America and Africa may be attributed to biomass burning in dry seasons, likely due to poor representation of aerosol loads in satellite algorithms (Pinker *et al.*, 2000).

Existing literature shows that SW_{down} and LW_{down} derived from satellite data have generally smaller biases than reanalysis because they are more constrained by observations (Hicke, 2005; Betts *et al.*, 2006). Climatologies of SW_{down} and LW_{down} in ERA-40 and NCEP-DOE reanalysis were compared globally against ISCCP-SRB data (Betts *et al.*, 2006). The biases in the climatology of the reanalyses are significant, more for NCEP-DOE than ERA40. Over the northern continents in summer, NCEP-DOE has too little cloud cover, so that SW_{down} is too large. The corresponding ERA40 biases are mixed and generally smaller.

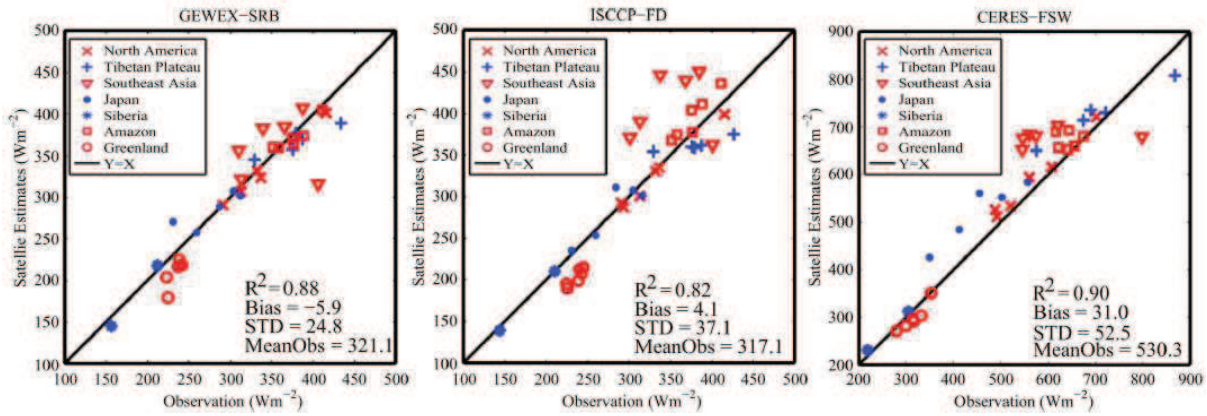

Figure 3.6 Comparison of three-year mean SW_{down} between satellite estimates and ground measurements at 36 sites in seven regions, averaged from three hourly values over 2000–2002 (after Gui *et al.*; 2010).

Using global GEBA data, Hicke (2005) compared mean average daily SW_{down} from NCEP-NCAR and ISCCP-FD over each month for the period 1984–2000. ISCCP-FD estimates had substantially reduced errors relative to ground-based observations compared to NCEP-NCAR. Mean global NCEP-NCAR computed growing season solar radiation exceeded that from ISCCP-FD by 16%, likely as a result of lower cloudiness within the NCEP reanalyses compared to satellite observations.

Xia *et al.* (2006) showed that NCEP-NCAR annual averages for 1984–2000 SW_{down} exceeded surface stations in China from 40 Wm^{-2} to more than 100 Wm^{-2}. Different trends were also observed in surface observations and NCEP data. The same study found that ISCCP-FD SW_{down} agreed well in northern China (north of 35ºN) with less than 10 Wm^{-2} bias. Bias increased south of 35ºN to 17–29 Wm^{-2}.

Monthly and annual SW_{down} ERA-40 and ERA-Interim data were evaluated against observations in three large river basins, the Amazon, Mississippi and Mackenzie (Betts *et al.*, 2009). In the Amazon, seasonal patterns in both ERA reanalysis matched ISCCP-FD data. Clear-sky SW_{down} in ERA-Interim has decreased by 16 Wm^{-2} with respect to ERA 40, closer to the ISCCP-FD observations than ERA-40. However both reanalysis seasonal estimates underestimated ISCCP-FD for all-sky conditions, with substantially lower estimates in ERA-Interim than ERA-40, probably because of the differences in the aerosol climatology between ERA-40 and ERA-Interim. This underestimation is observed as well in the Mississippi, although not as much as in

the Amazon. In summer the ERA-Interim clear-sky fluxes are very close to the ISCCP clear-sky flux. The surface all-sky SW_{down} estimate from the ISCCP dataset is less than the reanalyses for most of the year. Similar results to the Mississippi were obtained for the Mackenzie.

In the Princeton dataset SW_{down} adjusts the systematic biases in NCEP-NCAR data using the GEWEX-SRB climatology and a historic cloud dataset (Troy and Wood, 2009). The dataset has been extended through 2008 and updated using the GEWEX-SRB v3.0 product. For 1984–2006, monthly downward shortwave was scaled directly to SRB, without using the cloud dataset to adjust for trends. The dataset was evaluated by Troy and Wood (2009) together with ERA-40 reanalysis, NCEP-NCAR, and satellite ISCCP-SRB, against ground station data in Northern Eurasia sourced from the World Radiation Data Centre (WRDC), a subset of GEBA. Mean daily SW_{down} annual biases were within approximately ±3 Wm^{-2} for all the gridded datasets except the NCEP-NCAR reanalysis. Seasonal differences were as large as 20 Wm^{-2}. ERA-40 consistently estimated lower SW_{down}; this was attributed to differences in cloud cover between ERA-40 and ISCCP-SRB and PGF, which use ISCCP cloud cover. The ISCCP-SRB dataset had the smallest bias and RMSE compared to the station observations.

3.3 Summary and recommendations

A literature review was conducted to assess the quality and accuracy of climate forcing data required as inputs in W3RA-LUM, including: daily precipitation (P), incoming shortwave radiation (SW_{down}) and temperature in terms of near surface air temperature (T_a). A more in-depth evaluation was performed for precipitation data because of its importance in the hydrologic cycle and its variability in space and time. The recommendations presented here for variables other than precipitation are based on the literature review findings.

In terms of precipitation, review findings showed that satellite-based precipitation performed better during warm seasons and in the tropics, although overestimating total precipitation. Reanalysis data outperformed satellite-based precipitation during winter and in higher latitudes. Scaling precipitation using gauge data, as in TRMM V6, reduced observed bias in many areas

globally. To address inter-annual and inter-decadal precipitation variability, only reanalysis data with long-term time-series were considered for scenario modelling.

Long-term time-series of NCEP-DOE, ERA-Interim and JRA-25 reanalyses and Princeton precipitation were systematically evaluated against gauge-based precipitation analysis in Australia and south and east Asia. Princeton agreed better than the reanalysis for monthly correlation and root mean square error and daily precipitation intensity frequency and therefore was considered more suitable for the hydrological modelling experiments conducted here.

Global monthly, annual and climatological surface temperature anomalies from reanalysis had very similar values. At the daily scale, compared daily maximum and minimum temperature probability density functions from ERA-40, JRA-25 and NCEP-DOE were dissimilar with large regional differences, but overall no reanalysis showed more skill than the aforementioned two when compared against regional observational temperature data. Princeton used ground-based data to correct known temperature biases in NCEP-NCAR.

Surface shortwave radiation derived from satellite data generally has smaller biases than reanalysis because they are more constrained by observations. Of the three satellite-based incoming shortwave radiation estimates, GEWEX-SRB appeared superior to the other two. Globally, the biases in the climatology of the re-analyses are considerable. Princeton adjusted the systematic biases in NCEP-NCAR shortwave radiation data using the GEWEX-SRB climatology and a historic cloud data set.

Climate inputs other than precipitation, at least at daily scale, have less spatial variability. Given the bias correction used for these variables in Princeton using ancillary data that appeared of reasonable quality, these are also considered for the hydrological modelling experiments conducted here.

Chapter 4 Parameterising pan-tropical scale models of groundwater hydrology and baseflow generation

Contents

Journal article - **Peña-Arancibia, J. L.**, A. I. J. M. van Dijk, M. Mulligan, and L. A. Bruijnzeel (2010), The role of climatic and terrain attributes in estimating baseflow recession in tropical catchments, **Hydrology and Earth System Sciences**, 14(11), 2193-2205.

Hydrol. Earth Syst. Sci., 14, 2193–2205, 2010
www.hydrol-earth-syst-sci.net/14/2193/2010/
doi:10.5194/hess-14-2193-2010

Hydrology and Earth System Sciences

The role of climatic and terrain attributes in estimating baseflow recession in tropical catchments

J. L. Peña-Arancibia[1,2,3], **A. I. J. M. van Dijk**[3], **M. Mulligan**[1], **and L. A. Bruijnzeel**[2]

[1]CSIRO Land and Water, GPO 1666, Black Mountain ACT, Australia
[2]Environmental Monitoring and Modelling Research Group, Department of Geography, King's College London, Strand, London WC2R 2LS, UK
[3]Faculty of Earth and Life Sciences, VU University Amsterdam, De Boelelaan 1085-1087, 1081 HV, Amsterdam, The Netherlands

Received: 13 June 2010 – Published in Hydrol. Earth Syst. Sci. Discuss.: 1 July 2010
Revised: 15 October 2010 – Accepted: 27 October 2010 – Published: 4 November 2010

Abstract. The understanding of low flows in rivers is paramount more than ever as demand for water increases on a global scale. At the same time, limited streamflow data to investigate this phenomenon, particularly in the tropics, makes the provision of accurate estimations in ungauged areas an ongoing research need. This paper analysed the potential of climatic and terrain attributes of 167 tropical and sub-tropical unregulated catchments to predict baseflow recession rates. Daily streamflow data ($m^3\ s^{-1}$) from the Global River Discharge Center (GRDC) and a linear reservoir model were used to obtain baseflow recession coefficients (k_{bf}) for these catchments. Climatic attributes included annual and seasonal indicators of rainfall and potential evapotranspiration. Terrain attributes included indicators of catchment shape, morphology, land cover, soils and geology. Stepwise regression was used to identify the best predictors for baseflow recession coefficients. Mean annual rainfall (MAR) and aridity index (AI) were found to explain 49% of the spatial variation of k_{bf}. The rest of climatic indices and the terrain indices average catchment slope (SLO) and tree cover were also good predictors, but co-correlated with MAR. Catchment elongation (CE), a measure of catchment shape, was also found to be statistically significant, although weakly correlated. An analysis of clusters of catchments of smaller size, showed that in these areas, presumably with some similarity of soils and geology due to proximity, residuals of the regression could be explained by SLO and CE. The approach used provides a potential alternative for k_{bf} parameterisation in ungauged catchments.

Correspondence to:
J. L. Peña-Arancibia
(jorge.pena_arancibia@kcl.ac.uk)

1 Introduction

The gradual depletion of water stored in a catchment during dry weather constitutes the drainage or baseflow recession (Tallaksen, 1995). The understanding of quantities and temporal patterns of baseflow are central to water resources management, particularly in catchments with marked streamflow seasonality (Vogel and Kroll, 1992; Bruijnzeel, 2004; Brandes et al., 2005).

In recent years, several assessments of global water resources have been conducted using hydrological models and land surface models (LSMs); mainly in response to increase in water demand and potential impacts of climatic and land use change (Vörösmarty et al., 2000; Oki and Kanae, 2006). Linear conceptual storage-discharge models have been used to simulate baseflow recession in many of these models. In many cases, the linear reservoir application in global hydrological models used fixed parameter values, e.g. the routing HD model (Hagemann and Dümenil, 1998), macro-PDM (Arnell, 1999, 2003) and WGHM (Döll et al., 2003). Values obtained from drainage theory have been used in PCR-GLOBWB (Van Beek and Bierkens, 2008) whereas calibrated values were used in the global application of WASMOD-M (Widen-Nilsson et al., 2007) and in an application of the Catchment Land Surface Model (CLSM) to the Somme River Basin (Gascoin et al., 2009). The use of drainage theory is questionable at large scales and hindered by the uncertain quality of data needed to estimate various parameters. For example, the theoretical approach of Brutsaert and Nieber (1977), one of the few analytical ways to obtain aquifer parameters from hillslope to catchment scales, was used by Zecharias and Brutsaert (1988) to advance a proportionality relationship between the recession coefficient and aquifer characteristics:

Published by Copernicus Publications on behalf of the European Geosciences Union.

$$k_{\mathrm{bf}} \propto \frac{K D \alpha}{Y L} \quad (1)$$

where K is hydraulic conductivity, D is aquifer thickness , α is slope, Y is storativity and L a characteristic flow path length. Many of the aquifer parameters are not readily available in the tropics (and elsewhere); in particular data on aquifer hydraulic conductivity and thickness are sparse and scattered and cannot be considered representative of large areas. Also, the density of streamflow station data – used on a routine basis to calibrate conceptual models – is not spatially uniform, particularly in remote forested areas. Moreover, calibration approaches are not practical for global applications because of the large number of locations for which separate calibrations would be needed (Nijssen et al., 2001). Nijssen et al. (2001) modelled the seasonal discharge of 26 large basins in the world (including the Amazon, Congo and Mekong) using data from the Global River Discharge Center (GRDC) based in Koblenz-Germany. From these data, they estimated baseflow recession coefficients (k_{bf}) to parameterise the conceptual quasi-linear baseflow reservoir component of the VIC model (Liang et al., 1994). Baseflow recession coefficients were determined for 347 stations that had good quality data using a linear regression on the log-transformed discharges and then interpolated to the nearest areas.

On the other hand, several studies have correlated terrain attributes – including catchment morphology and soil type – to estimate k_{bf} in different climatic and physiographic regions or for geological formations across the world (e.g. Post and Jakeman, 1996; Yu et al., 2002; Brandes et al., 2005). Most studies have focused on catchments with areas $<200\,\mathrm{km}^2$ and located in common physiographic regions of similar climate. Van Dijk (2010) included climatic attributes in addition to terrain attributes to analyse the relationship with k_{bf} for 183 mainly temperate Australian catchments with a large geographical spread and encompassing different climates. The results showed that baseflow recession from a linear reservoir was best explained by climatic attributes, with catchment aridity index (AI, the ratio of rainfall to potential evapotranspiration) explaining 27% of the variation in derived recession coefficients. No correlations were found with catchment morphology or geology; however, spatial coherence of the residual unexplained variation showed that another 53% of the variation was spatially correlated over distances of 100–150 km. This was probably associated with terrain factors not captured by the available data and the large geographical spread of individual catchments (Van Dijk, 2010).

Motivated by the latter results, the objective of the present study is to identify the dominant climatic and terrain attributes that control the variance of k_{bf} in tropical and subtropical catchments. There is a dearth of studies that have investigated these relationships in the tropics and most of them were limited to small geographic regions (e.g. Yu et al., 2002; Mwakalila et al., 2002). In this study, catchment baseflow recession coefficients were determined from GRDC daily streamflow data ($\mathrm{m}^3\,\mathrm{s}^{-1}$) using a linear reservoir model. Although research indicates that low flows during dry periods can be adequately approximated by linear reservoirs (Zecharias and Brutsaert, 1988; Vogel and Kroll, 1992; Chapman, 1999; Fenicia et al., 2006, Van Dijk, 2010), this may not be the case in every catchment, in which some hydrological processes may lead to a non-linear behaviour. The choice of a linear model was made by taking into account that the aforementioned global hydrological models use a linear reservoir to estimate baseflow. Building equations based on the climatic and terrain indices that best explain k_{bf} in gauged catchments to estimate this parameter in ungauged catchments is a subsidiary objective of this study. These equations can be potentially used to parameterise k_{bf} in global hydrological models.

2 Theory

Several reviews on baseflows and recession analysis can be found in the existing literature (Tallaksen, 1995; Wittenberg, 1999; Smakhtin, 2001). In this paper, only a summary of the rationale and the main equations involved in baseflow recession analysis are presented. The theoretical framework of this study follows the one presented in Van Dijk (2010).

A linear reservoir model requires a recession coefficient (k_{bf}) to separate daily streamflow data into baseflow and quickflow and is expressed as:

$$Q_{\mathrm{bf}} = -k_{\mathrm{bf}} S \quad (2)$$

where Q_{bf} (in $\mathrm{mm\,day}^{-1}$) is the flow rate during the baseflow recession period, S (mm) is reservoir storage. The constant k_{bf} is expressed in day^{-1}.

Streamflow data representative of baseflow needs not to be affected by stormflow. It is assumed that stormflow affects streamflow for a period of T_{QF} days after the event peak flow (Van Dijk, 2010). Van Dijk (2010) found that for catchments in Australia, the number of data pairs decreased exponentially with increasing T_{QF} period. Vogel and Kroll (1992) considered baseflow recession to start when the 3-day streamflow moving average begins to decrease, and the recession to end when the 3-day moving average start to increase. A period of 5 days (T_{QF5}) was considered a useful compromise between representative low flow conditions and data availability. Increasing the window size to more days would have resulted in many catchments being dropped from the analysis. In addition, by using a large T_{QF}, results may be biased because only a small number of long baseflow recessions would be used to determine k_{bf} (Van Dijk, 2010). On the other hand, 5 days was assumed a sufficient time to avoid influence of storm flow on the hydrograph recession. This criterium was considered to construct Q and Q^* (Q of the previous day) data pairs representative of baseflow conditions for each gauging station. All days with zero streamflow

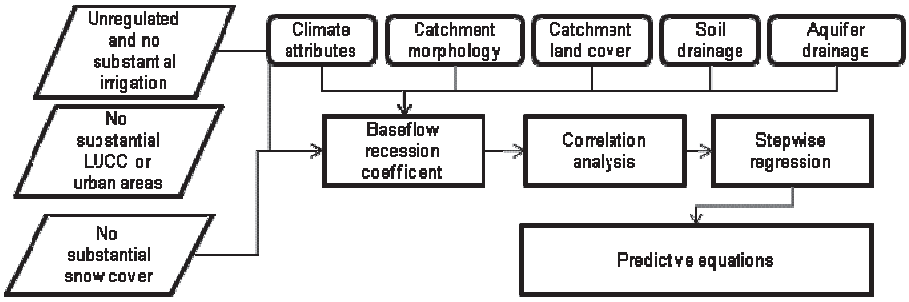

Fig. 1. Methodology flowchart. Unregulated catchments without substantial land use and land cover change (LUCC) and with snow, irrigation or urban extent <5% are selected for the analysis. Streamflow had to have at least 5 years of data , 30 runoff events and 30 Q–Q^* data pairs.

and or missing data were also excluded. By using a representative number of Q–Q^* data pairs it was possible to estimate the recession coefficient k_{bf}. The procedure to obtain k_{bf} and the influence of using different windows sizes on k_{bf} will be described further on.

The relationship between initial storage (S_0 in mm) and S after t days is defined by:

$$S = S_0 e^{-k_{\mathrm{bf}} t} \tag{3}$$

By combining Eqs. (2) and (3) for time step $t = 1$, provided that both Q and Q^* represent baseflow and $Q_0 = Q^*$, baseflow recession can be represented by the exponential decay function:

$$Q = Q e^{-k_{\mathrm{bf}} t} \tag{4}$$

3 Methodology

Time-series of catchment streamflow hydrographs for 1175 tropical and sub-tropical stations with >5 years of data were obtained from the Global Runoff Database (GRDB) from the GRDC. Additional data for 272 stations in tropical and subtropical Queensland (Australia) were obtained from the Department of Environment and Resource Management Queensland (DERM). Stations with more than 30 runoff events (defined as the number of times that daily average streamflow is exceeded) and more than 30 data pairs Q–Q^* characteristic of low flow conditions were selected for the analysis. Data in $\mathrm{m^3\,s^{-1}}$ were subsequently converted to $\mathrm{mm\,d^{-1}}$. Furthermore, stations were geo-referenced using the Hydrosheds river network data (Lehner et al., 2008). Catchments not affected by regulation were identified using a pan-tropical dam dataset (Saenz and Mulligan, 2010) representing the only available dataset (to the authors' knowledge) providing the actual catchment areas of reservoirs on a pan-tropical scale. In addition, GLOBCOVER land use data (Arino et al., 2008) and the MODIS 500-m map of global urban extent (Schneider et al., 2009) were used to check for catchments that may have snowmelt influence and irrigation areas, and large urban centres respectively. Only catchments with less than 5% snow cover, irrigation or uban extent were used in the analysis. Areas not affected by extensive deforestation during the period of analysis, which would likely have an impact on the recession coefficient trend, were determined from the map of areas of rapid land cover change provided by Lepers et al. (2005). Catchments complying with these criteria were considered unregulated for the purpose of this study.

Relevant catchment climatic, physiographic and geological attributes previously used in baseflow recession analysis were derived using terrain analysis and available climatic, geological or soils data. A preliminary analysis of frequency distributions for k_{bf} and various climatic indices and catchment attributes was conducted to assess applicable correlations methods. Furthermore, a non-parametric correlation matrix was used to determine the degree of correlation between recession constants and catchment attributes. Finally, predictive relationships were obtained using stepwise regression. Figure 1 presents a summary flowchart of the procedure described above.

3.1 Climatic and terrain attributes of pan-tropical catchments

Several climatic and terrain attributes with a demonstrated correlation with baseflow parameters (e.g. Post and Jakeman, 1996; Brandes et al., 2005; Van Dijk, 2010) were derived for each catchment. A summary of parameters, their original resolution and source are summarised in Table 1. Climatic attributes included annual and seasonal descriptors of rainfall and potential evapotranspiration and were defined as follows:

- Mean annual rainfall (MAR) expressed in $\mathrm{mm\,y^{-1}}$ obtained from the WORLDCLIM dataset (Hijmans et al., 2005).
- Potential evapotranspiration (PET) in $\mathrm{mm\,y^{-1}}$ estimated using the Hargreaves et al. (1985) model formulation and parameterised as described in Trabucco et al. (2008).

Table 1. Summary of climatic and terrain attributes used in the present study.

Parameter	Resolution		Source
	Temporal	Spatial	
MAR ($mm\,y^{-1}$)	Monthly average climatology 1950–2000	1 × 1 km grid	WORLDCLIM (Hijmans et al., 2005)
PET ($mm\,y^{-1}$)	Monthly average climatology 1950–2000	1 × 1 km grid	Trabucco et al. (2008; available at: http://www.csi.cgiar.org)
AI	NA	1 × 1 km grid	Calculated from MAE and PET
TMI	NA	1 × 1 km grid	Calculated from monthly rainfall and monthly PET
SI	NA	1 × 1 km grid	Calculated from monthly rainfall
CE ($m^2\,m^{-1}$)	NA	NA	Hydrosheds 1 km DEM (Lehner et al., 2010)
SLO (%)	NA	90 × 90 m grid	Hydrosheds 90 m DEM (Lehner et al., 2010)
DD ($km\,km^{-2}$)	NA	90 × 90 m grid	Hydrosheds 90 m river network available at http://hydrosheds.cr.usgs.gov/hydro.php
TC (%)	NA	1 × 1 km grid	AVHRR Tree Cover Continuous fields (DeFries et al., 2000; available at: http://glcf.umd.edu/data/treecover/data.shtml)
SDI	NA	9 × 9 km grid	ISRIC-WISE derived soil properties (Batjes, 2006)
DPI	NA	NA	WHYMAP (2010)

– Aridity index (AI = MAR/PET)

– Thornthwaite Moisture Index (TMI, Thornthwaite, 1948). An overall measure of precipitation effectiveness on a monthly basis. It is estimated using monthly rainfall and PET totals from the above mentioned datasets as follows:

$$\mathrm{TMI} = \frac{\sum_{m=1}^{12} (100 s_m - 60 d_m)}{\mathrm{PET}} \quad (5)$$

where s is the monthly water surplus and d is the monthly water deficit ($mm\,mo^{-1}$).

– Seasonality index. The seasonality index (SI, Walsh and Lawler, 1981) is defined as the sum of the absolute deviation of mean monthly rainfall ($\bar{X}_m$) from the overall monthly mean divided by the mean annual rainfall (MAR):

$$\mathrm{SI} = \frac{1}{\mathrm{MAR}} \sum_{m=1}^{12} \left| \overline{X_m} - \frac{\mathrm{MAR}}{12} \right| \quad (6)$$

The SI varies from zero (when all months have the same rainfall) to 1.83 (when all rainfall occurs in a single month): values <0.19 indicate a very equable rainfall regime, whereas values between 0.20 and 0.99 indicate a seasonal rainfall regime and values >1 a short wet season.

Terrain attributes included indicators of catchment shape, morphology, land cover, soils and geology.

– Catchment shape, defined by catchment elongation (CE) in km^2 surface area per km of catchment length, or by the ratio of a circle with the same area as the catchment to the catchment's length (Post and Jakeman, 1996).

– Mean catchment rainfall weighted slope (SLO) (%). To account for spatial variability in rainfall, each catchment slope pixel is scaled using normalised mean catchment rainfall data. By scaling SLO in this way, areas that may produce more runoff due to spatial differences in rainfall have more weight in the final mean catchment slope computation.

– Catchment drainage density (DD) in km per km^2, defined by the total length of streams per square kilometre of catchment area.

– Catchment tree cover percentage (TC), from AVHRR Tree Cover Continuous fields (DeFries et al., 2000).

– Soil unit weighted infiltrability class (SDI), obtained from the ISRIC-WISE Soil Derived Properties database (Batjes, 2006). The final values were obtained using an area weighted average of dominant soils comprising each soil unit.

Categorical information on drainage potential index (DPI) according to geology and climate was obtained from WHYMAP (2010). WHYMAP included eleven classes: Class I to V correspond to the presence of a major groundwater basin with very high, high, medium, low and very low drainage rates respectively. Classes VI to IX correspond to complex hydrogeological structure and very high, high, medium and low drainage rates respectively. Class X and XI correspond to local and shallow aquifers with high and low drainage rates respectively.

3.2 Estimation of recession coefficient k_{bf}

Methods to obtain k_{bf} from baseflow data pairs include linear regression through the origin, linear regression on log-transformed baseflow data pairs and optimisation techniques (e.g. Wittenberg, 1999; Tularam and Ilahee, 2008). For this study, recession coefficients were estimated by fitting Eq. (4) to the baseflow data pairs using the mean relative error (ε_{MRE}) as the objective function and a multi-start downhill simplex search method (Van Dijk, 2010):

$$\varepsilon_{MRE} = \frac{1}{n}\sum\left|\frac{Q}{Q_{est}} - 1\right| \quad (7)$$

where Q_{est} is Q predicted from Eq. (4). By using the relative agreement between estimated and observed streamflows, this formulation does not use absolute values which could bias the results and gives equal weighting to all data pairs. However weighting influence by very low or very large values when using different objective functions cannot be entirely avoided. In addition, by estimating a mean baseflow recession constant from many observed recession segments, the problem of time variability (per event or seasonal) in baseflow recession is partially overcome (Tallaksen, 1995).

3.3 Statistical analysis

A correlation matrix was used to determine the correlation between various catchment attributes and the recession coefficients. The attributes with the best individual explanatory values were combined into a stepwise multiple regression equation. Exponential, logarithmic and power functions were computed to link potential predictors to k_{bf}, and the best regression was selected to subsequently predict k_{bf}. Attributes that co-correlated were not considered in the subsequent stepwise regression. After selecting the best equation, the same types of regression were computed for both the absolute and relative residual variance and the remaining potential predictors, until no further variation was explained by adding these.

4 Results

4.1 Assembling a pan-tropical dataset for baseflow modelling

Catchment boundaries were obtained from the Hydrosheds 1 km river network (Lehner et al., 2010). Only catchments with a relative error of less than 10% between the GRDC reported surface areas and the river network derived areas were considered in the analysis. After controlling for regulation, snow and lake influence, urban and irrigation areas, and land use change; the analysis resulted in a database comprising 167 catchments worldwide (Fig. 2a). Of the 167 catchments, 50% had a catchment area <1000 km^2 and 90% <6000 km^2. The median was 850 km^2.

The catchment assemblage encompassed many tropical climates (Fig. 2b). A large number of stream gauging stations were located in Australia. No stations complying with the aforementioned requirements were found in the Amazon or Congo Basins. Most stations in these basins had monthly records or short daily records, which excluded them from the present analysis of daily flows.

4.2 Estimation of recession coefficient k_{bf}

The overall mean k_{bf} for the 167 analysed catchments was of 0.08 ± 0.053 (std. dev.) day^{-1}. The distribution was positively skewed. Higher values were found in arid catchments and lower values in wetter catchments. In addition, lower values were generally found in catchment closer to the coastline. The mean relative error (ε_{MRE}) was 0.97 ± 0.38 m^3 s^{-1}. The distribution of ε_{MRE} for different mean daily baseflow ranges is shown in Fig. 3.

In Australia, the lowest values of k_{bf} (0.02–0.08 day^{-1}) were generally found in catchments that lie closer to the east and north coastlines. Catchments located in the more arid interior had values of 0.11–0.18 day^{-1}. In Southeast Asia, the fully humid Malayan Peninsula had values of 0.02–0.06 day^{-1}. Continental Southeast Asia showed values of 0.04–0.07 day^{-1}. The highest values in Africa were found in Namibia (0.20 day^{-1}) and in the catchments located in the northernmost of the Sahel (0.17 day^{-1}). Catchments located closer to the coastline in West Africa and Central Africa (Congo and Zambia) generally showed values of $\sim$0.035 day^{-1}, as did temperate catchments in South Africa. Catchments located in the Andes had values of 0.03–0.08 day^{-1}. Catchments in Panama, Costa Rica Nicaragua

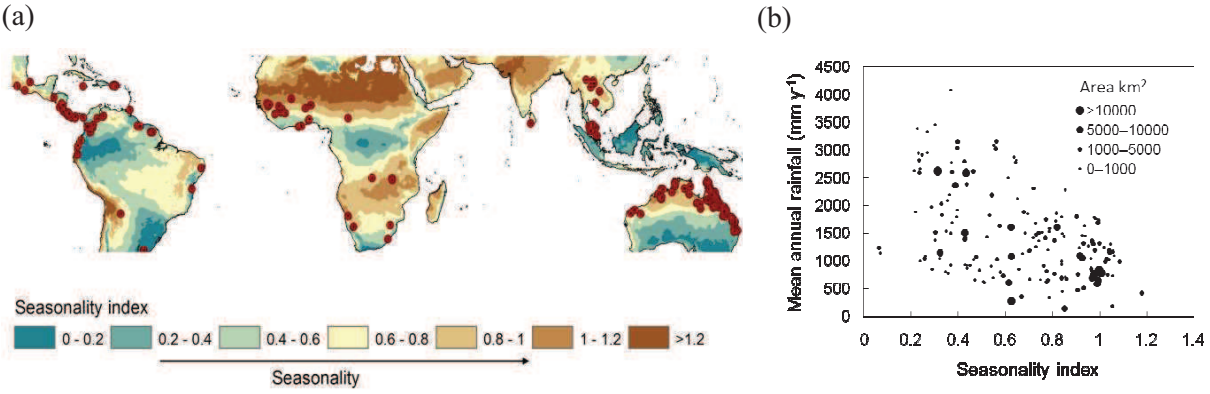

Fig. 2. Distribution of catchments in the dataset: **(a)** Geographic distribution **(b)** In terms of climate using the seasonality index (SI; Walsh and Lowler, 1981). Symbol sizes in **(b)** indicate catchment areas in km^2.

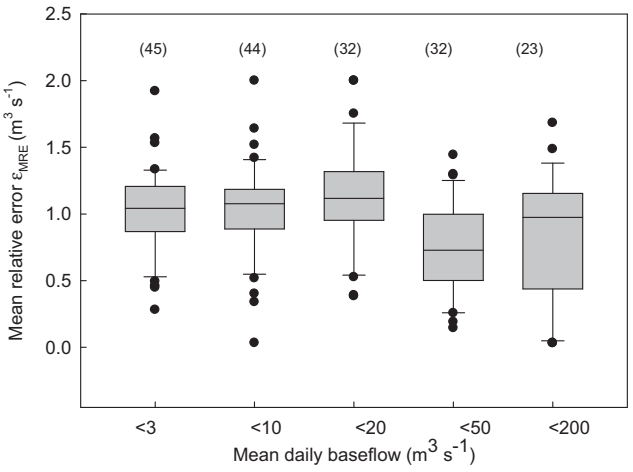

Fig. 3. Distribution of the mean relative error for different mean daily baseflow ranges. The number in brackets is the sample size per range.

and Honduras had mostly values around 0.03–0.09 day^{-1} whereas catchments in Puerto Rico had values of 0.05 day^{-1}. In tropical Mexico, catchments close to the coastline had values of 0.03–0.10 days.

The stability of recession coefficients was assessed by varying the window size T_{QF} from 0–20 days. Results for six catchments with different climate regimes and geographical areas are illustrated in Fig. 4a–f. Increasing T_{QF} results in a reduction of k_{bf} , with the fastest decrease occurring in the first days 0–3 days. The rate of reduction diminishes after 5–10 days in most cases. Complex patterns occur when window size increased beyond 10 days. Similar variations of k_{bf} and Q–Q^* pairs were also observed for temperate Australian catchments in the study of Van Dijk (2010).

4.3 Statistical analyses

Visual inspection of scatter plots (Fig. 5) already suggested catchment recession coefficients to be correlated to various climatic attributes. Of the respective terrain attributes, only slope and tree cover appeared to show some correlation (Fig. 5e and f). The rest of the catchment attributes did not reveal a clear pattern (not shown). In addition, different aquifer drainage potential classes did not seem to have any influence on k_{bf} either (Fig. 5).

Recession coefficient data showed a positively skewed distribution and thus a non-parametric Spearman rho test was used in the correlation analysis. The correlation matrix is presented in Table 2. Significant strong correlations were found between k_{bf} and most climatic attributes; slope and tree cover. As expected, cross-correlations occurred between all climatic attributes. In addition, cross-correlations between slope, tree cover and climatic attributes were also observed. The best correlations for k_{bf} were with MAR and the Thornthwaite Moisture Index TMI (non-parametric $r^* = -0.65$). AI also showed good correlation with k_{bf} ($r^* = -0.64$). Regression equations were computed for k_{bf} vs. MAR and AI, results are shown in Fig. 6 (no power or exponential regression were possible for negative values of TMI).

A two-parameter exponential relationship of MAR and AI explained 49% of the variance in k_{bf}. Only marginal improvement was achieved with the stepwise regression when including the weakly correlated catchment elongation (CE, $r^* = 0.138$). The other catchment terrain attributes with explanatory value were cross-correlated to climatic attributes and therefore not used in the multivariate analysis. The equations and summary statistics of all regressions are shown in Table 3.

A subset of catchments that were smaller and geographically close to each other, contiguous in some cases, were analysed to see whether the correlation of catchment terrain properties with k_{bf} was confounded by the large geographical

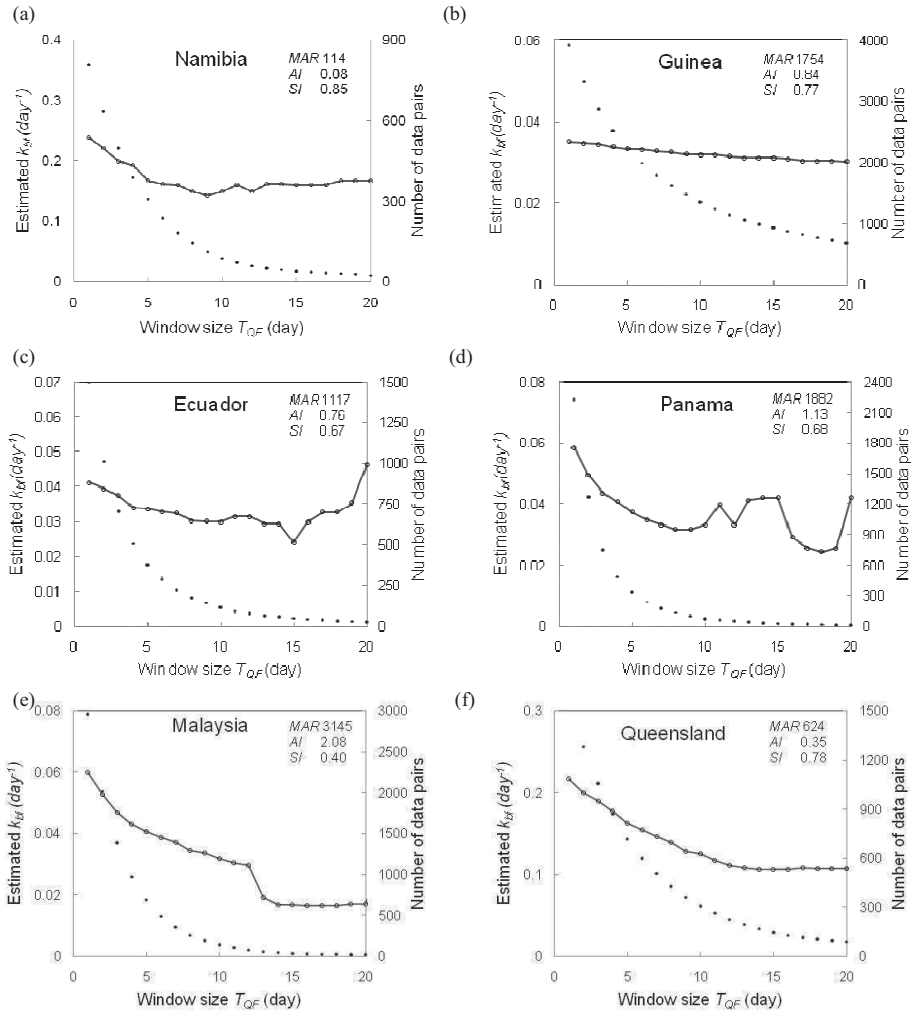

Fig. 4. Variation of estimated recession coefficient k_{bf} (closed lines) and number of Q–Q^* data pairs (dots) with an increase in T_{QF} from 0 to 20 days. Values for mean annual rainfall (MAR in mm y^{-1}), aridity index (AI) and seasonality index (SI) is show for each catchment gauge data.

area and the different climates covered by the overall dataset (cf. Fig. 2a). Relatively smaller groups of catchments ($<300\,\mathrm{km}^2$) were selected in north, central and south Queensland and in Puerto Rico. Only clusters of larger catchments (500–$3000\,\mathrm{km}^2$) were left for analysis and so they were selected in the absence of data more suited to the purpose, in any case only two catchments were larger than 1500 km^2. These were located in Panama, Senegal and Malaysia. Relative residuals of the original regression of k_{bf} and MAR were analysed using scatter plots and non-parametric correlation. Only slope and catchment elongation showed significant correlations ($r^* = 350$ and -250 respectively). Although correlations were weak, scatter plots of such properties versus relative residuals showed some degree of spatial organisation by location (Fig. 7).

5 Discussion

5.1 Pan tropical catchment dataset

In the present study, great care was taken in producing a good quality daily streamflow dataset of unregulated flows (using the georeferenced dam dataset of Saenz and Mulligan) for tropical landscapes. A good range of climatic landscapes and rainfall regimes has been covered, but data from hydrologically important areas such as the Amazon and Congo basins are not yet represented in the analysis. Needless to say, their inclusion is highly desirable.

5.2 Characteristics of recession coefficients

In general, higher (faster) recession coefficients were observed for drier catchments. In the most arid catchments (e.g. Namibia, arid parts of Australia) streamflow is typically

Table 2. Spearman rank correlation matrix of recession coefficients and catchment attributes. k_{bf} correlations with climatic and catchment attributes are shown in bold.

	k_{bf}	MAR	PET	AI	TMI	SI	CE	SLO	DD	TC	SD	DPI
k_{bf}												
MAR	**−0.650****											
PET	**0.291****	−0.453**										
AI	**−0.639****	0.979**	−0.608**									
TMI	**−0.649****	0.987**	−0.564**	0.996**								
SI	**0.170***	−0.436**	0.649**	−0.534**	−0.469**							
CE	**0.138***	0.119	−0.068	0.105	0.108	0.008						
SLO	**−0.380****	0.528**	−0.693**	0.613**	0.587**	−0.499**	0.100					
DD	**0.016**	0.064	−0.210**	0.088	0.086	−0.005	0.027	0.171*				
TC	**−0.425****	0.578**	−0.577**	0.636**	0.618**	−0.436**	0.161*	0.592**	0.353**			
SD	**0.007**	0.003	0.294**	−0.056	−0.019	0.390**	0.064	−0.304**	0.191**	−0.02		
DPI	**0.003**	0.025	−0.005	0.012	−0.084	0.019	0.048	−0.017	0.287**	−0.003	−0.01	

* Correlation is significant at the 0.05 level.
** Correlation is significant at the 0.01 level.

Table 3. Summary of results, including r^2 and standard error of estimate (SEE) for the exponential, logarithmic and power regressions linking k_{bf} with MAR and AI ($n = 167$).

Equation	r^2	SEE
$k_{bf} = 0.0356 + 0.2273 \times e^{-0.0014\text{MAR}}$	0.4850	0.0382
$k_{bf} = 0.5247 - 0.0619 \times \ln(\text{MAR})$	0.4447	0.0396
$k_{bf} = 10.4370 \times \text{MAR}^{-0.7050}$	0.3850	0.0510
$k_{bf} = 0.0394 + 0.2087 \times e^{-2.2282\text{AI}}$	0.4865	0.0382
$k_{bf} = 0.0692 - 0.0552 \times \ln(\text{AI})$	0.4414	0.0397
$k_{bf} = 0.0580 \times \text{AI}^{-0.6210}$	0.3720	0.0515

ephemeral and consequently mainly event driven. The presence of fast-draining perched aquifers may also explain higher k_{bf}. By contrast, lower recession coefficients (slower drainage) were found for most of the humid tropics. Although there were no good quality data to account for the effects of soil depth and aquifer porosity, deep soils and permeable regoliths are widely present in tropical landscapes; and are likely to represent an important source of baseflow (Chappell et al., 2007). A recent three-year study in a small catchment underlain by very deep soils in the central Amazon Basin by Tomasella et al. (2008) showed an important contribution to the groundwater system by the extended unsaturated zone. Both unsaturated and groundwater flow showed a delayed response to rainfall and most of the seasonal variability in streamflow tended to be dampened by either one or the other.

5.3 Predictors of recession coefficients

Climatic attributes proved to be the best predictors of k_{bf}, with MAR and AI together explaining 49% of the variance. The exponential and logarithmic regression equations for AI and MAR had very similar goodness-of-fit statistics but due to the nature of the fitted equations estimation errors appeared higher for drier catchments in all equations. For wetter catchments, both logarithmic and power relations approached the asymptotic value of 0.05 too gradually. The robustness of the equations for MAR and AI intervals was checked using box and whisker plots of relative residuals for all equations. The exponential equations for MAR and AI were slightly more robust than the other equations for all intervals, and MAR was only marginally better than AI (Fig. 8).

Of the terrain attributes, rainfall weighted slope (SLO), tree cover percentage (TC) and catchment elongation (CE) showed significant although weaker correlations with k_{bf}. The first two attributes were not included in stepwise regressions due to the cross-correlation with MAR. A relationship between tree cover, catchment slope and MAR is intuitively possible, for instance in the case of steep mountainous terrain where difficulty of access increases the chances of forest conservation and topography and altitude lead to enhanced orographic rainfall. The negative weaker correlation between catchment elongation (CE) and k_{bf} was also intutively possible, impliying the rounded catchments will drain faster than wider catchments of similar area (e.g. Post and Jakeman, 1996). Rainfall weighted slope also showed a negative correlation, opposite to the one expected from theory as in Zecharias and Brutsaert (1988, Eq. 1) and to results from similar correlation studies (Mwakalila et al., 2002; Brandes et al., 2005). The negative correlation between recession coefficients and rainfall weighted slope is counterintuitive; what common sense tells is that rugged catchments drain quicker than flatter ones (e.g. Post and Jakeman, 1996). However this effect may have less relevance when catchment areas are larger and other effects such as climate or complex topography/geology override the effects of slope, this was

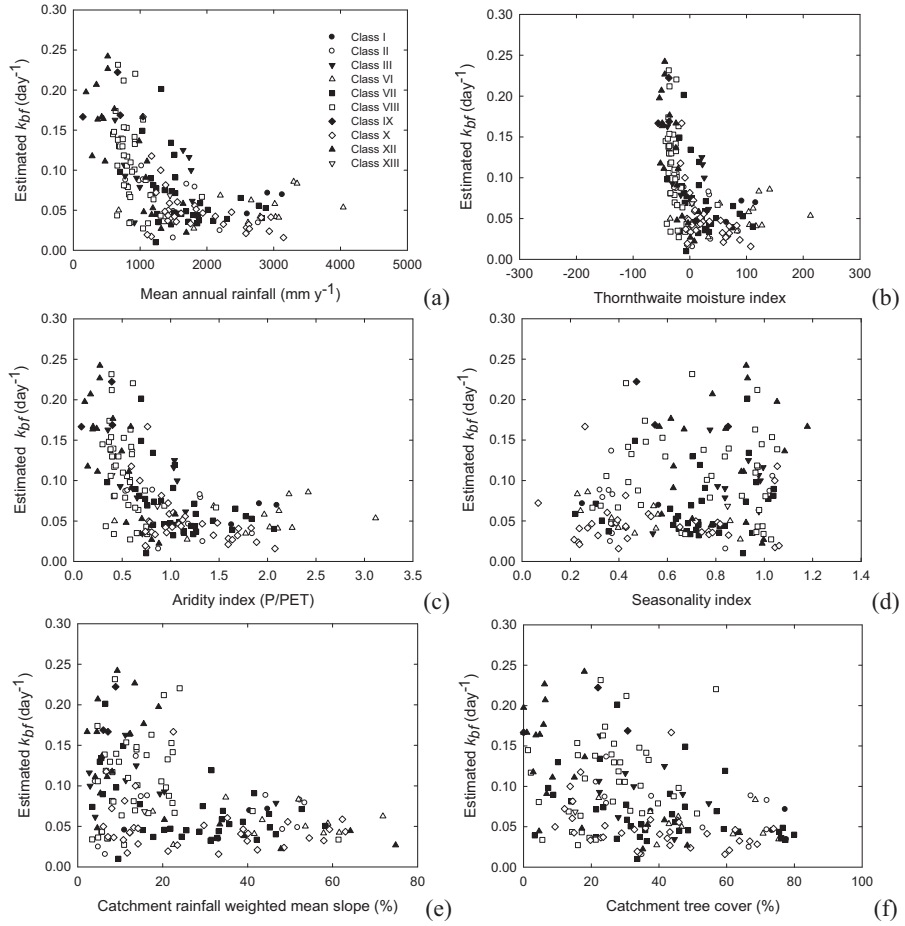

Fig. 5. Scatter plots of recession coefficient k_{bf} versus **(a)** MAR, **(b)** TMI, **(c)** AI, **(d)** SI, **(e)** SLO and **(f)** TC. Symbols denote a proxy for aquifer drainage potential from WHYMAP (2010).

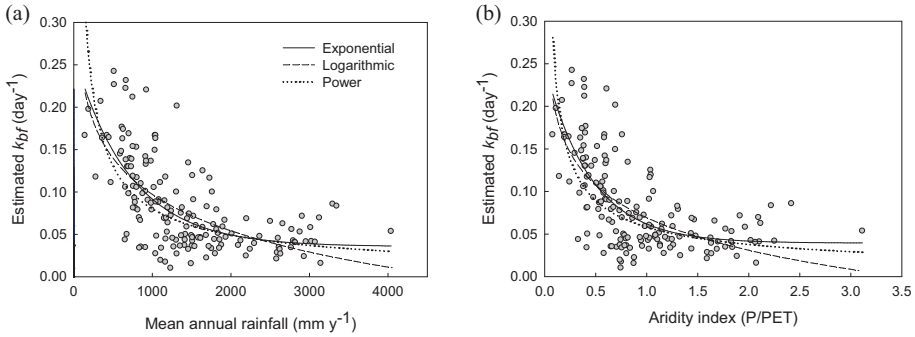

Fig. 6. Regression equations for **(a)** MAR versus k_{bf} and **(b)** AI versus k_{bf}.

also observed in Post and Jakeman (1996) but their results were not conclusive. A similar negative correlation was reported in Van Dijk (2010). The geology proxy used in the analysis, aquifer drainage potential, did not reveal any pattern with k_{bf} (Fig. 3) and its low correlation value indicated no influence on recession coefficients (Table 2). One would expect that geology and associated derivatives play a central role in groundwater recession rates. This may well be ascribed to the lack of detailed geology at a global scale and the variety and geographic extent and distribution of catchments use in the study. Besides more detailed data, more robust methodologies could be used to include these attributes and the other catchment terrain attributes as covariates in regression equations. For example Detenbeck et al. (2005) used

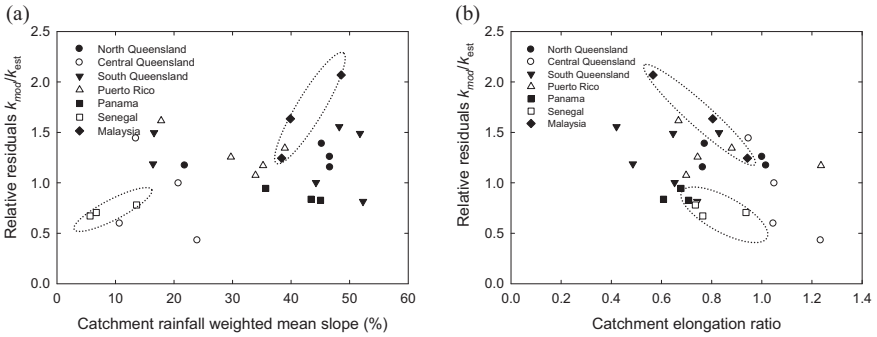

Fig. 7. Scatter plot of relative residuals (ratio of modelled to hydrograph-based estimated k_{bf}) versus **(a)** rainfall weighted slope of catchment (SLO) and **(b)** catchment elongation (CE). Elongated ellipses around Malaysian and Senegal data points are shown to illustrate possible correlations of residuals at smaller scales for geographically close catchments.

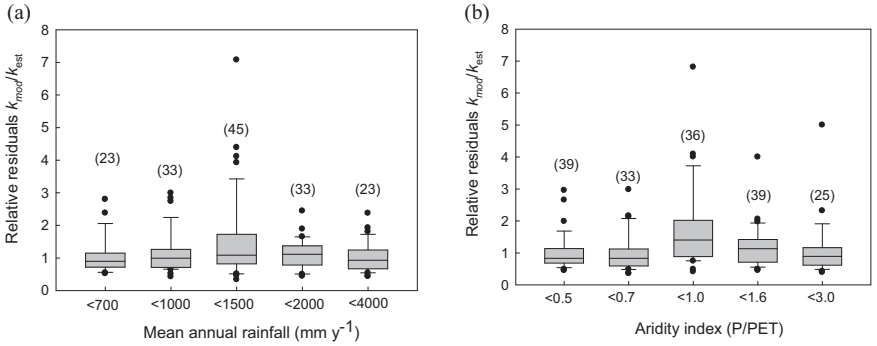

Fig. 8. Box and whiskers plot of relative residuals for exponential equations linking k_{bf} to **(a)** a range of mean annual rainfall classes (MAR). **(b)** Idem for aridity index (AI) range. The number in brackets is the sample size per range.

principal component analysis (PCA) to reduce dimensionality in an analysis to determine correlations between flow and velocity metrics in the North and South Shores of western Lake Superior (USA).

Pan-tropical maps of k_{bf} extending to 30° N and 35° S were derived using the MAR regression equation and the lower and upper bounds of the 95% confidence interval. The resulting catchment k_{bf} values are plotted in the map showing the original value (Fig. 9). A reasonable agreement is observed between original values and the ones using the regression equation.

The analysis of relative residuals for smaller catchments showed that catchment attributes such as slope (SLO) and elongation ratio (CE) had weak correlations with k_{bf}. Studies in catchments $<100\,km^2$ (e.g. Post and Jakeman, 1996; Brandes et al., 2005) also showed the explanatory power of terrain attributes and soils with respect to k_{bf} or other baseflow associated parameters. The present study and Van Dijk (2010) have demonstrated a more important role of climatic characteristics in relation to baseflow recessions across the tropics and Australia at catchments scales $>100\,km^2$. Van Dijk (2010, Fig. 7 for the AI vs. k_{bf} plot) obtained similar power relationships between MAR, AI and baseflow recessions respectively for temperate Australian catchments. Estimates of k_{bf} using the equations derived in the present study produced slightly higher estimates in these catchments, but the form of the relationships were similar. Differences between the rainfall data, and the Priestley-Taylor PET formulation in Van Dijk (2010) with the Hargreaves formulation in the present study may explain these differences.

The current empirical equations for the estimation of k_{bf} are necessarily subject to the limitations and uncertainties of the data used to derive them. There is no dense network of streamflow gauges in much of the tropics; the same can be said of the spatial density of gauges used to interpolate rainfall surfaces in the WORLDCLIM dataset (Hijmans et al., 2005). Furthermore, the estimation of k_{bf} was performed using long-term monthly climatologies, which would also yield long-term k_{bf} estimates. Coefficients will vary seasonally and interannually, with different k_{bf} estimates for dry-wet years and seasons.

It is expected that better rainfall data will result in more accurate relationships in the future. In addition, better soil and geological data may also improve the predictions.

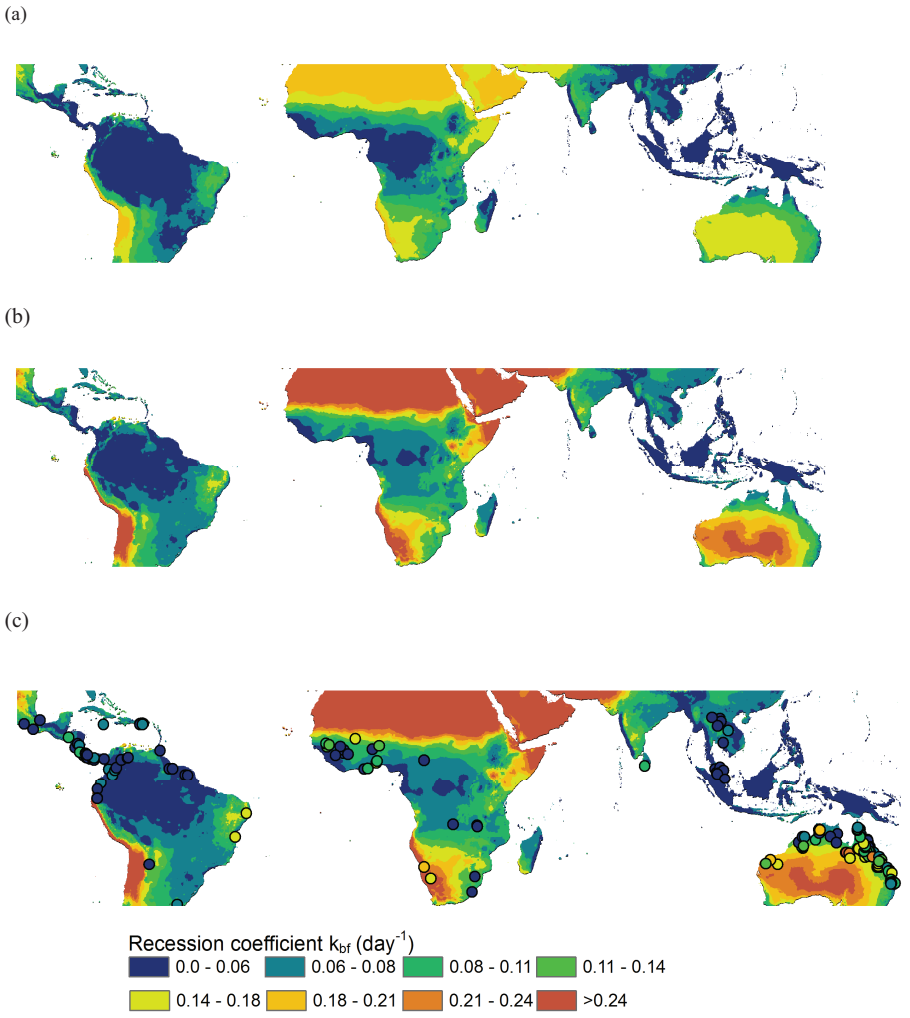

Fig. 9. Pan-tropical map of baseflow recession coefficient using the exponential regression equation and mean annual rainfall (MAR): **(a)** equation representing the lower and **(b)** upper bounds of the 95% confidence interval and **(c)** original regression equation. Symbol colours represent estimated k_{bf} values of the 167 catchments used in this study.

6 Summary and conclusions

This study analysed the potential of various climatic and terrain attributes to estimate baseflow recession coefficients (k_{bf}) for 167 unregulated tropical and subtropical catchments with areas $>200\,km^2$. Linear reservoir theory was used to estimate k_{bf} from daily streamflow data ($m^3\,s^{-1}$) obtained from the Global River Discharge Center (GRDC). Stepwise regression showed the overriding importance of climatic attributes over terrain ones at this scale. The best predictors for baseflow recession coefficient were mean annual rainfall (MAR) and aridity index (AI) together explaining 49% of the variance.

The interaction between climate and surface and subsurface attributes also plays an important role at smaller scales. For example, catchment elongation (CE), a measure of catchment shape, was also found to be statistically significant, although weakly correlated. An analysis of clusters of catchments of smaller size, showed that in these areas with presumably similar soils and geology, residuals of the regression could be explained by average catchment slope (SLO) and CE.

Although climatic characteristics explained a great deal of the variation in k_{bf}, baseflow is catchment-specific and dependent on the rainfall spatial and temporal patterns, land cover and land use, catchment morphology, infiltration opportunities and soil water holding capacity, configuration of the groundwater system and timing of groundwater discharge to the stream. The differences in k_{bf} found in humid and arid catchments show the interconnection of climate and surface and subsurface characteristics of catchments: ephemeral and consequently mainly event-driven streamflow as well as the occurrence of fast-draining perched aquifers may explain the higher recession coefficients observed in drier catchments.

The lowest recession coefficients in the humid tropics may be attributed to excess rainfall recharging deep soils and porous aquifers present in these areas (e.g. volcanic belts Central Amazonia, sandstone basin forms in Northeast Thailand). These sources may be an important source of baseflow during dry weather.

If better data are obtained for these surface and subsurface attributes, the prediction of baseflow in ungauged areas can be improved accordingly.

Acknowledgements. The authors gratefully acknowledge the funding from Microsoft Research and the Basin Focal Project Andes, a project of the CGIAR Challenge Program on Water and Food (CPWF). The GRDC Runoff Data Center and DERM Queensland are also thanked for providing the streamflow data. The authors are also grateful to Hannah Cloke from King's College London for providing valuable comments on the research.This study was conducted during an internship carried on in CSIRO Land and Water, Canberra-Australia and is part of the PhD dissertation of the first author.

Edited by: N. Verhoest

References

Arino, O., Bicheron, P., Achard, F., Latham, J., Witt, R., and Weber, J. L.: GLOBCOVER The most detailed portrait of Earth, Esa Bulletin-European Space Agency, 24–31, 2008.

Arnell, N. W.: A simple water balance model for the simulation of streamflow over a large geographic domain, J. Hydrol., 217, 314–335, 1999.

Arnell, N. W.: Effects of IPCC SRES* emissions scenarios on river runoff: a global perspective, Hydrol. Earth Syst. Sci., 7, 619–641, doi:10.5194/hess-7-619-2003, 2003.

Batjes, N. H.: ISRIC-WISE derived soil properties on a 5 by 5 arc-minutes global grid (version 1.0). Report 2006/02 ISRIC World Soil Information, Wagenigen 2006. (Available at: http://www.isric.org/isric/webdocs/Docs/ISRIC_Report_2006_02.pdf, data available at: http://www.isric.org last access: 17 May 2010), 2010.

Brandes, D., Hoffmann, J. G., and Mangarillo, J. T.: Base flow recession rates, low flows, and hydrologic features of small watersheds in Pennsylvania, USA, J. Am. Water Resour. Assoc., 41, 1177–1186, 2005.

Bruijnzeel, L. A.: Hydrological functions of tropical forests: not seeing the soil for the trees?, Agr. Ecosyst. Environ., 104, 185–228, doi:10.1016/j.agee.2004.01.015, 2004.

Brutsaert, W. and Nieber, J. L.: Regionalized Drought Flow Hydrographs From A Mature Glaciated Plateau, Water Resour. Res., 13, 637–644, 1977.

Chapman, T.: A comparison of algorithms for stram flow recession and baseflow separation. Hydrological Processes, 13, 601–604, 1999.

Chappell, N. A., Sherlock, M., Bidin, K., Macdonald, R., Najman, Y., and Davies, G.: Runoff processes in Southeast Asia: Role of soil, regolith, and rock type, Forest Environments in the Mekong River Basin, Part 1, 3–23, 2007.

Defries, R. S., Hansen, M. C., Townshend, J. R. G., Janetos, A. C., and Loveland, T. R.: A new global 1-km dataset of percentage tree cover derived from remote sensing, Glob. Change Biol., 6, 247–254, 2000.

Detenbeck, N. E., Brady, V. J., Taylor, D. L., Snarski, V. M., and Batterman, S. L.: Relationship of stream flow regime in the western Lake Superior basin to watershed type characteristics, J. Hydrol., 309, 258–276, 2005.

Doll, P., Kaspar, F., and Lehner, B.: A global hydrological model for deriving water availability indicators: model tuning and validation, J. Hydrol., 270, 105–134, 2003.

Fenicia, F., Savenije, H. H. G., Matgen, P., and Pfister, L.: Is the groundwater reservoir linear? Learning from data in hydrological modelling, Hydrol. Earth Syst. Sci., 10, 139–150, doi:10.5194/hess-10-139-2006, 2006.

Gascoin, S., Ducharne, A., Ribstein, P., Carli, M., and Habets, F.: Adaptation of a catchment-based land surface model to the hydrogeological setting of the Somme River Basin (France), J. Hydrol., 308, 105–116, 2009.

Hagemann, S. and Dumenil, L.: A parametrization of the lateral waterflow for the global scale, Clim. Dynam., 14, 17–31, 1998.

Hijmans, R. J., Cameron, S. E., Parra, J. L., Jones, P. G., and Jarvis, A.: Very high resolution interpolated climate surfaces for global land areas, Int. J. Climatol., 25, 1965–1978, doi:10.1002/joc.1276, 2005.

Lehner, B., Verdin, K., and Jarvis, A.: Hydrosheds technical documentation. Version 1.1. (Data available from: http://hydrosheds.cr.usgs.gov, last access 17 May 2010), 2008.

Lepers, E., Lambin, E. F., Janetos, A. C., DeFries, R., Achard, F., Ramankutty, N., and Scholes, R. J.: A synthesis of information on rapid land-cover change for the period 1981–2000, Bioscience, 55, 115–124, 2005.

Liang, X., Lettenmaier, D. P., Wood, E. F., and Burges, S. J.: A Simple Hydrologically Based Model Of Land-Surface Water And Energy Fluxes For General-Circulation Models, J. Geophys. Res.-Atmos., 99, 14415–14428, 1994.

Mwakalila, S., Feyen, J., and Wyseure, G.: The influence of physical catchment properties on baseflow in semi-arid environments, J. Arid Environ., 52, 245–258, doi:10.1006/jare.2001.0947, 2002.

Nijssen, B., O'Donnell, G. M., Lettenmaier, D. P., Lohmann, D., and Wood, E. F.: Predicting the discharge of global rivers, J. Clim., 14, 3307–3323, 2001.

Oki, T. and Kanae, S.: Global hydrological cycles and world water resources, Science, 313, 1068–1072, doi:10.1126/science.1128845, 2006.

Post, D. A. and Jakeman, A. J.: Relationships between catchment attributes and hydrological response characteristics in small Australian mountain ash catchments, Hydrol. Process, 10, 877–892, 1996.

Saenz, L. and Mulligan, M.: Development and validation of a georeferenced tropics-wide database of dams, Water Resour. Res., to be submitted, 2010.

Schneider, A., Friedl, M. A., and Potere, D.: A new map of global urban extent from MODIS satellite data, Environ. Res. Lett., 4, 044003, doi:10.1088/1748-9326/4/4/044003, 2009.

Smakhtin, V. U.: Low flow hydrology: a review, J. Hydrol., 240, 147–186, 2001.

Tallaksen, L. M.: A Review Of Baseflow Recession Analysis, J.

Hydrol., 165, 349–370, 1995.
Thornthwaite, C. W.: An Approach toward a Rational Classification of Climate, Geogr. Rev., 38, 55–94, 1948.
Tomasella, J., Hodnett, M. G., Cuartas, L. A., Nobre, A. D., Waterloo, M. J., and Oliveira, S. M.: The water balance of an Amazonian micro-catchment: the effect of interannual variability of rainfall on hydrological behaviour, Hydrol. Process., 22, 2133–2147, doi:10.1002/hyp.6813, 2008.
Tularam, G. U. and Ilahee, M.: Exponetial smoothing method of base flow separation and its impact on continuous loss estimates, American Journal of Environmental Sciences, 4, 136–144, 2008.
van Beek, L. P. H., and Bierkens, M. F. P.: The Global Hydrological Model PCR-GLOBWB: Conceptualization, Parameterization and Verification, 2008. Report Department of Physical Geography,Utrecht University, Utrecht, The Netherlands, available at: http://vanbeek.geo.uu.nl/suppinfo/vanbeekbierkens2009.pdf, last access: 17 May 2010.
van Dijk, A. I. J. M.: Climate and terrain factors explaining streamflow response and recession in Australian catchments, Hydrol. Earth Syst. Sci., 14, 159–169, doi:10.5194/hess-14-159-2010, 2010.
Vogel, R. M. and Kroll, C. N.: Regional Geohydrologic-Geomorphic Relationships for the Estimation of Low-Flow Statistics, Water Resour. Res., 28, 2451–2458, 1992.
Vorosmarty, C. J., Green, P., Salisbury, J., and Lammers, R. B.: Global water resources: Vulnerability from climate change acid population growth, Science, 289, 284–288, 2000.
Walsh, R. P. D. and Lawler, D. M.: Rainfall seasonality: description, spatial patterns and change through time, Weather, 36, 201–209, 1981.
WHYMAP – World-wide Hydrogeological Mapping and Assessment Programme. Groundwater resources of the world 2010, Data available from http://www.bgr.de/app/fishy/GoogleEarth/whymap.kml, last access: 17 May 2010.
Widen-Nilsson, E., Halldin, S., and Xu, C. Y.: Global water-balance modelling with WASMOD-M: Parameter estimation and regionalisation, J. Hydrol., 340, 105–118, doi:10.1016/j.jhydrol.2007.04.002, 2007.
Wittenberg, H.: Baseflow recession and recharge as nonlinear storage processes, Hydrol. Process., 13, 715–726, 1999.
Yu, P. S., Yang, T. C., and Liu, C. W.: A regional model of low flow for Southern Taiwan, Hydrol. Process., 16, 2017–2034, 2002.
Zecharias, Y. B. and Brutsaert, W.: Recession Characteristics Of Groundwater Outflow And Base-Flow From Mountainous Watersheds, Water Resour. Res., 24, 1651–1658, 1988.

Chapter 5 Model implementation and evaluation

Contents

5.1 Introduction

This chapter describes the pan-tropical implementation of the W3RA-LUM model and presents an evaluation of modelled against observed streamflows. The main features of the model are described in detail as well as the modifications introduced to make the model amenable to modelling the streamflow impacts of land use and land cover change (LUCC) through incorporation of the Soil Conservation Service Curve Number Method (SCS-CN, USDA, 1986). The SCS-CN method is currently the only method for global application of LUCC scenarios impact modelling that has a strong empirical basis and is responsive to both differences soil in type and level of soil degradation. The emphasis of the description – including the processes simulated, associated equations and model structure – is on those model components that were modified (to allow hypothesis testing) in the original AWRA-L model on which the W3RA-LUM model is largely based (Van Dijk, 2010a; Van Dijk and Renzullo, 2011). For a description of the model components not covered here, the reader is referred to Appendix D. The modifications and parameter estimation methods are described in detail below and include a brief discussion of estimated parameter values (Section 5.3.1).

Several processes represented in AWRA-L were described using well-established relationships (Van Dijk, 2010a). Others followed a data-driven 'downward' approach (*e.g.* Sivapalan *et al.*, 2003), which resulted in a reduction of model dimensionality whilst still achieving acceptable results compared to more complex formulations (Van Dijk, 2010b; Van Dijk, 2010c). In order to understand the *raison d'être* of the structure and equations describing some of the processes simulated in W3RA-LUM, a background summary of the approach used in the development and implementation of AWRA-L is provided in Section 5.2. Previous model applications pertaining to LUCC studies are also discussed in this section. Section 5.3 describes the methods used for the implementation of W3RA-LUM pan-tropically. Results are presented and analysed in Section 5.4 and discussed in LUCC scenario modelling context in Section 5.5. Finally conclusions are drawn in Section 5.6.

5.2 Background

5.2.1 Approach for model development

Hydrological models attempt to describe naturally occurring hydrological processes. A model's complexity will often be dictated by the problem (*i.e.,* hypothesis) at hand and the processes that require a detailed description to address it. The use of the catchment scale, at which many hypotheses are typically tested, has frequently required simplifications of complex hydrological processes at smaller scales that have proved sufficiently robust at describing observations made at larger scales (*e.g.* streamflow, Savenije, 2001). Models grow in complexity when there is a need to address different hypotheses about the processes underlying a hydrological system (Beven, 2006). The additional assumptions and input parameters required to explain the other hypotheses will likely require more calibration to reproduce observations. This may result in more than one parameter set with similar explanatory value (Oreskes *et al.*, 1996). A model in this situation may be over-parameterised and suffer from structural equivalence or 'equifinality' (Beven, 1996). Even if an 'optimal' model is defined, equifinality may still occur if during the calibration the optimum parameter values obtained compensate for errors in input and output data (*e.g.* streamflow data used in calibration) and initial boundary conditions (Beven, 2006).

The aim of AWRA-L – to produce interpretable water balance component estimates, and as much as possible agree with water balance observations at a continental scale (Van Dijk, 2010a) – entailed predictions in different environments and with limited observational data. Thus a compromise needed to be found between the simplest alternative formulation that could explain observed aspects of the catchment water balance and the complexity of the processes required to be modelled.

A data-driven 'downward' approach was followed for model development (Klemeš, 1983; Sivapalan *et al.*, 2003). Climatological inputs and streamflow observations were available for several hundred catchments of (size range of 5−2000 km^2) across Australia. Quality-controlled streamflow data and interpolated climatic data were used to estimate storm flow (260 catchments) and baseflow (183 catchments) using storm flow recession and baseflow separation techniques respectively (Van Dijk, 2010b, Van Dijk, 2010c). These were

subsequently used to test and calibrate several variants of lumped and/or distributed models (in the case of soil water balance) commonly used in catchment modelling, including storm runoff models (Van Dijk, 2010c), (non)linear reservoir variants of groundwater flow models (Van Dijk, 2010b) and soil water balance models (Van Dijk and Marvanek, 2010). The climatic and biophysical conditions of the catchments used in the latter analysis also included catchments with (sub)tropical conditions, although most were located in temperate southeast Australia (Van Dijk, 2010c).

A version of Akaike's Final Prediction Error Criterion (FPEC; Akaike, 1970) and Nash-Sutcliffe model efficiency (NSME; Nash and Sutcliffe, 1970) were used to guide interpretation for model adoption. The version of FPEC used in AWRA-L considers the number of degrees of freedom in a penalisation factor used to scale the estimated prediction error; this provides an objective metric to explain the trade-off between the number of fitting parameters and the remaining unexplained variation in observations. The approach was also used to investigate whether parameters could be related to catchment climatic and geomorphologic attributes to increase the likelihood of predictive performance in ungauged catchments. Equations with explanatory value that described the parameters in terms of these catchment characteristics were obtained using step-wise regression[1]. The following main conclusions were drawn with respect to the selection of a storm runoff model (Van Dijk, 2010c, more details to follow in Section 5.3.1.2):

- Four model structures with similar functional form to the SCS-CN method and with a maximum of six parameters were investigated.
- A non-linear response model with two or three parameters provided the optimal model structure for modelling storm flow in 260 catchments in Australia, with a median Nash Sutcliffe model efficiency of 0.64.

The main soil water balance fluxes (groundwater recharge, effective infiltration and soil water uptake by roots or soil evaporation) were estimated in order to evaluate alternative soil water balance models. The following main conclusions were drawn with respect to the selection of a soil water balance model (Van Dijk and Marvanek, 2010, more details to follow in Section 5.3.1.3):

[1] Chapter 4 provides an example of how a similar approach was used to parameterise the groundwater recession coefficient in W3RA-LUM using pan-tropical streamflow data.

- A simplified two-parameter soil water balance model based on the Richards' equation (Richards, 1931) and the Brooks-Corey relationships (Brooks and Corey, 1964) was compared to similar explicit soil moisture accounting (ESMA) routines used in several lumped catchment models.
- The simplified model captured the characteristic behaviour of a free-draining soil profile and was consistent with more computationally demanding numerical solutions of the Richards' equation.
- Conceptually, the simplified model had advantages over the lumped models used, with parameter values agreeing better with *a priori* values.

The following main conclusions were drawn with respect to the selection of a groundwater flow model (Van Dijk, 2010b, more details to follow in Section 5.3.1.4):

- Baseflow estimates obtained with the one-parameter linear reservoir approach were as good as those obtained with a non-linear two parameter reservoir approach.

The 'data-driven' approach, besides combining the power of pooling data from hundreds of catchments in Australia (*e.g.* Sivapalan, 2009), strives to develop the most parsimonious model components that agree well with observations for very dissimilar hydrologic environments. The approach entailes that (*i*) increases in complexity need to be justified by an increased ability to explain observed phenomena (by using the Akaike's Final Prediction Error Criterion); (*ii*) model components are formulated in such a way as to be consistent with physical laws and principles, and catchment hydrological process knowledge and; (*iii*) formulations have a minimum number of parameters, particularly parameters that are poorly predictable *a priori*.

AWRA-L outputs, including streamflow, evaporative fluxes and soil moisture, have been extensively evaluated in Australia (*e.g.* Van Dijk and Warren, 2010) and the model is currently used operationally to produce water balance information by the Australian Bureau of Meteorology (Band *et al.*, 2012; Stenson *et al.*, 2012).

5.2.2 Previous evapotranspiration and land use impact studies using AWRA-L

King *et al.* (2011) performed a multi-model comparison of actual evapotranspiration (*AET*) estimates, which included three dynamic models and five satellite-based *AET* models. Among the former was an uncalibrated version of AWRA-L (v 0.5). Two types of evaluation are of interest here: (1) 8-day averaged *AET* time-series estimated by the model were compared against flux tower estimates for six sites in Australia with different climates and land covers; and (2) long-term mean annual *AET* estimated by the model against long-term mean annual *AET* values obtained from catchment water balance for 568 catchments in Australia. In evaluation (1) AWRA-L performed well for most sites except in an open water area site (mean coefficient of determination r^2=0.83 and relative bias Relbias=-0.16%, excluding the open water site). In evaluation (2) AWRA-L performed similarly to the land surface models and better than the satellite-based estimates (r^2=0.56 and Relbias=-3.5%).

Overall, *AET* products from the two dynamic models (including AWRA-L) and one satellite algorithm (see Guerschmann *et al.*, 2009 for details) provided the best estimates.

Van Dijk *et al.* (2012, see Attachment C for full details) used AWRA-L and a formulation of the Budyko framework[2] (Budyko, 1974) that included vegetation cover types to assess the likely causes of the documented weak influence of vegetation cover on streamflow from non-experimental catchments with mixed land cover (*e.g.* Zhang *et al.*, 2004; van Dijk *et al.*, 2007; Oudin *et al.*, 2008; Donohue *et al.*, 2010; Peel *et al.*, 2010). A formulation of the Budyko framework that accounted for vegetation – the so-called Zhang model (Zhang *et al.*, 2001) – successfully detected land cover influence in a global streamflow dataset of mostly small (<1 km^2) catchments with homogenous land cover. The *'w'* parameter in the Zhang *et al.* (2001) model can be interpreted as a measure of the vegetation's transpiration efficiency and was found to be different for forests (w_{forest}=2.0) and herbaceous vegetation (w_{herb}=0.5) after calibration.

[2] Budyko postulated that the long-term average annual evapotranspiration from catchments is determined by rainfall and available energy and formulated a simple model that showed good agreement with the long-term water balance for catchments in the former USSR (Zhang *et al.*, 2008).

Contrary to the idealised conditions of small catchment experiments in which a strong signal of land cover is typically well established (and generally translated into noticeably lower long-term water yield in catchments with mostly forest cover compared to catchments with mostly herbaceous cover; see also Brown *et al.*, 2005), the above mentioned studies exploring the effects of mixed land cover on streamflow either reported a much smaller influence, no statistically significant influence, or even an influence contrary to what was expected (at least for some vegetation and climate types). As also highlighted in Chapter 2, the use of a variant of the Budyko framework demonstrated only a weak signal of LUCC (in this case 40% of *Acacia* woodland removal) in the Comet catchment (16,440 km^2).

In the study of Van Dijk *et al.* (2012), the Zhang *et al.* (2001) model was used to detect land cover influence in 278 catchments in Australia having mixed land cover. Part of the aim of the former study was to assess if a stronger land cover signal could be detected with a more complex model (AWRA-L in this case) than with the Zhang model. However, any process model incorporating vegetation dynamics could have been chosen to test this hypothesis. The Zhang formulation was re-arranged to predict mean annual streamflow using optimised values for w_{forest} and w_{herb} values and the respective fractions of catchment cover, $FCOV_{forest}$ and $FCOV_{grass}$ respectively. Resulting optimised parameter values were very close (w_{forest}=1.98 and w_{herb}=1.91) and this translated into an average water use of forest cover only 2% greater than that of herbaceous cover. Further, reducing the model to a single parameter yielded a w value of 1.95. These results support the findings of the weak influence of vegetation cover in the studies previously referred to (Zhang *et al.*, 2004; Van Dijk *et al.*, 2007; Oudin *et al.*, 2008; Donohue *et al.*, 2010; Peel *et al.*, 2010). Subsequently, uncalibrated AWRA-L predictions of mean streamflow for the same 278 catchments, but using hypothetical scenarios of full forest or full herbaceous cover, were compared to the equivalent Zhang model with generic values for w (2.0 and 0.5 for forest and herbaceous vegetation cover, respectively), thus depicting the same vegetation cover conditions as used for the AWRA-L predictions (*i.e.,* full forest or full herbaceous cover). Uncalibrated AWRA-L predictions were able to reproduce the differences between forest and herbaceous cover predicted by the Zhang model with generic values for w (Figure 5.1).

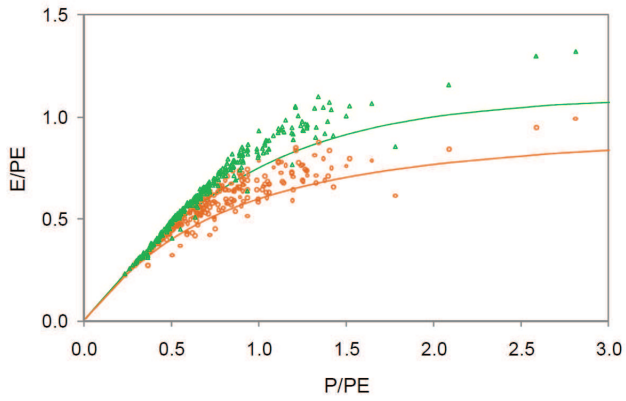

Figure 5.1 Comparison of uncalibrated AWRA-L simulated streamflow for the 278 catchments for full forest cover (green triangles) and herbaceous cover (orange circles) and the Zhang model for full forest cover (green line) and herbaceous cover (orange line). The Y and X axis correspond to the ratio of evapotranspiration (*E*) to potential evapotranspiration (*PE*) and precipitation (*P*) to *PE* respectively (after van Dijk *et al.*, 2012).

The ability of the uncalibrated AWRA-L to reproduce streamflow (Table 1, see Appendix F) was better than that of the Zhang model as depicted in Figure 5.1, and also better than that of model variants with calibrated *w* parameters. It was concluded that AWRA-L satisfactorily predicted streamflow in the 278 catchments with mixed land cover and that it produced a land cover signal of similar or higher magnitude as the Zhang model. A corollary finding of the previous result is that AWRA-L can also be useful in predicting the hydrological impacts of LUCC in scenario modelling, although further testing is required with respect to sensitivity of the model to LUCC (see Chapter 6). The study also advanced other biophysical, climatic and methodological issues that may well prevent Budyko-type models from detecting a strong vegetation cover signal in catchments with mixed land cover (see Appendix F).

5.3 Methodology

5.3.1 W3RA-LUM Model description

The technical description – including the appendices to which it refers – of the hydrological processes simulated by W3RA-LUM and the corresponding equations and justifications of structure or specific parameter values, is largely based on Van Dijk's (2010a) description of AWRA-L, except for the modifications introduced here. These modifications and specific model

parameters values, either as part of AWRA-L or W3RA-LUM development, are described in detail below.

W3RA-LUM is a one-dimensional grid-based land surface model that uses lumped models of water balance of the soil, groundwater and surface water stores applied to individual grid cells. W3RA-LUM currently runs at a 1° grid resolution and at a daily time-step, commensurate with the resolution of high-quality long-term climatic data available for LUCC studies (as discussed more fully in Chapter 3).

The current model makes the fundamental assumption that lateral redistribution of water between grid cells can be ignored without having an impact on water balance estimates. This assumption is generally acceptable for the grid cell resolution used here, although it is likely to be violated areas having large surface water bodies or in areas that receive important surface and/or groundwater inflows. Lateral water redistribution of surface, subsurface and groundwater movement (*e.g.* floods, irrigation or lateral groundwater inflows, run off – run on processes) becomes significant at higher resolutions and are key at the hillslope scale. Arising from the previous assumption, it follows that precipitation within the grid cell is the only source of water and that all sources of lateral discharge occur within the cell.

Other processes not yet simulated in the model are:

- River routing, although aggregation for larger catchments over monthly periods might not be greatly affected by the lack of routing *per se*.
- River management such as regulation, reservoir operation and human extraction.

Under these assumptions and model structural simplifications, mainly lack of routing, model outputs are best interpreted as local fluxes in catchments up to the model's grid resolution (*i.e.,* 10,000 km^2).

The following processes are simulated in W3RA-LUM: (*i*) partitioning of incident precipitation into interception evaporation and net precipitation; (*ii*) partitioning of net precipitation into infiltration, infiltration-excess surface runoff, and saturation-excess runoff; (*iii*) snow melt and snow accumulation; (*iv*) vertical water movement in a topsoil store, including infiltration, drainage and soil water evaporation; (*v*) vertical water movement in a shallow soil store

including incoming (from the above store) and exiting drainage (to the store below) and root water uptake (transpiration); (*vi*) vertical water movement in a deep soil store (*idem* as for shallow soil store); (*vii*) vertical water movement in a groundwater store including recharge, capillary rise and discharge; and (*viii*) surface water body dynamics, including inflows from surface runoff and river discharge, open water evaporation and catchment water accumulation (flooding). In addition, vegetation cover is dynamically adjusted through a simple model that predicts water-related vegetation phenology[3]. The model design attempts to integrate simulated processes in a modular fashion to allow flexibility and the inclusion of alternative processes. The design also considers easy linkage to other data streams via data assimilation (*cf.* Van Dijk, 2011) and multi-objective global calibration (Zhang *et al.*, 2011). These features have been identified as promising pathways in advancing hydrological modelling methods (Buytaert *et al.*, 2008).

A flux diagram of the aforementioned processes is shown in Figure 5.2. The process equations of the model components that differ from the original AWRA-L model, enclosed by the red dashed box in Figure 5.2, are described in Section 5.3.1.

The version of the model used here simplifies subgrid variation in vegetation cover by considering only two 'hydrological response units' (HRUs):

- Deep-rooted tall vegetation ('forest') which can use water from shallow and deep soil layers.
- Shallow-rooted short vegetation ('herbaceous') which can only use water from shallow soil layers.

Each HRU can be parameterised differently according to vegetation and soil characteristics. Deep-rooted tall vegetation continues to have access to soil water during dry periods and has a canopy that fluctuates less over time than does the canopy of shallow-rooted vegetation, as a response to the availability of water (Van Dijk *et al.,* 2010a). It follows that, soil and energy balances are simulated separately for each HRU (Figure 5.2, large green box). Although it is a far from a complete representation of land cover types, the system is flexible and can

[3] *phenology*: relating to cyclical biological events in response to climatic conditions, in particular greening and senescence in response to water availability.

incorporate any number of HRUs, subjected to increases in computational capacity. Moreover, the use of the SCS-CN method implicitly adds characteristics of other land use and land covers to these HRUs by regulating the partition of precipitation reaching the soil into infiltration and/or runoff (see Section 5.3.1.2 for details).

- Groundwater and streamflow dynamics are simulated at the grid cell scale and therefore have only one set of parameters (Figure 5.2, large yellow box).

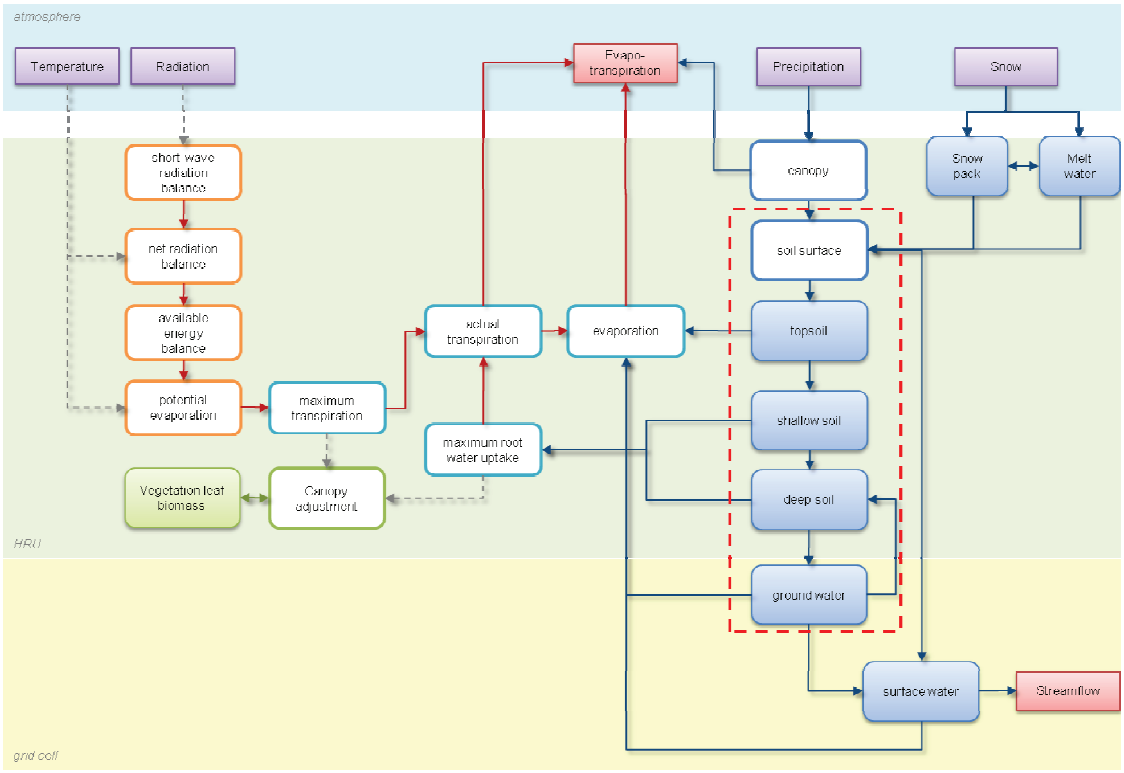

Figure 5.2 Flux diagram of the W3RA-LUM model structure (modified from Van Dijk, 2010a): the minimum input data requirements (purple boxes); fluxes lost from the grid cell (red boxes); water fluxes (blue arrows); energy and vapour fluxes (red arrows); functional relationships (dashed grey arrows); water balance model components described (blue rounded boxes); the surface radiation and energy balance (orange); vapour fluxes (cyan); and vegetation phenology (green). Solid blue and green colours represent dynamic model states updated from one time step to the next; outlined boxes represent transformations and partitioning. Enclosed in the red dashed box are the components of the model that were modified here.

5.3.1.1 Mass balance

The mass balance equations used to describe the soil water balance are as follows (Van Dijk *et al.*, 2010a):

Canopy partitioning of precipitation (P_g) into net precipitation (P_n) and interception evaporation (E_i, see Appendix D2.2):

$$P_n(t) = P_g(t) - E_i(t) \quad \text{5-1}$$

A snow melt model using a degree-day factor from the HBV snow model (Bergström, 1995) was incorporated into the model. Net precipitation (P_n) falls as snow if the average daily temperature falls below 0°. Snow may melt and/or may refreeze. Snow accumulates as solid snow pack in a solid snow storage (S_{SS}, in mm) or melt water in a liquid water storage (S_{SL}, in mm) up to a certain maximum holding capacity, any surplus reaches the top soil and is partitioned into surface runoff (Q_R) and infiltration (I) (no storage term):

Soil surface partitioning of net precipitation (P_n)

$$I(t) = P_n(t) - Q_R(t) \quad \text{5-2}$$

Surface top soil water balance, comprising top soil water storage (S_0), infiltration, soil evaporation (E_S) and top soil drainage (D_0):

$$S_0(t+1) = S_0(t) + I(t) - E_s(t) - D_0(t) \quad \text{5-3}$$

Shallow soil water balance, comprising shallow soil water storage (S_S), shallow root water uptake (U_S), top soil drainage (D_0) from the layer above, and shallow soil water drainage (D_S):

$$S_s(t+1) = S_s(t) + D_0(t) - U_S(t) - D_S(t) \quad \text{5-4}$$

Deep soil water balance, comprising deep soil water storage (S_D), D_S, capillary rise from the groundwater (Y), deep root water uptake (U_D), and deep drainage (D_D):

$$S_D(t+1) = S_D(t) + D_S(t) + Y(t) - U_D(t) - D_D(t) \quad \text{5-5}$$

Groundwater balance, comprising ground water storage (S_g), D_D, Y, groundwater evaporation (E_g) and groundwater discharge (Q_g):

$$S_g(t+1) = S_g(t) + D_D(t) - E_g(t) - Q_g(t) - Y(t) \quad \text{5-6}$$

River water balance, comprising surface water storage (S_r), Q_R, Q_g, and stream discharge (Q_{stream}):

$$S_r(t+1) = S_r(t) + Q_R(t) + Q_g(t) - E_r(t) - Q_{stream}(t) \quad \text{5-7}$$

The remainder of the present description will focus on the processes and/or parameters that were modified relative to AWRA-L (see red dashed box in Figure 5.2), notably: (*i*) Soil surface partitioning of net precipitation into surface runoff and infiltration, (*ii*) soil water balance, and (*iii*) groundwater dynamics.

5.3.1.2 Surface runoff (Q_R)

The following equations describing surface runoff were selected using the 'downward' approach mentioned in Section 5.2. The terms between brackets in equation 5-8 can be interpreted as describing infiltration excess and saturation overland flow, respectively (Van Dijk, 2010a):

$$Q_R = \left((1 - f_{sat}) \frac{P_n}{P_n + S_{\max}} + f_{sat} \right) (P_n - I_i), \quad \text{5-8}$$

with

$$I_i = \min(P_n, I_0),$$

and

$$f_{sat} = \min\left(1, \max\left(\frac{S_G}{S_{Gref}}, f_{water}\right)\right), \quad \text{5-9}$$

where Q_R is estimated event surface runoff (mm), f_{sat} is the groundwater saturated area fraction (dimensionless), f_{water} is the fraction area covered by water (dimensionless), P_n is the net event precipitation (mm), and I_i is the initial infiltration (mm). The other terms (I_0, S_{max}, S_{Gref}) are

parameters that were either estimated using reasonable values *a priori* or were inferred using relationships with catchment climatic and/or geomorphologic attributes (see below).

Parameter estimation

The initial infiltration I_i represents the initial amount of precipitation required to wet the soil before any surface runoff begins. Using streamflow data from 260 catchments in south-eastern Australia, a median initial retention capacity I_0 of 8 mm was derived, whereas optimising rather than prescribing I_0 led to only minimal improvement in model performance improvement (Van Dijk, 2010b). It is noted that the effects of precipitation interception are implicit in the values of I_0=8 mm estimated by Van Dijk from the streamflow data (2010c), whereas in W3RA-LUM these are computed separately through a canopy interception loss model (see Appendix D2.2). A conservative default estimate of I_0=1 mm was adopted here in order to consider other initial losses (*i.e.,* initial infiltration losses and surface storage losses) in the SCS-CN method (see below).

The parameter S_{Gref}, representing the hypothetical groundwater storage at which the entire catchment area is saturated, was related to catchment mean annual precipitation (*MAP*, in mm). *MAP* explained 28% of the variation in S_{Gref} among the cited 260 catchments (Section 5.2.1) according to:

$$S_{Gref} = 8.15 MAP^{2.34} . \qquad 5\text{-}10$$

This formulation of S_{Gref} suggests that the groundwater-saturated area fraction (f_{sat}, Eq. 5-9) increases faster with increasing groundwater storage for a catchment with lower precipitation than for a catchment with comparatively higher precipitation. This may be related to partial-area runoff responding to high intensity precipitation, possibly in fast-draining (perched) saturated areas or degraded areas with limited infiltrability and limited natural storage characteristic (*e.g.* Petheram *et al.*, 2008, although for Northern Australia).

The parameter S_{max} (in mm), interpreted as the potential soil maximum storage capacity for which half of net precipitation on unsaturated soils is able to infiltrate and the other half runs off, was estimated here following the SCS-CN method. The two terms between brackets in

Equation 5-8 can be interpreted to describe infiltration excess and saturation overland flow respectively. The first term of equation 5-8 describing infiltration excess overland flow is mathematically equivalent to the surface runoff term in the SCS-CN ($Q_{CN,}$ mm d^{-1}) method:

$$Q_{CN} = \frac{\left(P_g - I_a\right)^2}{\left(P_g - I_a\right) + S_{\max}}, \qquad 5\text{-}11$$

where P_g is gross event precipitation (mm) and I_a is the initial abstraction loss (interception, initial infiltration losses and surface storage losses). To avoid an independent estimation of I_a in the SCS-CN method, a linear relationship with S_{max} was proposed: $I_a=\lambda S_{max}$, where λ is the initial abstraction ratio. The linear relationship was empirically justified on the basis of measurements made in catchments of less than 5 ha (Ponce and Hawkins, 1996). Although there was considerable scatter in the data, 50% of the values fell between 0.095 and 0.38. A value of λ=0.2 was then adopted (Ponce and Hawkins, 1996). Unfortunately, the details of the data sources underlying the relationship have been lost (Hawkins *et al.*, 2009). Using λ=0.2 in Equation 5-11 yields:

$$Q_{CN} = \left(\frac{P_n}{P_n + S_{\max}}\right) P_n . \qquad 5\text{-}12$$

For convenience, S_{max} was converted into a dimensionless parameter (ranging between 0 for maximum theoretical storage to 100 for zero storage) commonly referred to as the curve number (CN):

$$S_{\max} = \frac{25400}{CN} - 254 . \qquad 5\text{-}13$$

Curve numbers were originally estimated using recorded rainfall-runoff data from small instrumented catchments in the USA (Hawkins *et al.*, 2009). Each catchment was assumed to be represented by a Hydrologic Soil Group (HSG) and a Hydrologic Soil Condition (HSC). The SCS-CN method considers four HSGs corresponding to different classes of final infiltration rates (*i.e.,* from a soil after prolonged wetting): group A with high infiltration rates, B, C and D with intermediate, low and very low infiltration rates respectively (USDA, 1986). The effect of land cover and/or treatment is characterised by the HSC. The three types of HSC considered in the

SCS-CN method (good, fair and poor) depend on the effects of land use and cover type on infiltration and surface runoff generation. For instance, a good hydrologic condition indicates that the soil has low surface runoff potential. Soil condition is generally determined in the field by considering such factors as vegetation density, litter and surface roughness (USDA, 1986). Tables and charts for the derivation of CN values for different types of land cover and land use, Hydrologic Soil Condition (HSC) were produced, but unfortunately the original data for only a few sites are currently documented and most have been lost (Hawkins *et al.*, 2009). Although empirical in its derivation, different authors have justified the equations on theoretical grounds (*e.g.* Schaake *et al.,* 1996; Yu, 1998; Mishra and Singh, 2003). The method has been successful because of its simplicity and continues to be used authoritatively (see, among others, Beck *et al.*, 2009; Wang *et al.*, 2012; El-Hames, 2012). In addition, there have been numerous efforts to enhance its robustness (*e.g.* Mishra and Singh, 1999; Michel *et al.*, 2005).

Recent progress in remote sensing-based mapping of land use and land cover and the availability of soil maps at a global scale makes the estimation of a global map of CN feasible, albeit within the limitations and uncertainties of the respective data sources. However, due to the fact that CN values were originally developed using regional data (*i.e.,* mid-West of the US), care should be exercised when translating some of these CN values to regions with very different climate and soils (Ponce and Hawkins, 1996; Descheemaeker *et al.*, 2008; Sartori *et al.*, 2008).

Published CN values for different HSGs, land cover and HSCs were sourced and/or modified from USDA (1986) and Hong and Adler (2008) (Table 5-1). A method similar to the one used by Hong and Adler (2008) was followed in order to obtain a global map of CN values using and/or modifying existing global maps of (among others) land cover and land use, HSC and HSG. Hong and Adler (2008) considered only land cover and land use and HSG to derive a CN map for soils with fair hydrologic conditions. Here, HSC was explicitly considered, and a global satellite-derived proxy of land degradation, expressed in terms of trends in the long-term rain-use efficiency (RUE) adjusted normalised difference vegetation index (NDVI), was used to determine HSC pan-tropically. Bai *et al.* (2008) derived a global proxy for land degradation using trends of 15-day, 8 km grid cell, and estimates of NDVI for 1981–2003 to infer areas with

a long-term decline in ecosystem function and productivity (in terms of NDVI) that were not related to precipitation effects. Here, each grid cell of the Bai *et al.* (2008) global map was ascribed a HSC type based on the slope (or lack thereof) of the negative RUE adjusted normalised NDVI trend. A global map of HSC was obtained by ascribing good hydrologic conditions to grid cells with positive or no trend, fair to grid cells with trends between 0 and -0.02 and poor to trends lower than -0.02 (Figure 5.3a). Although this is a subjective classification, the resulting pan-tropical map of HSC showed a reasonable agreement with the Bai *et al.* (2008) land degradation categories (Figure 5.3b and c).

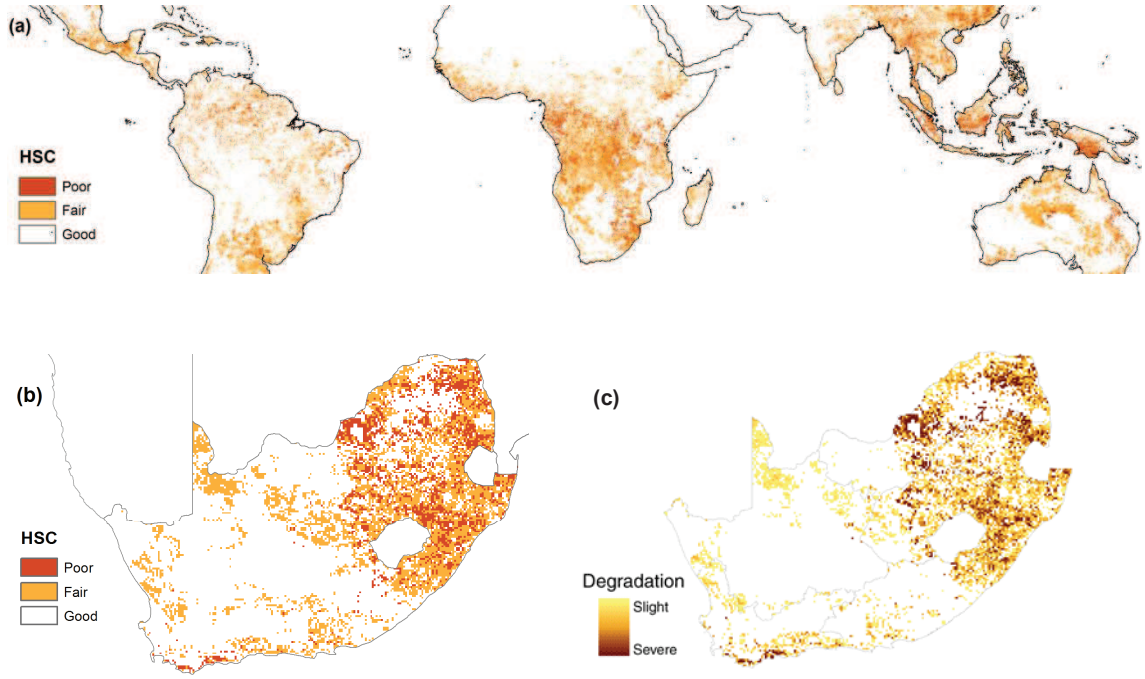

Figure 5.3 (a) Classification of Hydrologic Soil Condition (HSC) based on trends of RUE adjusted normalised NDVI (Bai *et al.*, 2008, see text for explanation); (b) comparison of HSCs in South Africa with (c) land degradation categories as defined in Bai *et al.* (2008). Note that Swaziland, Lesotho and bordering countries are masked out in the latter two maps.

Next, the 1 km grid cell Harmonised World Soil Database (HWSD; Nachtergaele *et al.*, 2012) based on the FAO Soil Map of the World (FAO, 1977) was used to obtain a global map of HSGs. The FAO Soil Map of the World was prepared mainly for agricultural purposes and soil classifications are mostly based on edaphic and pedological characteristics. Consequently, most of the detailed mapping was performed in areas with agricultural land use, whereas

uplands, mountains and forested areas were poorly sampled. Perhaps the greatest disadvantage of the map is the coarse resolution and the qualitative information on hydraulic properties (Terribile *et al.*, 2011). Despite these limitations, the FAO map is still the only worldwide soil classification that provides consistent, harmonised soil characteristics for each soil unit (Eswaran *et al.*, 2002) and has been used in several large-scale hydrologic modelling applications (*e.g.* Döll *et al.*, 2003; Gudmundsson *et al.*, 2012; Zhao *et al.*, 2012).

As previously mentioned, the SCS-CN method considers four HSGs: group A with high final infiltration rates, and groups B, C and D with intermediate, low and very low final infiltration rates respectively (USDA, 1986). The SCS HSG classification rules were developed for soils in the USA and are mainly based on soil texture. There are no established criteria to apply the same rules outside the USA. For instance, generally well-drained Ferralsols (FAO soil classification; IUSS Working Group WRB, 2006) would be classified as type D or C due to their clay content (Sartori *et al.*, 2008). Here, HSGs were equated to the qualitative FAO drainage classification based on soil types and adjusted for tropical soil characteristics (Table 5-2) to obtain a global map of HSGs (Figure 5.4).

The currently used classification has limitations inherited not only from the coarse scale of the FAO map on which it is based, but also from the fact that soil types with potentially different drainage characteristics are lumped together by necessity. For example, different Ferralsols may well exhibit different drainage characteristics based on differences in their clay mineralogy (Nortcliff and Thornes, 1989; Tomasella and Hodnett, 1997; Elsenbeer, 2001). In general, clay mineralogy affects soil permeability because of its effects on aggregate stability and structure (Driessen *et al.*, 2001). This is also case for the Acrisols Groups in the FAO classification; these soils are in reality of the 'Acrisol-Alisol' type which is not yet mapped separately at the global scale (Chappell *et al.*, 2007). Alisols are comparable to Acrisols but less strongly weathered and have a dense argicllic B horizon containing 2:1 clay minerals that restrict drainage (Driessen *et al.*, 2001). Conversely, Acrisols proper have low activity clays (mainly kaolinite and some gibbsite) and are generally well drained (Driessen *et al.*, 2001).

Table 5-1 Curve numbers (CN) for land use and land cover classification and Hydrological Soil Groups (HSGs) for fair, poor and good soil hydrologic conditions (HSCs) (modified after USDA (1986) and Hong and Adler (2008)).

Land use/land cover	CN Hydrologic Soil Group											
	Fair HSC*				Poor HSC*				Good HSC*			
	A	B	C	D	A	B	C	D	A	B	C	D
Water bodies	N/A	N/A	N/A	N/A	N/A	N/A	N/A	N/A	N/A	N/A	N/A	N/A
Evergreen needle leaf	36	60	73	79	45	66	77	83	30	55	70	77
Evergreen broad leaf	30	58	71	77	39	64	75	81	24	53	68	75
Deciduous needle leaf	40	64	77	83	49	70	81	87	34	59	74	81
Deciduous broad leaf	42	66	79	85	51	72	83	89	36	61	76	83
Mixed forests	38	62	75	81	68	79	86	89	49	69	79	84
Woodlands	61	71	81	89	91	88	92	97	72	78	85	92
Wooded grass lands	55	70	80	87	80	84	89	93	56	70	80	86
Closed shrub lands	45	65	75	80	64	75	82	85	35	57	70	76
Open shrub lands	49	69	79	84	68	79	86	89	39	61	74	80
Grasslands	49	69	79	84	68	79	86	89	39	61	74	80
Croplands	67	78	85	89	72	81	88	91	61	70	77	80
Bare ground	72	82	83	87	72	82	83	87	72	82	83	87
Urban and built-up	80	85	90	95	80	85	90	95	80	85	90	95

* Hydrologic condition indicates the effects of cover type and treatment on infiltration and runoff and is generally estimated from density of plant and residue cover on sample areas. Good hydrologic condition indicates that the soil usually has a low runoff potential for that specific hydrologic soil group, cover type, and treatment (USDA, 1986).

Table 5-2 Equivalent of FAO drainage class and SCS Hydrologic Soil Group (HSG)

FAO Drainage class		HSG	
1	Very Poor	D	Very low infiltration rates
2	Poor	D	
3	Imperfectly	C	Low infiltration rates
4	Moderately Well	B	Moderate infiltration rates
5	Well	A	High infiltration rates
6	Somewhat Excessive	A	
7	Excessive	A	

The 1 km grid cell resolution UMD Global Land Cover Classification of Hansen *et al.* (2000) was used to characterise land use pan-tropically. The land cover categories in the UMD map are a close match to those listed in Table 5-1.

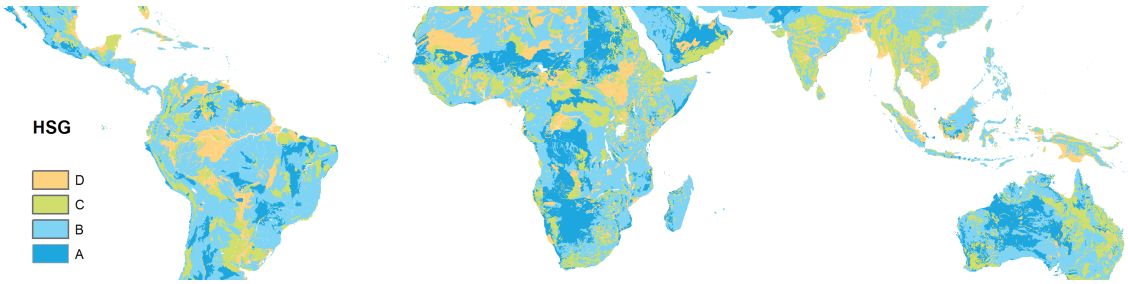

Figure 5.4 Map of Hydrologic Soil Groups (HSG) across the tropics based on the Harmonised World Soil Database (HWSD; Nachtergaele *et al.*, 2012).

The HSC map was resampled to the 1 km grid cell resolution of the land use/land cover and the HSG maps. Subsequently CN values were obtained by linking the latter maps to the corresponding CN values in Table 5-1. The resulting CN map was resampled to 1° grid cell resolution by averaging the respective CNs in the 1 km grid cell UMD map, the result of which is shown in Figure 5.5a. Surface runoff amounts for a uniformly distributed design event rainfall of 50 mm (using Equation 5-12) across the tropics are shown in Figure 5.5b. Finally, the W3RA-LUM parameter S_{max} was obtained from CN values using Equation 5-13.

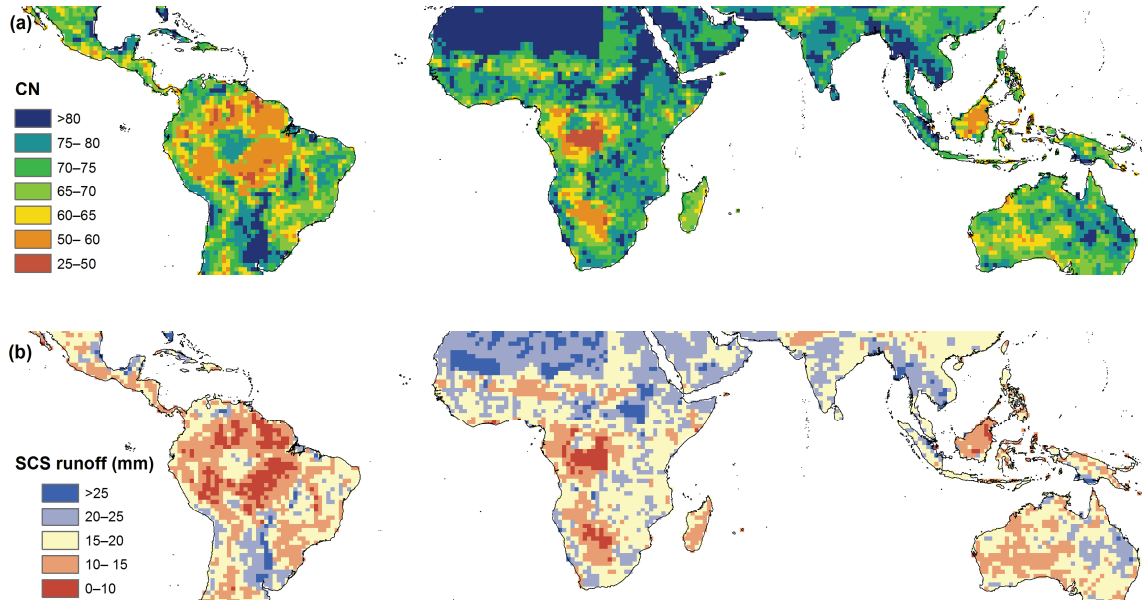

Figure 5.5 (a) Pan-tropical CN values for current conditions; and (b) surface runoff for a uniformly distributed design rainfall of 50 mm.

Pan-tropical values of CN in Figure 5.5a are normally distributed (mean=71 and standard deviation=8) with 90% of the values falling between 60 and 91. Upon visual inspection, some of the values reported here appear to be different from those reported in Hong and Adler (2008). The cause of this discrepancy may well be the fact that the HSG classification used by Hong and Adler (2008) was based on soil texture only and not on different HSCs. For example, values of CN are high in the Amazon and in the Congo's forests (~75–95). In terms of the prevailing land cover and soil types this seems counterintuitive since both areas have generally well drained Ferralsols as dominant soil type (FAO, 1977). According to Table 5-1, even for poor HSCs, their CN values should be between 39 and 64. The values reported here are similar to validated empirical values in various tropical locations and elsewhere (for tropical locations, see Dilshad and Peel, 1994; Sartori *et al.*, 2008; Descheemaeker *et al.*, 2008).

5.3.1.3 Soil water drainage (D_z)

Soil water content in W3RA-LUM is expressed in relative terms (*i.e.,* as a fraction of the amount held at field capacity) and is defined as follows:

$$w_z = \frac{S_z}{S_{zFC}} \text{ ,} \qquad \text{5-14}$$

where S_z (mm) is the amount of water stored in layer z (with the subscript z replaced by 0, S or D as appropriate to denote topsoil, shallow soil, or deep soil, respectively), and S_{zFC} (mm) the available water content at field capacity. Soil water content is assumed to represent the difference between remaining water in layer z one day after a saturation event (similar to the definition of field capacity) and the remaining soil water remaining when soil evaporation (in the case of S_0) or root water uptake (in the case of S_S and S_D) cease.

Soil drainage (for each layer) is defined as follows:

$$D_Z = f_{drain} S_z \text{ ,} \qquad \text{5-15}$$

and

$$f_{drain} = \max\left(K_{FC}, 1 - \frac{1}{w_z} \right) \text{ ,} \qquad \text{if } w_z > 1 \qquad \text{5-16}$$

$$f_{drain} = K_{FC} \exp\left[-\beta (1 - w_z) \right] \text{ ,} \qquad \text{if } w_z \leq 1 \qquad \text{5-17}$$

where D_z is the drainage from layer z (mm d^{-1}), f_{drain} is the drainage fraction (dimensionless), K_{FC} is the drainage fraction at field capacity (dimensionless) and β drainage function exponent (dimensionless).

Parameter estimation

The parameters K_{FC}, β and S_{FC} were calibrated by fitting Equation 5-15 against values of groundwater recharge and effective infiltration obtained from streamflow observations in 198 Australian catchments (Van Dijk and Marvanek, 2010). Instead of the three soil layers conceptualised in AWRA-L, a single free draining soil layer was used here. This is not expected to affect the estimated values of K_{FC} and β (Van Dijk *et al.*, 2010a). To estimate the moisture fluxes going in and out of the soil layer, it was assumed that the rise in baseflow was equal to the amount of groundwater recharge and that effective soil infiltration and retention was equal to the difference between net precipitation and storm flow. Also, actual evapotranspiration (*AET*)

was estimated independently (Guerschman *et al.*, 2009) by scaling potential evapotranspiration (E_0) using vegetation indices derived from the Moderate Resolution Imaging Spectroradiometer (MODIS). Estimated *AET* included transpiration by vegetation, interception losses and soil evaporation. Values obtained for the parameter β (median=4.5, range=0.7–8.4) and K_{FC} (median=0.029, range=0.01–0.3) were in accordance with *a priori* estimates from pedotransfer functions. Testing showed that β could be prescribed at 4.5 with minimal impact on model performance. A relationship that explained 40% of the variance in K_{FC} values was found with catchment humidity ($H=P/E_0$):

$$K_{FC} = 0.0685H^{3.18}. \qquad 5\text{-}18$$

This equation suggests that soils in wetter catchments are better drained and is consistent with published differences in soil drainage and infiltration capacity (everything else being equal) between humid- and arid-zone soils (Van Dijk, 2010a). This is most likely to reflect an enhanced infiltration capacity under more humid conditions due to a better developed vegetation cover and associated biological processes. Minimum catchment greenness (a measure of deep-rooted vegetation) explained 24% of the variance in storage at field capacity (S_{FC}).

In AWRA-L the top (S_0), shallow (S_S) and deep (S_D) soil layers have been assigned 30, 200 and 1000 mm storage capacity respectively. These values were adopted from a relationship between satellite-observed vegetation greenness (MODIS Enhanced Vegetation Index) and catchment moisture status that explained 24% of the variance between catchments. The relationship suggested a storage of around 1000 mm for forested catchments and 140 mm for catchments with little forest cover, in accordance with values for plant available water capacity in Australia (Van Dijk, 2010a).

To derive comparable spatially distributed soil water contents pan-tropically, the overall soil water storage capacity of the soil layer under consideration at field capacity is defined in W3RA-LUM as follows:

$$S_{zFC} = D_z \times \theta_{zFC}, \qquad 5\text{-}19$$

where D_z is soil layer depth (mm) and θ_{zFC} (mm mm^{-1}) is the fractional soil water content at field capacity.

Representative soil depths and fractional water content at field capacity were obtained from data found in the public domain. For D_0 and θ_{0FC}, the median depths and fractional soil water content at field capacity for the top soil, respectively, were obtained from the WISE Soil Profile Data produced by the International Soil Reference and Information Centre (ISRIC, Batjes, 2008). This database includes data for some 4382 soil profiles from 149 countries. Soil profiles obtained for the tropics accounted for almost 80% of the database, with Africa holding 41%, followed by South America and the Caribbean (18%), Southeast Asia (13%), and South Asia and Oceania (8%). S_{0FC} values for the entire soil profiles were subsequently spatially distributed by linking the data for each soil group with the corresponding soil units in the Harmonised World Soil Database.

Soil depths D_S and D_D were obtained from the 1° grid cell resolution Global Dataset of Ecosystem Rooting Depths (Schenk and Jackson, 2002) using the depths containing 50% and 95% of all roots respectively. The Schenk and Jackson (2002) database considers 475 vertical root profiles from 209 geographic locations and uses linear regression models linking plant life-form dominance, climate, and soil variables. These simple linear models explained as much as 50% of the variance in rooting depths for various biomes and highlighted that much deeper rooting depths were found in (seasonally) water limited ecosystems such as those found in eastern Amazonia and the Sahel. Water content at field capacity for the shallow (θ_{SFC}) and deep soil (θ_{DFC}) layers were sourced from the 1° grid cell resolution Global Gridded Surfaces of Selected Soil Characteristics (Global Soil Data Task, 2000), both based on the FAO Soil Map of the World (FAO, 1977) and the World Inventory of Soil Emission Potentials (WISE) WISE pedon-database (also produced by ISRIC) (Batjes, 1995). The aforementioned rooting depth and soil water content at field capacity data were specifically developed for use in land surface models (Schenk and Jackson, 2002). Figure 5.6 shows the spatial distribution of soil water content at field capacity for W3RA-LUM soil storages.

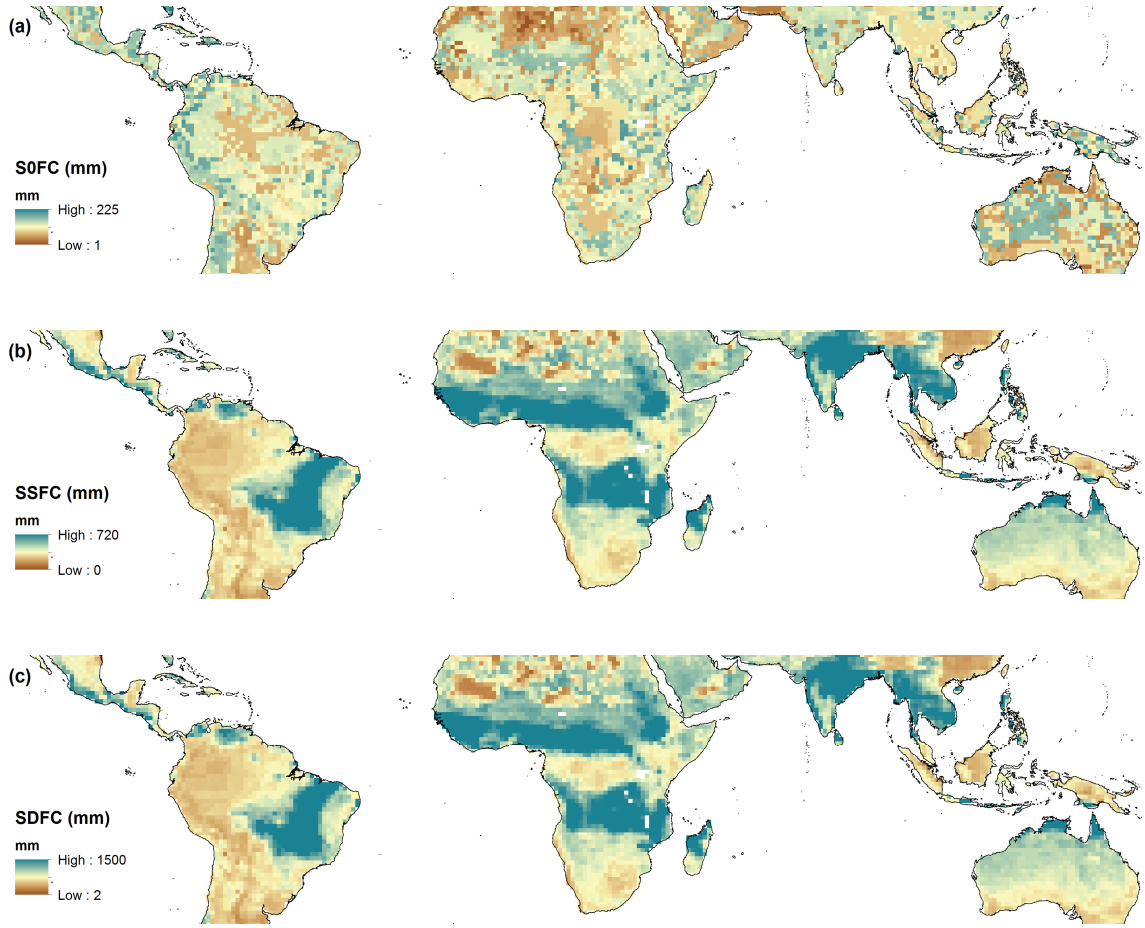

Figure 5.6 Spatial distribution of water storage capacity at field capacity for (a) the top (S_{0FC}), (b) shallow (S_{SFC}) and (c) deep (S_{DFC}) soil layers.

The resulting map shows deep storage capacity in areas characterised by dry and wet cycles (*e.g.* Brazil, the Sahel, Northern Australia). This is consistent with observed rooting depths of trees in such water-limited environments. In fact, there are cases for which much deeper rooting depths have been reported in these areas (see Canadell *et al., 1996)*, although soil water content may be modulated and concentrated in shallower soils horizons by hydraulic lift under these conditions (Burgess *et al.*, 1998).

5.3.1.4 Groundwater discharge (Q_g)

W3RA-LUM uses a one-parameter linear reservoir to simulate groundwater discharge (Q_g):

$$Q_g = \left[1 - \exp\left(-K_g\right)\right] S_g \,, \qquad 5\text{-}20$$

where S_g is the groundwater reservoir storage (mm) and considered a state variable and K_g is the groundwater drainage coefficient (mm d^{-1}).

Parameter estimation

Linear and non-linear reservoir (where S_g is raised by an exponent β_g) model variants were evaluated using estimated groundwater discharge (Q_g) patterns derived from baseflow recession data for 183 Australian catchments (Van Dijk, 2010b). In doing so, it was assumed that groundwater discharge was the only source of baseflow, although other sources of 'delayed flow' (Ward, 1984) may also be part of the estimated 'baseflow', such as slow draining soils or perched groundwater stores. Using a two-parameter non-linear reservoir did not add much more explanatory value than the one-parameter linear reservoir whereas the derived β_g were generally close to unity (Van Dijk, 2010b).

Chapter 4 described in detail how the groundwater drainage coefficient K_g was estimated using streamflow data for 167 unregulated catchments in the (sub)tropics. The approach followed was similar to the one in Van Dijk (2010b). The mean K_g was 0.08 d^{-1} (±0.053 standard deviation) with a positively skewed distribution. The shortest recession half-times occurred in the driest catchments, and lower values in wetter catchments. A relationship that explained 49% of the observed variance was found with catchment humidity (H):

$$K_g = 0.0580H^{-0.6210} \qquad 5\text{-}21$$

An analysis of a subset of geographically close catchments, showed that in these areas, presumably with some similarity of soils and geology, residuals of the regression could be explained by slope and catchment elongation.

5.3.2 Data

Meteorological forcing data

Gridded meteorological data for daily precipitation (P in mm), incoming shortwave radiation (SW_{down} in Wm^{-2}), and minimum and maximum temperature ($T_{min,max}$ in ºC) are the minimum requirements to force W3RA-LUM. A literature review was conducted to assess the quality and

accuracy of climate forcing data (Chapter 3). In addition, a systematic evaluation of the performance of reanalysis or reanalysis-based precipitation data was performed against gauge-based precipitation analyses for Australia and South and East Asia. It was found that the Princeton precipitation dataset (Sheffield *et al.*, 2006) agreed better than the reanalysis data in terms of monthly correlation, root mean squared error and daily precipitation intensity frequency, and therefore its use was considered for the hydrological modelling experiments conducted here. Climate inputs other than precipitation, at least at the daily scale, have less spatial variability than precipitation. Given the bias-correction applied to the aforementioned meteorological variables in the Princeton database using ancillary data of reasonable quality, these were also considered for use in the current hydrological modelling experiments. The version of the dataset used here included 61 years of daily time series of P, SW_{down}, and $T_{min,max}$ from 1948 to 2008. Effective air pressure (p_{air}) was also available from Princeton and was used instead of the average air pressure at sea level commonly assumed for Australia (*ca.* 1,015 hPa).

Biophysical data

The vegetation cover fractions for each HRU were estimated from the 500 m grid cell resolution map of tree cover as derived from MODIS reflectance data for the period 2000–2001 (Hansen *et al.*, 2003). The higher resolution of this dataset compared to previous data (*e.g.* DeFries *et al.*, 2000) enables a more accurate determination of forest extent, particularly in areas of fragmented forests. Each grid cell provided percentages of woody vegetation, herbaceous vegetation, and bare ground and also discriminated for open water surfaces. Other biophysical data used in the energy balance (see Van Dijk, 2010a for details) included an albedo climatology derived from MODIS white-sky albedo (Moody *et al.*, 2005) (http://modis-atmos.gsfc.nasa.gov/ALBEDO/) and a wind speed climatology (1983–1993) from NASA (http://eosweb.larc.nasa.gov/sse/*)* to compute aerodynamic conductance for the estimation of plant transpiration (see Appendix D.2.3).

Streamflow data

Daily streamflow data for 1432 catchments with an area smaller than 10,000 km^2 (*i.e.,* less than the model's 1° grid cell) were obtained from the Global Runoff Data Centre (GRDC,

http://grdc.bafg.de/) and Australian state agencies through the Water Information Research and Development Alliance (WIRADA), which form part of a larger global database consisting of 6192 catchments assembled for a GEWEX[4] forecasting project (*e.g.* Van Dijk *et al.*, accepted). All stations had at least 10 years of data. Catchments with a runoff coefficient greater than 1.2 where omitted from the analysis to account for basin size, precipitation and streamflow errors. This more relaxed catchment screening criteria was used because of scale differences between observations and the model grid cell, particularly the mismatch between catchment and grid cell precipitation. Catchments were also screened for the presence of flow regulation using two dam datasets (Lehner *et al.*, 2008; Mulligan *et al.*, 2009) which provided the locations of dams and their dam catchment areas (the latter only for the Mulligan *et al.* dataset). In addition, long-term seasonal data for 12 large basins were obtained from the Global Runoff Data Center (GRDC).

5.3.3 Simulation and evaluation

The W3RA-LUM model was run pan-tropically using daily Princeton climate forcing data for the years 1948–2008 and with the parameterisation described in previous sections. The model warm-up used the full 61 years of the Princeton data (1948–2008) to account for climatic variability, then the model was rerun using the states reached at the end of 2008. This was done due to the long time needed for deeper soil stores in very arid regions to reach dynamic equilibrium.

Two types of model evaluation were performed: (1a) A comparison of monthly time-series of W3RA-LUM modelled streamflow against monthly observed streamflow for the 1461 catchments with an area smaller than the model's 1° grid cell. (1b) The same comparison but for modelled monthly streamflow from a version of W3RA (Van Dijk *et al.*, accepted) which used calibrated parameters from AWRA-L version 1.0 (AWRA-L 1.0). AWRA-L 1.0 was calibrated against daily streamflow observations data for 160 Australian catchments, resulting in a substantial improvement of simulated streamflow (Viney *et al.*, 2011). In addition, the comparison also included streamflow (also at 1° cell resolution) from the four hydrological models (CLM, Mosaic, NOAH, and VIC) that form part of the Global Land Data Assimilation

[4] The Global Energy and Water Cycle Experiment (GEWEX) is an integrated program of research, observations, and scientific activities ultimately aiming to the prediction of global and regional climate change (http://www.gewex.org).

system (GLDAS; Rodell *et al.*, 2004). (2) Comparison long-term seasonal modelled streamflow to observed long-term seasonal streamflow for 12 large (>10,0000 km^2) (sub)tropical basins.

The following agreement indicators were computed for evaluation 1a and b (1461 small catchments):

- Density plots of observed and modelled average annual streamflow for all catchments,
- the slope of the linear regression and coefficient of determination for the previous plot,
- plots of the cumulative distribution of relative bias between modelled and observed streamflows and
- plots of the cumulative distribution functions of the parametric (Pearson's) coefficient of correlation between modelled and observed monthly streamflow for all stations.

The following caveats should be considered when interpreting the results from the above evaluation (1a and b):

- Scaling errors: the comparison is performed between a grid cell of 1° resolution (*i.e.,* 10,000 km^2) and with catchment areas varying from 152–4049 km^2. It follows that the input data, particularly precipitation (also 1° resolution) may well not be representative of a catchment. This uncertainty in precipitation inputs will be propagated and may have a strong impact on modelled streamflow.
- Unknown river regulation: although care was taken to filter out regulated catchments using information on the location and catchment areas of dams, it is very difficult to verify other types of streamflow regulation and water extraction for various productive activities.
- Possible errors in streamflow records.
- The different forcing data used for the GLDAS models as well as differences in model structure can be expected to be an important factor underlying possible dissimilar results.

The following agreement indicators were computed for evaluation 2 (12 large basins):

- Observed and modelled average annual streamflows for all large basins,

- the coefficient of determination for the relationship between observed and modelled long-term seasonal streamflows,
- the root mean squared error (RMSE) for the observed and modelled long-term seasonal streamflows and
- plots of averaged and observed long-term seasonal streamflows.

The following caveats should be considered before interpreting the results from evaluation 2:

- Scaling errors may be attenuated in this larger-scale comparison due to grid cell aggregation; however this attenuation could be partly due to compensating errors caused by the averaging of streamflow amounts between cells.
- Differences in time-periods used for comparison: the GRDC long-term seasonal streamflows for different gauging stations correspond to different periods and are compared directly with no attempt of harmonisation. This is mainly because, besides dates of the start and end of the records, there is not enough information in the GRDC database to assess which data were used to compute the long-term seasonal streamflows. This would require the analysis of the underlying daily streamflow data.
- Effects of river regulation: some of the basins used in the comparison were considered to be strongly affected by regulation (see Section 5.5) and various forms of water withdrawal (*e.g.* irrigation). This version of W3RA-LUM does not include a reservoir regulation model.
- Errors due to routing may affect modelled streamflow, although this might not be very important for the proper prediction of long-term seasonal streamflow, differences in wet season peaks and recessions may occur.

5.4 Results

Comparison of modelled and observed streamflow in 1461 small catchments

The density plots of modelled versus observed streamflows from 1461 small catchments in Figure 5.7 shows that the W3RA-LUM model underestimates streamflow for the more humid catchments and overestimates streamflow for the more arid catchments. It explains 63% of the variance in mean annual streamflow. Around 40% of W3RA-LUM mean annual modelled

streamflow was within ±50% of observations whereas this was around 48% for W3RA (not shown). In terms of annual relative bias, cumulative distribution functions between modelled and observed streamflow for all models in the comparison show that W3RA-LUM is more positively biased than W3RA and slightly more negatively biased than CLM, whereas the other three GLDAS models are negatively biased (Figure 5.8a). The performance of W3RA-LUM is similar to that of CLM and W3RA and better than that of the other models in terms of (parametric) correlation coefficient (*R*) for monthly flows.

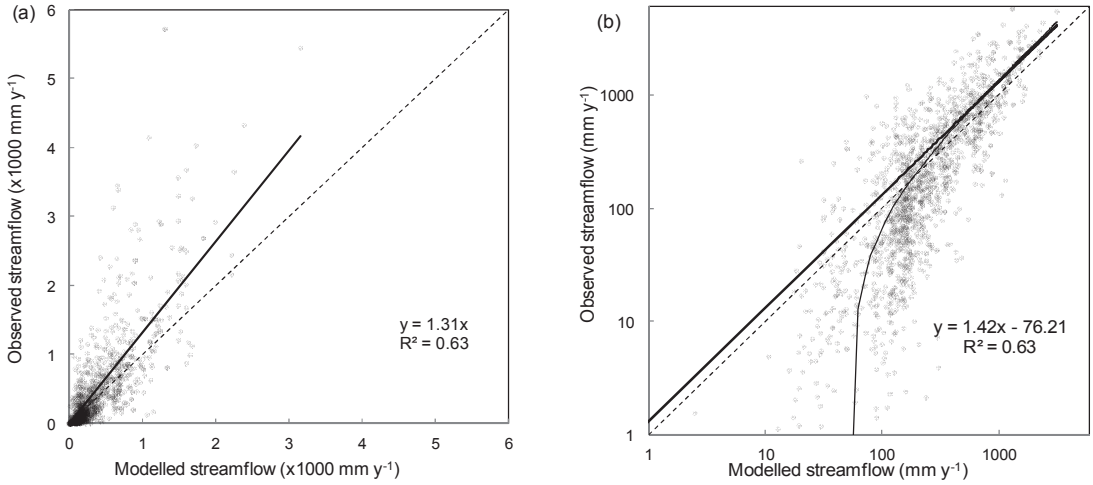

Figure 5.7 Density plots using (a) normal and (b) logarithmic axes for observed and modelled mean annual streamflow for 1461 small catchments including a linear regression (through the origin for the normal axis) and the coefficient of determination.

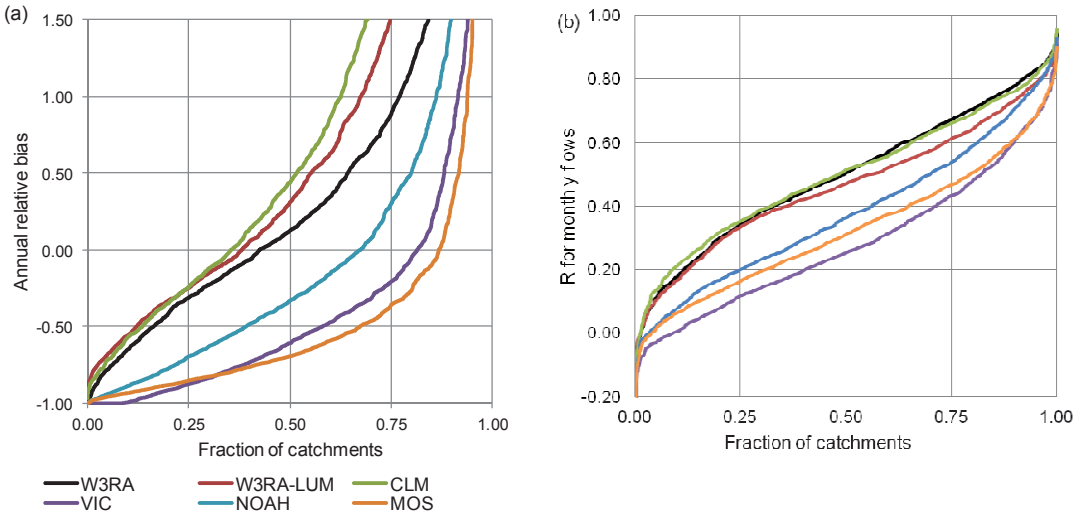

Figure 5.8 Cumulative distribution functions for modelled and observed streamflow from 1461 small catchments. (a) Annual relative bias and (b) parametric (Pearson's) correlation coefficient for monthly flows. W3RA-LUM, W3RA and the GLDAS models where used in the comparison (see text for details).

Comparison of modelled and observed streamflow in 12 large basins

Modelled long-term monthly streamflow for the grid cells covering 12 large (>10,0000 km^2) (sub)tropical basins was averaged over the entire area draining to the GRDC gauging station (Table 5-3) and compared to observed streamflows. Table 5-3 summarises basin characteristics and evaluation results whereas Figure 5.9 shows the corresponding seasonal streamflow patterns.

Table 5-3 Summary of basic characteristics and an evaluation of streamflow modelling results, including mean annual streamflow (Q_{tot}), Spearman's rank correlation coefficient (r) and the root mean squared error (RMSE) for 12 large tropical river basins.

				mean Q_{tot} (mm y^{-1})		Monthly	
GRDC ID	River	Station	Area (km^2)*	W3RA-LUM	GRDC	r	RMSE
1147013	Congo	Kinshasa-East	3747320	34	27	0.41	11.45
1159100	Orange	Vioolsdrif	866486	8	1	0.22	9.18
2186800	Xi Jiang	Wuzhou	329705	55	50	0.98	10.64
2854300	Krishna	Vijayawada	251355	45	17	0.86	30.29
2856900	Godavari	Polavaram	299320	43	27	0.96	21.57
2964130	Chao Phraya	Wat Pho Ngam	120693	40	10	0.79	35.73
3206720	Orinoco	Puente Angostura	836000	105	97	0.97	16.82
3629000	Amazonas	Obidos - Porto	4680000	83	94	0.99	11.21
3649250	Tocantins	Porto Nacional	177800	47	33	0.99	21.30
3651900	Sao Francisco	Traipu	622520	30	29	0.95	11.19
5101200	Burdekin	Clare	129876	22	6	0.94	20.70
5101300	Fitzroy	Yaamba	136398	18	3	0.74	18.81

***** Upstream area reported for the GRDC station. Areas used to average simulated streamflow predicted by W3RA-LUM were within 10% of GRDC areas.

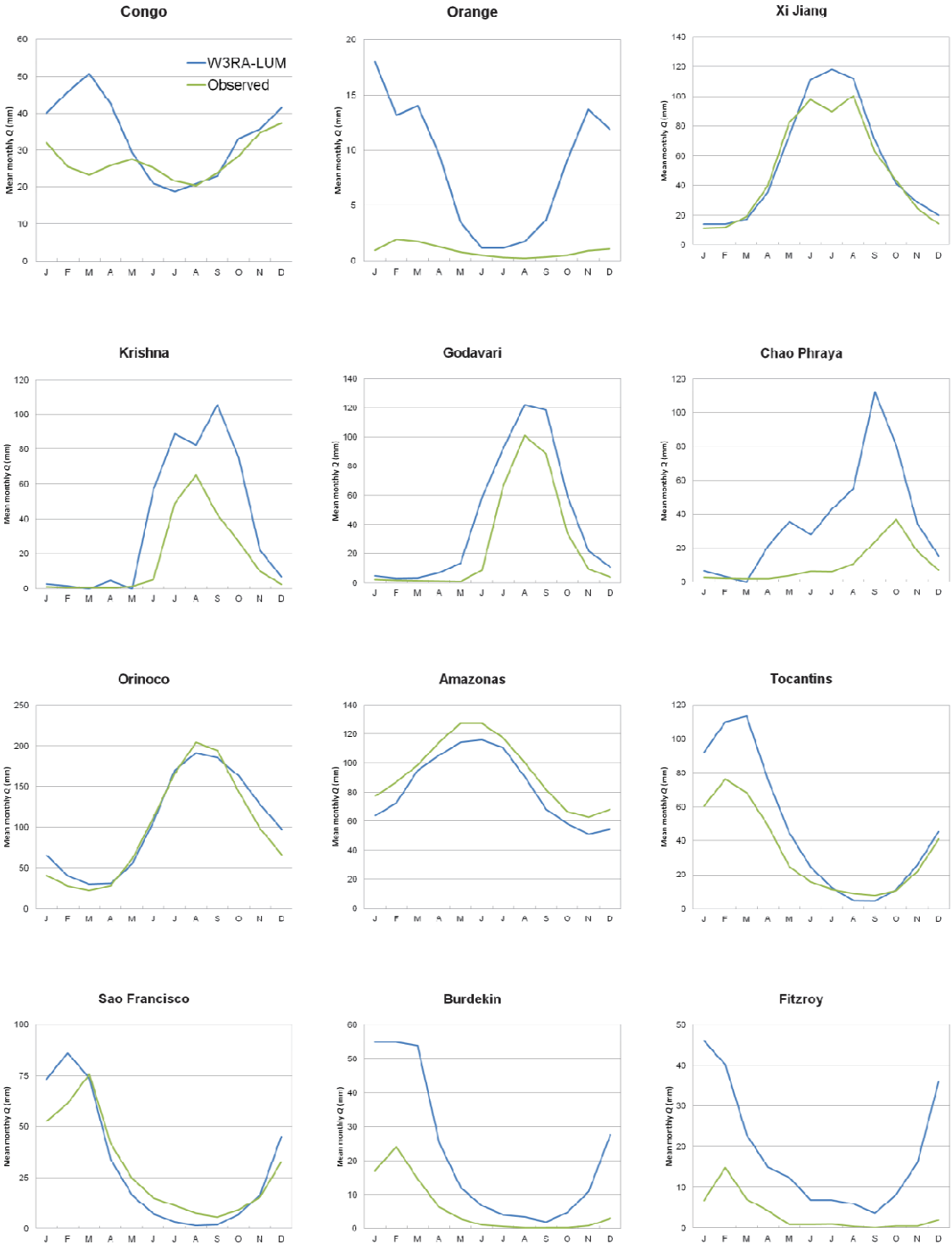

Figure 5.9 W3RA-LUM modelled (blue line) and observed (green line) long-term seasonal streamflow for 12 large (>10,000 km^2) (sub) tropical basins.

The long-term seasonal streamflow patterns simulated by W3RA agree reasonably well with observed patterns, indicating that the flow dependence on precipitation is appropriately

represented, but magnitudes differ particularly during the wet period in the more arid basins (*e.g.* Burdekin, Fitzroy). Except for the Orinoco and the Amazon, modelled streamflow was higher than observed. Generally, modelled streamflow showed more variability than observed streamflow whereas the onset of the wet period and the annual streamflow peak occurred earlier than was observed.

5.5 Discussion

The results indicate that streamflow simulated with W3RA-LUM has a reasonable performance compared to observations and outputs obtained with various other hydrological models. Although the estimated magnitudes are different, the obtained correlations for monthly flows suggest that the model is capturing the seasonal patterns of streamflow. The potential causes for the discrepancies between measured and modelled streamflow were covered in the caveats listed in the methodology (Section 5.5.3) and apply both to the present and other global hydrological models. Most global hydrological models, even calibrated ones, overestimate runoff in arid and semi-arid catchments (*e.g.* Widén-Nilsson *et al.*, 2007 and references therein). Besides river regulation and other withdrawals, some models do not simulate the various processes that may result in substantial internal losses in arid and semi-arid basins, such as open water evaporation and evaporation from riparian and irrigated areas (Widén-Nilsson *et al.*, 2007).

The model inter-comparison (Figure 5.8) highlighted the reasonable performance of W3RA-LUM. The model's estimates were better than those obtained with most other models used in the comparison in terms of monthly correlation, although positive bias is evident. Monthly streamflow simulations by the calibrated W3RA model showed better agreement with observed streamflow in terms of bias and correlation although this improvement came at a cost. The aim of the calibrated version was to better reproduce observed streamflow but this exerted and undue influence on other hydrological processes. For example, the calibrated parameters resulted in soil evaporation estimates that were substantially greater than in the (non-calibrated) version W3RA-LUM. The model's structure prevents unsustainable soil water withdrawal (*i.e.,* does not permit negative soil moistures to develop), and as a consequence there must be a compensation of water withdrawal by vegetation which is affected by an unrealistic change in

the factors that control evapotranspiration such as vegetation leaf area index (Neil Viney; CSIRO, pers. comm.).

Seasonal streamflow patterns for large river basins were also more or less captured by the model (with few exceptions). In some of the examined basins, river regulation is undoubtedly an important factor for the obtained differences between modelled and observed streamflow (Table 5-3), with large dams located along the main river stem in many systems (Figure 5.10). Of all the basins used in this analysis, the Amazonas/Orinoco and the Congo were considered to be the least affected by regulation or irrigation withdrawals (Nilsson *et al.*, 2005), although averaging between grid cells may be partly responsible for the observed good agreement. As an example of a river basin that is heavily affected by regulation, the Oranje river (Figure 5.10a), runs through a marked precipitation gradient. There are five dams situated along the main river stem, but there are many smaller ones in the basin's runoff-producing upland subcatchments (Lehner *et. al.*, 2008, not shown). Losses due to irrigation withdrawals, open water evaporation and evapotranspiration from riparian vegetation along the river's course in the arid Namib/Kalahari Desert also contribute to the marked differences between observed and modelled streamflow. In the case of the Congo, other global models specifically used for streamflow simulation, also overestimated and enhanced streamflow variability (Döll *et al.*, 2003; Widén-Nilsson *et al.*, 2007), as again observed in the seasonal streamflow predicted by W3RA-LUM. This may be partly due to errors in observed streamflow.

Regulation will not only distort modelled seasonal flow patterns, particularly in basins that experience long delays in the release of water, but it also controls the flow during the dry season. In areas strongly affected by regulation, any impacts of LUCC on dry season flows may well be (much) less pronounced or even irrelevant in terms of water quantity. This is more relevant in seasonally semi-arid areas than in humid areas, since a larger proportion of precipitation will be stored in reservoirs. However, for most dam systems the stored amount will be small relative to the total precipitation or streamflow (Mark Mulligan, King's College London, pers. comm.).

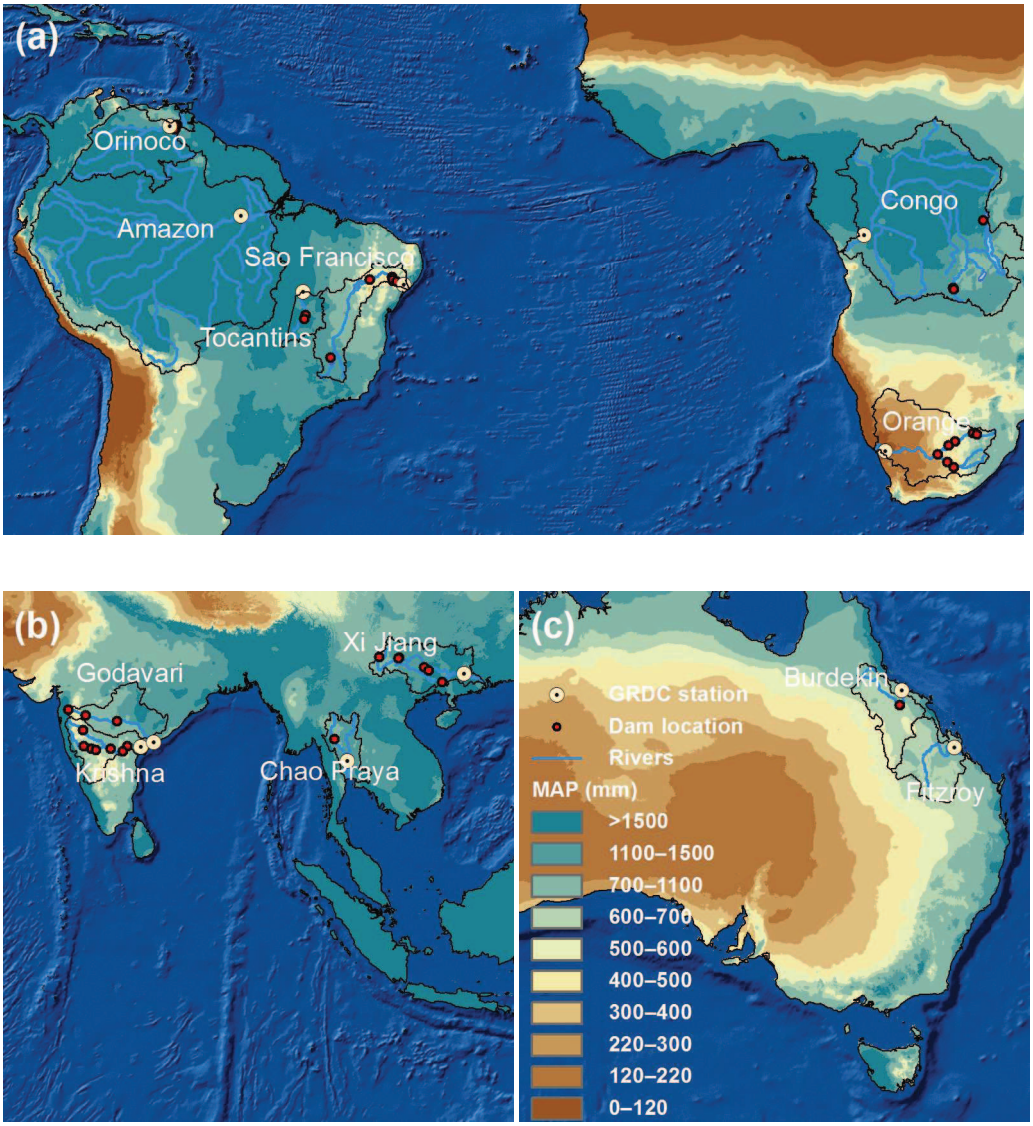

Figure 5.10 River basin boundaries (black lines), location of dams along the main river stem (red dots), and location of GRDC gauging stations used in the analysis (black/yellow dots). Colour scale represents the mean annual precipitation according to WORLDCLIM (Hijmans *et al.*, 2005).

5.6 Summary and conclusion

This chapter provided a detailed description of the development and implementation of the W3RA-LUM model for potential land use and land cover change (LUCC) scenario modelling framework. The Soil Conservation Service Curve Number Method (SCS-CN) was chosen to translate impacts of LUCC on the production of surface runoff (storm flows) as a function of soil

type and degree of surface degradation. The SCS-CN method is currently the only method available for the global application of these scenarios that has a strong empirical basis.

The model development philosophy of W3RA-LUM, based on AWRA-L (Van Dijk, 2010a), strived towards a parsimonious representation of simulated hydrological processes. In addition, the emphasis was on utilising parameters that could be reasonably estimated *a priori* or that could be related to catchment climatic characteristics. This approach may enhance model performance when applied in ungauged catchments.

A background review highlighted the capabilities of AWRA-L to capture the hydrological impacts of vegetation dynamics and change, and to reproduce patterns and estimates of actual evapotranspiration for a variety of Australian environments. These capabilities were not evaluated separately for W3RA-LUM. However, the processes associated with vegetation dynamics (including the corresponding model structure and parameter values) were largely identical and thus these capabilities should remain similar. More tests are to be conducted in Chapter 6 to further elucidate W3RA-LUM's capability to represent the effects of LUCC.

To use the SCS-CN method within W3RA-LUM, various indicators of land cover and soil surface condition had to be computed globally. A method to obtain curve numbers (CNs) pan-tropically was devised and adjusted to represent the characteristics of tropical soils. The resulting CN values were within design CNs reported for various tropical sites and elsewhere.

An evaluation of modelled against observed streamflow was performed for 1411 catchments with an area much less than the grid cell scale of the modelling (10,000 km^2), as well as for 12 large (>10,000 km^2) (sub)tropical river basins. The results indicate that W3RA-LUM shows a reasonable performance compared to observations and, especially, other hydrological model, particularly in terms of capturing monthly flows and seasonal patterns.

Besides model structure parsimony, uncertainty in parameter values, scale factors (contrasts between catchment and grid cell sizes), and errors in climate and streamflow data, there are various anthropogenic influences on streamflow that are difficult to quantify (notably river regulation and water withdrawals) and have an unknown influence on model performance.

Based on the present findings the following scenario modelling recommendations are made:

- Model outputs are best interpreted as local fluxes in catchments having a size up to the model's grid resolution.
- At this scale and for larger aggregations, the unknown influence of river regulation on model outputs needs to be quantified.
- Due to uncertainty in model outputs and bias, results should be interpreted in geographically relative rather absolute terms.

  Further testing is required to assess the capabilities of W3RA-LUM to represent the hydrological effects of vegetation dynamics and LUCC.

Chapter 6 Modelling the pan-tropical impact of LUCC and surface degradation on dry season flows and comparison with empirical observations at sites across the tropics

Contents

6.1 Introduction

Land use and land cover change (LUCC), deforestation in particular, have a direct effect on hydrology through changes in the partition of rainfall into water that is either evaporated or runs-off. LUCC is frequently accompanied by changes in surface infiltration characteristics (Lal, 1996; Elsenbeer *et al.*, 1999; Ilstedt *et al.*, 2007). At the catchment scale, these changes can cause a decrease or an increase in baseflow, depending on the trade-off between the associated changes in vegetation water use (the 'pump' effect) and infiltration (the 'sponge effect'; Bruijnzeel, 2004). The so-called soil 'sponge' effect of forests promotes baseflow by enhancing infiltration rates due to the effects of high soil organic matter and a well-developed root network, creating abundant bioporosity (Bonell, 2005). Water that is not evaporated or directly lost to streams via rapid surface runoff, infiltrates and is stored in the soil or the groundwater system and ultimately released as baseflow. If due to LUCC the infiltration capacity of the soils is strongly diminished, and if prevailing precipitation intensities are greater than this infiltration capacity, then overland flow occurrence will be enhanced (*e.g.* Bonell and Williams, 2009; Peña-Arancibia *et al*., 2012). The associated decrease in infiltration may cause reductions in soil profile moisture storage (and thus percolation), which will reduce the storage of groundwater and thus groundwater flows. This redistribution of water assumes additional importance if it takes place in catchments dominated by a seasonal precipitation regime (wet-dry cycles). Under such conditions, infiltration and percolation feed a groundwater system, which in turns feeds springs that maintain the stream during the dry season. In these catchments, the seasonal distribution of streamflow throughout the year is more important than total annual water yield *per se*, as water availability during the dry season is both crucial to sustaining ecosystems and an adequate water supply for productive activities (Poff and Ward, 1989; Bruijnzeel, 2004; Maneta *et al*., 2009).

In the tropics, agricultural expansion since the 1980s – estimated at 629 million ha (FAO, 2006) – occurred mostly at the expense of previously undisturbed forests (Gibbs *et al.*, 2010). The productivity of post-forest LUCC generally decreased because of soil degradation and/or conversion to less productive agro-ecosystems (DeFries and Bounoua, 2004). According to Bai

et al. (2008), some 23% of the terrestrial land suffers from degradation, mostly in the tropics. In the absence of major policy changes and technological innovations, it is estimated that 30–87 million ha of agricultural land will have to be taken out of production due to land degradation, again mostly in tropical countries (Lambin and Meyfroidt, 2011), whereas another 125–416 million ha would be needed to sustain global demand of agricultural products under future population and consumption projections (Meyfroidt and Lambin, 2011). Given the current population growth and LUCC trends, this expansion will likely take place in forested lands in tropical developing countries (*e.g.* Hartemink *et al*., 2008). Concurrently, there is evidence that more intensive farming practices have triggered new land degradation processes at large scales across tropical landscapes (Loker, 1994; Turkelboom *et al.*, 2008). When more and more land is converted to intensively cultivated or grazed lands, the absence of adequate soil conservation practices is likely have an impact on soil infiltrability and therefore on dry season flows (Bruijnzeel, 1990; Ziegler *et al*., 2009).

At the regional to global scales, modelling studies of the impact of LUCC on hydrology have mainly focused on the streamflow impacts induced by vegetation change through changes in vegetation water use (*e.g.* Gordon *et al.*, 2005; Mulligan and Burke, 2005; Trabucco *et al*., 2008; Mao and Cherkauer, 2009; Mishra *et al*., 2010). On the other hand, only a handful of regional studies have focused on the importance of changes in soil physical characteristics as a result of LUCC in order to explain hydrologic change (*e.g.* Mahé *et al*., 2005; Beck *et al*., 2013). Ascertaining the full pan-tropical impacts of LUCC – *i.e.,* including both vegetation and soil changes – on dry season flows is the main aim of this chapter. This aim (*cf.* Chapter 1), incorporates the following specific objectives: (*i*) to define reference hydrological conditions under natural forest conditions; (*ii*) to evaluate where tropical LUCC can be expected to have the greatest impacts on dry season flows; and based on corresponding changes in evapotranspiration and infiltration (*iii*) to assess potential areas for land rehabilitation and regeneration of hydrological services in degraded areas through reforestation.

Hydrological modelling with W3RA-LUM and three maps depicting (a) potential forest cover, (b) current and (c) future forest cover were used to attain these objectives. To make W3RA-LUM amenable to this type of LUCC scenario modelling, the model's structure and parameterisation were modified as described in Chapter 5. Besides changes in land cover that directly affect evapotranspiration (*AET*), the new model structure (akin to the Soil Conservation Service Curve Number Method; USDA, 1986) permits the modification of those soil parameters that affect surface infiltration characteristics (see Section 5.3.1.1 for details).

The respective hypotheses that were advanced to address the above objectives are represented by the following four situations (see also Figure 1.3, Chapter 1):

(I) In situation A, deforestation associated with small or no changes in surface infiltration characteristics (in the case of low impact logging, soil conservation measures, low rainfall erosivity, stable soil aggregates or a combination thereof; *cf.* Edwards, 1979) will invariably lead to an increase of dry season flows, due to the smaller water use and interception of the grasses and crops replacing the forest.

(II) In situation B, deforestation (loss of the 'pump' effect) associated with negative changes in surface infiltration characteristics (loss of the 'sponge' effect due to soil compaction, logging and/or mechanized agriculture or a combination thereof) can either decrease or increase dry season flows, depending on the trade-off between the associated changes in vegetation water use and infiltration, respectively.

(III) In situation C, forestation accompanied by little changes in surface infiltration characteristics will invariably lead to a decrease of dry season flows, due to the larger water use and interception of the forests replacing grasses and crops.

(IV) In situation D, forestation associated with negative changes in surface infiltration characteristics (*e.g.*, due to the poor soil building capacity of the planted species or repeated surface disturbance during forest maturation in the form of

litter removal, understory harvesting, or grazing; *cf.* Ghimire *et al*., 2013) will invariably lead to a decrease in dry season low flows due to the higher water use and rainfall interception losses of the forest vegetation, *i.e.,* the forest acts predominantly as a 'pump'. Conversely, if surface infiltration characteristics are positive (*e.g.*, the development over time of a layer of organic matter that enhances moisture retention and a root network that enhances infiltration; *cf.* Ghimire *et al*., 2013), dry season flows can either decrease or increase again depending on the trade-off between the associated changes in vegetation water use and infiltration, respectively.

Two types of analyses are conducted here to test these hypotheses: (1) vegetation water use and infiltration changes are used in a pan-tropical sensitivity analysis to determine the impacts of LUCC on evapotranspiration and streamflow. This sensitivity analysis is also conducted at sites for which there is published observational evidence of changes in dry season flows due to LUCC. (2) Pan-tropical 'what if' modelling scenarios are used to assess the historical and future impacts of LUCC. Spatial maps are derived in (1) and (2) to identify 'hotspots' in which LUCC may have important impacts on dry season flows.

This chapter is organised as follows. The next section describes: (a) the global maps used for scenario modelling; (b) the approach for the sensitivity analysis; (c) the approach for the 'what if' scenarios and; (d) a description of the indicators used to assess LUCC impacts on streamflow. Subsequently, results are presented for (b) and (c), followed by discussion and conclusion.

6.2 Methodology

6.2.1 LUCC maps

Three global forest cover maps resampled to 1° grid cell resolution and representing different epochs were used in scenario modelling: (1) potential or undisturbed past forest cover, (2) current forest cover and (3) future forest cover. The three maps were used to determine (a) the forest cover loss from undisturbed to current conditions and (b) the projected forest cover loss,

from current to future forest cover based on currently observed trends. Each of the maps is discussed briefly below.

Potential forest cover (B98)

Billington *et al*. (1998), hereafter referred to as B98, compiled an original forest cover map from various regional maps in order to calculate total original forest loss. The map shows the extent of global forest cover before large pre-agricultural human impact (*i.e.,* roughly prior to 1500 A.D.). Billington *et al*. (1998) estimates suggest that about 47% of the land surface (or 6.2 billion ha) was covered with forests. Although humans managed forest before agriculture, most of the forest loss in the tropics may have occurred in the last two centuries (Shvidenko *et al*., 2005). The original forest map used here was amended to include areas not classified as forests but that are currently under forest cover today (see Mulligan, 2010 for details).

Current forest cover (H03)

The current forest cover map, hereafter referred to as H03, was estimated from the 500 m grid cell resolution tree cover derived from MODIS reflectance data for the period 2000–2001 (Hansen *et al.*, 2003).

Future forest cover (DNP06)

The future forest cover map developed by De Noblet-Ducoudré and Peterschmitt (2006), hereafter referred to as DNP06, was derived from the IMAGE (Integrated Model to Assess the Global Environment) model (Alcamo *et al.*, 1998). IMAGE simulates LUCC in each region as driven by demands for food, timber and biofuels, in addition to changes in climate. The land use change scenarios were used in the IPCC Third Assessment Report on Climate Change (IPCC, 2001). The scenario used here (A1b) corresponds to moderate demand forces and represents a conservative estimate of future LUCC (*e.g.* DeFries and Bounoua, 2004). The grid cell resolution is 0.5°, while the temporal resolution is every 10 years from 1990 to 2100 and showing changes in crop fraction in each 0.5° grid cell. The year 2100 was used here to represent future forest cover.

6.2.2 Sensitivity analysis

Sensitivity analysis for selected sites

This analysis, similar to the one conducted by Mao and Cherkauer (2009), was performed to understand the sensitivity of hydrologic responses to cover type and soil conditions and to compare these with documented cases of impacts of LUCC on dry season flows introduced in Chapter 1 and 2. Firstly, W3RA-LUM simulations were run in multiple grid cells for different combinations of forest cover percentage and associated soil conditions (SC) in several tropical locations for which previous observations are available. A list of approximate locations and climatic characteristics is presented in Table 6-1. Some relevant details of the LUCC impacts on hydrology at each site are provided below.

Table 6-1 Approximate location of grid cells used in sensitivity analysis and associated climatic characteristics including: mean annual precipitation (MAP), mean annual potential evapotranspiration (PET) and precipitation seasonality index (SI) for the years 1948–2008. Climatic characteristics were computed from the Princeton climate dataset (Sheffield *et al*., 2006).

Location	Lat	Long	MAP (mm y^{-1})	PET (mm y^{-1})	SI*	Main reference
Upper Konto (Indonesia)	7.52°S	112.24°E	1964	1526	0.65	Rijsdijk and Bruijnzeel (1991)
Babati (Tanzania)	4.15 °S	35.46°E	712	2075	0.87	Sandström (1995)
Tocantins (Brazil)	11.05°S	48.25°W	1503	1911	0.82	Costa *et al.* (2003)
Upper Mahaweli (Sri Lanka)	7.12 °N	80.40°E	1878	2033	0.37	Bruijnzeel (2004)

* SI indicates the intra-annual seasonality of precipitation. It varies from zero (all months with the same precipitation) to 1.83 (all precipitation occurring in one month): values <0.19 indicate very equal precipitation, whereas values between 0.20 and 0.99 indicate a seasonal regime and values >1 a short wet season.

In the upper Konto catchment in East Java, 33% of the original forest was replaced by rainfed cropping; the subsequent increase in sealed surfaces such as roads and settlements reduced the infiltration opportunities in those areas (Rijsdijk and Bruijnzeel, 1991; Rijsdijk *et al*., 2007). The excess water associated with reduced evapotranspiration following forest clearing, did not override the loss of soil and groundwater recharge due to diminished infiltration, thereby, changing the seasonal distribution of streamflow and reducing dry season flows.

Sandström (1995) established that the observed increase in peak flows in sub-humid Babati (northern Tanzania) since mid-1940s was caused by accelerated forest clearance and not climatic variability. The loss of bioporosity due to precipitation impact on exposed soil surfaces and human-induced compaction was deemed key to the reduced surface infiltration rates.

Costa *et al.* (2003) analysed a 50-year long time series of streamflow for the large (175,360 km^2) Tocantins Basin in Amazonia, separating the record into a period with relatively little LUCC (1949–1968), and a period during which 49% percent of the catchment was cleared for agriculture and pasture (1979–1998). Although precipitation did not change significantly over the entire period, the results indicated that the mean annual streamflow increased by 24% and the wet season peak occurred one month earlier (see Figure 6 in Costa *et al.*, 2003). The increase was ascribed to a reduction in evapotranspiration and infiltration and a concurrent increase in streamflow.

Another example of decreased dry season flows was observed in the 1,100 km^2 upper Mahaweli catchment in Sri Lanka, which was ascribed to conversion of tea plantations to annual cropping and home gardens, without appropriate soil conservation measures (Madduma Bandara and Kurupuarachchi (1988) in Bruijnzeel, 2004). Precipitation and streamflow time-series for the 1940–1980 period showed that, although there was no significant change in precipitation, there was an overall increase in wet season flows and a slight decrease in dry season flows.

Three different sensitivity simulations with W3RA-LUM were conducted for each of these four locations: (*i*) sensitivity to changes in forest cover percentage, (*ii*) sensitivity to changes in soil condition (SC), and (*iii*) sensitivity to changes in both forest cover and SC. Forest cover was assumed to be either 0% or 100%, whereas the soil parameters were varied according to forest presence or absence. Runoff Curve Numbers for the two forest cover percentages were computed by supplanting the dominant forest type (according to the UMD Global Land Cover Classification, see Section 5.3.1.2) with grasslands and *vice versa*. It was also assumed that in the case of a change in SC, any decrease in forest cover was associated with a change from good to poor hydrologic SC (*cf.* Table 5-1), thus depicting the most extreme case of soil disturbance and *vice versa* for increases in forest cover. Subsequently, the simulations were run

for each location and parameterisation using daily Princeton precipitation data for the years 1948–2008 as forcing (Sheffield *et al*., 2006). Long-term intra-annual plots of streamflow were used to interpret the results.

In summary, the following simulations were run: (1) 100% forest cover (100FC), (2) 0% forest cover (*i.e.,* 100% grass cover, 0FC) and no associated soil change, (3) 100% forest cover and maximum negative change in soil conditions (*i.e.,* 100% forest cover + SC or 100FCSC), the most hypothetical of the four simulations (*i.e.,* rarely occurs in practice), to separate the impact of a change in infiltration characteristics from that of altered vegetation water use, and (4) 0% forest cover and maximum negative change in soil conditions (*i.e.,* 0% forest cover + SC or 0FCSC).

Pan-tropical sensitivity

Sensitivity simulations were conducted at the pan-tropical scale using model runs corresponding to the 100FC, 0FC and 0FCSC scenarios. The 100% forest percentage cover was assigned to all grid cells containing ≥5% forest cover according to the B98 map. The 5% threshold was chosen to filter some semi-desert areas from the analysis. Spatial maps of indicators of streamflow regime alterations (see Section 6.2.4) were used to interpret the results.

6.2.3 'What if' scenarios

The 'what if' scenarios were used to identify 'hotspots' in which LUCC may have impacted, or may impact dry season flows. Three simulations were conducted using the three land cover maps described in Section 6.2.1 and associated runoff Curve Numbers computed as described in Section 5.3.1.2. As in the sensitivity analysis, runoff Curve Numbers for the forest cover percentages pertaining to each forest cover map were computed by supplanting the dominant forest type with grasslands. In addition, any decrease in forest cover was associated with a change from good to poor hydrologic SC. Subsequently, spatial maps of indicators of streamflow regime alterations were used to interpret the results.

To visualise the extent of LUCC for historical and future forest cover loss (Figure 6.1a and b), losses were estimated by subtracting the fraction corresponding to the expansion in other land uses (at the expense of forest) in each 1° grid cell. To derive the future forest cover map, it was assumed that already existing grassland/cropland will still be used as such in the future and that there is only continued expansion of agricultural land. In the tropics, projected decreases in the area under agriculture were limited to a few small areas in Southeast Asia (*i.e*. elsewhere the agricultural land area increased).

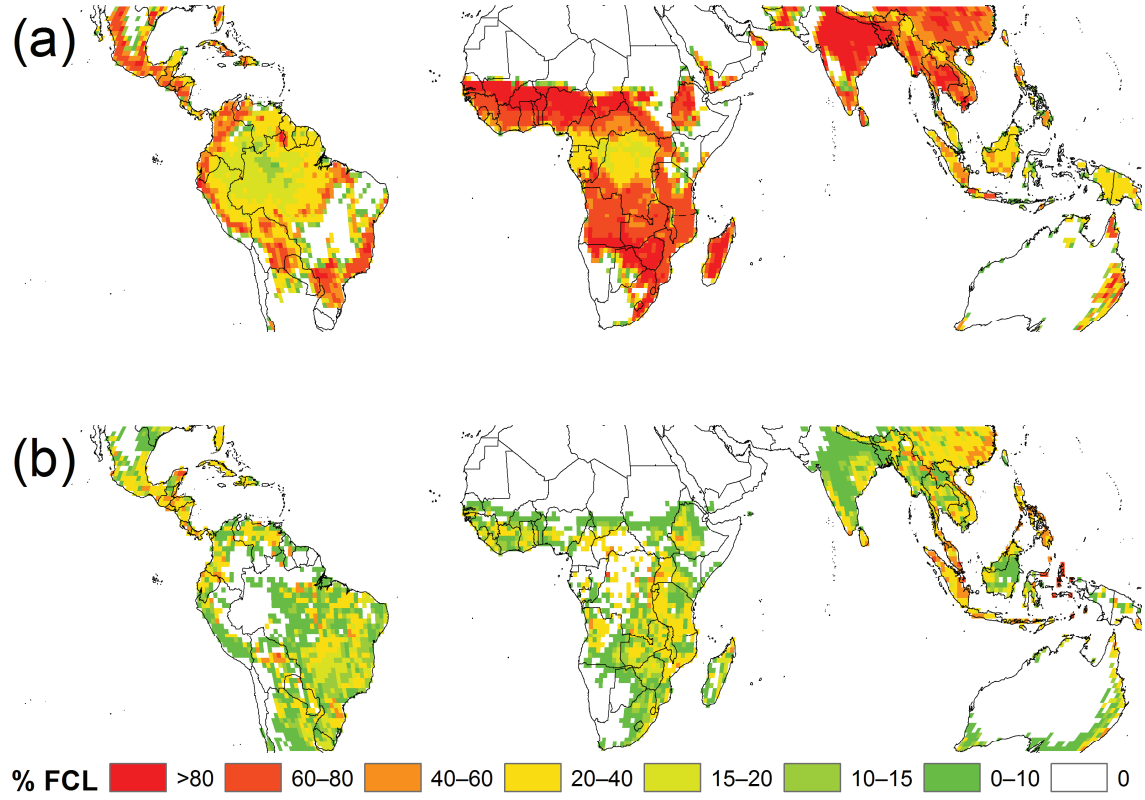

Figure 6.1 Scenarios of percentage forest cover loss (%FCL): (a) % FCL between the potential forest cover (B98) and the current forest cover (H03), *i.e.,* B98-H03. (b) %FCL between the present and a future forest cover (*i.e.,* in 2100) due to continued agricultural expansion (DNP06), *i.e.,* H03-DNP06.

The forest cover loss from undisturbed to current conditions shows a large reduction (> 40%) in the Andes, Central America, south-eastern Brazil, Sub-Saharan and southern Africa, most of

Asia and part of Australia (Figure 6.1a). In some cases this loss may be realistic (*e.g.* expansion of croplands in India, Southeast Asia, China and south-eastern Brazil; see Goldewijk and Ramankutty, 2004), in others this may be the result of the coarse resolution of the potential forest cover map. In the case of future forest cover loss, results show the maximum decrease in remote and undisturbed forest lands to be less than 20% in areas of central Amazonia, eastern Congo, Borneo, Sulawesi and Papua New Guinea. In other remote and undisturbed lands the decrease is generally less than 7% (Figure 6.1b). Conversely, the decrease in forest cover for grid cells with greater than 30% but less than 60% current forest cover under original conditions (*i.e.,* less dense types of forest or woodlands in climates with seasonal rainfall) is more intensive, more widespread and occurs for different types of forests.

It is noted that the proximity of these more seasonal and less dense forests to densely populated areas (representing higher extraction pressures) and their often rich agricultural soils make them more vulnerable to deforestation than humid forests (*e.g.* Songer *et al*., 2009).

6.2.4 Indicators of streamflow regime alterations

Three indicators based on monthly streamflow data were computed to locate grid cells for which streamflow regime has been altered by LUCC. The indicators were taken (and partly modified) from Döll *et al*. (2009). The following indicators were computed:

- The indicator for the effect of LUCC on long-term mean annual streamflow (ILTA) computes the relative difference in long-term mean annual streamflows before and after LUCC.
- The indicator for the effect of LUCC on streamflow seasonal amplitude (ISA) computes the relative difference in long-term mean seasonal amplitude (month with highest streamflow minus the month with the lowest streamflow) before and after LUCC.
- The indicator for the effect of LUCC on low flows (ILF) computes the number of months with decreased total flows out of four months with low flows, after LUCC compared to prior conditions. A period of four months of low flows was selected since in many areas the dry season lasts longer (Foster and Chilton, 1993).

Due to the uncertainty in model input data (particularly rainfall), predicted streamflow outputs and overall model bias, the resulting indicators are interpreted mostly in relative rather than absolute terms (see Section 5.6). In addition, due to the coarse scale of the analysis, the derived indicator values should be considered as first estimates only and used mainly to identify 'hotspots' of hydrological change after LUCC.

6.3 Results

6.3.1 Sensitivity analysis

Sensitivity analysis for selected sites

Three of the four study sites used in the sensitivity analysis have a strong seasonal precipitation (*P*) regime, with the wet season peaking in December-March, and a distinctive dry season extending several months during the May-October period (Figure 6.2). The exception is the upper Mahaweli basin in monsoonal Sri Lanka which has a bimodal precipitation regime peaking around April and November. In the upper Konto and Tocantins basins, the mean ratio of monthly *P* to the corresponding number of days with *P* (MPDR, a proxy of rainfall intensity) was <15 mm mo^{-1} per rain day in most months (Figure 6.2 and c), whereas it was >15 in the Mahaweli basin (Figure 6.2d). Relative to the amounts of monthly *P*, the sub-humid Babati site (Tanzania) had the highest MPDR (Figure 6.2b).

The mean annual results of the two most extreme simulations (i.*e*., 100FC and 0FCSC) are summarised in Table 6-2 and show that generally the higher long-term evapotranspiration ($\overline{E_{tot}}$) associated with the 100FC simulations results in a reduction in streamflow ($\overline{Q_{tot}}$).

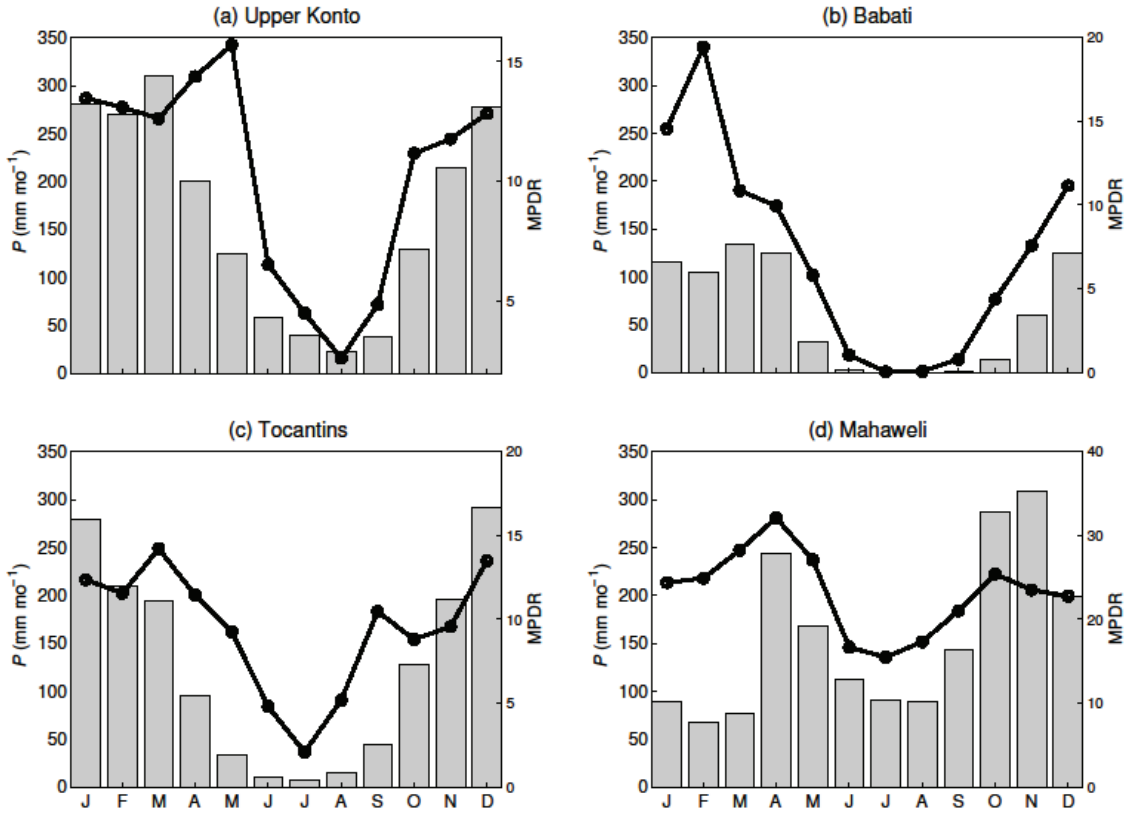

Figure 6.2 Mean monthly rainfall (*P* in mm, grey bars) and the mean ratio of monthly rainfall amount to the number of days with precipitation (MPDR, black line) for the years 1948–2008 as computed from the Princeton climate dataset (Sheffield *et al*., 2006) for the four catchments chosen for the sensitivity analysis.

The differences in $\overline{E_{tot}}$ range from 12 to 38%, whereas the range is -60– -27% in $\overline{Q_{tot}}$. On the other hand, the higher infiltration in the 100FC simulation shows a more commensurate contribution of baseflow ($\overline{Q_g}$) and storm flow ($\overline{Q_R}$) to $\overline{Q_{tot}}$ in the Tocantins (44 and 66% for $\overline{Q_R}$ and $\overline{Q_g}$, respectively) and upper Mahaweli (48 and 62% for $\overline{Q_R}$ and $\overline{Q_g}$, respectively) sites. Conversely, in the 0FCSC simulation, $\overline{Q_{tot}}$ is dominated by $\overline{Q_R}$, with much of the excess $\overline{Q_{tot}}$ due to reduced $\overline{E_{tot}}$ being translated into $\overline{Q_R}$ (61 and 74% in the Tocantins and upper Mahaweli, respectively) rather than $\overline{Q_g}$.

Table 6-2 Mean annual streamflow ($\overline{Q_{tot}}$), storm flow ($\overline{Q_R}$), baseflow ($\overline{Q_g}$) and evapotranspiration ($\overline{E_{tot}}$) with corresponding differences (prefix Δ) for two simulation scenarios, *i.e.,* 100% forest cover (100FC, in bold) and the completely deforested case with poor soil hydrological conditions (0FCSC, in italics) (see Section 6.2.2). Numbers in brackets correspond to the differences expressed in percentages.

	Tocantins	Mahaweli	Upper Konto	Babati
$\overline{Q_{tot}}$ (mm y^{-1})	**230**	**509**	**672**	**50**
	518	*884*	*933*	*127*
$\Delta\overline{Q_{tot}}$	-288 (-55)	-375 (-42)	-261 (-27)	-77 (-60)
$\overline{Q_R}$ (mm y^{-1})	**102**	**248**	**166**	**42**
	316	*655*	*422*	*116*
$\Delta\overline{Q_R}$	-214 (-67)	-407 (-62)	-256 (-60)	-74 (-63)
$\overline{Q_g}$ (mm y^{-1})	**129**	**261**	**507**	**8**
	202	*229*	*511*	*10*
$\Delta\overline{Q_g}$	-73 (-36)	32 (14)	-4 (-1)	-2 (-20)
$\overline{E_{tot}}$ (mm y^{-1})	**1273**	**1370**	**1292**	**662**
	985	*993*	*1031*	*586*
$\Delta\ \overline{E_{tot}}$	288 (29)	377 (38)	261 (25)	76 (12)

Streamflow in the upper Konto catchment is dominated by baseflow $\overline{Q_g}$ in the 100FC simulation (66%) whereas in the 0FCSC simulation its contribution is reduced to 25%. Conversely, $\overline{Q_{tot}}$ in the Babati catchment is dominated by storm flow $\overline{Q_R}$ (84 and 91% for the 100FC and 0FCSC simulations, respectively). Proportionally speaking, the differences in baseflow associated with the two scenarios are the main underlying cause of the predicted overall changes in $\overline{Q_{tot}}$, since the increase in storm flow in the 0FCSC simulation is around 60% in all catchments. Despite the increase in storm flow in all sites, the absolute difference in baseflow $\Delta\overline{Q_g}$ for the upper Konto and Babati were very small. In these two cases, the mean annual increase in infiltration converted to $\overline{Q_g}$ compensated the increase in $\overline{E_{tot}}$.

Looking at seasonal patterns for the upper Konto associated with the different land covers and soil hydrologic conditions, E_{tot} *and* Q_{tot} behave similarly in simulations with the same land cover, regardless of contrasts in soil conditions (Figure 6.3). E_{tot} responses to forest removal (with or without soil deterioration) show a decline during the dry season that is both delayed and deepened compared to the 100FC scenario (Figure 6.3b). The latter indicates lowered soil water availability in the shallow soil during this time of the year causing a further reduction into dry season E_{tot} by the grassland. A (very) slight reduction in Q_{tot} is observed during the dry months of June-August in the 0FCSC scenario compared to the 100FC case (Figure 6.3a). Nonetheless, changes in SC redistributed the components of Q_{tot}, with simulations with a (negative) change in SC having higher Q_R and lower Q_g, respectively (Figure 6.3c and d). Wet season flows (Q_{tot}) are enhanced in both simulations with 0FC whereas the seasonal peak occurs one month earlier (Figure 6.3a).

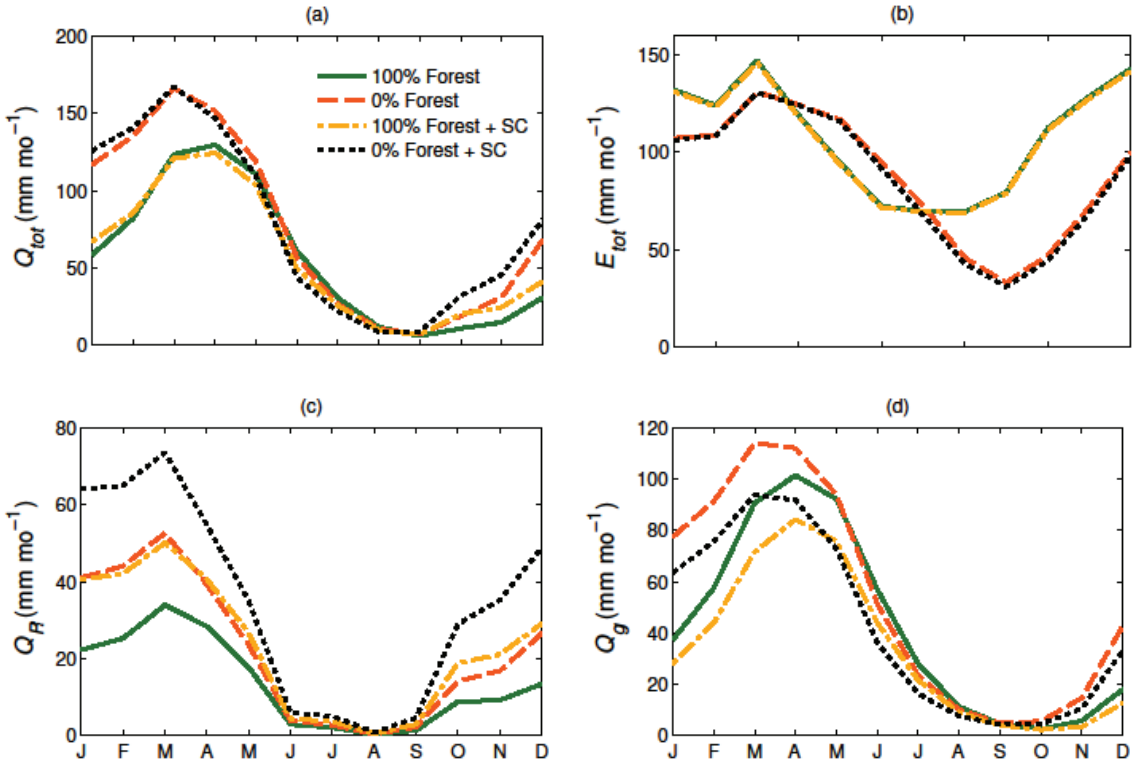

Figure 6.3 Mean monthly simulated (a) streamflow (Q_{tot}), (b) evapotranspiration (E_{tot}), (c) storm flow (Q_R) and (d) baseflow (Q_g) for 1948–2008 for the upper Konto catchment. Each coloured line represents simulations depicting different vegetation and changes in soil conditions; the term SC in the legend refers to changes in soil conditions limiting infiltrability: 100% Forest (100FC, green solid line), 0% Forest (0FC, orange dashed line), 100% Forest +SC (100FCSC, yellow line) and 0% Forest + SC (0FCSC, black dotted line).

In the sub-humid Babati catchment, changed soil conditions are more important than differences in vegetation cover *per se* (*i.e.*, E_{tot}). The two simulations with negative changes in SC have higher wet season flows than simulations without SC, regardless of forest presence or absence (Figure 6.4a). E_{tot} almost stops in the dry season in the 0FC simulations (Figure 6.4b) and this may be related to insufficient water storage in the shallow soil compartment under the prevailing sub-humid conditions. Higher E_{tot} is simulated for grass than for forest during the wet season. Simulations with 100FC sustain E_{tot} during the dry season (Figure 6.4b). Most of the changes in Q_{tot} result from changes in Q_R, with a negligible effect of changes in Q_g (Figure 6.4c and d).

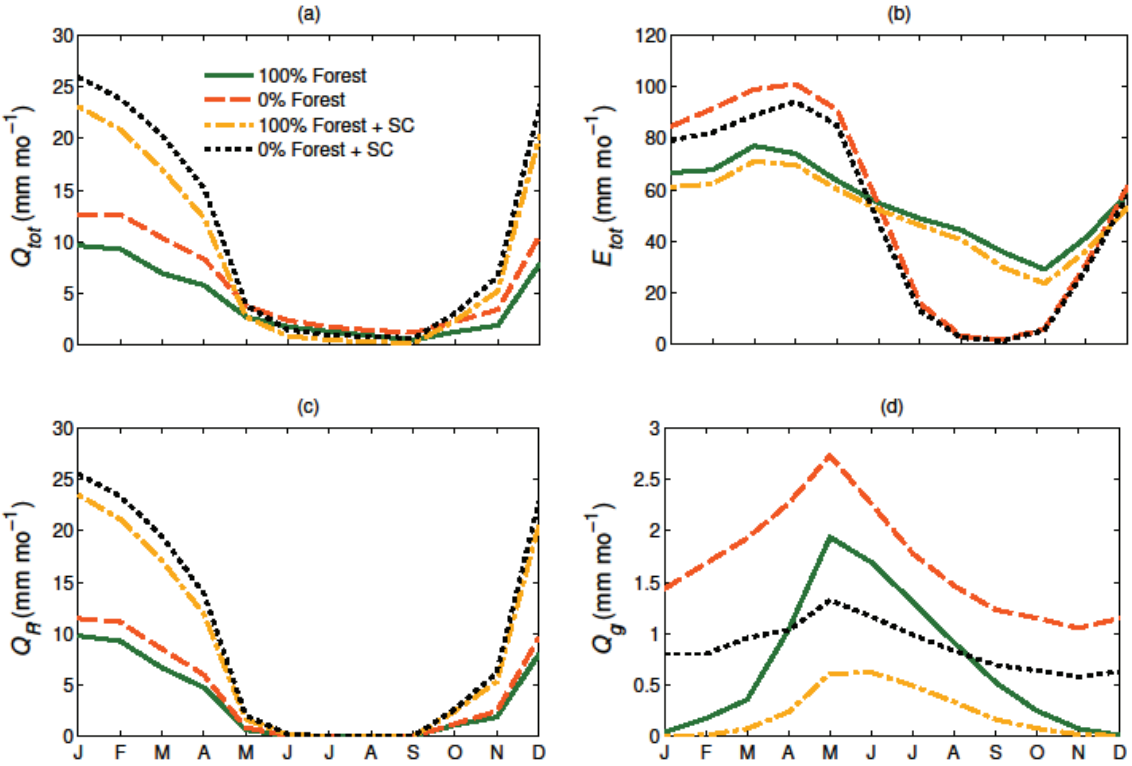

Figure 6.4 Idem as in Figure 6.3 but for the Babati catchment.

Vegetation cover is relatively more important than soil conditions in the Tocantins basin when it comes to explaining changes in seasonal streamflow patterns associated with the different scenarios (Figure 6.5). Patterns of E_{tot} in the Tocantins are similar to those in Babati, although there is sufficient water storage in the shallow soil layer to sustain some E_{tot} for the grassland

during the dry season. The amount of Q_g appears to be modulated by SC (Figure 6.5a) since seasonal peaks occurring one month earlier are observed in the simulations with changed SC. The latter results in a very slight reduction of initial dry season flows. The seasonal pattern for Q_R, naturally, varies according to rainfall (Figure 6.2c), whereas in scenarios with no negative change in SC it seems that soils 'carry over' water from the wet to the dry season, maintaining a delayed streamflow in the form of Q_g (Figure 6.5d).

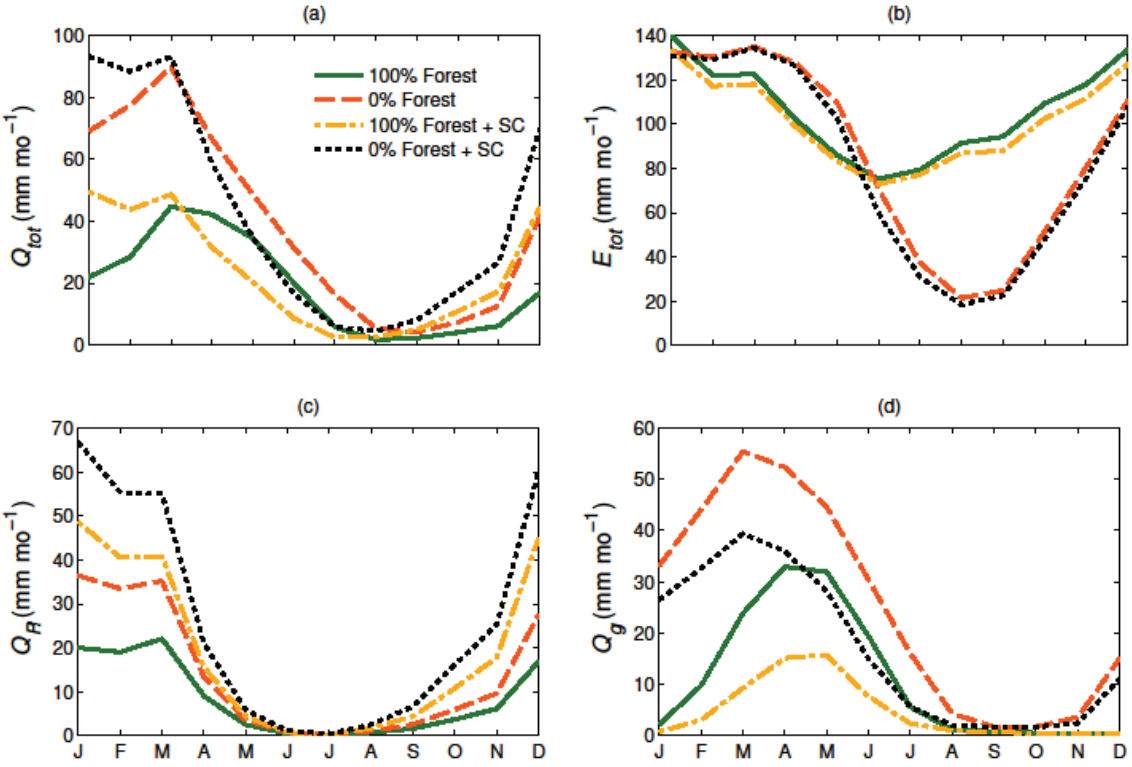

Figure 6.5 Idem as in Figure 6.3 but for the Tocantins basin.

In the humid upper Mahaweli catchment, the higher E_{tot} associated with the 100FC simulations (Figure 6.6b) results in generally less Q_{tot} throughout most of the year than in the simulations with 0FC (Figure 6.6b). The recession of Q_{tot} appears to be controlled by SC, with faster recessions observed in the simulations involving changed SC. Simulations with 0FC also have higher flows during the short dry season. The seasonal peak in flows is one month ahead (November vs. December) in the simulations with changed SC (Figure 6.6a).

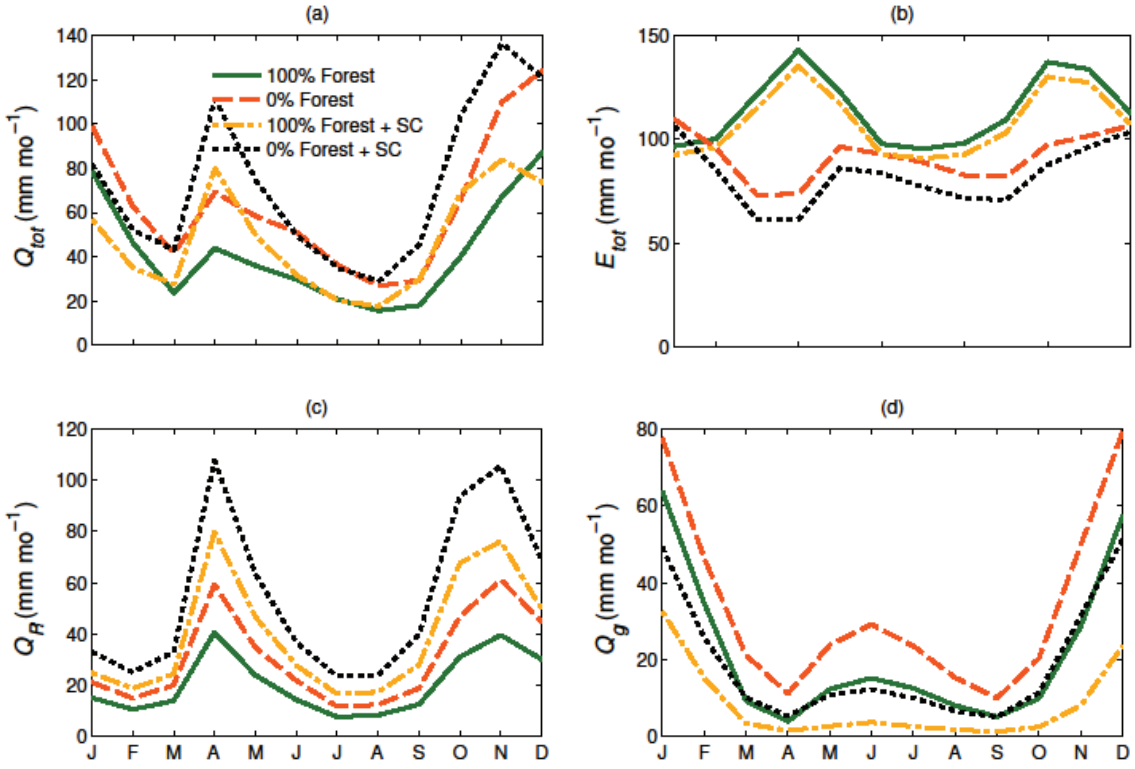

Figure 6.6 Idem as in Figure 6.3 but for the Mahaweli catchment.

Pan-tropical sensitivity analysis

Expressed as the percentage difference in long-term mean annual streamflow associated with completely forested (100FC) and deforested conditions (0FC) shows the long-term mean annual streamflow ($\overline{Q_{tot}}$) to increase pan-tropically after the removal of forests. This increase is 18% on average if only the vegetation cover changes, whereas it amounts to 26% if vegetation cover changes alongside soil conditions. Pan-tropical maps of the spatial variability in response to deforestation show that these changes vary geographically both for the 100FC and 0FC comparison (Figure 6.7a) and the 100FC and 0FCSC comparison (Figure 6.7b). In the former case, substantial increases in $\overline{Q_{tot}}$ (>30%) are observed in areas with high rainfall but also in some areas with seasonal rainfall (*e.g.* the Brazilian *cerrado* zone, Madagascar, Peninsular Southeast Asia, Sub-Saharan East Africa, northern Australia, north-east and west India, western Mexico), whereas the increases are smaller in more arid and semi-arid areas (eastern Brazil, southern Madagascar, inland Australia, central India, northern Mexico). On the other

hand, a similarly substantial increase is also observed in the more arid areas for the deforestation *cum* soil degradation case (100FC-0FCSC) (Figure 6.7b).

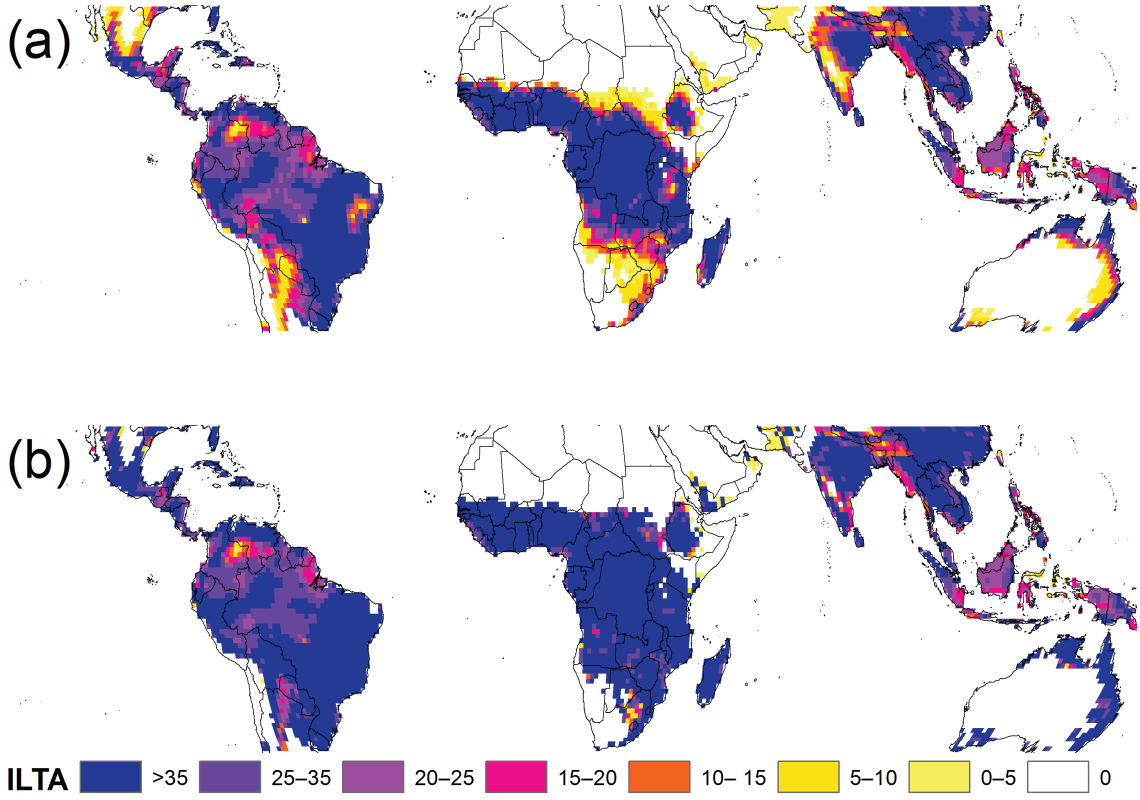

Figure 6.7 Relative change in long-term mean annual streamflow (ILTA) under LUCC impact and undisturbed conditions, expressed as a percentage of the long-term mean annual streamflow under undisturbed conditions for (a) deforestation only (100FC-0FC); (b) deforestation plus soil degradation (100FC-0FCSC).

The relative change in long-term mean annual streamflow (ILTA) are better illustrated in the form of cumulative percentage plots, where catchment humidity (HI=*P*/PET with PET being potential evapotranspiration) appears to be a good indicator of ILTA (Figure 6.8a and b). Differences in ILTA for 100FC-0FC (Figure 6.8a) and 100FC-0FCSC (Figure 6.8b) are more pronounced in more water-limited areas (HI<0.9) and less in energy-limited areas (HI>1.3).

Similarly, in terms of the seasonality index (SI; indicates the intra-annual seasonality of precipitation, see Table 6-1 for an explanation), ILTA increases especially in more seasonal areas (SI>0.6) after forest removal (Figure 6.8c). On the other hand, ILTA values do not vary

much in the case of forest removal followed by soil degradation, indicating smaller post-forest water use possibly as a consequence of reduced infiltrability and enhanced Q_R (Figure 6.8d).

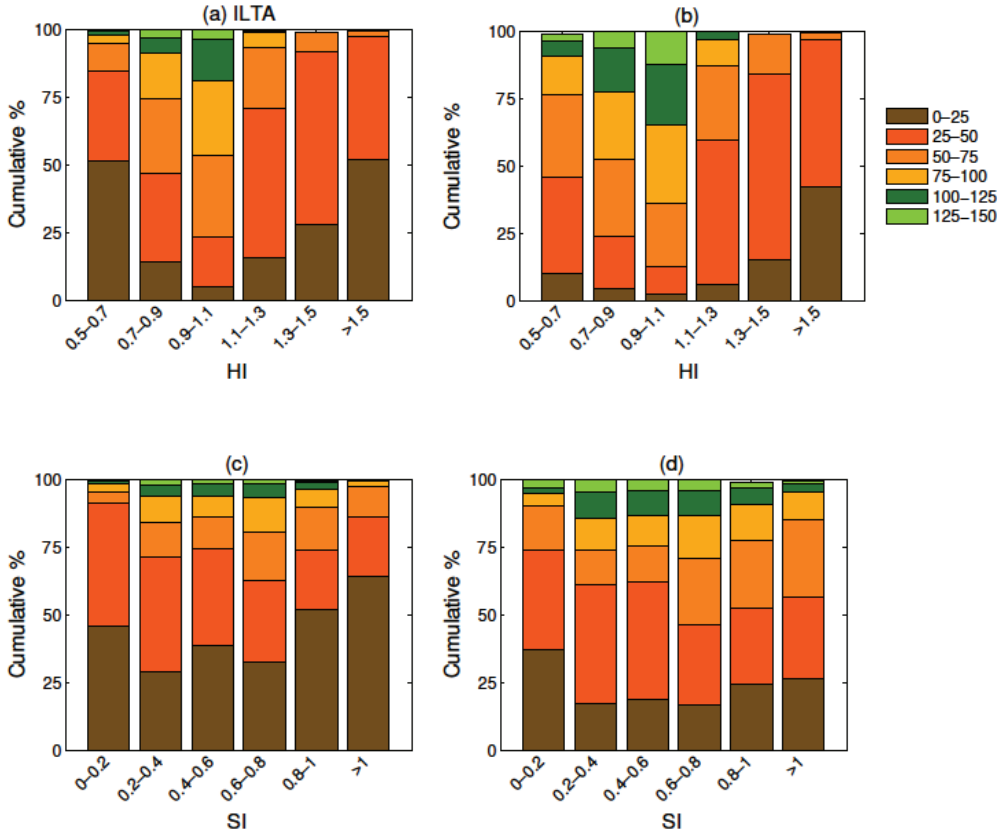

Figure 6.8 Cumulative percentage relative change change in long-term mean annual streamflow (ILTA) by humidity index (HI) for (a) 100FC-0FC; (b) 100FC-0FCSC. Colours represent different ranges in the percentage increase in ILTA, (c) and (d) idem but for the seasonality index (SI).

The patterns obtained for the differences in seasonal amplitude indicator (ISA) between the respective scenarios are similar to those found for ILTA, suggesting that most of the increase in $\overline{Q_{tot}}$ occurs during the wet season, particularly for the aforementioned arid and semi-arid areas in the 100FC-0FCSC scenario (Figure 6.9b). There are some exceptions, however. For example, not much change (0–1%) is found in some areas in the Congo and central South America in either scenario (Figure 6.9). In these humid areas, high rainfall may well translate into sufficient water storage in the shallow and deep soil storages. Because of the resulting commensurate increase in all months, ISA changes may not be as marked (although ILTA may increase). Pan-tropically, the average change in ISA is 11% for the deforestation scenario and 20% for the deforestation plus soil degradation scenario.

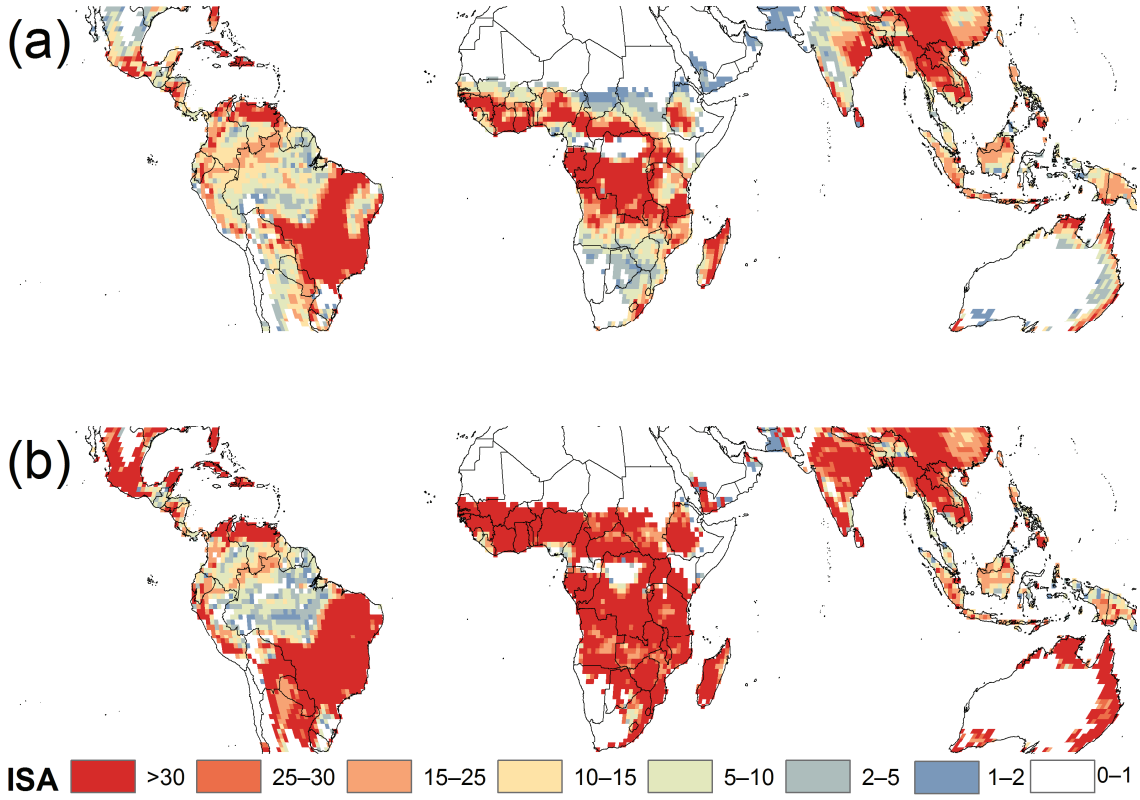

Figure 6.9 Difference between long-term mean seasonal amplitude (ISA) under LUCC impacts and prior conditions, expressed as a percentage of the amplitude under prior conditions for (a) 100FC-0FC; and (b) 100FC-0FCSC. See text for explanation.

The results for the third indicator of streamflow change, *i.e.,* the number of months with decreased Q_{tot} during the four-month low flow season (ILF), are only shown for the 100FC-0FCSC comparison (Figure 6.10). Results for the 100FC-0FC comparison were trivial and showed all months in the 0FC case to have higher Q_{tot} as would be expected on the basis of the corresponding reduction in E_{tot}. In areas with ILF>0, different combinations of climatic and/or physical characteristics captured by the model (*i.e.,* soil water holding capacity, vegetation type, surface infiltration conditions) are potentially important for the modelled LUCC impacts on dry season flows. The simulation results show areas with a reduction in Q_{tot} for some of the driest months, despite the decreases in E_{tot} associated with the conversion from forest to grassland, as also simulated before for some low flow months in the upper Konto or Tocantins catchments. As such, the surface degradation effect appears to override the evaporation effect for some of the driest months in these cases. Figure 6.10 shows several clusters of ILF>0, notably in Central America, northern South America, the Andes, Bolivia, Brazil, the Caribbean, Congo,

Gabon, Tanzania, Ethiopia, South Africa, Madagascar, India, Bangladesh, and several countries in Southeast Asia.

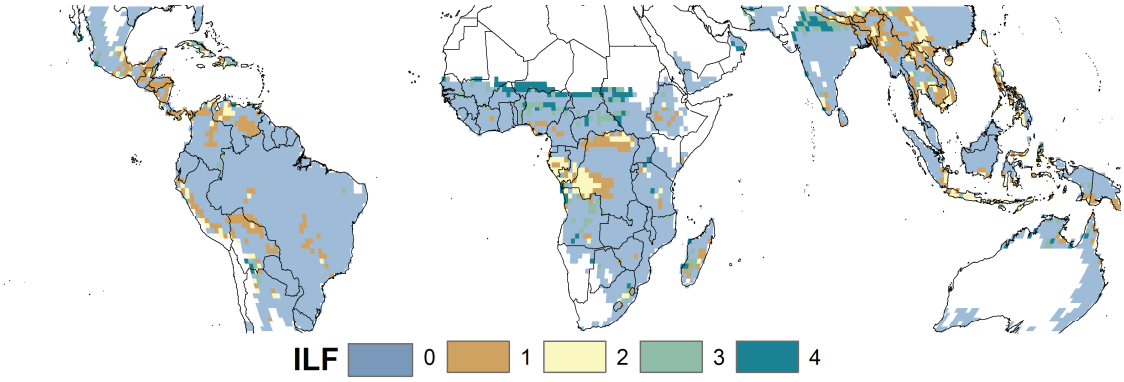

Figure 6.10 Number of months with modelled decreases in dry season flows (ILF) out of four months with low flows following deforestation and surface degradation (100FC–0FCSC). See text for explanation.

To shed further light on the possible causes underlying the patterns shown in Figure 6.10, the distributions of selected climatic and physical characteristics (including model inputs, parameters and state variables) of two cell sample populations were examined for the 100FC simulations: (*i*) all model grid cells (n = 3743, excluding semi-desert areas with MAP<400 mm y^{-1} where dry season flows may be small or nonexistent) and (*ii*) all modelled grid cells with ILF>0 (n = 704). The two populations were compared using normalised probability distribution plots (Figure 6.11).

Of all the climatic and physical characteristics examined, probabilistic distributions of the mean humidity index (HI), potential maximum soil water storage capacity for rainfall events (S_{max}), soil water content in the shallow and deep stores (S_{tot}), and groundwater recession coefficient (K_g) for the two model grid cell sample populations suggested a difference in climate type between the two samples, and a different way of partitioning net rainfall into surface runoff and infiltration (which is then evaporated or released as baseflow).

In terms of climatic attributes, cells with ILF>0 had higher HI-values (mean 1.20 ± 0.47 standard deviation) than all model cells (0.70 ± 0.58 standard deviation) (Figure 6.11a). Mean annual precipitation (MAP) and seasonality index (SI) probability distribution functions did not differ much between the two samples (not shown).

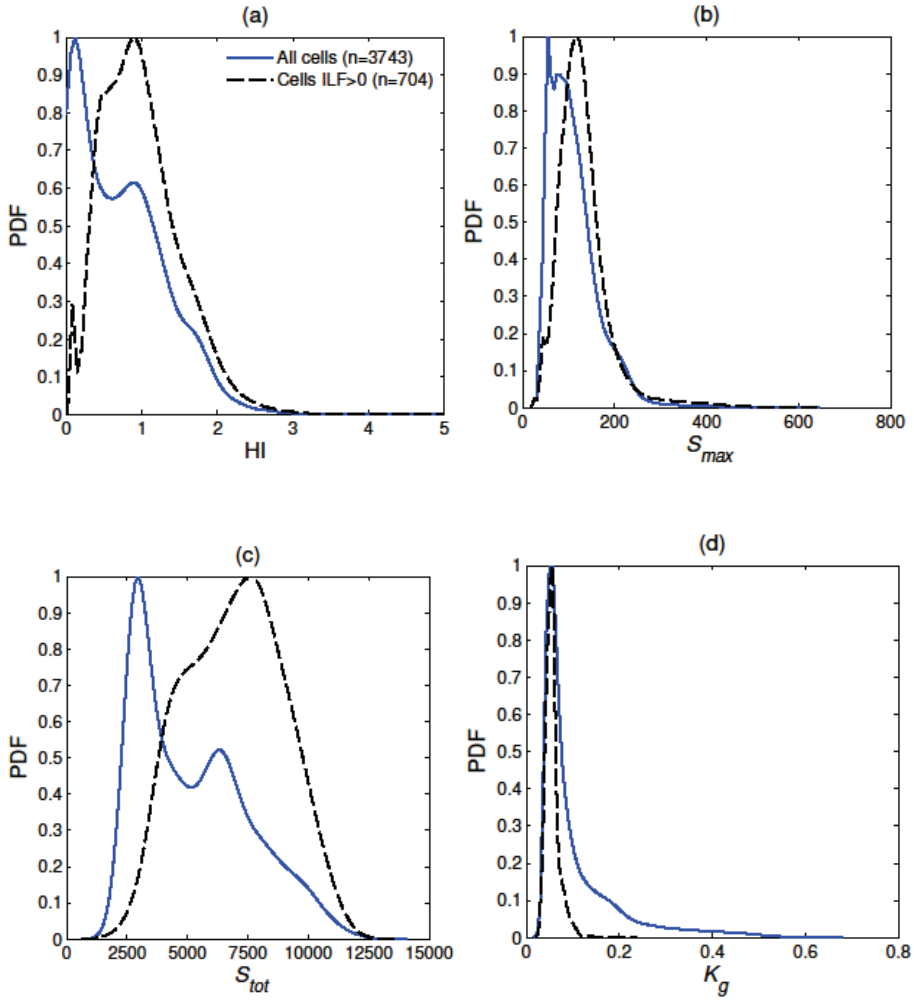

Figure 6.11 Normalised probability distribution functions (PDF) of all model grid cells (solid blue lines) and of all model grid cells with ILF>0 (dashed black lines) for mean annual values (1948–2008) of (a) humidity index (HI), (b) potential maximum soil water storage capacity for rainfall events (S_{max}), (c) soil water content in the shallow and deep stores (S_{tot}) and (d) groundwater recession coefficient (K_g).

The two physical model parameters, S_{max} and K_g had different probabilistic distributions (Figures 6.11b and d). The PDF of S_{max} in all model grid cells exhibited a greater skew than that for the cells with ILF>0. This was also the case for K_g; K_g for most model cells with ILF>0 was 0.06 d^{-1}

on average (corresponding to a half-time of approximately 12 days) compared to 0.11 d^{-1} (half-time *ca.* 6 days) for all model grid cells.

The most dissimilar PDFs were found for the state variable soil water content in the shallow and deep stores (S_{tot}). A noticeably negatively skewed and bimodal probabilistic distribution was computed for S_{tot} in all model cells, whereas that for the model cells with ILF>0 indicated their soils to remain wetter. It should be noted that cells with MAP<400 mm y^{-1} were excluded from this analysis. Hence the bimodality of the PDF for all cells cannot be completely ascribed to grid cells located in dry or very dry areas. A summary of cell sample statistics is given in Table 6-3.

Table 6-3 Comparison of climatic and physical characteristics of all model grid cells with those of cells with ILF>0. Climatic characteristics include means and standard deviations (in brackets) of: mean annual precipitation (MAP), humidity index (HI) and seasonality index (SI). Physical characteristics include: potential maximum soil water storage capacity for rainfall events (S_{max}), soil water content in the shallow and deep stores (S_{tot}), and the groundwater recession constant (K_g).

Characteristics	All grid cells (n=3743)	Grid cells ILF>0 (n=704)
Climatic		
MAP (mm y^{-1})	1513 (±652)	1690 (±747)
HI	0.70 (±0.58)	1.20 (±0.47)
SI	0.63 (±0.28)	0.62 (±0.19)
Physical		
S_{max}	112 (±62)	135 (±76)
$S_{tot} = S_s + S_d S_0$ (mm y^{-1})	5449 (±4586)	7531 (±3742)
S_{totFC} (mm)	832 (±367)	1200 (±370)
K_g (day^{-1})	0.11 (±0.09)	0.06 (±0.01)

6.3.2 'What if' scenarios

As observed earlier in the sensitivity scenario modelling, pan-tropical removal of forests in the two 'what if' scenarios (*cf.* Section 6.2.3) led to an increase in ILTA. ILTA increases appeared to be generally commensurate to percentage forest cover loss (%FCL, Figure 6.12). ISA changes also followed similar patterns to those shown by the sensitivity scenarios and are not shown here. The main concern of this experiment, however, are the results of the third indicator of

changes in streamflow, *i.e.,* the number of months with decreased Q_{tot} during the four months of low flows (ILF) (Figure 6.13a and b). Not surprisingly, areas with ILF>0 when comparing the current and undisturbed forest cover situations (i.e. B98–H03) were similar to the areas found during the sensitivity simulations (comparing 100FC and 0FCSC), due to the high %FCL associated with B98–H03. Besides the clusters already observed in Figure 6.10, new clusters were identified in West Africa (Benin, Guinea and Togo) and India. It should be noted that the percentages of forest cover in B98FC and 100FC may be different, and so will be the associated runoff Curve Numbers, which may go some way toward explaining some of the differences between Figures 6.10 and 6.13a.

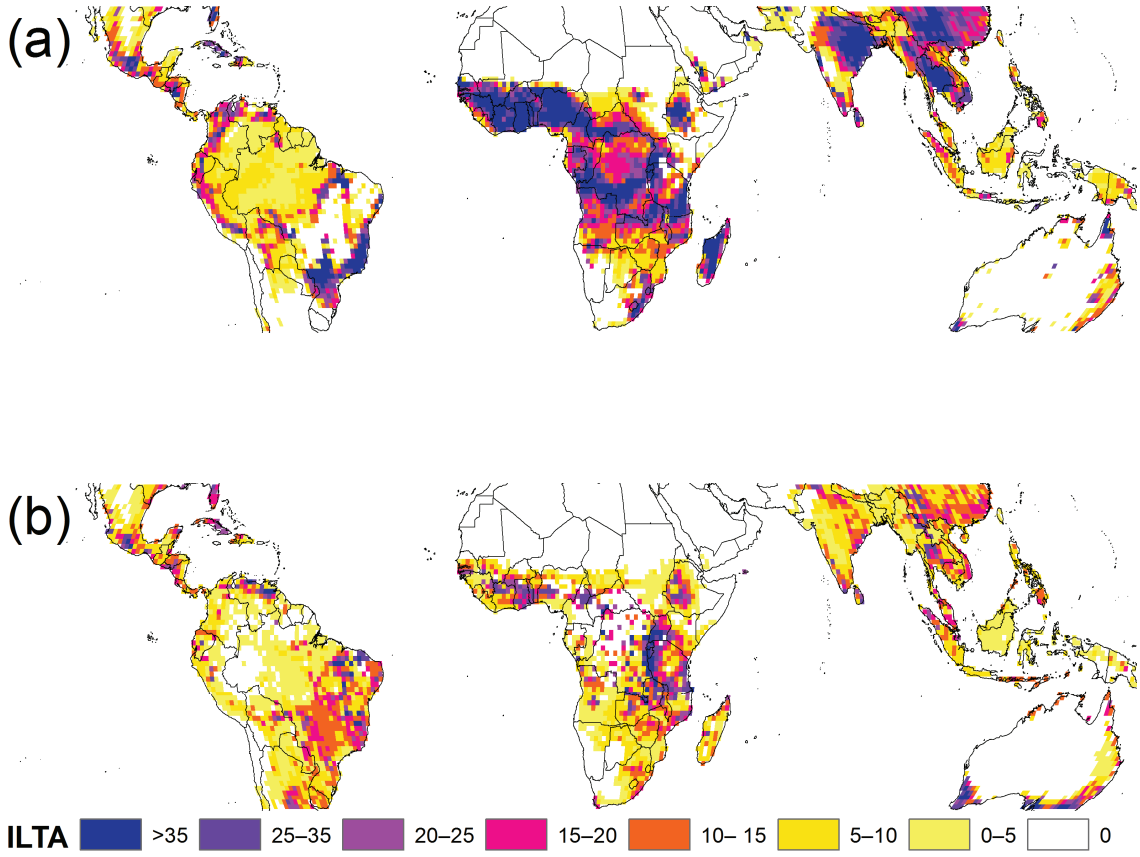

Figure 6.12 Difference between long-term mean annual streamflow (ILTA) under LUCC impacts and prior conditions, expressed as a percentage of long-term mean annual streamflow under prior conditions for (a) (B98-H03); (b) (H03-DNP06). See text for explanation.

Similarly, clusters of ILF>0 identified in the H03-DNP06 scenario (future forest loss) roughly compare to those found for B98-H03, and again correspond to areas affected by relatively high

values of %FCL (Figure 6.13b). However, %FCL values in some of these clusters are not as large as in B98-H03, which may be caused by the non-linearity of LUCC impacts on hydrology, as also inferred from the results obtained with the site sensitivity analysis.

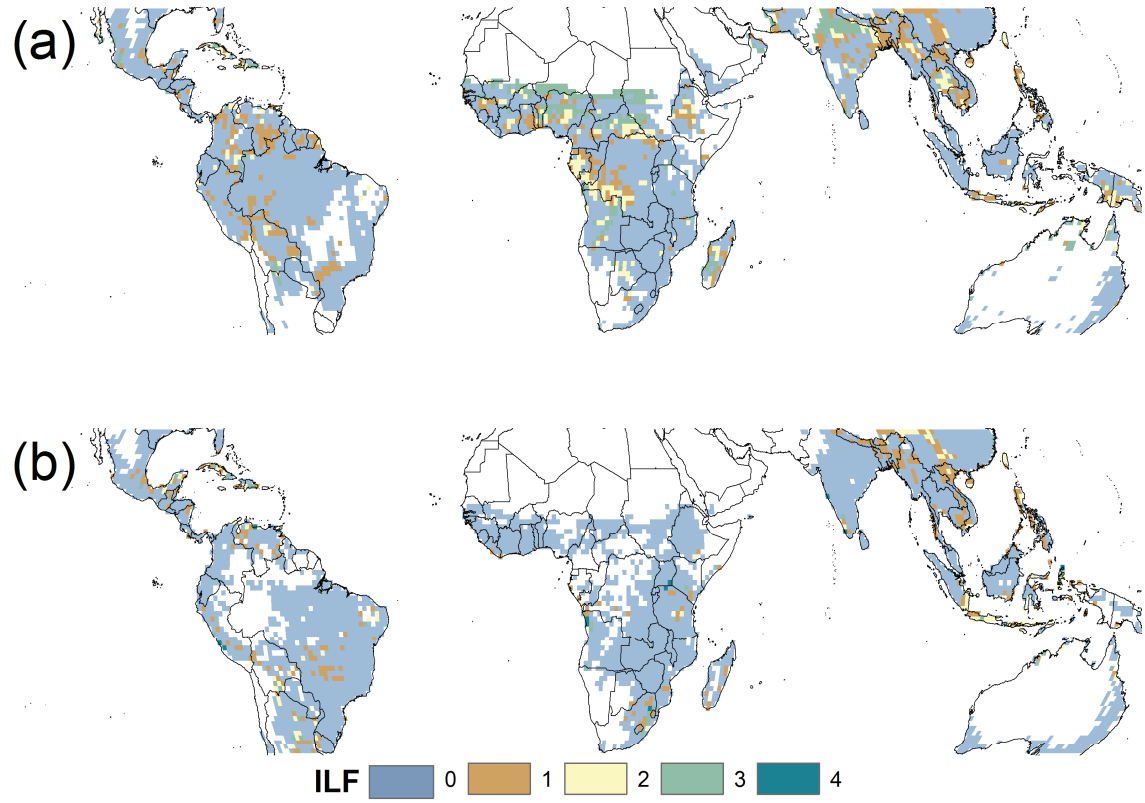

Figure 6.13 Number of months with modelled decrease in dry season flows (ILF) out of four months with low flows under LUCC impacts and prior conditions for (a) deforestation until present (B98-H03); and (b) future deforestation (H03-DNP06). See text for explanation.

6.4 Discussion

Sensitivity analysis for selected sites

On a long-term mean annual basis, the higher $\overline{E_{tot}}$ in the simulations with 100% forest cover resulted in a reduction in total streamflow, $\overline{Q_{tot}}$ at all four sites under consideration. The inclusion of soil surface degradation impacts (through the Soil Conservation Service Curve Number approach) when shifting from forest to a grass cover; resulted in higher absolute

baseflows ($\overline{Q_g}$), except for the Mahaweli catchment; whereas storm flows ($\overline{Q_R}$) increased by around 60% across all sites. Despite the increase in storm flow in all sites, the absolute difference in baseflow ($\Delta\overline{Q_g}$) for the upper Konto and Babati were very small. In these two cases, the mean annual increase in infiltration converted into $\overline{Q_g}$ compensated the increase in $\overline{E_{tot}}$.

On a seasonal basis, changes in flow patterns varied between sites, with some interesting dynamics pertaining to dry season flows (Figures 6.3–6.6). Changes in CN associated with poor soil conditions controlled infiltration and the recession of streamflow at the end of the wet season through an increase in monthly Q_R and thus faster recession; this had an impact on dry season flows in some catchments.

In the upper Konto catchment, the patterns (but not the magnitudes) of mean seasonal Q_{tot} as modelled in the 100% forest cover (100FC) and 0% forest cover and negative changes in soil condition (*i.e.,* 100% grass cover, 0FCSC) scenarios were similar to the ones observed by Rijsdijk and Bruijnzeel (1991) (see Figure 1.2, Chapter 1). The observed and modelled slight reduction in dry season flows in the 0FCSC scenario was ascribed to a loss of infiltration opportunities due to poor soil conservation practices and an increase in sealed surfaces.

The increase in modelled peak Q_{tot} during the wet season in the 0FCSC simulations for the Babati catchment is consistent with the reported increase (Sandström, 1995). Most of the simulated increase was due to overland flow during the wet season. The higher MPDR in relation to monthly *P* in the Babati area translated into a substantial difference in streamflow associated with the same land cover but different soil conditions (Figure 6.4). The loss of bio-porosity was deemed key for the observed increase in peak flows (Sandström, 1995), which appeared to be the mechanism governing overland flow occurrence, rather than changes in vegetation cover in this sub-humid environment where the natural vegetation consists of scrub rather than tall forest.

In the Tocantins river basin, the simulated patterns (although not the magnitudes) in mean seasonal Q_{tot} for the 100FC and 0FCSC simulations were similar to the ones observed by Costa

et al. (2003) (see their Figure 6) for periods before and after LUCC, respectively. As in these simulations, the inferred reduction in infiltration opportunities advanced by Costa *et al*. (2003) was not great enough to produce a marked reduction in dry season flows, although there were changes in streamflow recession and overall redistribution of dry season flows (Figure 6.5).

The simulation results for the upper Mahaweli catchment (Figure 6.6) did not support the slight decrease in dry season flows reported in Bruijnzeel (2004) that was mainly ascribed to poor soil conservation measures. However, in this particular case tea plantations (not forest) were replaced by annual cropping and home gardens. Therefore, a more pertinent comparison would have been that between the 0FC and 0FCSC scenarios, in which case a very slight decrease in streamflow during one month of the dry season was simulated (Figure 6.6a).

The above results were site-specific and reflected the representation of various physical processes in the model, the specific parameter values used and the experimental design (*i.e.,* forest presence versus absence). With respect to transpiration (E_t), the current model version mainly considers the effects of soil water availability, since this most likely will have the greatest impact in seasonal tropical environments (Costa *et al.*, 2010). Other factors such as energy availability and canopy wetness duration may play a similarly important role in more humid environments such as rain forests or montane cloud forests (Giambelluca *et al*., 2009; Costa *et al.*, 2010). Some of these aspects are incorporated in the model through its interception evaporation (E_i) routine (*cf.* Van Dijk, 2010).

Sensitivity simulations for the catchments with marked rainfall seasonality (Babati and Tocantins) showed higher E_{tot} for grassland at the end of the wet season (*cf.* Figures 6.4b and 6.5b). This is consistent with the idea that grasses adopt a less conservative water-use strategy compared to trees (Rodriguez-Iturbe *et al.*, 2001; Rodriguez-Iturbe and Porporato, 2004). Observations of daily mean or maximum transpiration rates made from flux towers being similar or even higher for grasses and grasslands compared to trees and forests support this finding (Teuling *et al.*, 2010). Results by Williams *et al.* (2012) using data for 167 flux tower sites located mostly in temperate environments suggested annual E_t from grasslands was 9% higher than for forests. The fact that the eddy covariance method used to estimate E_t is generally unreliable during rainfall and thus it is so for estimating E_i may partly explain the latter results.

However, in some shrub-dominated environments, such as Amazonian *cerrado* (*i.e.,* parts of the Tocantins basin) and sub-humid Babati, the LAI of grasses during the wet season was comparable or higher than that of trees and shrubs, with soil water content in the shallow soil (up to 1 m) being strongly and positively correlated to grass LAI (Hoffman *et al.*, 2005).

In the present sensitivity simulations, E_t for grass reached a minimum at the end of the dry season in the more water-limited environments, or stopped altogether (*e.g.* at the Babati site; Figure 6.4b). Figure 6.14 shows the soil water contents in the deep (S_d) and shallow (S_s) storage compartments used in the Tocantins simulations for different percentages of forest cover. Water content in S_s (Figure 6.14a) was insufficient to maintain rates of dry season evapotranspiration for 100% grass cover (*cf.* Figure 6.5b). Indeed, typical *cerrado* vegetation has a grassy layer that becomes inactive during the dry season (Giambelluca *et al.*, 2009). Conversely, rainfall that infiltrated during the wet season was 'carried over' to S_d (Figure 6.14b) and this modulated dry season evapotranspiration by the forest (Figure 6.5b). Negrón Juarez *et al.* (2007) concluded for a seasonal Amazonian forest site that under normal or below-normal dry season rainfall conditions, more than 75% of E_{tot} is supplied by soil water below 1 m depth, whereas during a rainier dry season, this would be about 50%. Soil moisture found at <1 m depth is typically recharged by rainfall during the wet season.

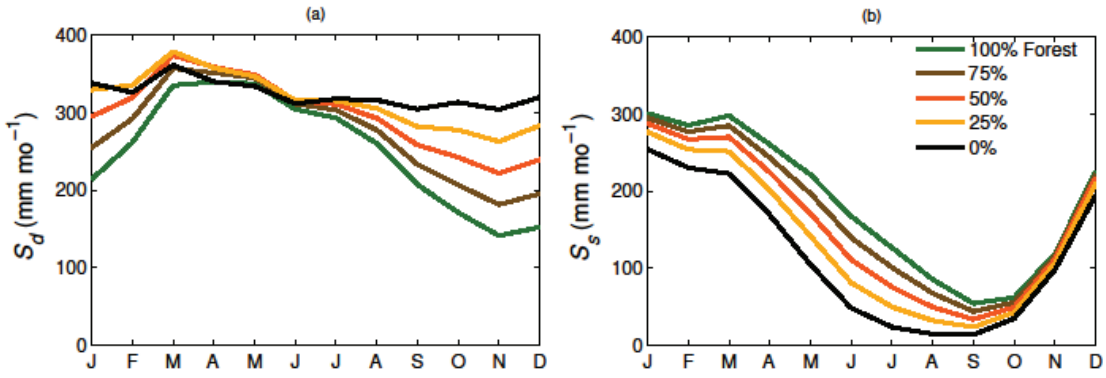

Figure 6.14 Water contents in (a) deep (S_d) and (b) shallow (S_s) soil water storage compartments in the Tocantins simulations for different percentages of forest cover.

Similar E_{tot} and soil moisture dynamics were also observed for grasses and eucalypt woodlands in a savannah in the seasonal tropics of northern Australia (Hutley *et al.*, 2010). Deep roots in forests are likely to become more important in maintaining high rates of E_t in the dry season because of their ability to access deeper soil water (Nepstad *et al.*, 1994). In an Amazonian rain forest, monthly E_t peaked during the dry season, presumably because of the higher atmospheric evaporative demand in the dry season (less cloud cover) and deep roots having continued access to soil water (da Rocha *et al.*, 2004).

Model sensitivity to imposed LUCC at these sites and elsewhere will depend on additional factors that were not considered in the current model, including: cloud cover, rainfall intensities, mixed vegetation cover, topography and geology not captured by parameters in the model's structure.

Pan-tropical sensitivity analyses

The previous site sensitivity analyses suggested that the representation of several relevant hydrological processes (particularly for the seasonal tropics) as well as the response of the model to imposed LUCC are reasonable; even if deviating in absolute terms from observations. Due to the many uncertainties in the forcing and land cover data, scale issues, and other processes that the model does not capture, the results should be considered to be an indication of the scale of change associated with LUCC, rather than an exact prediction of change (Coe *et al.*, 2011).

In terms of the percentage difference in the long-term mean annual streamflow indicators (ILTA) for forested and non-forested conditions, long-term mean annual streamflow ($\overline{Q_{tot}}$) increases by 18% on average if only vegetation cover changes and infiltration opportunities are maintained, whereas it increases by an additional 8% if infiltration opportunities are reduced. To a large extent, this additional increase occurs in more water-limited and seasonal environments, whereas the changes are less marked in more humid environments (Figure 6.8). Similar patterns were simulated for the difference in the seasonal flow amplitude indicator (ISA) which indicated most of the increase in $\overline{Q_{tot}}$ may occur during the wet season. The results obtained for these two indicators suggested that dry season flows may well be negatively impacted by LUCC

in areas where the seasonal distribution of streamflow is important. In fact, 97% of the grid cells in which the indicator for the effect of LUCC on low flows (ILF) was <4 had a seasonal rainfall regime (SI>0.2), and 64% had a marked seasonal regime (SI>0.6).

The statistics (Table 6-3) and probability distribution functions for various physical and model parameters derived for grid cells with ILF>0 after LUCC provided a rationale for identifying the characteristics of areas in which dry season flows are likely to be more sensitive to LUCC impacts.

In terms of site Humidity Index (HI), 65% of the grid cells with ILF>0 had an HI>1, whereas 90% had an HI>0.65. The PDF for HI was also less negatively skewed for the grid cells with ILF>0 than that for all model grid cells with MAP>400 mm y^{-1} (Figure 6.11a). In the case of seasonal climates, this surplus of *P* over PET occurs generally during 3–6 months of wet season. Some of this surplus may infiltrate (and be available for E_t) or will run off, depending on the changes in soil infiltration characteristics associated with LUCC, and prevailing rainfall intensities. Site sensitivity simulations also illustrated the role of rainfall intensity and the infiltration capacity of soils, with higher intensities resulting in more overland flow and greater storm flow volumes (Figures 6.3c–6.6c). The distribution of S_{max} (a proxy for soil infiltrability) for grid cells with ILF>0 was less negatively skewed that that for all model grid cells (Figure 6.11b), suggesting the former soils to be more capable of accommodating higher rainfall intensities. Common LUCC in the tropics, such as mechanised forest clearing for timber harvesting and cattle ranching, or intensive agriculture cause a number of disturbances (particularly loss of organic matter and increased compaction) to the soil surface (Alegre and Cassel, 1996; Wemple and Jones, 2003; Sidle *et al.*, 2004; Grip *et al.*, 2005; Negishi *et al.*, 2008). The degree of soil disturbance determines the change in infiltration opportunities and volumetric soil moisture content. With respect to the role of S_{tot}, deep soils with high water storage capacities (and by implication better infiltration opportunities) may also 'carry over' soil moisture from the wet to the dry season. These effects are illustrated in Figure 6.15 through the normalised probability functions of S_{max} and S_{tot} for all model grid cells with ILF>0 in the 100FC and 0FCSC scenarios. The PDF for S_{max} is more negatively skewed in the 0FCSC scenario than in 100FC whereas the mean has decreased from 135 mm mo^{-1} in the 100FC simulation to 52 mm mo^{-1} in 0FCSC (Figure

6.15a). This translated in S_{tot} being substantially lower (*i.e*. drier soils) in the 0FCSC scenario than in 100FC (Figure 6.15b).

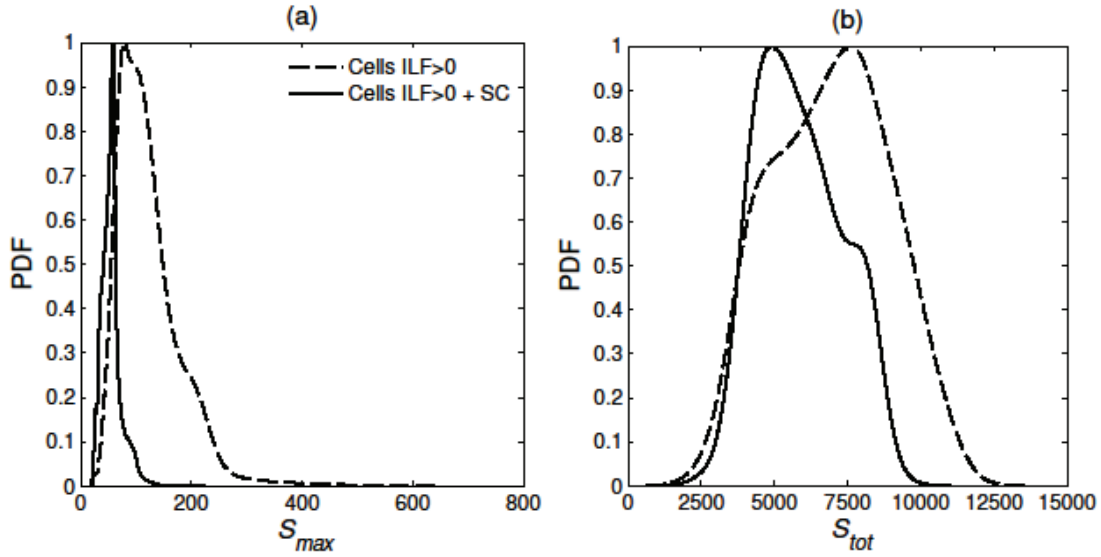

Figure 6.15 Normalised probability distribution functions (PDF) for all model grid cells with ILF>0 for 100FC (dashed lines) and for 0FCSC (solid lines) for mean annual values (1948–2008) of (a) potential maximum soil water storage capacity for rainfall events (S_{max}), and (b) soil water content in the shallow and deep stores (S_{tot}).

The mean groundwater recession coefficient (K_g) for all grid cells with ILF>0 implied a half-time that was roughly twice the value for all model grid cells (i.e. ca. 12 and 6 days, respectively; *cf.* Table 6-3). The equation normally used to describe rates of baseflow recession (Section 5.3.1.4; *cf*. Peña Arancibia *et al.*, 2010) corresponds to the part of the hydrograph associated with prolonged periods with little or no rainfall. As such, it illustrates in a general way the nature of the groundwater storages feeding the streamflow (Tallaksen, 1995). However, the recession data were limited to 167 tropical catchments and the role of deep soils and permeable regoliths and lithologies could not be established (Peña Arancibia *et al.*, 2010). Deep soils and permeable regoliths are widely present in tropical landscapes (Chappell *et al.*, 2007), and their lagging effect is expected to reduce seasonal streamflow variability as well as sustain flows during the dry season. In particularly porous catchments, dry season flows may contribute up to 30% of all streamflow (see Le Maître and Colvin (2008) for an example from temperate southern Africa). In karst-dominated landscapes, as in the mountain areas of North-west Vietnam, baseflow contributions to total flows may be up to 80% (Tam *et al.*, 2001).

The map showing the spatial distribution of the third indicator of changes in streamflow after LUCC, *i.e.,* the number of months with decreased Q_{tot} during the four months with low flows (ILF) in the B98-H03 deforestation scenario directs attention to areas with potential for boosting dry season flows through (re)forestation. The grid cells with ILF>0 are located in similar regions as found in the pan-tropical sensitivity scenarios (compare Figures 6.13a and Figure 6.10). Therefore, they share certain climatic and physical (through estimated model parameters) characteristics that make them more sensitive to LUCC-induced changes in dry season flows. Forestation and the associated recovery of infiltration possibilities in such areas (and others with similar characteristics) may reduce seasonal streamflow variability and even enhance streamflow during the dry season. Many of these areas coincide with the Global Map of Forest Restoration Opportunities (*cf.* Minnemeyer *et al*., 2011; http://www.wri.org/project/forest-landscape-restoration) and the map of Lepers *et al.* (2005) showing the main areas of rapid forest cover changes over the period 1980–2000. The rising demands for arable land and water in these areas also highlight the future pressure on the agricultural land base and water resources (Vörosmarty *et al*., 2000).

It may take many years (even decades) to observe the potentially beneficial effects on dry season flows afforded by improved infiltration after forestation (Bruijnzeel, 2004; Scott *et al*., 2005; Zhou *et al*., 2010). Intensive grazing typically results in compaction by continuous cattle trampling of soil and thus decreased infiltrability (Alegre and Cassel, 1996; Martinez and Zinck, 2004). The (partial) recovery of soil infiltration characteristics in affected areas often takes one or two decades of uninterrupted vegetation development (Alegre and Cassel, 1996; Zhou *et al.*, 2002; Ilstedt *et al*., 2007; Ziegler *et al.*, 2001, 2009). Zimmermann *et al.* (2006) showed that the effect of 13 years of grazing was still measurable in a teak plantation after 10 years of post-grazing growth, with a slow recovery of infiltrability when compared to soils with shorter periods of grazing. Ghimire *et al.* (2013) measured infiltration capacities in reforestation stands in the Middle Hills of Nepal after 25 years and found serious reductions in surface hydraulic conductivities due to continued over-exploitation of the forests. Nevertheless, 'real-world' cases

of large-scale forestation of severely degraded areas and posterior enhancement of dry season flows are slowly beginning to be published in the literature as more long-term streamflow data become available (*e.g.*, Zhou *et al.*, 2010; Wilcox and Huang, 2010).

Forestation with fast-growing exotic species having high water use such as eucalyptus and pines may negate the beneficial effects of increased infiltration opportunities (see Bruijnzeel, 2004 and references therein; Scott *et al*., 2005). A combination of soil conservation measures, targeted forestation of 'hot spots' and careful selection of (indigenous) species with lower water use (Gush, 2009) may provide a positive trade-off between enhanced infiltration opportunities and increased water use and thus boost dry season flows.

Streamflow regime regulation should also be considered when interpreting the spatial patterns of changes in low flow durations following deforestation (Figure 6.13a). Man-made reservoirs are purposely built to increase water availability during the dry season for irrigation, domestic and industrial uses, hydropower generation and/or flood protection. Impacts of LUCC on dry season flows in regulated areas will likely be offset by the presence of dams (Döll *et al.*, 2009). The effects of regulation are not yet considered in W3RA-LUM. Nor do atmospheric feedbacks that may be important when the scale of LUCC is in the order of the model grid cell (100,000 km^2). However, besides modelling or theoretical results (*e.g.* Wang and Eltahir, 2000, Makarieva and Groshkov, 2007; Sheil and Murdiyarso, 2009; but see Meesters *et al.*, 2009), no physical evidence of a major negative impact on rainfall was found after large-scale forest clearing in Amazonia and elsewhere (Wilk *et al.*, 2001; Costa *et al.*, 2003; Angelini *et al.*, 2011).

6.5 Conclusion

This chapter investigated the pan-tropical impacts of land use and land cover change (LUCC) on hydrology, particularly dry season flows. The model used here, W3RA-LUM, was tailored to not only simulate changes in vegetation cover, but also changes in soil condition that limit infiltration opportunities. W3RA-LUM was used in four site sensitivity experiments together with pan-tropical hydrological modelling to: (*i*) define reference hydrological conditions under natural forest conditions; (*ii*) evaluate where tropical LUCC can be expected to have the greatest

impacts on dry season flows; and - on the basis of changes in evapotranspiration and infiltration - (*iii*) to assess potential areas for rehabilitation and regeneration of hydrological services in degraded areas through reforestation.

Besides model structural limitations and data uncertainties, various hydrological responses were simulated through simplistic changes in vegetation cover (replacing a 100% forest cover with 100% grass cover) and soil conditions (good and poor soil conditions, following the Soil Conservation Service Curve Number approach), which do not necessarily reflect the true dynamics of LUCC in the 'real world'. Despite these limitations, the results obtained suggested that the representation of several relevant hydrological processes in the seasonal tropics, and the response of the model to LUCC were reasonable.

Sensitivity analyses were performed at four tropical sites, three with documented (negative) impacts of LUCC on dry season flows, which provided some interesting insights. To a reasonable extent, the simulated impacts of LUCC (although not replicating the observed magnitudes themselves) on catchment hydrological functioning resembled observed streamflow patterns. On an annual basis, the higher evapotranspiration derived in simulations with 100% forest cover resulted in a corresponding reduction in streamflow compared to simulations with 100% grass cover. Intra-annually, results showed significant impacts of LUCC on the way rainfall is partitioned into evapotranspiration (E_{tot}) and the two streamflow components, baseflow (Q_g) and stormflow (Q_R). Vegetation changes and soil condition changes affected groundwater recharge and the amount of overland flow, which resulted in altered Q_R and Q_g. Generally, simulations with 100% grass cover and poor soil conditions gave a faster rate of streamflow recession at the end of the wet season, whereas wet season flows also peaked around a month earlier than in simulations with 100% forest cover and good soil conditions. Good soil conditions also appeared to modulate the seasonal variability of streamflow. In addition, contrasting rainfall intensities between sites (in terms of the ratio of monthly rainfall totals per number of rainy days per month) highlighted the capacity of soils to either infiltrate more net rainfall or produce more runoff.

Pan-tropical sensitivity analyses for scenarios with or without full forest cover and/or good or poor surface conditions showed an increase in mean annual streamflow of 18% if only

vegetation changes were taken into account. The amount increased to 26% if there were concurrent changes in soils from good to poor surface conditions. A large amount of the latter additional increase in mean annual streamflow occurred in more water-limited and seasonal environments, whereas the changes were less marked in more humid environments. These results highlight the potentially negative impact of LUCC on dry season flows in areas where the distribution of streamflow during the year is more important than total water yield. In addition, the results show that for some areas there was a reduction in Q_{tot} for some of the driest months after forest removal, despite the corresponding decreases in E_{tot}. An indicator for the change in (the duration of) low flows was used to asses which combinations of climatic and/or physical catchment characteristics captured by the model (*i.e.,* soil water holding capacity, vegetation type, surface infiltration capacity, and rate of baseflow recession) were potentially important for the direction and magnitude of LUCC impacts on dry season flows. The physical (related to model parameters) and climatic characteristics were used to determine those areas (forested and pre-degraded state) in which LUCC and any consequent reduction of infiltration opportunities might have a negative impact on dry season flows. The results may be summarised as follows:

- There is sufficient rainfall in excess of potential evapotranspiration during the wet season to recharge deeper soil profiles and/or the groundwater system.
- The surface soil infiltration capacity can accommodate prevailing rainfall intensities during the wet season.
- There is sufficient soil water storage to 'carry over' rainfall infiltrated during the wet season.
- A sufficiently long 'buffer time' (in terms of groundwater recession coefficient) that modulates the release of water stored in the deep soil profile or saturated zone as baseflow.

Following the same rationale, deforested or deforested and degraded areas with similar characteristics were considered for forestation and potential recovery of infiltration possibilities, which in turn could enhance streamflow during the dry season. Some of the areas identified in this way coincide with areas targeted by ongoing reforestation and restoration initiatives.

However, it is not known if and to what extent these areas are currently experiencing water scarcity issues.

There are many more factors to be considered in such areas which translate into a need for more detailed modelling and field investigations at the catchment or hillslope scale. Recent advances in remote sensing allowed the dynamic quantification of hydrological parameters related to 'above ground' factors that control the water balance (*i.e.,* incoming solar radiation, precipitation and biophysical parameters related to vegetation cover and LUCC) that are sophisticated and accurate enough for their use in hydrological modelling. However, the understanding of the underlying subsurface factors (soil and geological substrate hydraulic characteristics) that affect evapotranspiration, infiltration, soil water retention, groundwater recharge and movement is of equal importance to close the knowledge gap in the forest 'pump' and 'sponge' paradigm. Overall, the results presented provide the first comprehensive pan-tropical overview of the impacts of forest removal and reforestation on streamflow. In addition, the present results direct attention to areas where some of the mentioned climatic and physical characteristics appear to be important in governing site vulnerability to changes in dry season flows, both in terms of decreased flows after surface degradation and possibly enhanced flows after vegetation restoration.

Chapter 7 Summary, conclusions and future research needs

Contents

7.1 Summary and conclusions

The land use and land cover change (LUCC) that alter the hydrological functioning of a landscape in the context of this research incorporate both changes in plant evaporation and soil hydraulic properties (specifically the partitioning of (net)rainfall into water that infiltrates into the soil or water that runs-off along the soil surface). These two impacts of LUCC can be metaphorically compared to changing a hydrological 'pump' (through plant evaporation) and a 'sponge' (through factors governing infiltration rates such as the effects of organic matter and soil bioporosity). The balance between these two impacts will determine the net hydrological change resulting from LUCC. Chapter 1 reviewed a number of case studies, from local to regional scales, in which a reduction of dry season flows occurred after forest removal, due to a loss in infiltration opportunities to the extent that soil moisture storage and thus groundwater recharge were critically reduced (*i.e.*, loss of the 'sponge' effect).

Earlier research has shown that agricultural expansion and intensification of agricultural practices in the tropics have triggered widespread land degradation processes which may have caused adverse changes in soil physical properties, reducing soil surface infiltration capacity and enhancing the intensity and frequency of overland flow and surface erosion. In the light of ongoing LUCC throughout the tropics and concerns over their potential impacts on dry season flows, hydrological analysis and modelling was performed to assess where tropical LUCC can be expected to have the greatest impacts on dry season flows. The present focus is on dry season flows since for much of the tropics this is the period when changes in water availability have their greatest impact on agricultural, domestic and other water-dependent activities. In addition to understanding where such problems might occur, this thesis examined already degraded areas where forestation could rehabilitate and regenerate so-called hydrological ecosystem services.

7.1.1 Identifying hydrological impacts of LUCC on streamflow metrics at the regional scale

Chapter 2 reviewed several published case studies of forest cover change impacts on long-term streamflow at the regional scale for various parts of the tropics (*i.e.*, catchments with an area >10,000 km^2). At the time of the review, only seven studies at this scale were reported in the published literature. Although the area of forest removed in six of the studies was large enough (19 to 63%) to increase annual streamflow post-LUCC (*i.e.*, as is typically reported for small experimental catchments), three studies showed no increase (*cf.* Table 1 in Chapter 2). In addition to these contrasting results, the role of climate variability was not fully addressed in some of these studies. Furthermore, more recently published evidence suggested that the role of climate variability may have played a part in the observed increases in streamflow in at least two of the mentioned studies and thus the purported impacts of LUCC on streamflow deserved further scrutiny.

Quality long-term (*i.e.*, >20 years) daily rainfall and streamflow data for two large (>10,000 km^2) catchments located in the seasonal tropics of Australia which underwent woodland conversion to grazing land were analysed to test the trade-off between the associated 'pump' and 'sponge' effects at the river basin scale. Earlier work in the area (Ive *et al.*, 1976; Thornton *et al.*, 2007; Bonell and Williams, 2009) had demonstrated declining infiltration rates after converting woodlands to grazing land. For one of the two investigated catchments (the Comet river basin, 16,449 km^2) Siriwardena *et al.* (2006) had postulated that most of the observed increase in mean annual streamflow between the pre- (1920–1949) and post-LUCC (1970–1999) periods could be attributed to a 45% removal of *Acacia* woodland whereas part of the increase in flow was explained in terms of a concurrent increase in rainfall. The objective of the present study also included the isolation of LUCC from climate variability effects on streamflow. Several published approaches providing 'multiple lines of evidence' were used to achieve these objectives. In doing so, it was established that most of the increase in observed streamflow was related to climate variability, although a period immediately post-LUCC showed an increase in streamflow related to a reduction in evapotranspiration (*i.e.*, a reduction in the 'pump' effect). It

was also demonstrated that LUCC enhanced storm flows of all magnitudes and somewhat decreased slower flows, possibly as a consequence of reduced infiltration (*i.e.*, a reduction of the 'sponge' effect); although this decrease was not reflected in a decrease in dry season flows *per se*. The present findings also suggested that some of the simple but successful techniques for detecting the strong influence of land cover in small catchments on long-term streamflow (*i.e.*, Budyko-type[1] models) might not be able to do so in large catchments with mixed land cover (*cf.* Oudin *et al.*, 2008 and Chapter 5, Appendix C; see Section 7.2.1 for additional details). Furthermore, Chapter 2 highlighted the importance of climate variability and the difficulty to separate the impact of LUCC from effects of climate variability in observed flows. Therefore, long-term climatic data were used for the subsequent scenario modelling in order to account for the typically observed variability.

Summarising, this study contributed to the understanding of LUCC impacts on streamflow in large 'real-world' catchments through the application of several inference methods that investigated not only changes in annual water yields but also seasonal and daily streamflow metrics. The results highlighted an increase in storm flows and a reduction in slower flows which, given the ongoing intensification of LUCC across the tropics, may result in water resource relevant changes to dry season flows.

Publication of research

Peña-Arancibia, J. L., A. I. J. M. van Dijk, J. P. Guerschman, M. Mulligan, L. A. Bruijnzeel, and T. R. McVicar (2012), Detecting changes in streamflow after partial woodland clearing in two large catchments in the seasonal tropics, **Journal of Hydrology**, 416/417, 60-71.

7.1.2 Model implementation, parameterisation and input data

The "World-Wide Water Resources Assessment system – Land Use Model" (W3RA-LUM) was used here to simulate the hydrological impacts of LUCC and to achieve the thesis aims and objectives. A key requirement was that W3RA-LUM had to be sensitive to the land cover signal

[1] Budyko postulated that the long-term average annual evapotranspiration from catchments is determined by rainfall and available energy and formulated a simple model that showed good agreement with the long-term water balance for catchments in the former USSR (Zhang *et al.*, 2008).

in ‘real-world’ catchments with mixed land cover and various degrees of land degradation. Modelling experiments using daily long-term streamflow and rainfall time series from 278 catchments with mixed land cover in Australia and the process model Australian Water Resources Assessment system Landscape hydrology (AWRA-L, Van Dijk, 2010; on which the vegetation water use module in W3RA-LUM is based, sharing the same parameter values) demonstrated that this more complex (but uncalibrated) process model had the ability to reproduce an observed land cover signal in streamflow time-series of similar or higher magnitude than a calibrated Budyko-type model (*cf.* Chapter 5, Appendix C). Step-wise regression analysis showed that climate factors other than potential evapotranspiration and rainfall (the most commonly used inputs in Budyko-type models), such as daily rainfall intensity, had a considerable influence on streamflow and were good predictors of land cover hydrological behaviour for some land cover types. These improved results constituted the decisive factor when selecting a process model capable of assessing the impacts of LUCC on dry season flows at a daily time scale across the tropics.

Publication of research

Van Dijk, A. I. J. M., **J.L. Peña-Arancibia** and L. A. Bruijnzeel (2012), Land cover and water yield: inference problems when comparing catchments with mixed land cover. **Hydrology and Earth System Sciences,** 16*,* 3461-3473.

In Chapter 5, the structure of W3RA-LUM was modified to incorporate not only the changes in LUCC that directly affect evapotranspiration (already present in AWRA-L), but also those that affect the partitioning of infiltration and runoff by using the Soil Conservation Service Curve Number Method (SCS-CN; USDA, 1986). The SCS-CN method translates the impacts of LUCC on the production of surface runoff (‘storm flows’) and is currently the only method for global application of LUCC infiltration impacts scenarios that has a strong empirical basis and is responsive to soil type and degradation scenarios. The method included the development of a hydrologic soil condition indicator based on a global proxy of current land degradation status. This proxy was derived from trends in the long-term rain-use efficiency (RUE) adjusted normalised difference vegetation index (NDVI) (Bai *et al.*, 2008), enabling a more realistic

representation of current land condition in a global Curve Number map. This new feature was subsequently used for scenario modelling using land cover maps that represented: (*i*) pre-agricultural forest cover; (*ii*) current forest cover, and (*iii*) future forest cover based on projected deforestation rates. Corresponding changes in runoff Curve Numbers for the areas experiencing deforestation in the respective maps were computed by supplanting the dominant forest type (distinguished per climatic zone) with grasslands. In addition, any decrease in forest cover was associated with a change from 'good' to 'poor' hydrologic soil conditions (*sensu* SCS, 1986), thereby representing the most extreme case of reduction in soil infiltration characteristics. These structural modifications and typification of Runoff Curve Numbers according to soil conditions are a novel use in the study of the hydrological impacts of LUCC at the pan-tropical scale. Most modelling studies, both in the tropics and elsewhere, that have investigated LUCC impacts on hydrology focused solely on changes in evapotranspiration and not on any corresponding changes in infiltration (for exceptions see Beck *et al.*, 2013; Ghimire *et al.*, 2013).

The structural modifications to the W3RA-LUM model enabled a more realistic representation of hydrological processes for modelling LUCC impacts on hydrology through the incorporation of changes that affect both evapotranspiration and infiltration.

Data for parameters that represent groundwater flow movement are few and far between, particularly with respect to aquifer thickness and hydraulic conductivity. Therefore, in Chapter 4 an approach was devised to parameterise and test a conceptual linear storage-discharge model to simulate the shape of the recession hydrograph, considered here as being representative of baseflow. The drainage characteristics of 167 tropical and sub-tropical catchments represented by the linear reservoir baseflow recession constant k_{bf} were linked empirically through statistical regression techniques to parameters representing catchment climate, geology and morphology. It was shown that the best predictors of k_{bf} were climatic, whereas terrain and geological characteristics were of secondary importance. This finding was partly considered as a justification for the use of the grid cell as the spatial modelling unit and the simplified representation of a 'catchment', thereby avoiding complex grid and vector model hybrids to emulate catchment boundaries. Next, an empirical relation was derived to spatially estimate k_{bf} from catchment aridity (the ratio of rainfall to potential evapotranspiration), which is readily

available from spatial climatic datasets at a pan-tropical scale. This relationship explained 49% of the observed variance in k_{bf}. The differences in k_{bf} for dry and humid zones demonstrated the interconnection between climate and subsurface characteristics of catchments. Higher (faster) recession coefficients were observed for the drier catchments, highlighting mainly event-driven streamflow and/or fast draining perched aquifers. Conversely, the lower (slower) recession coefficients found for the more humid catchments and may be attributed to excess rainfall recharging deeper soils and porous aquifers.

Summarising, this study provided the best climatic and terrain descriptors for baseflow recession in 167 (sub)tropical catchments. An equation was then derived to parameterise the recession coefficient of a linear reservoir pan-tropically. This is of utmost importance in the modelling of dry season flows (i.e., the timing of the release of water stored in the deep soil profile or saturated zone as baseflow).

Publication of research

Peña-Arancibia, J. L., A. I. J. M. van Dijk, M. Mulligan, and L. A. Bruijnzeel (2010), The role of climatic and terrain attributes in estimating baseflow recession in tropical catchments, **Hydrology and Earth System Sciences**, 14(11), 2193-2205.

In Chapter 3, a literature review was conducted to assess the strengths and weaknesses of commonly used climate forcing data needed as inputs in W3RA-LUM, which included daily precipitation (P in mm), incoming shortwave radiation (SW_{down} in Wm^{-2}) and minimum and maximum temperatures ($T_{min,max}$ in ºC). A more in-depth evaluation was performed for precipitation, which is both the most significant component of the hydrologic cycle and more variable in space and time than all other climatic variables. Two high-resolution gauge-only daily precipitation analyses available for Australia and South and East Asia were used as a reference to evaluate the respective precipitation datasets. The present results showed that the bias-corrected precipitation from the 50-Year High-Resolution Global Dataset of Meteorological Forcings for Land Surface Modelling developed by Sheffield et al. (2006) at Princeton University (referred to hereafter as the 'Princeton' data), was more accurate in reproducing the observed rainfall for both monthly accuracy metrics and daily rainfall intensity metrics (with daily metrics being crucial for surface hydrological processes, particularly infiltration and runoff generation).

As such, the Princeton data were considered as input for the hydrological modelling experiments conducted in Chapter 6. The other climatic variables in the Princeton dataset were also bias-corrected using ancillary data of reasonable quality; thus they were also used in the later modelling experiments.

Publication of research

Peña-Arancibia, J. L., A. I. J. M. van Dijk, M. P. Stenson, and N. R. Viney (2011) Opportunities to evaluate a landscape hydrological model (AWRA-L) using global data sets **MODSIM 2011**, 19th International Congress on Modelling and Simulation Modelling and Simulation Society of Australia and New Zealand, December 2011, 4071-4077 pp.

Peña-Arancibia, J. L., A. I. J. M. van Dijk L.J. Renzullo, and M. Mulligan (2013), Evaluation of precipitation estimation accuracy in reanalyses, satellite products and an ensemble method for regions in Australia and in South and East Asia, **Journal of Hydrometeorology**, 14, 1323-1333.

7.1.3 Modelling the pan-tropical impact of LUCC and surface degradation on dry season flows and comparison with empirical observations at sites across the tropics

In Chapter 6, W3RA-LUM was used in four site-sensitivity experiments ahead of pan-tropical hydrological modelling. Sensitivity analyses were performed for four catchments with documented (negative) impacts of LUCC on dry season flows. To investigate the hydrological impacts of LUCC (forest removal and soil surface degradation) simplistic changes in vegetation cover (replacing a 100% forest cover with 100% grass cover) and soil conditions (representing 'good' and 'poor' soil conditions where 'good' is considered to denote soils with a high infiltration rate; SCS, 1986) were modelled. The simulated impacts of LUCC on catchment hydrological functioning resembled observed streamflow patterns at the four sites (although not replicating the observed magnitudes themselves). The implemented experiments affected groundwater recharge and the amount of overland flow, which resulted in altered storm flow and baseflow. Faster rates of streamflow recession and peaks occurring about a month earlier were observed for simulations with 100% grass cover and poor soil conditions compared to simulations with 100% forest cover and good soil conditions. Good soil conditions also appeared to dampen the seasonal variability of streamflow.

Sensitivity analyses similar to the site sensitivity experiments described above were also performed pan-tropically. Scenarios without a full forest cover showed an increase in mean annual streamflow of 26% if there were concurrent changes in soils from 'good' to 'poor' surface conditions, as opposed to 18% when soil conditions did not change. The increase was more pronounced in more water-limited and seasonal environments, whereas the seasonal amplitude of streamflow also increased by similar amounts, highlighting a potentially stronger negative impact of LUCC on dry season flows in these areas. Moreover, the results showed that for some areas there was a reduction in streamflow for some of the driest months after forest removal and advanced soil degradation, despite the corresponding decreases in evapotranspiration. Statistical analysis was used to investigate the climatic and physical characteristics for which forest removal and any consequent reduction of infiltration opportunities might have a negative impact on dry season flows in these areas (forested and pre-degraded state) and included the following (Objective 2): (*i*) there is sufficient rainfall in excess of potential evapotranspiration during the wet season to recharge deeper soil profiles and/or the groundwater system; (*ii*) the surface soil infiltration capacity can accommodate prevailing rainfall intensities during the wet season; (*iii*) there is sufficient soil water storage to 'carry over' rainfall infiltrated during the wet season; and (*iv*) a sufficiently long 'buffer time' (in terms of groundwater recession coefficient) that modulates the release of water stored in the deep soil profile or saturated zone as baseflow.

Results from pan-tropical modelling using both current forest cover and future forest cover maps were used to identify 'hotspots' in which forest removal and concurrent advanced soil degradation may have a negative impact on dry season flows (Objectives 1 and 2). Areas that showed a reduction in streamflow for some of the driest months despite the increases in evapotranspiration associated with the conversion from forest to grassland and allowing advanced soil degradation to occur included: Central America, northern South America, the Andes, Bolivia, Brazil, the Caribbean, Congo, Gabon, Tanzania, Ethiopia, South Africa, Madagascar, India, Bangladesh, and several countries in Southeast Asia (Chapter 6, Figure 6.10).

Similarly, but using modelling results for the pre-agricultural forest cover and current forest cover situations, areas with similar climatic and biophysical characteristics but deforested and/or degraded according to Bai *et al.* (2008) were then identified for forestation with associated potential for recovery of infiltration (Objective 3). Some of the areas coincided with areas targeted by ongoing reforestation and restoration initiatives (*cf.*Minnemeyer *et al*., 2011; http://www.wri.org/project/forest-landscape-restoration) and the map of Lepers *et al.* (2005) showing the main areas of rapid forest cover changes over the period 1980–2000. However, no attempt was made as yet to assess if and to what extent these areas are currently experiencing water scarcity issues.

Publication of research

Peña-Arancibia, J. L., M. Mulligan, L. A. Bruijnzeel and A.I.J.M van Dijk (in prep.), Pan tropical modelling of the effects of land use and land cover change on dry season flows. **Agriculture Ecosystems & Environment,** manuscript in preparation.

7.2 Future research needs

Several possible research avenues have emerged from the present work which are grouped below in the following three subjects: (*i*) identifying hydrological impacts of LUCC in streamflow records; (*ii*) improvements to the W3RA-LUM for pan-tropical LUCC impact analyses; (*iii*) further analysis of modelling results.

7.2.1 Identifying hydrological impacts of LUCC in streamflow records

As new datasets become publicly available, there will be opportunities for analysing the hydrological impacts of LUCC on streamflow for additional 'real-world' catchments. The opening of the United States Geological Survey's (USGS) Landsat data archive (Woodcock *et al*., 2008) will make possible the retrospective analysis of catchments having significant LUCC, in a more accurate fashion than is currently possible using MODIS-based data on LUCC. Methods to monitor LUCC at national scales in an operational fashion exist and are in use in several

countries (Hansen *et al.*, 2012): *e.g.*; terra-i (www.terra-i.org) for the whole of Latin America, the PRODES product from Brazil's National Institute for Space Research (INPE), the Australia National Carbon Accounting System (NCAS) forest classification product (used in Chapter 2) from the Commonwealth Scientific and Industrial Research Organisation (CSIRO) and the National Land Cover Dataset (NLCD) from the USGS. For example, NCAS data provide the presence or absence of forests at 25 m resolution for fifteen time-periods since 1972. In the case of persistent cloud cover, as tends to be the case in many humid tropical areas, MODIS can be used to temporally disaggregate the Landsat images (*cf.* Broich *et al.*, 2011).

The acquisition of tropical hydrometric data is still a major challenge. In the case of rainfall, the inaccuracies and regional and seasonal biases of satellite-derived and reanalysis data make their direct use questionable where there are better sources. It was demonstrated in Chapter 3 the use of *in situ* rainfall station data to improve rainfall estimates in satellites and reanalyses products, particularly the correction of satellite biases in tropical locations. Regrettably, observational hydrometric data collection – including rainfall, streamflow and other meteorological variables – is in decline (Bonell *et al.*, 1993; Wohl *et al.*, 2012) (Figure **7.1**1), especially in the tropics.

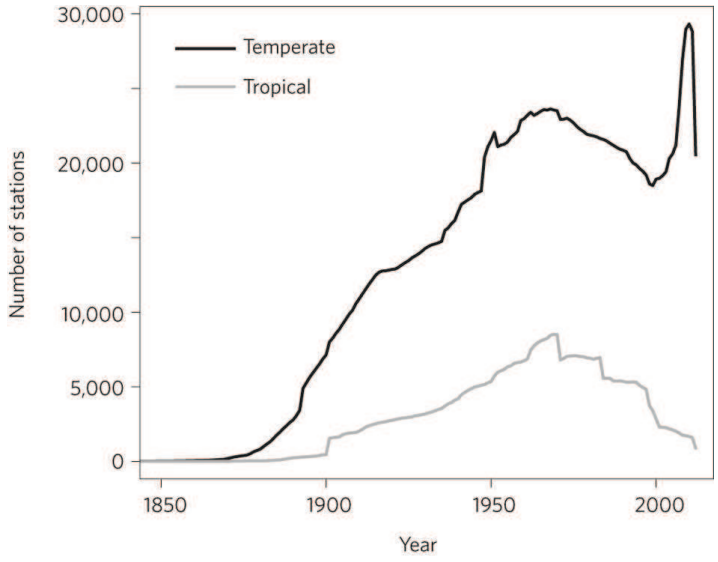

Figure 7.1 Number of precipitation stations in the Global Historical Climatology Network data set for each year (after Wohl *et al.*, 2012).

Long-term, high-quality, pan-tropical streamflow data are also limited, particularly at the daily time-scale. For the current research, daily streamflow data for 1175 tropical and sub-tropical stations with >5 years of data were selected from the Global Runoff Database (GRDB) of the Global Runoff Data Centre (http://www.bafg.de/GRDC/EN/Home/homepage_node.html), which is the main repository for freely-available global streamflow data. However, many of the station records terminated in the 1980s. Within Australia, the Bureau of Meteorology (www.bom.gov.au) is compiling and centralising all available hydrometric data. During this research, several other Australian 'real-world' catchments with long-term streamflow data and concurrent LUCC were identified using NCAS data. Although situated outside of the tropics, these provide an interesting opportunity to extend the research to catchments in temperate Australia. The availability of these hydrometric data and more detailed biophysical data (*e.g.*, LUCC dynamics, soil depth maps, soil hydraulic properties and groundwater systems) may be of help in the investigation of the trade off between changes in the 'pump' and 'sponge' effects associated with LUCC in different Australian settings.

7.2.2 Improvements to W3RA-LUM for pan-tropical LUCC impact analysis

The calibrated variant of W3RA (Van Dijk *et al.*, accepted) using daily streamflow observations for 160 Australian catchments performed equally or better than other global models from the Global Land Data Assimilation System (GLDAS; Rodell *et al.*, 2004) when evaluated against monthly observed streamflow for 1461 catchments (Chapter 5). However, to reproduce measured monthly streamflows required unrealistic values for parameters that control evapotranspiration such as vegetation leaf area index (LAI). Ongoing investigations with AWRA-L in continental Australia have included remotely sensed near-surface soil moisture and LAI in a multi-objective calibration scheme, which marginally improved streamflow predictions but noticeably improved modelled LAI and soil moisture estimates (Zhang *et al*., 2011). The results obtained with W3RA-LUM using the parameter set obtained by Zhang *et al.* (2011) can be evaluated against streamflow for the 1461 aforementioned catchments as was done in Chapter 5 with the default parameter set.

Existing flow networks at 1º grid cell resolution (Oki and Sud, 1998) can be used to implement a routing algorithm for W3RA-LUM which in turn can be used to compare the modelled streamflow to gauge data. This improvement is crucial to analyse upstream-downstream interactions depending on the location and pattern of the LUCC. In addition, routing which accounts for delays in large dams (*e.g.*, Hanasaki *et al.*, 2006) can be implemented using existing dam datasets (Mulligan *et al.*, 2009).

7.2.3 Further analysis of modelling results

The analyses provided here focused on long-term intra-annual impacts of LUCC on streamflow. Whilst this can help to determine 'hotspots' where tropical LUCC can be expected to have the greatest impacts on dry season flows, the availability of long-term (1948–2008) daily time-series permits other types of analyses as well. For example, a streamflow drought analysis can be performed in each grid cell for the scenarios investigated (*e.g.*, Hisdal *et al.*, 2001). The dry season can be defined in each grid cell and indices of drought frequency and severity can be computed, which will provide a quantitative metric rather than the qualitative metric used for dry season flows here. In addition, it will be possible to compute trends of drought frequency and severity during the dry season.

References

Akaike, H. (1970), Statistical predictor identification, Ann. Inst. Stat. Math., 22, 203-217.

Alcamo, J. M., R. Leemans and E. Kreileman (1998), Global change scenarios of the 21st century - Results from the IMAGE 2.1 model. London: Elsevier.

Alegre, J. C., and D. K. Cassel (1996), Dynamics of soil physical properties under alternative systems to slash-and-burn, Agriculture Ecosystems & Environment, 58(1), 39-48.

Allen, R. G., L. S. Pereira, D. Raes, and M. Smith (1998), Crop evapotranspiration - Guidelines for computing crop water requirements. Food and Agricultural Organisation of the United Nations, Rome.

Allen, R. G., L. S. Pereira, M. Smith, D. Raes, and J. L. Wright (2005), FAO-56 dual crop coefficient method for estimating evaporation from soil and application extensions, Journal of irrigation and drainage engineering, 131, 2-13.

Angelini, I. M., M. Garstang, R. E. Davis, B. Hayden, D. R. Fitzjarrald, D. R. Legates, S. Greco, S. Macko, and V. Connors (2011), On the coupling between vegetation and the atmosphere, Theoretical and Applied Climatology, 105(1-2), 243-261.

Arino, O., P. Bicheron, F. Achard, J. Latham, R. Witt, and J.L. Weber (2008), GLOBCOVER The most detailed portrait of Earth, Esa Bulletin-European Space Agency(136), 24-31.

Arnell, N. W. (1999), A simple water balance model for the simulation of streamflow over a large geographic domain, Journal of Hydrology, 217(3-4), 314-335.

Arnell, N. W. (2003), Effects of IPCCSRES emissions scenarios on river runoff: a global perspective, Hydrology and Earth System Sciences, 7(5), 619-641.

Bai, Z. G., Dent, D. L., Olsson, L. and M. E. Schaepman (2008) Proxy global assessment of land degradation, Soil use and Management, 24, 223-234.

Band, L. E. (2011), Commentary on the progress of the Australian Water Resources Assessment development, paper presented at Water Information Research and Development Alliance Science Symposium, August 2011. Melbourne. Retrieved November 5, 2012 <http://www.csiro.au/WIRADA-Science-Sympsosium-Proceedings>.

Batjes, N. H. (2008), ISRIC-WISE Harmonized Global Soil Profile Dataset (Ver. 3.1). Report 2008/02, ISRIC - World Soil information, Wagenigen. Retrieved November 5, 2012 < http://www.isric.org/isric/webdocs/docs//ISRIC_Report_2008_02.pdf>.

Batjes, N. H. (2010) ISRIC-WISE derived soil properties on a 5 by 5 arc-minutes global grid (version 1.0). Report 2006/02 ISRIC World Soil Information, Wagenigen 2006. Retrieved November 5, 2012 <http://www.isric.org/isric/webdocs/Docs/ISRIC_Report_2006_02.pdf>.

Batjes, N. H. (ed.). (1995), A homogenized soil data file for global environmental research: A subset of FAO, ISRIC and NRCS profiles (Version 1.0). Working Paper and Preprint 95/10b, International Soil Reference and Information Centre, Wageningen, The Netherlands.

Beck, H. E., L. A. Bruijnzeel, A. I. J. M. van Dijk, T. R. McVicar, F. N. Scatena, and J. Schellekens (2013), The impact of forest regeneration on streamflow in 12 meso-scale humid tropical catchments, Hydrol. Earth Syst. Sci. Discuss., 10, 3045-3102.

Beck, H. E., R. A. M. de Jeu, J. Schellekens, A. I. J. M. van Dijk, and L. A. Bruijnzeel (2009), Improving Curve Number Based Storm Runoff Estimates Using Soil Moisture Proxies, IEEE Journal of Selected Topics in Applied Earth Observations and Remote Sensing, 2(4), 250-259.

Berg, A. A., J. S. Famiglietti, J. P. Walker, and P. R. Houser (2003), Impact of bias correction to reanalysis products on simulations of North American soil moisture and hydrological fluxes, Journal of Geophysical Research-Atmospheres, 108(D16), 4490.

Bergstrom, S. (1995), The HBV model, in Computer Models of Watershed Hydrology, edited by Singh, V. P., pp. 443-476, Water Resource Publications, Highlands Ranch, Colorado, USA.

Best, M. J., et al. (2011), The Joint UK Land Environment Simulator (JULES), model description - Part 1: Energy and water fluxes, Geoscientific Model Development, 4(3), 677-699.

Betts, A. K., J. H. Ball, P. Viterbo, A. Dai, and J. Marengo (2005), Hydrometeorology of the Amazon in ERA-40, J. Hydrometeorol., 6(5), 764-774.

Betts, A. K., M. Kohler, and Y. C. Zhang (2009), Comparison of river basin hydrometeorology in ERA-Interim and ERA-40 reanalyses with observations, Journal of Geophysical Research-Atmospheres, 114, D02101.

Betts, A. K., M. Zhao, P. A. Dirmeyer, and A. C. M. Beljaars (2006), Comparison of ERA40 and NCEP/DOE near-surface data sets with other ISLSCP-II data sets, Journal of Geophysical Research-Atmospheres, 111(D22), D22S04.

Beven, K. (2006), A manifesto for the equifinality thesis, Journal of Hydrology, 320(1-2), 18-36.

Billington, C., V. Kapos, M. Edwards, S. Blyth and S. Iremonger (1996), Estimated Original Forest Cover Map: A First Attempt. World Conservation Monitoring Center, Cambridge. Retrieved 23 March, 2012 < http://www.wcmc.org.uk/>..

Bloeschl, G., S. Ardoin-Bardin, M. Bonell, M. Dorninger, D. Goodrich, D. Gutknecht, D. Matamoros, B. Merz, P. Shand, and J. Szolgay (2007), At what scales do climate variability and land cover change impact on flooding and low flows?, Hydrological Processes, 21(9), 1241-1247.

Blöschl, G., S. Ardoin-Bardin, M. Bonell, M. Dorninger, D. Goodrich, D. Gutknecht, D. Matamoros, B. Merz, P. Shand, and J. Szolgay (2007), At what scales do climate variability and land cover change impact on flooding and low flows?, Hydrological Processes, 21(9), 1241-1247.

Bonell, M. (2005), Runoff generation in tropical forests, Forests, Water and People in the Humid Tropics, Tropics, edited by M. Bonell and L. A. Bruijnzeel, 314-406, Cambridge University Press, Cambridge.

Bonell, M., and J. Balek (1993), Recent scientific developments and research needs in hydrological processes of the humid tropics, in Hydrology and Water Management in the Humid Tropics, edited by M. Bonell, M. M. Hufschmidt, and J.S. Gladwell, pp. 167-260, Cambridge University Press, Cambridge.

Bonell, M., and J. Williams (2009), A review of hydrology research within the open eucalypt woodlands of tropical semiarid Australia: a possible source of baseline information for the West African Sahel, Secheresse, 20(1), 31-47.

Bonell, M., and J. Williams (2009), A review of hydrology research within the open eucalypt woodlands of tropical semiarid Australia: a possible source of baseline information for the West African Sahel, Secheresse, 20(1), 31-47.

Bonell, M., and L. A. Bruijnzeel (2004), Forests, water and people in the humid tropics: past, present and future hydrological research for integrated land and water management, Cambridge University Press, Cambridge, UK. 925 pp.

Bonell, M., B. K. Purandara, B. Venkatesh, J. Krishnaswamy, H. A. K. Acharya, U. V. Singh, R. Jayakumar, and N. Chappell (2010), The impact of forest use and reforestation on soil hydraulic conductivity in the Western Ghats of India: Implications for surface and sub-surface hydrology, Journal of Hydrology, 391(1-2), 49-64.

Bosch, J. M., and J. D. Hewlett (1982), A review of catchment experiments to determine the effect of vegetation changes on water yield and evapo-transpiration, Journal of Hydrology, 55(1-4), 3-23.

Bosilovich, M. G., F. R. Robertson, and J. Chen (2011), Global Energy and Water Budgets in MERRA, J. Clim., 24(22), 5721-5739.

Bosilovich, M. G., J. Y. Chen, F. R. Robertson, and R. F. Adler (2008), Evaluation of global precipitation in reanalyses, Journal of Applied Meteorology and Climatology, 47(9), 2279-2299.

Brandes, D., J. G. Hoffmann, and J. T. Mangarillo (2005), Base flow recession rates, low flows, and hydrologic features of small watersheds in Pennsylvania, USA, Journal of the American Water Resources Association, 41(5), 1177-1186.

Bridge, B. J., J. J. Mott, W. H. Winter, and R. J. Hartigan (1983), Improvement in soil structure resulting from sown pastures on degraded areas in the dry savanna woodlands of northern Australia, Australian Journal of Soil Research, 21(1), 83-90.

Broich, M., M. C. Hansen, P. Potapov, B. Adusei, E. Lindquist, and S. V. Stehman, (2011), Time-series analysis of multi-resolution optical imagery for quantifying forest cover loss in Sumatra and Kalimantan, Indonesia. International Journal of Applied Earth Observation and Geoinformation, 13, 277-291.

Brooks, R. H., and A. T. Corey (1964), Hydraulic properties of porous media, Hydrological Papers (Colorado State University), 3.

Brown, A. E., L. Zhang, T. A. McMahon, A. W. Western, and R. A. Vertessy (2005), A review of paired catchment studies for determining changes in water yield resulting from alterations in vegetation, Journal of Hydrology, 310(1-4), 28-61.

Bruijnzeel, L. A. (1990), Hydrology of moist tropical forests and effects of conversion: a state of knowledge review, UNESCO International Hydrological Programme and Free University Amsterdam.

Bruijnzeel, L. A. (1990), Hydrology of moist tropical forests and effects of conversion: a state of knowledge review, Unesco International Hydrological Programme, Paris, France, 224 pp.

Bruijnzeel, L. A. (2002), Hydrology of tropical montane cloud forests: a reassessment, paper presented at Proceedings of the Second International Colloquium on Hydrology and Water Management of the Humid Tropics, UNESCO, Paris and CATHALAC, Panama City, Panama.

Bruijnzeel, L. A. (2004), Hydrological functions of tropical forests: not seeing the soil for the trees? Agriculture Ecosystems & Environment, 104(1), 185-228.

Bruijnzeel, L. A., and J. Proctor (1995), Hydrology and biogeochemistry of tropical montane cloud forests: what do we really know?, in Tropical Montane Cloud Forests, edited by L. S. Hamilton, J. O. Juvik and F. N. Scatena, pp. 38-78, Springer Ecological Studies.

Bruijnzeel, L. A., M. Mulligan, and F. N. Scatena (2011), Hydrometeorology of tropical montane cloud forests: emerging patterns, Hydrological Processes, 25(3), 465-498.

Brutsaert, W., and J. L. Nieber (1977), Regionalized drought flow hydrographs from a mature glaciated plateau, Water Resources Research, 13(3), 637-644.

Bruun, T. B., A. de Neergaard, D. Lawrence, and A. D. Ziegler (2009), Environmental Consequences of the Demise in Swidden Cultivation in Southeast Asia: Carbon Storage and Soil Quality, Human Ecology, 37(3), 375-388.

Budyko, M. I. (1974), Climate and Life, Academic Press, New York, 508 pp.

Bureau of Meteorology - BOM (2010), La Niña – Detailed Australian Analysis. Retrieved November 5, 2012 < http://www.bom.gov.au/climate/enso/lnlist/>. >.

Burgess, S. S. O., M. A. Adams, N. C. Turner, and C. K. Ong (1998), The redistribution of soil water by tree root systems, Oecologia, 115(3), 306-311.

Buytaert, W., D. Reusser, S. Krause, and J. P. Renaud (2008), Why can't we do better than Topmodel?, Hydrological Processes, 22(20), 4175-4179.

Caesar, J., L. Alexander, and R. Vose (2006), Large-scale changes in observed daily maximum and minimum temperatures: Creation and analysis of a new gridded data set, Journal of Geophysical Research-Atmospheres, 111(D5), D05101.

Calder, I. R. (2002), Forests and Hydrological services: Reconciling public science and perceptions, Land Use and Water Resources Research, 2, 2.1-2.12.

Calder, I. R. (2007), Forests and water-Ensuring forest benefits outweigh water costs, Forest Ecology and Management, 251(1-2), 110-120.

Canadell, J., R. B. Jackson, J. R. Ehleringer, H. A. Mooney, O. E. Sala, and E. D. Schulze (1996), Maximum rooting depth of vegetation types at the global scale, Oecologia, 108(4), 583-595.

Chandler, D. G. (2006), Reversibility of forest conversion impacts on water budgets in tropical karst terrain, Forest Ecology and Management, 224(1-2), 95-103.

Chandler, D. G., and M. F. Walter (1998), Runoff responses among common land uses in the uplands of Matalom, Leyte, Philippines, Transactions of the ASAE, 41(6), 1635-1641.

Chapman, T. (1999), A comparison of algorithms for stream flow recession and baseflow separation, Hydrological Processes, *13*(5), 701-714.

Chappell, N. A. (2010) Soil pipe distribution and hydrological functioning within the humid tropics: a synthesis, Hydrological Processes, 24, 1567-1581.

Chappell, N. A., M. Sherlock, K. Bidin, R. Macdonald, Y. Najman, and G. Davies (2007), Runoff processes in Southeast Asia: Role of soil, regolith, and rock type, in Forest Environments in the Mekong River Basin edited, by H. Swada, M. Araki, N.A. Chappell, J.V. LaFrankie, A. Shimizu, 3-23, Springer-Verlag, Tokyo (2007),

Chiacchio M., Arabini E., Wild M. (2010), Development of a gridded surface solar radiation dataset from the Global Energy Balance Archive. EGU General Assembly 2010, held 2-7 May, 2010 in Vienna, Austria, p.10918

Chiew, F. H. S., and T. A. McMahon (1991), The applicability of Morton and Penman evapotranspiration estimates in rainfall-runoff modeling, Water Resources Bulletin, 27(4), 611-620.

Coe, M. T., E. M. Latrubesse, M. E. Ferreira, and M. L. Amsler (2011), The effects of deforestation and climate variability on the streamflow of the Araguaia River, Brazil, Biogeochemistry, 105(1-3), 119-131.

Colloff, M. J., K. R. Pullen, and S. A. Cunningham (2010), Restoration of an Ecosystem Function to Revegetation Communities: The Role of Invertebrate Macropores in Enhancing Soil Water Infiltration, Restoration Ecology, 18, 65-72.

Cornish, P. M., and R. A. Vertessy (2001), Forest age-induced changes in evapotranspiration and water yield in a eucalypt forest, Journal of Hydrology, 242(1-2), 43-63.

Costa, M. H., A. Botta, and J. A. Cardille (2003), Effects of large-scale changes in land cover on the discharge of the Tocantins River, Southeastern Amazonia, Journal of Hydrology, 283(1-4), 206-217.

Costa, M. H., M. C. Biajoli, L. Sanches, A. C. M. Malhado, L. R. Hutyra, H. R. da Rocha, R. G. Aguiar, and A. C. de Araujo (2010), Atmospheric versus vegetation controls of Amazonian tropical rain forest evapotranspiration: Are the wet and seasonally dry rain forests any different?, Journal of Geophysical Research-Biogeosciences, 115, G0402.

da Rocha, H. R., M. L. Goulden, S. D. Miller, M. C. Menton, L. Pinto, H. C. de Freitas, and A. Figueira (2004), Seasonality of water and heat fluxes over a tropical forest in eastern Amazonia, Ecological Applications, 14(4), S22-S32.

Dadson, S. J., V. A. Bell, and R. G. Jones (2011), Evaluation of a grid-based river flow model configured for use in a regional climate model, Journal of Hydrology, 411(3-4), 238-250.

Daniel, J. A., K. Potter, W. Altom, H. Aljoe, and R. Stevens (2002), Long-term grazing density impacts on soil compaction, Transactions of the Asae, 45(6), 1911-1915.

de Moraes, J. M., A. E. Schuler, T. Dunne, R. d. O. Figueiredo, and R. L. Victoria (2006), Water storage and runoff processes in plinthic soils under forest and pasture in Eastern Amazonia, Hydrological Processes, 20(12), 2509-2526.

de Noblet-Ducoudré, N. and J. Y. Peterschmitt (2006), Designing historical and future land-cover maps at the global scale for climate studies. Retrieved 20 March, 2012 < http://www.cnrm.meteo.fr/ensembles/public/data/LandUseMaps_Informations.pdf>.

de Rosnay, P., J. Polcher, K. Laval, and M. Sabre (2003), Integrated parameterization of irrigation in the land surface model ORCHIDEE. Validation over Indian Peninsula, Geophysical Research Letters, 30(19), GL018024.

Dee, D. P., et al. (2011), The ERA-Interim reanalysis: configuration and performance of the data assimilation system, Quarterly Journal of the Royal Meteorological Society, 137(656), 553-597.

Defries, R. S., M. C. Hansen, and J. R. G. Townshend (2000), Global continuous fields of vegetation characteristics: a linear mixture model applied to multi-year 8 km AVHRR data, International Journal of Remote Sensing, 21(6-7), 1389-1414.

Defries, R. S., M. C. Hansen, J. R. G. Townshend, A. C. Janetos, and T. R. Loveland (2000), A new global 1-km dataset of percentage tree cover derived from remote sensing, Global Change Biology, 6(2), 247-254.

DeFries, R., and L. Bounoua (2004), Consequences of land use change for ecosystem services: a future unlike the past, GeoJournal, 61(4), 345-351.

Descheemaeker, K., J. Poesen, L. Borselli, J. Nyssen, D. Raes, M. Haile, B. Muys, and J. Deckers (2008), Runoff curve numbers for steep hillslopes with natural vegetation in semi-arid tropical highlands, northern Ethiopia, Hydrological Processes, 22(20), 4097-4105.

Detenbeck, N. E., V. J. Brady, D. L. Taylor, V. M. Snarski, and S. L. Batterman (2005), Relationship of stream flow regime in the western Lake Superior basin to watershed type characteristics, Journal of Hydrology, 309(1-4), 258-276.

Deuchars, S. A., J. Townend, M. J. Aitkenhead, and E. A. FitzPatrick (1999), Changes in soil structure and hydraulic properties in regenerating rain forest, Soil Use and Management, 15(3), 183-187.

Dilshad, M., and L. J. Peel (1994), Evaluation of the USDA Curve Number Method for Agricultural Catchments in the Australian Semiarid Tropics, Australian Journal of Soil Research, 32(4), 673-685.

Döll, P., F. Kaspar, and B. Lehner (2003), A global hydrological model for deriving water availability indicators: model tuning and validation, Journal of Hydrology, 270(1-2), 105-134.

Döll, P., K. Fiedler, and J. Zhang (2009), Global-scale analysis of river flow alterations due to water withdrawals and reservoirs, Hydrology and Earth System Sciences, 13(12), 2413-2432.

Donohue, R. J., M. L. Roderick, and T. R. McVicar (2007), On the importance of including vegetation dynamics in Budyko's hydrological model, Hydrology and Earth System Sciences, 11(2), 983-995.

Donohue, R. J., M. L. Roderick, and T. R. McVicar (2010), Can dynamic vegetation information improve the accuracy of Budyko's hydrological model?, Journal of Hydrology, 390(1-2), 23-34.

Donohue, R. J., T. R. McVicar, and M. L. Roderick (2010), Assessing the ability of potential evaporation formulations to capture the dynamics in evaporative demand within a changing climate, Journal of Hydrology, 386(1-4), 186-197.

Driessen, P., Deckers, J., Spaargaren, O., and Nachtergaele, F. (2001), Lecture notes on the major soils of the world, FAO, Rome, 35-37.

Dyhr-Nielsen, M. (1986), Hydrological Effect of Deforestation in the Chao Phraya Catchment in Thailand. International Symposium on Tropical Forest Hydrology and Application, Chiangmai, Thailand, p. 12.

Ebert, E. E., J. E. Janowiak, and C. Kidd (2007), Comparison of near-real-time precipitation estimates from satellite observations and numerical models, Bulletin of the American Meteorological Society, 88(1), 47-64.

Edwards, K. A. (1979), The water balance of the Myeba experimental catchments. East African Agricultural and Forestry Journal, 43, 231-247.

El-Hames, A. S. (2012), An empirical method for peak discharge prediction in ungauged arid and semi-arid region catchments based on morphological parameters and SCS curve number, Journal of Hydrology, 456, 94-100.

Elkaduwa, W. K. B. and R. Sakthivadive (1998), Use of historical data as a decision support tool in watershed management: A case study of the Upper Nilwala basin in Sri Lanka. Research Report 26. Colombo, Sri Lanka: International Water Management Institute. Retrieved June 24, 2012 < http://www.iwmi.cgiar.org/Publications/>.

Ellis, E., and R. Pontius (2010), Land-use and land-cover change, Encyclopedia of Earth. Cleveland. Washington, D.C.: Environmental Information Coalition, National Council for Science and the Environment. First published in the Encyclopedia of Earth April 18, 2010, last revised date May 11, 2011. Retrieved March 20, 2012 <http://www.eoearth.org/article/Land-use_and_land-cover_change>.

Elsenbeer, H. (2001), Hydrologic flowpaths in tropical rainforest soilscapes - a review, Hydrological Processes, 15(10), 1751-1759.

Elsenbeer, H., B. E. Newton, T. Dunne, and J. M. de Moraes (1999), Soil hydraulic conductivities of latosols under pasture, forest, and teak in Rondonia, Brazil, Hydrological Processes, 13 (9), 1417-1422.

Essery, R., and D. B. Clark (2003), Developments in the MOSES 2 land-surface model for PILPS 2e, Global and Planetary Change, 38(1-2), 161-164.

Eswaran, H., T. Rice, R. Ahrens, B.A. Stewart (2002), Soil Classification: A global desk reference. CRC Press, Boca Raton, Florida.

FAO (2006), Global Forest Resources Assessment 2005. Progress towards sustainable forest management. Retrieved 20 March, 2012 <http://www.fao.org/docrep/008/a0400e/a0400e00.htm>..

FAO (2010), Global forest land-use change from 1990 to 2005. Retrieved 20 March, 2012 <http://foris.fao.org/static/data/fra2010/RSS_Summary_Report_lowres.pdf>..

FAO, 1993. Forest Resources Assessment 1990 – Tropical Countries, Rome. Retrieved 5 November, 2012 <http://www.ciesin.columbia.edu/docs/002-471/002-471.html>.

Fekete, B. M., C. J. Vorosmarty, J. O. Roads, and C. J. Willmott (2004), Uncertainties in precipitation and their impacts on runoff estimates, J. Clim., 17(2), 294-304.

Fenicia, F., H. H. G. Savenije, P. Matgen, and L. Pfister (2006), Is the groundwater reservoir linear? Learning from data in hydrological modelling, Hydrology and Earth System Sciences, 10(1), 139-150.

Fensham, R. J., and R. J. Fairfax (2003), Assessing woody vegetation cover change in north-west Australian savanna using aerial photography, International Journal of Wildland Fire, 12(3-4), 359-367.

Fensham, R. J., R. J. Fairfax, and S. R. Archer (2005), Rainfall, land use and woody vegetation cover change in semi-arid Australian savanna, Journal of Ecology, 93(3), 596-606.

Fernandes, K., R. Fu, and A. K. Betts (2008), How well does the ERA40 surface water budget compare to observations in the Amazon River basin?, Journal of Geophysical Research-Atmospheres, 113(D11), D11117.

Foley, J. A., et al. (2005), Global consequences of land use, Science, 309(5734), 570-574.

Foster, S. D. D. and P. J. Chilton (1993), Groundwater Systems in the Humid Tropics, in Hydrology and Water Management in the Tropics, edited by M. Bonell, M. M. Hufschmidt and J. S. Gladwell, 261-273, Cambridge University Press, Cambridge.

Fu, G., N. R. Viney, S. P. Charles, and J. Liu (2010), Long-Term Temporal Variation of Extreme Rainfall Events in Australia: 1910-2006, Journal of Hydrometeorology, 11(4), 950-965.

Fu, P.B. (1981), On the calculation of the evaporation from land surface Sci. Atmos. Sin., 22–31 (in Chinese).

Furby, S. (2002) Land Cover Change: Specification for Remote Sensing Analysis, National Carbon Accounting System Technical Report No. 9, Australian Greenhouse Office, Canberra.

Garcia, N. O., and C. R. Mechoso (2005), Variability in the discharge of South American rivers and in climate, Hydrological Sciences Journal-Journal Des Sciences Hydrologiques, 50(3), 459-478.

Gascoin, S., A. Ducharne, P. Ribstein, M. Carli, and F. Habets (2009), Adaptation of a catchment-based land surface model to the hydrogeological setting of the Somme River basin (France), Journal of Hydrology, 368(1-4), 105-116.

Gash, J. H. C. (1979), An analytical model of rainfall interception by forests, Royal Meteorological Society, Quarterly Journal, 105, 43-55.

Gash, J. H. C., C. R. Lloyd, and G. Lachaud (1995), Estimating sparse forest rainfall interception with an analytical model, Journal of Hydrology, 170(1-4), 79-86.

Germer, S., C. Neill, T. Vetter, J. Chaves, A. V. Krusche, and H. Elsenbeer (2009), Implications of long-term land-use change for the hydrology and solute budgets of small catchments in Amazonia, Journal of Hydrology, 364(3-4), 349-363.

Ghimire, C. P., L. A. Bruijnzeel, M. Bonell, N. Coles, M.W. Lubczynski and D.A. Gilmour (2013), The effects of sustained forest use on hillslope soil hydraulic conductivity in the Middle Mountains of Central Nepal. Ecohydrology, doi: 10.1002/eco.1367.

Giambelluca, T. W. (2002), Hydrology of altered tropical forest, Hydrological Processes, 16(8), 1665-1669.

Giambelluca, T. W., F. G. Scholz, S. J. Bucci, F. C. Meinzer, G. Goldstein, W. A. Hoffmann, A. C. Franco, and M. P. Buchert (2009), Evapotranspiration and energy balance of Brazilian savannas with contrasting tree density, Agricultural and Forest Meteorology, 149(8), 1365-1376.

Giambelluca, T. W., M. A. Nullet, A. D. Ziegler, and L. Tran (2000), Latent and sensible energy flux over deforested land surfaces in the eastern Amazon and northern Thailand, Singapore Journal of Tropical Geography, 21(2), 107-130.

Gibbs, H. K., A. S. Ruesch, F. Achard, M. K. Clayton, P. Holmgren, N. Ramankutty, and J. A. Foley (2010), Tropical forests were the primary sources of new agricultural land in the 1980s and 1990s, Proceedings of the National Academy of Sciences of the United States of America, 107(38), 16732-16737.

Gilgen, H., and A. Ohmura (1999), The Global Energy Balance Archive, Bulletin of the American Meteorological Society, 80(5), 831-850.

Gilmour, D. A., M. Bonell, and D. S. Cassells (1987), The effects of forestation on soil hydraulic-properties in the middle hills of Nepal - a preliminary assessment, Mountain Research and Development, 7(3), 239-249.

Global Soil Data Task (2000), Global Gridded Surfaces of Selected Soil Characteristics (IGBP-DIS). Available on-line at <http://www.daac.ornl.gov>. from Oak Ridge National Laboratory Distributed Active Archive Center, Oak Ridge, Tennessee, U.S.A.

Godsey, S., and H. Elsenbeer (2002), The soil hydrologic response to forest regrowth: a case study from southwestern Amazonia, Hydrological Processes, 16(7), 1519-1522.

Goldewijk, K. K., and N. Ramankutty (2004), Land cover change over the last three centuries due to human activities: the availability of new global data sets, GeoJournal, 61(4), 335-344.

Gordon, L. J., W. Steffen, B. F. Jonsson, C. Folke, M. Falkenmark, and A. Johannessen (2005), Human modification of global water vapor flows from the land surface, Proceedings of the National Academy of Sciences of the United States of America, 102(21), 7612-7617.

Gottschalck, J., J. Meng, M. Rodell, and P. Houser (2005), Analysis of multiple precipitation products and preliminary assessment of their impact on global land data assimilation system land surface states, J. Hydrometeorol., 6(5), 573-598.

Grip, H., J. M. Fritsch, and L. A. Bruijnzeel (2004), Soil and water impacts during forest conversion and stabilization to new land use, in: Forests, Water, and People in the Humid Tropics: Past, Present and Future Hydrological Research for Integrated Land and Water Management, 561-589, edited by M. Bonell and L. A. Bruijnzeel, Cambridge University Press, Cambridge.

Grip, H., J. M. Fritsch, and L. A. Bruijnzeel (2005), Soil and water impacts during forest conversion and stabilisation to new land use, Forests, Water and People in the Humid Tropics, edited by M. Bonell and L.A. Bruijnzeel, 561-589, Cambridge University Press, Cambridge.

Gu, G., R. F. Adler, G. J. Huffman, and S. Curtis (2007), Tropical rainfall variability on interannual-to-interdecadal and longer time scales derived from the GPCP monthly product, J. Clim., 20(15), 4033-4046.

Gudmundsson, L., et al. (2012), Comparing Large-Scale Hydrological Model Simulations to Observed Runoff Percentiles in Europe, Journal of Hydrometeorology, 13(2), 604-620.

Guerschman, J. P. (2009), Remote Sensing of open water: why, where, when and how much?, in CSIRO Earth Observation Workshop, 31 March 2009, Canberra.

Guerschman, J. P., A. I. J. M. Van Dijk, G. Mattersdorf, J. Beringer, L. B. Hutley, R. Leuning, R. C. Pipunic, and B. S. Sherman (2009), Scaling of potential evapotranspiration with MODIS data reproduces flux observations and catchment water balance observations across Australia, Journal of Hydrology, 369(1-2), 107-119.

Gui, S., S. Liang, K. Wang, L. Li, and X. Zhang (2010), Assessment of Three Satellite-Estimated Land Surface Downwelling Shortwave Irradiance Data Sets, Ieee Geoscience and Remote Sensing Letters, 7(4), 776-780.

Gupta, S. K., D. P. Kratz, A. C. Wilber, and L. C. Nguyen (2004), Validation of parameterized algorithms used to derive TRMM-CERES surface radiative fluxes, Journal of Atmospheric and Oceanic Technology, 21(5), 742-752.

Gush, M. B., and P. J. Dye (2009), Water-Use Efficiency within a Selection of Indigenous and Exotic Tree Species in South Africa as Determined Using Sap Flow and Biomass Measurements, in VII International Workshop on Sap Flow, edited by E. Fernandez and A. Diaz Espejo, pp. 323-330, Int Soc Horticultural Science, Leuven 1.

Hacker, J. B., and R. B. Waite (2001), Selecting buffel grass (Cenchrus ciliaris) with improved spring yield in subtropical Australia, Tropical Grasslands, 35(4), 205-210.

Hagemann, S., and L. Dumenil (1998), A parametrization of the lateral waterflow for the global scale, Climate Dynamics, 14(1), 17-31.

Hanasaki, N., S. Kanae, and T. Oki (2006), A reservoir operation scheme for global river routing models. Journal of Hydrology, 327, 22-41.

Hanasaki, N., S. Kanae, T. Oki, K. Masuda, K. Motoya, N. Shirakawa, Y. Shen, and K. Tanaka (2008), An integrated model for the assessment of global water resources Part 1: Model description and input meteorological forcing, Hydrology and Earth System Sciences, 12(4), 1007-1025.

Hansen, M. C., and T. R. Loveland, (2012), A review of large area monitoring of land cover change using Landsat data.Remote Sensing of Environment, 122, 66-74.

Hansen, M. C., R. S. Defries, J. R. G. Townshend, and R. Sohlberg (2000), Global land cover classification at 1km spatial resolution using a classification tree approach, International Journal of Remote Sensing, 21(6-7), 1331-1364.

Hansen, M. C., R. S. DeFries, J. R. G. Townshend, M. Carroll, C. Dimiceli, and R. A. Sohlberg (2003), Global percent tree cover at a spatial resolution of 500 meters: first results of the MODIS Vegetation Continuous Fields algorithm, Earth Interactions, 7(10), 1-15.

Hartemink, A. E., T. Veldkamp, and Z. Bai (2008), Land cover change and soil fertility decline in tropical regions, Turkish Journal of Agriculture and Forestry, 32(3), 195-213.

Hassler, S. K., B. Zimmermann, M. van Breugel, J. S. Hall, and H. Elsenbeer (2011), Recovery of saturated hydraulic conductivity under secondary succession on former pasture in the humid tropics, Forest Ecology and Management, 261(10), 1634-1642.

Hawkins, R. H., T. J. Ward, D. E. Woodward, and J. A. Van Mullen (2009), Curve Number Hydrology: State of the Practice, 105 pp., American Society of Civil Engineers, Reston, Virginia.

Hicke, J. A. (2005), NCEP and GISS solar radiation data sets available for ecosystem modeling: Description, differences, and impacts on net primary production, Global Biogeochemical Cycles, 19(2), GB2006.

Hijmans, R. J., S. E. Cameron, J. L. Parra, P. G. Jones, and A. Jarvis (2005), Very high resolution interpolated climate surfaces for global land areas, International Journal of Climatology, 25(15), 1965-1978.

Hirsch, R. M., J. R. Slack, and R. A. Smith (1982), Techniques of trend analysis for monthly water-quality data, Water Resources Research, 18(1), 107-121.

Hisdal, H., K. Stahl, L. M.Tallaksen, and S. Demuth, (2001), Have streamflow droughts in Europe become more severe or frequent? International Journal of Climatology, 21, 317-333.

Hoffmann, W. A., E. R. da Silva, G. C. Machado, S. J. Bucci, F. G. Scholz, G. Goldstein, and F. C. Meinzer (2005), Seasonal leaf dynamics across a tree density gradient in a Brazilian savanna. Oecologia 145, 307-316.

Holscher, D., J. Mackensen, and J. M. Roberts (2005), Forest recovery in the humid tropics: Changes in vegetation structure, nutrient pools and the hydrological cycle, Forests, Water and People in the Humid Tropics, Tropics, edited by M. Bonell and L. A. Bruijnzeel, 598-621.

Holscher, D., T. D. A. Sa, T. X. Bastos, and M. Denich (1997), Evaporation from young secondary vegetation in eastern Amazonia, Journal of Hydrology, 193(1-4), 293-305.

Hong, Y., and R. F. Adler (2008), Estimation of global SCS curve numbers using satellite remote sensing and geospatial data, International Journal of Remote Sensing, 29(2), 471-477.

Huete, A., K. Didan, T. Miura, E. P. Rodriguez, X. Gao, and L. G. Ferreira (2002), Overview of the radiometric and biophysical performance of the MODIS vegetation indices, Remote Sensing of Environment, 83, 195-213.

Huffman, G. J., R. F. Adler, D. T. Bolvin, G. J. Gu, E. J. Nelkin, K. P. Bowman, Y. Hong, E. F. Stocker, and D. B. Wolff (2007), The TRMM multisatellite precipitation analysis (TMPA): Quasi-global, multiyear, combined-sensor precipitation estimates at fine scales, J. Hydrometeorol., 8(1), 38-55.

Huschke, E. (ed.) (1959) Glossary of meteorology. American Meteorological Society. Retrieved August 28, 2012 < http://amsglossary.allenpress.com/glossary>.

Hutley L.B., Beringer J. (2010) Flux dynamics in a northern Australian tropical savanna, in Ecosystem Function in Savannas: Measurement and Modeling at Landscape to Global Scales, edited by M.J. Hill and N.P. Hanan, CRC/Taylor and Francis Press.

Ilstedt, U., A. Malmer, E. Verbeeten, and D. Murdiyarso (2007), The effect of afforestation on water infiltration in the tropics: A systematic review and meta-analysis, Forest Ecology and Management, 251(1-2), 45-51.

IPCC, (2001) Climate Change 2001: Synthesis Report. A Contribution of Working Groups I, II, and III to the Third Assessment Report of the Integovernmental Panel on Climate Change, edited by Watson, R.T. and the Core Writing Team, Cambridge University Press, Cambridge, United Kingdom, and New York, NY, USA, 398 pp.

IUSS Working Group WRB (2006) World Reference Base for Soil Resources 2006, second ed., World Soil Resources Reports No. 103, FAO, Rome. Retrieved November 5, 2012 < http://www.fao.org/ag/Agl/agll/wrb/doc/wrb2006final.pdf >.

IUSS Working Group WRB, 2006. World Reference Base for Soil Resources 2006, second ed. World Soil Resources Reports No. 103, FAO, Rome.

Ive, J. R., C. W. Rose, B. H. Wall, and B. W. R. Torssell (1976), Estimation and simulation of sheet run-off, Australian Journal of Soil Research, 14(2), 129-138.

Ive, J. R., C.W Rose, B.H. Wall, and B.W.R. Torssell (1976), Estimation and simulation of sheet run-off., Australian Journal of Soil Research, 14 (2), 129-138.

Jarvis, P. G., and K. G. McNaughton (1986), Stomatal control of transpiration: scaling up from leaf to region, Advances in ecological research, 15(1), 1-49.

Jeffrey, S. J., J. O. Carter, K. B. Moodie, and A. R. Beswick (2001), Using spatial interpolation to construct a comprehensive archive of Australian climate data, Environmental Modelling & Software, 16(4), 309-330.

Jones, H. G. (1998), Stomatal control of photosynthesis and transpiration, Journal of Experimental Botany, 49(90001), 387-398.

Joyce, R. J., J. E. Janowiak, P. A. Arkin, and P. P. Xie (2004), CMORPH: A method that produces global precipitation estimates from passive microwave and infrared data at high spatial and temporal resolution, J. Hydrometeorol., 5(3), 487-503.

Juhrbandt, J., C. Leuschner, and D. Holscher (2004), The relationship between maximal stomatal conductance and leaf traits in eight Southeast Asian early successional tree species, Forest Ecology and Management, 202(1-3), 245-256.

Kalnay, E., et al. (1996), The NCEP/NCAR 40-year reanalysis project, Bulletin of the American Meteorological Society, 77(3), 437-471.

Kanamitsu, M., W. Ebisuzaki, J. Woollen, S. K. Yang, J. J. Hnilo, M. Fiorino, and G. L. Potter (2002), NCEP-DOE AMIP-II reanalysis (R-2), Bulletin of the American Meteorological Society, 83(11), 1631-1643.

Kelliher, F. M., R. Leuning, M. R. Raupach, and E. D. Schulze (1995), Maximum conductances for evaporation from global vegetation types, Agricultural and Forest Meteorology, 73, 1-16.

King, E. A., et al. (2011), An operational actual evapotranspiration product for Australia, paper presented at Proceedings, Water Information Research and Development Alliance Science Symposium, August 2011. Melbourne. Retrieved November 5, 2012 <http://www.csiro.au/WIRADA-Science-Sympsosium-Proceedings>.

Klemes, V. (1983), Conceptualization and Scale in Hydrology, Journal of Hydrology, 65(1-3), 1-23.

Knyazikhin, Y., et al. (1999), MODIS Leaf Area Index (LAI) and Fraction of Photosynthetically Active Radiation Absorbed by Vegetation (FPAR) Product (MOD15) Algorithm Theoretical Basis Document. Retrieved November 5, 2012 < http://modis.gsfc.nasa.gov/data/atbd/atbd_mod15.pdf>.

Krinner, G., N. Viovy, N. d. Noblet-Ducoudre, J. Ogee, J. Polcher, P. Friedlingstein, P. Ciais, S. Sitch, and I. C. Prentice (2005), A dynamic global vegetation model for studies of the coupled atmosphere-biosphere system, Global Biogeochemical Cycles, 19(1), GB1015-GB1015.

Lakshmi, V., K. Czajkowski, R. Dubayah, and J. Susskind (2001), Land surface air temperature mapping using TOVS and AVHRR, International Journal of Remote Sensing, 22(4), 643-662.

Lal, R. (1987), Tropical Ecology and Physical Edaphology, Wiley, New York, pp. 732.

Lamb, D., P. D. Erskine, and J. A. Parrotta (2005), Restoration of degraded tropical forest landscapes, Science, 310(5754), 1628-1632.

Lambin, E. F., and P. Meyfroidt (2011), Global land use change, economic globalization, and the looming land scarcity, Proceedings of the National Academy of Sciences of the United States of America, 108(9), 3465-3472.

Langford, K. J. (1976), Change in yield of water following a bushfire in a forest of eucalyptus regnans, Journal of Hydrology, 29(1-2), 87-114.

Le Maître, D. C., and C. A. Colvin (2008), Assessment of the contribution of groundwater discharges to rivers using monthly flow statistics and flow seasonality, Water SA, 34(5), 549-564.

Lehner, B., C. Liermann, C. Revenga, C. Vörösmarty, B. Fekete, P. Crouzet, P. Döll. et al. (2008), High resolution mapping of the world's reservoirs and dams for sustainable river flow management. Frontiers in Ecology and the Environment. Source: GWSP Digital Water Atlas (2008). Map 81: GRanD Database (Dataset) (V1.0). Available online at <http://atlas.gwsp.org>.

Lehner, B., Verdin, K., and Jarvis, A. (2008) Hydrosheds technical documentation. Version 1.1. Retrieved November 5, 2012 < http://hydrosheds.cr.usgs.gov >.

Lepers, E., E. F. Lambin, A. C. Janetos, R. DeFries, F. Achard, N. Ramankutty, and R. J. Scholes (2005), A synthesis of information on rapid land-cover change for the period 1981-2000, Bioscience, 55(2), 115-124.

Leuning, R., Y. Q. Zhang, A. Rajaud, H. Cleugh, and K. Tu (2008), A simple surface conductance model to estimate regional evaporation using MODIS leaf area index and the Penman-Monteith equation, Water Resources Research, 44(10), W10419.

Li, M. X., and Z. G. Ma (2010), Comparisons of Simulations of Soil Moisture Variations in the Yellow River Basin Driven by Various Atmospheric Forcing Data Sets, Advances in Atmospheric Sciences, 27(6), 1289-1302.

Liang, S. L., K. C. Wang, X. T. Zhang, and M. Wild (2010), Review on Estimation of Land Surface Radiation and Energy Budgets From Ground Measurement, Remote Sensing and Model Simulations, Ieee Journal of Selected Topics in Applied Earth Observations and Remote Sensing, 3(3), 225-240.

Liang, X., D. P. Lettenmaier, E. F. Wood, and S. J. Burges (1994), A simple hydrologically based model of land-surface water and energy fluxes for general-circulation models, Journal of Geophysical Research-Atmospheres, 99(D7), 14415-14428.

Linhares, C.A. (2005), Influência do desflorestamento na dinâmica da resposta hidrológica na bacia do Rio Ji-paraná/RO (in Portuguese), doctoral thesis, Brazilian Institute for Space Research, INPE-13778-TDI/1052. Retrieved November 5, 2012 < http://mtc-m12.sid.inpe.br/col/sid.inpe.br/MTC-m13%4080/2005/09.06.13.50/doc/publicacao.pdf >.

Loker, W. M. (1994), Where's the beef - incorporating cattle into sustainable agroforestry system sin the amazon basin, Agroforestry Systems, 25(3), 227-241.

Lowe, L., R. J. Nathan, and R. Morden (2005), Assessing the impact of farm dams on streamflows; Part II: regional characterisation, Australian Journal of Water Resources, 9(1), 13-26.

Ma, L. J., T. J. Zhang, Q. X. Li, O. W. Frauenfeld, and D. Qin (2008), Evaluation of ERA-40, NCEP-1, and NCEP-2 reanalysis air temperatures with ground-based measurements in China, Journal of Geophysical Research-Atmospheres, 113(D15), D15115.

Ma, L. J., T. Zhang, O. W. Frauenfeld, B. S. Ye, D. Q. Yang, and D. H. Qin (2009), Evaluation of precipitation from the ERA-40, NCEP-1, and NCEP-2 Reanalyses and CMAP-1, CMAP-2, and GPCP-2 with ground-based measurements in China, Journal of Geophysical Research-Atmospheres, 114, D09105.

Macfarlane, C., S. K. Arndt, S. J. Livesley, A. C. Edgar, D. A. White, M. A. Adams, and D. Eamus (2007), Estimation of leaf area index in eucalypt forest with vertical foliage, using cover and fullframe fisheye photography, Forest Ecology and Management, 242(2-3), 756-763.

Madduma-Bandara, C. M., and T. A. Kuruppuarachchi (1988), Land-use change and hydrological trends in the upper Mahaweli basin, in Paper presented at the workshop on Hydrology of Natural and Man-made Forests in the Hill Country of Sri Lanka, p. 18.

Mahé, G., J. E. Paturel, E. Servat, D. Conway, and A. Dezetter (2005), The impact of land use change on soil water holding capacity and river flow modelling in the Nakambe River, Burkina-Faso, Journal of Hydrology, 300(1-4), 33-43.

Makarieva, A. M., and V. G. Gorshkov (2007), Biotic pump of atmospheric moisture as driver of the hydrological cycle on land, Hydrology and Earth System Sciences, 11(2), 1013-1033.

Malmer, A., D. Murdiyarso, L. A. Bruijnzeel, and U. Ilstedt (2010), Carbon sequestration in tropical forests and water: a critical look at the basis for commonly used generalizations, Glob. Change Biol., 16(2), 599-604.

Maneta, M. P., M. Torres, W. W. Wallender, S. Vosti, M. Kirby, L. H. Bassoi, and L. N. Rodrigues (2009), Water demand and flows in the Sao Francisco River Basin (Brazil) with increased irrigation, Agricultural Water Management, 96(8), 1191-1200.

Mao, D., and K. A. Cherkauer (2009), Impacts of land-use change on hydrologic responses in the Great Lakes region, Journal of Hydrology, 374(1-2), 71-82.

Marengo, J. A. (2004), Interdecadal variability and trends of rainfall across the Amazon basin, Theoretical and Applied Climatology, 78(1-3), 79-96.

Martinez, L. J., and J. A. Zinck (2004), Temporal variation of soil compaction and deterioration of soil quality in pasture areas of Colombian Amazonia, Soil & Tillage Research, 75(1), 3-17.

McJannet, D., J. Wallace, and P. Reddell (2007a), Precipitation interception in Australian tropical rainforests: II. Altitudinal gradients of cloud interception, stemflow, throughfall and interception, Hydrological Processes, 21(13), 1703-1718.

McVicar, T. R., et al. (2007), Developing a decision support tool for China's re-vegetation program: Simulating regional impacts of afforestation on average annual streamflow in the Loess Plateau, Forest Ecology and Management, 251(1-2), 65-81.

McVicar, T. R., T. G. Van Niel, L. T. Li, M. L. Roderick, D. P. Rayner, L. Ricciardulli, and R. J. Donohue (2008), Wind speed climatology and trends for Australia, 1975-2006: Capturing the stilling phenomenon and comparison with near-surface reanalysis output, Geophysical Research Letters, 35(20).

Meesters, A. G. C. A., A. J. Dolman, and L. A. Bruijnzeel (2009), Comment on 'Biotic pump of atmospheric moisture as driver of the hydrological cycle on land' by A. M. Makarieva and V. G. Gorshkov, Hydrol. Earth Syst. Sci., 11, 1013-1033, 2007, Hydrol. Earth Syst. Sci., 13(7), 1299-1305.

Mehta, V. K., P. J. Sullivan, M. T. Walter, J. Krishnaswamy, and S. D. DeGloria (2008), Impacts of disturbance on soil properties in a dry tropical forest in Southern India, Ecohydrology, 1(2), 161-175.

Meyfroidt, P., and E. F. Lambin (2011), Global Forest Transition: Prospects for an End to Deforestation, in Annual Review of Environment and Resources, Vol 36, edited by A. Gadgil and D. M. Liverman, pp. 343-371.

Michel, C., V. Andreassian, and C. Perrin (2005), Soil Conservation Service Curve Number method: How to mend a wrong soil moisture accounting procedure?, Water Resources Research, 41(2), W02011.

Mills, A. J., and M. V. Fey (2004), Frequent fires intensify soil crusting: physicochemical feedback in the pedoderm of long-term burn experiments in South Africa, Geoderma, 121(1-2), 45-64.

Minnemeyer, S., L. Laestadius and N. Sizer (2011), A World of Opportunity for Forest and Landscape Restoration, World Resources Institute>. Retrieved 28 March, 2012 < http://www.wri.org/project/forest-landscape-restoration>..

Mishra, S. K., and V. P. Singh (1999), Another look At SCS-CN Method, Journal of Hydrologic Engineering, 4(3), 257-264.

Mishra, S. K., and V. P. Singh (2003), Soil Conservation Service Curve Number (SCS-CN) Methodology, Kluwer Academic Publishers, Dordrecht, the Netherlands.

Mishra, V., K. A. Cherkauer, D. Niyogi, M. Lei, B. C. Pijanowski, D. K. Ray, L. C. Bowling, and G. Yang (2010), A regional scale assessment of land use/land cover and climatic changes on water and energy cycle in the upper Midwest United States, International Journal of Climatology, 30(13), 2025-2044.

Monin, A. S. and A. M. Obukhov (1954), Basic laws of turbulent mixing in the surface layer of the atmosphere. Tr. Akad. Nauk SSSR Geofiz. Inst 24, 163-187.

Monsi, M., and T. Saeki (1953), Über den Lichtfactor in den Pflanzengesellschaften und seine Bedeutung für die Stoffproduktion, Jpn. J. Bot., 14, 22-52.

Moody, E. G., M. D. King, S. Platnick, C. B. Schaaf, and F. Gao (2005), Spatially complete global spectral surface albedos: Value-added datasets derived from terra MODIS land products, IEEE Transactions on Geoscience and Remote Sensing, 43(1), 144-158.

Morton, D. C., R. S. DeFries, Y. E. Shimabukuro, L. O. Anderson, E. Arai, F. d. B. Espirito-Santo, R. Freitas, and J. Morisette (2006), Cropland expansion changes deforestation dynamics in the southern Brazilian Amazon, Proceedings of the National Academy of Sciences of the United States of America, 103(39), 14637-14641.

Morton, F. I. (1983), Operational estimates of areal evapo-transpiration and their significance to the science and practice of hydrology, Journal of Hydrology, 66(1-4), 1-76.

Moss, A. J. (1991), Rain-impact soil crust .1. Formation on a granite-derived soil. Australian, Australian Journal of Soil Research, 29(2), 271-289.

Mulligan M., Saenz-Cruz L., Van Soesbergen A., Smith V.T., Zurita L. (2009) Global dams database and geowiki. Version 1. Available online at <http://www.ambiotek.com/dams>.

Mulligan, M (2010), Modelling the tropics-wide extent and distribution of cloud forest and cloud forest loss, with implications for conservation priority, in Tropical Montane Cloud Forests, edited by L.A. Bruijnzeel, F.N. Scatena and L. S. Hamilton, pp. 14-38, Cambridge University Press, Cambridge.

Mulligan, M. and Burke, S.M. (2005). DFID FRP Project ZF0216 Global cloud forests and environmental change in a hydrological context, Ambiotek, 74 pp. Retrieved 20 March, 2012 <http://www.ambiotek.com/cloudforests/>..

Mulligan, M., J. Rubiano, M. Rincón-Romero (2010), Hydrology and land-cover change in tropical montane environments: the impact of pattern on process, in Tropical Montane Cloud Forests, edited by L.A. Bruijnzeel, F.N. Scatena and L. S. Hamilton, pp. 516-524, Cambridge University Press, Cambridge

Mutziger, A. J., C. M. Burt, D. J. Howes, and R. G. Allen (2005), Comparison of measured and FAO-56 modeled evaporation from bare soil, Journal of irrigation and drainage engineering, 131, 59-72.

Mwakalila, S., J. Feyen, and G. Wyseure (2002), The influence of physical catchment properties on baseflow in semi-arid environments, Journal of Arid Environments, 52(2), 245-258.

Nachtergaele F. et al. (2012), Harmonized World Soil Database, Version 1.2. Retrieved November 5, 2012 < http://webarchive.iiasa.ac.at/Research/LUC/External-World-soil-database/HWSD_Documentation.pdf>.

Nash, J. E., and J. V. Sutcliffe (1970), River flow forecasting through conceptual models part I - A discussion of principles, Journal of Hydrology, 10, 282-290.

Negishi, J. N., R. C. Sidle, A. D. Ziegler, S. Noguchi, and N. A. Rahim (2008), Contribution of intercepted subsurface flow to road runoff and sediment transport in a logging-disturbed tropical catchment, Earth Surface Processes and Landforms, 33(8), 1174-1191.

Negron Juarez, R. I., M. G. Hodnett, R. Fu, M. L. Goulden, and C. von Randow (2007), Control of dry season evapotranspiration over the Amazonian forest as inferred from observations at a southern Amazon forest site, Journal of Climate, 20(12), 2827-2839.

Nepstad, D.C., Carvalho, C.R., Davidson, E.A. et al. (1994), The role of deep roots in the hydrological and carbon cycles of Amazonian forests and pastures. Nature 372, 666-669.

New, M. G., M. Hulme, and P. D. Jones (2000) Representing twentieth-century space-time climate variability. Part II: Development of 1901-1996 monthly grids of terrestrial surface climate. Journal of Climate, 13, 2217-2238.

Nicholson, S. E. (2000), The nature of rainfall variability over Africa on time scales of decades to millenia, Glob. Planet. Change, 26(1-3), 137-158.

Nijssen, B., G. M. O'Donnell, D. P. Lettenmaier, D. Lohmann, and E. F. Wood (2001), Predicting the discharge of global rivers, Journal of Climate, 14(15), 3307-3323.

Nilsson, C., C. A. Reidy, M. Dynesius, and C. Revenga (2005), Fragmentation and flow regulation of the world's large river systems, Science, 308(5720), 405-408.

Nortcliff, S., S. M. Ross, and J. B. Thornes (1990), Soil moisture, runoff and sediment yield from differentially cleared tropical rainforest plots, in Vegetation and erosion: processes and environment, edited by J.B. Thornes. John Wiley & Sons.

Ohmura, A., et al. (1998), Baseline Surface Radiation Network (BSRN/WCRP): New precision radiometry for climate research, Bulletin of the American Meteorological Society, 79(10), 2115-2136.

Oki, T., and S. Kanae (2006), Global hydrological cycles and world water resources, Science, 313(5790), 1068-1072.

Oki, T., and Y.C. Sud (1998), Design of Total Runoff Integrating Pathways (TRIP) -A Global River Channel Network, pp. 1-37, Vol. 2.

Onogi, K., et al. (2007), The JRA-25 reanalysis, Journal of the Meteorological Society of Japan, 85(3), 369-432.

Oreskes, N., K. Shraderfrechette, and K. Belitz (1994), Verification, validation, and confirmation of numerical-models in the earth-sciences, Science, 263(5147), 641-646.

Oudin, L., V. Andréassian, J. Lerat, and C. Michel (2008) Has land cover a significant impact on mean annual streamflow? An international assessment using 1508 catchments, Journal of Hydrology, 357, 303-316.

Overgaard, J., D. Rosbjerg, and M. B. Butts (2006), Land-surface modelling in hydrological perspective - a review, Biogeosciences, 3(2), 229-241.

Pan, M., H. B. Li, and E. Wood (2010), Assessing the skill of satellite-based precipitation estimates in hydrologic applications, Water Resources Research, 46, W09535.

Peel, M. C. (2009), Hydrology: catchment vegetation and runoff, Progress in Physical Geography, 33(6), 837-844.

Peel, M. C., B. L. Finlayson, and T. A. McMahon (2007), Updated world map of the Koppen-Geiger climate classification, Hydrology and Earth System Sciences, 11(5), 1633-1644.

Peel, M. C., T. A. McMahon, and B. L. Finlayson (2010), Vegetation impact on mean annual evapotranspiration at a global catchment scale, Water Resources Research, 46, W09508.

Peña-Arancibia, J. L., A. I. J. M. v. Dijk, J. P. Guerschman, M. Mulligan, L. A. Bruijnzeel and T. R. McVicar (2012), Detecting changes in streamflow after partial woodland clearing in two large catchments in the seasonal tropics., Journal of Hydrology, 416/417, 60-71.

Peña-Arancibia, J. L., A. I. J. M. van Dijk, M. Mulligan, and L. A. Bruijnzeel (2010), The role of climatic and terrain attributes in estimating baseflow recession in tropical catchments, Hydrology and Earth System Sciences, 14(11), 2193-2205.

Peña-Arancibia, J. L., A. I. J. M. Van Dijk, M. P. Stenson, and N. R. Viney (2011), Opportunities to evaluate a landscape hydrological model (AWRA-L) using global data sets, paper presented at MODSIM2011, 19th International Congress on Modelling and Simulation Modelling and Simulation Society of Australia and New Zealand, December 2011.

Peña-Arancibia, J. L., A. I. J. M. Van Dijk, M. P. Stenson, and N. R. Viney (Unpublished), Data sets for the implementation of a global version of AWRA-L: Opportunities for further model evaluation, CSIRO: Water for a Healthy Country National Research Flagship, p. 32.

Peña-Arancibia, J. L., van Dijk, A. I. J. M., Renzullo, L.J. and M. Mulligan (2013), Evaluation of precipitation from reanalyses, satellite products and an ensemble in regions of Australia and East Asia, Journal of Hydrometeorology, 14, 1323-1333.

Petheram, C., T. A. McMahon, and M. C. Peel (2008), Flow characteristics of rivers in northern Australia: Implications for development, Journal of Hydrology, 357(1-2), 93-111.

Pinker, R. T., I. Laszlo, D. Goodrich, and G. Pandithurai (2000), Satellite estimates of surface radiative fluxes for the extended San Pedro Basin: sensitivity to aerosols, Agricultural and Forest Meteorology, 105(1-3), 43-54.

Pitman, A. J. (2003), The evolution of, and revolution in, land surface schemes designed for climate models, International Journal of Climatology, 23(5), 479-510.

Pitman, A. J., and S. E. Perkins (2009), Global and regional comparison of daily 2-m and 1000-hPa maximum and minimum temperatures in three global reanalyses, J. Clim., 22(17), 4667-4681.

Poff N. L. and J. V.Ward (1989), Implications of streamflow variability and predictability for lotic community structure: a regional analysis of streamflow patterns. Canadian Journal of Aquatic Sciences, 46, 1805-1818.

Ponce, V. M., and R. H. Hawkins (1996), Runoff Curve Number: Has It Reached Maturity?, Journal of Hydrologic Engineering, 1(1), 11-19.

Post, D. A., and A. J. Jakeman (1996), Relationships between catchment attributes and hydrological response characteristics in small Australian mountain ash catchments, Hydrological Processes, 10(6), 877-892.

Prihodko, L., and S. N. Goward (1997), Estimation of air temperature from remotely sensed surface observations, Remote Sensing of Environment, 60(3), 335-346.

Prince, S. D., S. J. Goetz, R. O. Dubayah, K. P. Czajkowski, and M. Thawley (1998), Inference of surface and air temperature, atmospheric precipitable water and vapor pressure deficit using Advanced Very High-Resolution Radiometer satellite observations: comparison with field observations, Journal of Hydrology, 213(1-4), 230-249.

Rawls, W. J., L. R. Ahuja, D. L. Brakensiek, and A. Shirmohammadi (1992), Infiltration and soil water movement, in Handbook of Hydrology, edited by D. R. Maidment, pp. 5.1-5.51, McGraw-Hill.

Rayner, D.P., Moodie, K.B., Beswick, A.R., Clarkson, N.M., Hutchinson, R.L. (2004), New Australian Daily Historical Climate Surfaces using CLIMARC. Queensland Department of Natural Resources and Mines. Retrieved November 5, 2012 < http://www.longpaddock.qld.gov.au/silo/CLIMARC/AustralianHistoricalDailyClimateSufacesUsingCLIMARC_nocover.pdf >.

Recha, J. W., J. Lehmann, M. T. Walter, A. Pell, L. Verchot, and M. Johnson (2012), Stream Discharge in Tropical Headwater Catchments as a Result of Forest Clearing and Soil Degradation, Earth Interactions, 16, 1-18.

Reich, P. B., I. J. Wright, J. Cavender-Bares, and J. M. Craine (2003), The Evolution of Plant Functional Variation: Traits, Spectra, and Strategies, International Journal of Plant Sciences, 164(s3), S143-S164.

Reich, P. B., M. B. Walters, and D. S. Ellsworth (1997), From tropics to tundra: Global convergence in plant functioning, Proceedings of the National Academy of Sciences, 94(25), 13730-13734.

Richards, J. H., and M. M. Caldwell (1987), Hydraulic lift: substantial nocturnal water transport between soil layers by Artemisia tridentata roots, Oecologia, 73(4), 486-489.

Richards, L. A. (1931), Capillary conduction of liquids through porous mediums, Physics -a Journal of General and Applied Physics, 1(1), 318-333.

Richey, J. E., C. Nobre, and C. Deser (1989), Amazon river discharge and climate variability - 1903 to 1985, Science, 246(4926), 101-103.

Rienecker, M. M., et al. (2011), MERRA: NASA's Modern-Era Retrospective Analysis for Research and Applications, J. Clim., 24(14), 3624-3648.

Rijsdijk, A., and L. A. Bruijnzeel (1991), Erosion, sediment yield and land use patterns in the upper Konto watershed, East Java, Indonesia, 150 pp, Konto River Project, Malang, Indonesia.

Rijsdijk, A., L. A. S. Bruijnzeel, and C. K. Sutoto (2007), Runoff and sediment yield from rural roads, trails and settlements in the upper Konto catchment, East Java, Indonesia, Geomorphology, 87(1-2), 28-37.

Ritchie, J. T. (1972), Model for predicting evaporation from a row crop with incomplete cover. Water Resources Research 8, 1204-1213.

Rodell, M., et al. (2004), The global land data assimilation system, Bulletin of the American Meteorological Society, 85(3), 381-394.

Rodriguez, D. A., J. Tomasella, and C. Linhares (2010), Is the forest conversion to pasture affecting the hydrological response of Amazonian catchments? Signals in the Ji-Parana Basin, Hydrological Processes, 24(10), 1254-1269.

Rodriguez-Iturbe, I., A. Porporato, F. Laio, and L. Ridolfi (2001), Plants in water-controlled ecosystems: active role in hydrologic processes and response to water stress - I. Scope and general outline, Advances in Water Resources, 24(7), 695-705.

Rodriguez-Iturbe, I., and A. Porporato (2004), Ecohydrology of water-controlled ecosystems: soil moisture and plant dynamics, 422pp. Cambridge University Press, Cambridge.

Rohde, K. (2005) Less compaction, more cover save soil, Australian Farm Journal, 42-43.

Rost, S., D. Gerten, A. Bondeau, W. Lucht, J. Rohwer, and S. Schaphoff (2008), Agricultural green and blue water consumption and its influence on the global water system, Water Resources Research, 44(9), WR006331.

Roth, C.H., Lawson, G., Cavanagh, D. (2002), Overview of Key Natural Resource Management Issues in the Burdekin Catchment, with Particular Reference to Water Quality and Salinity. CSIRO Land and Water. Retrieved November 5, 2012 <http://www.clw.csiro.au/publications/consultancy/2003/Burdekin_Catchment_Report_Condition_Study_Phase_1-2003.pdf >.

Ruane, A. C., and J. O. Roads (2007), 6-hour to 1-year variance of five global precipitation sets, Earth Interactions, 11.

Ryan, S.E., Porth, L.S. (2007), A tutorial on the piecewise regression approach applied to bedload transport data. Gen. Tech. Rep. RMRS-GTR-189. Fort Collins, CO, US Department of Agriculture, Forest Service, Rocky Mountain Research Station, p. 41. Retrieved November 5, 2012 <http://www.fs.fed.us/rm/pubs/rmrs_gtr189.pdf>.

Saenz, L. and Mulligan, M. (in prep.) Development and validation of a georeferenced tropics-wide database of dams, Water Resources Research.

Saha, S., et al. (2010), The NCEP Climate Forecast System Reanalysis, Bulletin of the American Meteorological Society, 91(8), 1015-1057.

Saito, M., A. Ito, and S. Maksyutov (2011), Evaluation of Biases in JRA-25/JCDAS Precipitation and Their Impact on the Global Terrestrial Carbon Balance, J. Clim., 24(15), 4109-4125.

Sandström, K. (1995), Forest and water-friends or foes? Hydrological implications of deforestation and land degradation in semi-arid Tanzania, 120 pp, PhD Thesis, Linkoping University, S-581 83 Linkoping Sweden.

Sapiano, M. R. P., and P. A. Arkin (2009), An Intercomparison and Validation of High-Resolution Satellite Precipitation Estimates with 3-Hourly Gauge Data, J. Hydrometeorol., 10(1), 149-166.

Sartori, A., A. Maia Genovez, and F. Lombardi Neto (2009), Tentative Hydrologic Soil Classification for Tropical Soils, paper presented at Advances in Water Resources and Hydraulic Engineering: Proceedings of 16th IAHR-APD Congress and 3rd Symposium of IAHR-ISHS, Springer Berlin Heidelberg.

Savenije, H. H. G. (2001), Equifinality, a blessing in disguise?, Hydrological Processes, 15(14), 2835-2838.

Scanlan, J. C., and E. R. Anderson (1981), Use of the heavy duty blade plough for control of woody regrowth in Central Queensland, Australian Weeds, 1(2), 10-12.

Schaake, J. C., V. I. Koren, Q. Y. Duan, K. Mitchell, and F. Chen (1996), Simple water balance model for estimating runoff at different spatial and temporal scales, Journal of Geophysical Research-Atmospheres, 101(D3), 7461-7475.

Schenk, H. J., and R. B. Jackson (2002), The global biogeography of roots, Ecological Monographs, 72(3), 311-328.

Schneider, A., M. A. Friedl, and D. Potere (2009), A new map of global urban extent from MODIS satellite data, Environmental Research Letters, 4(4), 044003.

Schulze, E. D., N. C. Turner, D. Nicolle, and J. Schumacher (2006), Species differences in carbon isotope ratios, specific leaf area and nitrogen concentrations in leaves of Eucalyptus growing in a common garden compared with along an aridity gradient, Physiologia Plantarum, 127(3), 434-444.

Scott, D. F., L. A. Bruijnzeel, and J. Mackensen (2005), The hydrological and soil impacts of forestation in the tropics, in Forests, Water and People in the Humid Tropics, edited by M. Bonell and L. A. Bruijnzeel, pp. 622-651, Cambridge University Press, Cambridge.

Sen, P. K. (1968), Estimates of regression coefficient based on Kendall's tau, Journal of the American Statistical Association, 63(324), 1379-1389.

Sheffield, J., G. Goteti, and E. F. Wood (2006), Development of a 50-year high-resolution global dataset of meteorological forcings for land surface modeling, Journal of Climate, 19(13), 3088-3111.

Sheil, D., and D. Murdiyarso (2009), How Forests Attract Rain: An Examination of a New Hypothesis, Bioscience, 59(4), 341-347.

Shu, Y., and Villholt K. G. (2012) Analysis of flow and baseflow trends in the Usangu catchment, Tanzania. 16th SANCIAHS National Hydrology Symposium. University of Pretoria, Pretoria, South Africa. Retrieved August 29, 2012 <http://www.ru.ac.za/static/institutes/iwr/SANCIAHS/2012/documents/047_Shu.pdf>.

Shuttleworth, W. J. (1992), Evaporation, in Handbook of Hydrology, edited by D. R. Maidment, pp. 4.1-4.53, McGraw-Hill.

Shvidenko, A., C. V. Braber, and R. Persson (2005) Forests and woodland systems, in Ecosystems and Human Well-Being: Volume I: Current State and Trends, edited by Hassan, R., R. Scholes, and N. Ash, 585-621, Island Press, Washington DC, USA.

Sidle, R. C., S. Sasaki, M. Otsuki, S. Noguchi, and A. R. Nik (2004), Sediment pathways in a tropical forest: effects of logging roads and skid trails, Hydrological Processes, 18(4), 703-720.

Simmons, A. J., K. M. Willett, P. D. Jones, P. W. Thorne, and D. P. Dee (2010), Low-frequency variations in surface atmospheric humidity, temperature, and precipitation: Inferences from reanalyses and monthly gridded observational data sets, Journal of Geophysical Research-Atmospheres, 115, D01110.

Simmons, A. J., P. D. Jones, V. D. Bechtold, A. C. M. Beljaars, P. W. Kallberg, S. Saarinen, S. M. Uppala, P. Viterbo, and N. Wedi (2004), Comparison of trends and low-frequency variability in CRU, ERA-40, and NCEP/NCAR analyses of surface air temperature, Journal of Geophysical Research-Atmospheres, 109(D24), D24115.

Siriwardena, L., B. L. Finlayson, and T. A. McMahon (2006), The impact of land use change on catchment hydrology in large catchments: The Comet River, Central Queensland, Australia, Journal of Hydrology, 326(1-4), 199-214.

Sitch, S., et al. (2003), Evaluation of ecosystem dynamics, plant geography and terrestrial carbon cycling in the LPJ dynamic global vegetation model, Global Change Biology, 9(2), 161-185.

Sivapalan, M. (2009), The secret to 'doing better hydrological science': change the question!, Hydrological Processes, 23(9), 1391-1396.

Sivapalan, M., L. Zhang, R. Vertessy, and G. Bloschl (2003), Preface - Downward approach to hydrological prediction, Hydrological Processes, 17(11), 2101-2111.

Smakhtin, V. U. (2001), Low flow hydrology: a review, Journal of Hydrology, 240(3-4), 147-186.

Sohn, S.J., C.Y. Tam, K. Ashok, and J.B. Ahn (2011), Quantifying the reliability of precipitation datasets for monitoring large□scale East Asian precipitation variations, Int. J. Clim. DOI: 10.1002/joc.2380 (In press; available in online).

Songer, M., M. Aung, B. Senior, R. DeFries, and P. Leimgruber (2009), Spatial and temporal deforestation dynamics in protected and unprotected dry forests: a case study from Myanmar (Burma), Biodiversity and Conservation, 18(4), 1001-1018.

Sorooshian, S., K. L. Hsu, X. Gao, H. V. Gupta, B. Imam, and D. Braithwaite (2000), Evaluation of PERSIANN system satellite-based estimates of tropical rainfall, Bulletin of the American Meteorological Society, 81(9), 2035-2046.

Stackhouse P.W., Gupta S.K., Cox S.J., Zhang T., Mikovitz J.C. and L.M. Hinkelman (2011), 24.5-Year SRB Data Set Released. GEWEX News, 21(1).

Stackhouse, P. W., S. K. Gupta, S. J. Cox, M. Chiacchio, and J. C. Mikovitz (2001), The WCRP/GEWEX Surface Radiation Budget Project release 2: An assessment of surface fluxes at 1 degree resolution, 485-488 pp.

Stednick, J. D. (1996), Monitoring the effects of timber harvest on annual water yield, Journal of Hydrology, 176(1-4), 79-95.

Stenson, M., et al. (2011), Operationalising the Australian Water Resources Assessment (AWRA) system, paper presented at Proceedings, Water Information Research and Development Alliance Science Symposium, August 2011. Melbourne. Retrieved November 5, 2012 <http://www.csiro.au/WIRADA-Science-Sympsosium-Proceedings>.

Stisen, S., and I. Sandholt (2010), Evaluation of remote-sensing-based rainfall products through predictive capability in hydrological runoff modelling, Hydrological Processes, 24(7), 879-891.

Suttles, J. T., and G. Ohring, 1986: Surface Radiation Budget for Climate Application. NASA RP-1169, 136 pp.

Tallaksen, L. M. (1995), A review of baseflow recession analysis, Journal of Hydrology, 165(1-4), 349-370.

Tam, V. T., T. M. N. Vu, and O. Batelaan (2001), Hydrogeological characteristics of a karst mountainous catchment in the northwest of Vietnam, Acta Geologica Sinica-English Edition, 75(3), 260-268.

Terink, W., R. Hurkmans, P. Torfs, and R. Uijlenhoet (2010), Evaluation of a bias correction method applied to downscaled precipitation and temperature reanalysis data for the Rhine basin, Hydrol. Earth Syst. Sci., 14(4), 687-703.

Terribile, F., A. Coppola, G. Langella, M. Martina, and A. Basile (2011), Potential and limitations of using soil mapping information to understand landscape hydrology, Hydrology and Earth System Sciences, 15(12), 3895-3933.

Teuling, A. J., et al. (2010), Contrasting response of European forest and grassland energy exchange to heatwaves, Nature Geoscience, 3(10), 722-727.

Thom, A. S. (1975), 3. Momentum, Mass and Heat Exchange of Plant Communities, Vegetation and the atmosphere: principles, 57.

Thornthwaite, C. W. (1948), An approach toward a rational classification of climate, Geographical Review, 38(1), 55-94.

Thornton, C. M., B. A. Cowie, D. M. Freebairn, and C. L. Playford (2007), The Brigalow Catchment Study: II. Clearing brigalow (Acacia harpophylla) for cropping or pasture increases runoff, Australian Journal of Soil Research, 45(7), 496-511.

Tian, Y. D., and C. D. Peters-Lidard (2010), A global map of uncertainties in satellite-based precipitation measurements, Geophysical Research Letters, 37, L24407.

Tian, Y. D., C. D. Peters-Lidard, J. B. Eylander, R. J. Joyce, G. J. Huffman, R. F. Adler, K. L. Hsu, F. J. Turk, M. Garcia, and J. Zeng (2009), Component analysis of errors in satellite-based precipitation estimates, Journal of Geophysical Research-Atmospheres, 114, D24101.

Todd, M. C., C. Kidd, T. J. Bellerby, and D. R. Kniveton (2001), A combined satellite infrared and passive microwave technique for estimation of small-scale rainfall, Journal of Atmospheric and Oceanic Technology, 18(5), 742-755.

Tomasella, J., and M. G. Hodnett (1997), Estimating unsaturated hydraulic conductivity of Brazilian soils using soil-water retention data, Soil Science, 162(10), 703-712.

Tomasella, J., M. G. Hodnett, L. A. Cuartas, A. D. Nobre, M. J. Waterloo, and S. M. Oliveira (2008), The water balance of an Amazonian micro-catchment: the effect of interannual variability of rainfall on hydrological behaviour, Hydrological Processes, 22(13), 2133-2147.

Tomer, M. D., and K. E. Schilling (2009), A simple approach to distinguish land-use and climate-change effects on watershed hydrology, Journal of Hydrology, 376(1-2), 24-33.

Trabucco, A., R. J. Zomer, D. A. Bossio, O. van Straaten, and L. V. Verchot (2008), Climate change mitigation through afforestation/reforestation: A global analysis of hydrologic impacts with four case studies, Agriculture Ecosystems & Environment, 126(1-2), 81-97.

Trancoso, R. (2006), Changes in Land Cover and Alterations in the Hydrological Response of Catchments in Amazonia. INPA/UFAM, p. 139.

Troy, T. J., and E. F. Wood (2009), Comparison and evaluation of gridded radiation products across northern Eurasia, Environmental Research Letters, 4(4), 045008.

Tularam, G.A. and M. Ilahee (2008), Exponential smoothing method of base flow separation and its impact on continuous loss estimates. American Journal of Environmental Sciences, 4, 136-144.

Tullberg, J. N., P. J. Ziebarth, and Y. X. Li (2001), Tillage and traffic effects on runoff, Australian Journal of Soil Research, 39(2), 249-257.

Turkelboom, F., J. Poesen, and G. Trebuil (2008), The multiple land degradation effects caused by land-use intensification in tropical steeplands: A catchment study from northern Thailand, Catena, 75(1), 102-116.

UNESCO (2009), The 3rd United Nations World Water Development Report: Water in a changing World. United Nations Educational Scientific and Cultural Organization, p. 349. Retrieved 5 November, 2012 <http://www.unesco.org/water/wwap/wwdr/wwdr3/pdf/WWDR3_Water_in_a_Changing_World.pdf>.

UNESCO (2013) UNESCO International Glossary of Hydrology. Retrieved 31 August, 2013 < http://webworld.unesco.org/water/ihp/db/glossary/glu/aglu.htm>.

Uppala, S. M., et al. (2005), The ERA-40 re-analysis, Quarterly Journal of the Royal Meteorological Society, 131(612), 2961-3012.

USDA (1986), Urban Hydrology of Small Watersheds. Technical release 55. United States Department of Agriculture (USDA). Retrieved June 24, 2012 < http://www.hydrocad.net/pdf/TR-55%20Manual.pdf>.

Valzano, F. P., R. S. B. Greene, and B. W. Murphy (1997), Direct effects of stubble burning on soil hydraulic and physical properties in a direct drill tillage system, Soil & Tillage Research, 42(3), 209-219.

Van Beek, L. P. H., and Bierkens, M. F. P. (2010) The Global Hydrological Model PCR-GLOBWB: Conceptualization, Parameterization and Verification, 2008. Report Department of Physical Geography,Utrecht University, Utrecht, The Netherlands. Retrieved November 5, 2012 < http://vanbeek.geo.uu.nl/suppinfo/vanbeekbierkens2009.pdf >.

Van der Weert, R., 1994. Hydrological Conditions in Indonesia, Delft Hydraulics, Jakarta, Indonesia, p. 72.

Van Dijk, A. I. J. M. (2010a), AWRA Technical Report 3. Landscape Model (version 0.5) Technical Description. CSIRO: Water for a Healthy Country National Research Flagship Canberra.

Van Dijk, A. I. J. M. (2010b), Climate and terrain factors explaining streamflow response and recession in Australian catchments, Hydrology and Earth System Sciences, 14(1), 159-169.

Van Dijk, A. I. J. M. (2010c), Selection of an appropriately simple storm runoff model, Hydrology and Earth System Sciences, 14(3), 447-458.

Van Dijk, A. I. J. M., and G. A. Warren (2010), AWRA Technical Report 4. Evaluation Against Observations. CSIRO: Water for a Healthy Country National Research Flagship. Canberra.

Van Dijk, A. I. J. M., and L. A. Bruijnzeel (2001), Modelling rainfall interception by vegetation of variable density using an adapted analytical model. Part 2. Model validation for a tropical upland mixed cropping system, Journal of Hydrology, 247(3-4), 239-262.

Van Dijk, A. I. J. M., and L. J. Renzullo (2011), Water resource monitoring systems and the role of satellite observations, Hydrology and Earth System Sciences, 15(1), 39-55.

Van Dijk, A. I. J. M., and R. J. Keenan (2007), Planted forests and water in perspective, Forest Ecology and Management, 251, 1-9.

Van Dijk, A. I. J. M., and S. Marvanek (2010), Derivation of a simplified soil drainage model. Rep., AWRA background paper 2010/1. WIRADA/CSIRO Water for a Healthy Country Flagship, Canberra.

Van Dijk, A. I. J. M., et al. (2011), Design and development of the Australian Water Resources Assessment system, paper presented at Proceedings, Water Information Research and Development Alliance Science Symposium, August 2011. Melbourne. Retrieved November 5, 2012 <http://www.csiro.au/WIRADA-Science-Sympsosium-Proceedings>.

Van Dijk, A. I. J. M., J. L. Peña Arancibia, and L. A. Bruijnzeel (2012), Land cover and water yield: inference problems when comparing catchments with mixed land cover, Hydrology and Earth System Sciences, 16, 1-13.

Van Dijk, A. I. J. M., J. L. Peña Arancibia, and L. A. Bruijnzeel (2011), Top-down analysis of collated streamflow data from heterogeneous catchments leads to underestimation of land cover influence Hydrol. Earth Syst. Sci. Discuss., 8 (2011), 4121–4150.

Van Dijk, A. I. J. M., J. L. Peña Arancibia, E. F. Wood, J. Sheffield and H. E. Beck (in press), Global analysis of seasonal streamflow predictability using an ensemble prediction system and observations from 6192 small catchments worldwide. Water Resources Research, 49(5), 2729-2746.

Vancutsem, C., P. Ceccato, T. Dinku, and S. J. Connor (2010), Evaluation of MODIS land surface temperature data to estimate air temperature in different ecosystems over Africa, Remote Sensing of Environment, 114(2), 449-465.

Vaze, J., D. A. Post, F. H. S. Chiew, J. M. Perraud, N. R. Viney, and J. Teng (2010), Climate non-stationarity - Validity of calibrated rainfall-runoff models for use in climate change studies, Journal of Hydrology, 394(3-4), 447-457.

Vila, D., R. Ferraro, and H. Semunegus (2010), Improved Global Rainfall Retrieval Using the Special Sensor Microwave Imager (SSM/I), Journal of Applied Meteorology and Climatology, 49(5), 1032-1043.

Villar, J. C. E., J. L. Guyot, J. Ronchail, G. Cochonneau, N. Filizola, P. Fraizy, D. Labat, E. de Oliveira, J. Julio Ordonez, and P. Vauchel (2009), Contrasting regional discharge evolutions in the Amazon basin (1974-2004), Journal of Hydrology, 375(3-4), 297-311.

Viney, N. R., A. I. J. M. Van Dijk and J. Vaze (2011), Comparison of models and methods for estimating spatial patterns of streamflow across Australia, paper presented at Proceedings, Water Information Research and Development Alliance Science Symposium, August 2011. Melbourne. Retrieved November 5, 2012 <http://www.csiro.au/WIRADA-Science-Sympsosium-Proceedings>.

Viramontes, D., and L. Descroix (2003), Changes in the surface water hydrologic characteristics of an endoreic basin of northern Mexico from 1970 to 1998, Hydrological Processes, 17(7), 1291-1306.

Vogel, R. M., and C. N. Kroll (1992), Regional geohydrologic-geomorphic relationships for the estimation of low-flow statistics, Water Resources Research, 28(9), 2451-2458.

Vorosmarty, C. J., B. Moore, III, A. L. Grace, M. P. Gildea, J. M. Melillo, B. J. Peterson, E. B. Rastetter, and P. A. Steudler (1989), Continental scale models of water balance and fluvial transport: an application to South America, Global Biogeochemical Cycles, 3(3), 241-265.

Vörösmarty, C. J., P. Green, J. Salisbury, and R. B. Lammers (2000), Global water resources: Vulnerability from climate change and population growth, Science, 289(5477), 284-288.

Walsh, R. P. D. and Lawler, D. M. (1981), Rainfall seasonality: description, spatial patterns and change through time, Weather, 36, 201–209.

Wang, G. L., and E. A. B. Eltahir (2000), Role of vegetation dynamics in enhancing the low-frequency variability of the Sahel rainfall, Water Resources Research, 36(4), 1013-1021.

Wang, X., T. Liu, and W. Yang (2012), Development of a robust runoff-prediction model by fusing the Rational Equation and a modified SCS-CN method, Hydrological Sciences Journal-Journal Des Sciences Hydrologiques, 57(6), 1118-1140.

Ward, R. C. (1984), On the response to precipitation of headwater streams in humid areas, Journal of Hydrology, 74(1-2), 171-189.

Wemple, B. C., and J. A. Jones (2003), Runoff production on forest roads in a steep, mountain catchment, Water Resources Research, 39(8), 1220.

Whitlock, C. H., et al. (1995), First Global WCRP Shortwave Surface Radiation Budget Dataset, Bulletin of the American Meteorological Society, 76(6), 905-922.

WHYMAP (2010) World-wide Hydrogeological Mapping and Assessment Programme. Groundwater resources of the world 2010. Retrieved November 5, 2012 < http://www.bgr.de/app/fishy/GoogleEarth/whymap.kml >.

Widen-Nilsson, E., L. Gong, S. Halldin, and C. Y. Xu (2009), Model performance and parameter behavior for varying time aggregations and evaluation criteria in the WASMOD-M global water balance model, Water Resources Research, 45, WR006695.

Widen-Nilsson, E., S. Halldin, and C.-Y. Xu (2007), Global water-balance modelling with WASMOD-M: Parameter estimation and regionalisation, Journal of Hydrology, 340(1-2), 105-118.

Wielicki, B. A., B. R. Barkstrom, E. F. Harrison, R. B. Lee, G. L. Smith, and J. E. Cooper (1996), Clouds and the earth's radiant energy system (CERES): An earth observing system experiment, Bulletin of the American Meteorological Society, 77(5), 853-868.

Wilcox, B. P., and Y. Huang (2010), Woody plant encroachment paradox: Rivers rebound as degraded grasslands convert to woodlands, Geophysical Research Letters, 37, L07402.

Wilk, J., L. Andersson, and V. Plermkamon (2001), Hydrological impacts of forest conversion to agriculture in a large river basin in northeast Thailand, Hydrological Processes, 15(14), 2729-2748.

Williams, C. A., et al. (2012), Climate and vegetation controls on the surface water balance: Synthesis of evapotranspiration measured across a global network of flux towers, Water Resources Research, 48, W06523.

Wittenberg, H. (1999), Baseflow recession and recharge as nonlinear storage processes, Hydrological Processes, 13(5), 715-726.

Wohl, E., et al., (2012), The hydrology of the humid tropics, Nature Climate Change, 2, 655-662.

Woodcock, C. E., et al., (2008) Free access to Landsat imagery, Science, 320, 1011-1011.

Wright, I. J., et al. (2004), The worldwide leaf economics spectrum, Nature, 428(6985), 821-827.

Xia, X. A., P. C. Wang, H. B. Chen, and F. Liang (2006), Analysis of downwelling surface solar radiation in China from National Centers for Environmental Prediction reanalysis, satellite estimates, and surface observations, Journal of Geophysical Research-Atmospheres, 111(D9), D09103.

Yatagai, A., K. Kamiguchi, O. Arakawa, A. Hamada, N. Yasutomi and A. Kitoh (2012) APHRODITE: Constructing a Long-term Daily Gridded Precipitation Dataset for Asia based on a Dense Network of Rain Gauges, Bulletin of American Meteorological Society, 93, 1401–1415.

Yilmaz, K. K., H. V. Gupta, and T. Wagener (2008), A process-based diagnostic approach to model evaluation: Application to the NWS distributed hydrologic model, Water Resources Research, 44(9), W09417.

Young, D. F., P. Minnis, D. R. Doelling, G. G. Gibson, and T. Wong (1998), Temporal interpolation methods for the Clouds and the Earth's Radiant Energy system (CERES) experiment, J. Appl. Meteorol., 37(6), 572-590.

Yu, B. (1998), Theoretical justification of SCS method for runoff estimation, Journal of Irrigation and Drainage Engineering-ASCE, 124(6), 306-310.

Yu, P. S., T. C. Yang, and C. W. Liu (2002), A regional model of low flow for southern Taiwan, Hydrological Processes, 16(10), 2017-2034.

Yue, S., and C. Y. Wang (2004), The Mann-Kendall test modified by effective sample size to detect trend in serially correlated hydrological series, Water Resources Management, 18(3), 201-218.

Yue, S., P. Pilon, and G. Cavadias (2002), Power of the Mann-Kendall and Spearman's rho tests for detecting monotonic trends in hydrological series, Journal of Hydrology, 259(1-4), 254-271.

Zecharias, Y. B., and W. Brutsaert (1988), Recession characteristics of groundwater outflow and base-flow from mountainous watersheds, Water Resources Research, 24(10), 1651-1658.

Zhang, B., Y. S. Yang, and H. Zepp (2004), Effect of vegetation restoration on soil and water erosion and nutrient losses of a severely eroded clayey Plinthudult in southeastern China, Catena, 57(1), 77-90.

Zhang, L., K. Hickel, W. R. Dawes, F. H. S. Chiew, A. W. Western, and P. R. Briggs (2004), A rational function approach for estimating mean annual evapotranspiration, Water Resources Research, 40(2), W02502.

Zhang, L., N. Potter, K. Hickel, Y. Zhang, and Q. Shao (2008), Water balance modeling over variable time scales based on the Budyko framework - Model development and testing, Journal of Hydrology, 360(1-4), 117-131.

Zhang, L., W. R. Dawes, and G. R. Walker (2001), Response of mean annual evapotranspiration to vegetation changes at catchment scale, Water Resources Research, 37(3), 701-708.

Zhang, Y. C., W. B. Rossow, A. A. Lacis, V. Oinas, and M. I. Mishchenko (2004), Calculation of radiative fluxes from the surface to top of atmosphere based on ISCCP and other global data sets: Refinements of the radiative transfer model and the input data, Journal of Geophysical Research-Atmospheres, 109(D19), D19105.

Zhang, Y., N. R. Viney, F. H. Chiew, A. I. J. M. Van dijk, and Y. Y. Liu (2011), Improving hydrological and vegetation modelling using regional model calibration schemes together with remote sensing data, in MODSIM2011, 19th International Congress on Modelling and Simulation. Modelling and Simulation Society of Australia and New Zealand, December 2011, http://www.mssanz.org.au/modsim2011/I4/zhang.pdf, edited by F. Chan, D. Marinova and R. S. Anderssen.

Zhao, F., F. H. S. Chiew, L. Zhang, J. Vaze, J.-M. Perraud, and M. Li (2012), Application of a Macroscale Hydrologic Model to Estimate Streamflow across Southeast Australia, Journal of Hydrometeorology, 13(4), 1233-1250.

Zheng, H., F. Chen, Z. Ouyang, N. Tu, W. Xu, X. Wang, H. Miao, X. Li, and Y. Tian (2008), Impacts of reforestation approaches on runoff control in the hilly red soil region of Southern China, Journal of Hydrology, 356(1-2), 174-184.

Zhou, G. Y., J. D. Morris, J. H. Yan, Z. Y. Yu, and S. L. Peng (2002), Hydrological impacts of reafforestation with eucalypts and indigenous species: a case study in southern China, Forest Ecology and Management, 167(1-3), 209-222.

Zhou, G., X. Wei, Y. Luo, M. Zhang, Y. Li, Y. Qiao, H. Liu, and C. Wang (2010), Forest recovery and river discharge at the regional scale of Guangdong Province, China, Water Resources Research, 46, W09503.

Ziegler, A. D., J. N. Negishi, R. C. Sidle, T. Gomi, S. Noguchi, and A. R. Nik (2007), Persistence of road runoff generation in a logged catchment in Peninsular Malaysia, Earth Surface Processes and Landforms, 32(13), 1947-1970.

Ziegler, A. D., J. Negishi, R. C. Sidle, P. Preechapanya, R. A. Sutherland, T. W. Giambelluca, and S. Jaiaree (2006), Reduction of stream sediment concentration by a riparian buffer: Filtering of road runoff in disturbed headwater basins of Montane mainland Southeast Asia, Journal of Environmental Quality, 35(1), 151-162.

Ziegler, A. D., T. B. Bruun, M. Guardiola-Claramonte, T. W. Giambelluca, D. Lawrence, and N. T. Lam (2009), Environmental Consequences of the demise in swidden cultivation in montane mainland Southeast Asia: Hydrology and Geomorphology, Human Ecology, 37(3), 361-373.

Ziegler, A. D., T. W. Giambelluca, L. T. Tran, T. T. Vana, M. A. Nullet, J. Fox, T. D. Vien, J. Pinthong, J. F. Maxwell, and S. Evett (2004), Hydrological consequences of landscape fragmentation in mountainous northern Vietnam: evidence of accelerated overland flow generation, Journal of Hydrology, 287(1-4), 124-146.

Ziegler, A. D., T. W. Giambelluca, R. A. Sutherland, M. A. Nullet, S. Yarnasarn, J. Pinthong, P. Preechapanya, and S. Jaiaree (2004), Toward understanding the cumulative impacts of roads in upland agricultural watersheds of northern Thailand, Agriculture Ecosystems & Environment, 104(1), 145-158.

Ziegler, A. D., T. W. Giambelluca, R. A. Sutherland, T. T. Vana, and M. A. Nullet (2001), Horton overland flow contribution to runoff on unpaved mountain roads: A case study in northern Thailand, Hydrological Processes, 15(16), 3203-3208.

Zimmermann, B., A. Papritz, and H. Elsenbeer (2010), Asymmetric response to disturbance and recovery: Changes of soil permeability under forest-pasture-forest transitions, Geoderma, 159(1-2), 209-215.

Zou, C. B., P. W. Barnes, S. Archer, and C. R. McMurtry (2005), Soil moisture redistribution as a mechanism of facilitation in savanna tree-shrub clusters, Oecologia, 145(1), 32-40.

Zou, X. M., and G. Gonzalez (1997), Changes in earthworm density and community structure during secondary succession in abandoned tropical pastures, Soil Biology & Biochemistry, 29(3-4), 627-629.

Appendix A - Glossary of hydrology related terminology

Baseflow - Part of the discharge which enters a stream channel mainly from groundwater, but also from lakes and glaciers during long periods when no precipitation or snowmelt occurs.

Baseflow recession - Period of decreasing baseflow discharge as indicated by the falling limb of a hydrograph starting from the peak.

Dry season flows - In certain types of climate, an annually recurring period of one or more months during which streamflow is at a minimum for the region.

Evapotranspiration - Quantity of water transferred from the soil and/or canopy to the atmosphere by evaporation and plant transpiration.

Groundwater recharge - Process by which water is added from outside to the zone of saturation of an aquifer, either directly into a formation, or indirectly by way of another formation.

Hydrograph - Graph showing the variation in time of some hydrological data such as stage, discharge, velocity, sediment load, etc. (hydrograph is mostly used for stage or discharge).

Hydrological response units - A basic computational unit assumed to be homogeneous in hydrologic response in terms of physical characteristics including soils, vegetation cover, topography, saturated area, etc.

Infiltration - Flow of water through the soil surface into a porous medium.

Infiltration capacity - Maximum rate at which water can be absorbed by a given soil per unit area under given conditions.

Infiltration-excess overland flow - Overfland flow occurring when the rate of precipitation on a surface exceeds the rate at which water can infiltrate the ground.

Interception - Process by which precipitation is caught and held by vegetation (canopy and litter structures) then may be lost by evaporation without reaching the ground.

Interflow - That portion of the precipitation which has not passed down to the water table, but is discharged from the area as subsurface flow into stream channels.

Land degradation - A temporary or permanent decline in the productive capacity of the land. This can be seen through a loss of biomass, a loss of actual productivity or in potential productivity, or a loss or change in vegetative cover and soil nutrients.

Land surface model - A one-dimensional computational model developed that describes ecological processes joined in many ecosystem models, hydrological processes found in hydrological models and flow of surface common in surface models using atmospheric models.

Overland flow - Flow of water over the ground before it enters a definite channel.

Percolation - Flow of a liquid through an unsaturated porous medium, e.g. of water in soil, under the action of gravity.

Perched aquifer - Groundwater body, generally of moderate dimensions, supported by a relatively impermeable stratum and which is located between a water table and the ground surface.

Porosity - Ratio of the volume of the interstices in a given sample of a porous medium, e.g. soil, to the gross volume of the porous medium, inclusive of voids.

Potential evapotranspiration - Maximum quantity of water capable of being evaporated in a given climate from a continuous stretch of vegetation covering the whole ground and well supplied with water. It thus includes evaporation from the soil and transpiration from the vegetation of a specified region in a given time interval, expressed as depth.

Runoff - That part of precipitation that appears as streamflow.

Saturated hydraulic conductivity - Property of a saturated porous medium which determines the relationship, called Darcy's law, between the specific discharge and the hydraulic gradient causing it.

Saturated zone - Part of the water-bearing material in which all voids, large and small, are filled with water. (IGH)

Saturation-excess overland flow - Overfland flow occurring when precipitation falling on saturated soil immediately produce surface runoff.

Soil bioporosity - Soil porosity created by plant roots and soil fauna.

Storm flow - That part of surface runoff which reaches the catchment outlet shortly after the precipitation starts.

Subsurface flow - Any flow below the surface of the ground which may contribute to interflow, base flow or deep percolation.

Water yield - Quantity of water derived from a unit area of a drainage basin in a given time interval.

Appendix B - Conference article

Peña-Arancibia, J. L., A. I. J. M. van Dijk, M. P. Stenson, and N. R. Viney (2011) Opportunities to evaluate a landscape hydrological model (AWRA-L) using global data sets, **MODSIM 2011**, 19th International Congress on Modelling and Simulation Modelling and Simulation Society of Australia and New Zealand, December 2011, 4071-4077 pp.

19th International Congress on Modelling and Simulation, Perth, Australia, 12–16 December 2011
http://mssanz.org.au/modsim2011

Opportunities to evaluate a landscape hydrological model (AWRA-L) using global data sets

Peña Arancibia J.L.[1,3], Van Dijk A.I.J.M.[1], Stenson, M.P.[2] and N.R. Viney[1]

[1]CSIRO Land and Water GPO Box 1666, Canberra ACT 2601 Australia

[2] CSIRO Land and Water, GPO Box 2583, Brisbane 4001, Australia

[3] Environmental Monitoring and Modelling Research Group, Department of Geography, King's College London, Strand, London WC2R 2LS, UK

Email: Jorge.PenaArancibia@csiro.au

Abstract: The Australian Water Resources Assessment system Landscape model (AWRA-L) aims to produce interpretable water balance component estimates covering all of Australia, and as much as possible agree with water balance observations, including point gauging data and satellite observations. The opportunities to evaluate AWRA-L water balance predictions in Australia are severely limited by the limited amount of field data (e.g. flux tower observations, soil moisture measurements) and the limited range of environments and conditions for which observations are available. Opportunities exist to further evaluate and improve AWRA-L model predictions by using global collations of in situ soil moisture, flux tower, and streamflow data available from the broader scientific community. To evaluate AWRA-L against these observations, global input data are required. We reviewed and compared results of published studies about meteorological data that could be used to parameterise AWRA-L globally. Review findings include:

- Satellite-based rainfall performs better during warm seasons and in the tropics, although overestimating total rainfall. Reanalysis data outperforms satellite-based rainfall during winter and in higher latitudes. Gauge bias-corrected TRMM 3B42V6 reduces observed bias in many areas globally. A blending approach may enhance rainfall quality estimates on a global scale, using rainfall from reanalysis in higher latitudes and satellite estimates such as TRMM 3B42V6 in mid-latitudes.
- Global monthly, annual and climatological surface temperature anomalies from reanalysis had very similar values. At the daily scale, compared daily maximum and minimum temperature probability density functions from ERA-40, JRA-25 and NCEP-DOE were dissimilar with large regional differences, but overall no reanalysis showed more skill than the other two when compared against regional observational temperature data.
- Surface shortwave radiation derived from satellite data generally has smaller biases than reanalysis because they are more constrained by observations. Of the three satellite-based incoming shortwave radiation estimates, GEWEX-SRB appeared superior to the other two. Globally, the biases in the climatology of the re-analyses are considerable.

The 60 year (1948–2008) Princeton Global Forcing (PGF) dataset with a spatial resolution of 1º and daily time step was considered an adequate compromise for trial simulations. PGF is based on the NCEP/NCAR reanalysis but uses several additional data sources to constrain and reduce bias in the meteorological variables. We implemented a prototype 1° resolution global hydrological model based on AWRA-L - referred to here as the World-Wide Water Resources Assessment system (W3RA). W3RA was parameterized with the same set of parameters used in AWRA-L except for baseflow coefficient, which was derived from a global analysis of baseflow recession. In addition, a snow module was added to simulate snowmelt and snow accumulation. Other data used included land cover maps based on MODIS reflectance data, albedo climatology derived from white-sky albedo and wind speed climatology.

As part of preliminary evaluation of W3RA, runoff estimates were compared against a Global Runoff Data Centre (GRDC) blend of observations and modeled runoff climatology. Ongoing evaluation will include comparisons against a quality controlled gauged daily flows in 167 unimpaired catchments located mostly in the tropics, a global data set of collated site soil moisture measurements, and evapotranspiration from a global network of flux towers.

Keywords *hydrology, global modelling, global data sets, AWRA-L, W3RA*

1. INTRODUCTION

The Australian Water Resources Assessment system Landscape model (AWRA-L) is a grid based distributed biophysical model that simulates water stores and flows in the vegetation, soil and local catchment groundwater systems (Van Dijk and Renzullo, 2011). As part of the requirements for model adoption in water balance assessment and water accounting for the whole of Australia, model outputs considered to provide a reliable indication of the quality of water balance were evaluated against observations (Van Dijk and Warren, 2010). Data used to perform model evaluation included daily streamflow data from over 300 catchments, eddy covariance flux tower evapotranspiration data at four sites, radar remote sensing (ASAR GM) derived top soil water content estimates and optical remote sensing (AVHRR, MODIS) derived vegetation fractional cover, leaf area index and greenness.

The opportunities to further evaluate AWRA-L water balance predictions in Australia are severely limited by the limited amount of field data. Flux tower observations and *in sit*u soil moisture measurements only represent a limited range of environments and conditions for which observations are available. Global collations of *in situ* soil moisture, flux tower, and streamflow data available from the broader scientific community can be used to further evaluate and improve AWRA-L. Additional benefits of having the model implemented on a global scale would be to compare model estimates to results from other global models and further identify potential improvements in model structure or parameterisation. To evaluate AWRA-L against these observations, global spatial model input data sets are required, particularly of daily rainfall, radiation, temperature, soils, and land cover. A review of the data needed to parameterize a global version of AWRA-L; daily meteorological forcing in particular, is the main focus of this paper. Based on findings of from published studies, we implemented a 1° resolution prototype "World-Wide Water Resources Assessment system" (W3RA). Simulated streamflow was compared with a Global Runoff Data Centre (GRDC) composite of observations and modeled runoff climatology (Fekete *et al.*, 2002).

2. METEREOLOGICAL FORCING DATA

2.1. Rainfall

Seven satellite-based rainfall products and five global atmospheric reanalysis of meteorological observations were reviewed (Table 1; acronyms explained in cited references). Several studies have been conducted to evaluate different rainfall products from satellite, reanalysis and climatologic data sets by comparing them to ground observations in areas with reliable gauge or radar coverage or through their predictive capability of state variables such as soil moisture or streamflow from hydrological or land-surface models (e.g. Ebert *et al.*, 2007; Tian *et al.*, 2009; Pan *et al.*, 2010; Tian and Peters-Lidard, 2010). Findings from most studies suggest a better agreement of satellite-based rainfall with baseline data over warm seasons whereas reanalysis rainfall outperformed the satellite estimates during the winter season on monthly and daily time-scales. It was also found in most studies that high (often convective) rainfall events are better captured by satellite estimates, although the amplitudes were generally overestimated (Ebert *et al.*, 2007; Tian *et al.*, 2009). The incorporation of surface rain gauge data, such as in TRMM 3B42V6, helped to reduce total errors; by adjusting the amplitudes of the hit biases and false precipitation. A global map of measurement uncertainties in daily satellite-based precipitation estimates were produced by Tian and Peters-Lidard (2010). Estimates tended to agree particularly well over areas with stronger precipitation, especially over the tropics. The performance at higher latitudes degraded considerably, especially above of 40° latitude. This was due to coverage by fewer sensors (e.g., lack of TRMM coverage), light precipitation events, snowfall, and in the case of land surfaces, snow and ice on the ground which produce a signal similar to precipitation. Tian *et al.* (2009) found that daily satellite-based rainfall estimates in continental US constantly missed about 20–80% of light precipitation (<10 mm d^{-1}) and that the amount of false precipitation can occasionally be exceedingly large, especially for winter in western USA. During winter, missed precipitation was a major contributor to the total errors (up to 40%) of TRMM-3B42RT, CMORPH, and PERSIANN, especially over complex terrain (Tian *et al.*, 2009).

Table 1. Main characteristics of daily or sub-daily global and quasi-global rainfall gridded data sets.

Dataset	Grid resolution	Frequency	Coverage	Period	Reference
Satellite					
TRMM-3B42 (RT or V6)	0.25º	3h	60ºS~60ºN	1998~	Huffman *et al.* (2007)
CMORPH	0.08º~0.25º	0.5, 3h	60ºS~60ºN	2002~	Joyce *et al.* (2004)
PERSIANN	0.25º	3, 6h	50ºS~50ºN	2000~	Sorooshian *et al.* (2000)
GPCP -1DD	1º	Daily	Global	1996~	Huffman *et al.* (2001)
Reanalysis					
ERA-40	1.125º	6h	Global	1957–2002	Uppala *et al.* (2005)
ERA-Interim	~0.7º	6h	Global	1989~	Simmons *et al.* (2007)
NCEP-NCAR	2.5º	6h	Global	1948~	Kalnay *et al.* (1996)
NCEP-DOE	2.5º	6h	Global	1957~	Kanamitsu *et al.* (2002)
JRA-25	1.25º	6h	Global	1979–2004	Onogi *et al.* (2007)

Daily reanalysis rainfall from ERA-interim, followed by ERA-40 were considered more accurate than both NCEP reanalysis when compared to relatively dense global or local rainfall gauge networks (e.g. Pan *et al.*, 2010) and generally outperformed the blended satellite estimates during the winter season over the continental USA, Australia, and Western Europe (Ebert *et al.*, 2007). ERA-40 produced reasonable monthly rainfall comparisons over the Northern Hemisphere continents, with some notable biases, but less so in tropics where it had high positive bias, except for a negative bias over the Amazon during the rainy season (Betts *et al.*, 2006; Bosilovich *et al.* 2008). The recent reanalysis JRA-25, showed good monthly rainfall comparisons in both the Northern Hemisphere continents and the tropical oceans, but varied in time according to the available observing systems, with additional satellite data improving precipitation and other hydrological data (Bosilovich *et al.* 2008). Rainfall in reanalysis data and impacts on water balance at a basin and global scale has been researched in some detail (Fekete *et al.*, 2004). Results showed that rainfall biases lead to errors in water balance calculations and uncertainties of similar magnitude in humid areas and larger over arid and semi-arid areas. Several studies have aimed to address reanalysis rainfall errors by correcting for biases (e.g. Betts *et al.*, 2005) with resulting improved water balances. Following this line, the 1° and 3-hourly 50-year daily meteorological Princeton Global Forcing (PGF) (1948–2008) dataset was developed by Sheffield *et al.* (2006). It was based on the NCEP-NCAR reanalysis and included corrections for known rainfall biases and rain day statistics using the latest global meteorological data sets and TRMM rainfall data. This dataset has been compared to ERA-40 and used in large-scale hydrological modelling to simulate soil moisture in the Yellow River Basin and showed better inter and intra-annual patterns (Li and Ma, 2010).

2.2. Surface air temperature

Absolute global daily temperature (T_a) observations are available from reanalysis. Monthly, annual and climatological T_a anomalies from aggregated daily estimates had very similar values in most reanalysis data sets including both ERA reanalysis, JRA-25 and NCEP-NCAR; when compared to station interpolated gridded global data sets such as HadCRUT3 (Simmons *et al.*, 2004; Onogi *et al.*, 2007). ERA-40 was closer to HadCRUT3 data than the NCEP-NCAR reanalysis, in all but the earliest years, reflecting the fact that surface observations were included in the ERA reanalysis (Simmons *et al.*, 2004). At the daily temporal scale, Pitman and Perkins (2009) compared daily maximum and minimum T_a probability density functions from ERA-40, JRA-25 and NCEP-DOE to regional observational data encompassing different environments in the absence of global observational data sets. Estimates of maximum T_a had large regional differences but overall no reanalysis showed more skill than the other two. All reanalysis failed to match observations of maximum T_a in the Amazon. For minimum T_a, all reanalysis showed reasonable agreement north of ~45º N, whereas ERA-40 appeared anomalous compared to the other reanalysis and to observations. Based on these results, Pitman and Perkins (2009) suggested the use of the 2-m air temperatures is not reliable and all reanalysis should be used independently to reflect uncertainty from input data. PGF also includes T_a estimates, NCEP-NCAR T_a was adjusted to match an earlier version of HadCRUT3 monthly and daily averages in order to correct for known temperature biases (Sheffield *et al.*, 2006).

2.3. Surface radiation

Global gridded radiation data sets, including incoming shortwave (SW_{down}) and longwave (LW_{down}) radiation, are available from satellite sensors and reanalysis. Existing literature shows that SW_{down} and LW_{down} derived from satellite data have generally smaller biases than reanalysis because they are more constrained by observations of atmospheric transmissivity (e.g. cloud cover) (Betts *et al.*, 2006). The International Satellite Cloud Climatology Project produced a global radiative flux data set (ISCCP-FD) on a 3-hourly, 280 km resolution for the period 1983–2006. Comparison of ISCCP-FD SW_{down} with the Baseline Surface Radiation Network (BSRN) data (Ohmura *et al.*, 1998) revealed a mean difference of 2 Wm^{-2} and an RMSE error of 19 Wm^{-2} (Zhang *et al.*, 2004). More recently, the GEWEX Surface Radiation Budget (GEWEX-SRB) Project has constructed a 24.5-year (July 1983 to December 2007) data set of surface SW_{down} and LW_{down} radiative fluxes (Stackhouse *et al.*, 2011). GEWEX SRB release 3.0 is produced on a 1º and 3-hourly resolution using satellite-derived cloud parameters and ozone fields, reanalysis meteorology, and a few other ancillary data sets. Validation of monthly average downward SW_{down} and LW_{down} fluxes with BSRN sites mean bias for SW_{down} fluxes is ~-4 W m^{-2} with an RMSE difference of 23 W m^{-2}. An examination of individual sites showed that most of this underestimation arose at polar sites; especially those located on the Antarctic coast, but these are much improved over previous versions (Stackhouse *et al*., 2011). Corresponding bias for the LW_{down} fluxes are only about -0.1 W m^{-2} with an RMSE difference of 11 W m^{-2}.

The Earth's Radiant Energy System Radiative Fluxes and Clouds instrument (CERES-FSW) provides SW_{down} and LW_{down} fluxes on a 1º and daily resolution. Gupta *et al.* (2004) evaluated instantaneous-footprint SW_{down} and LW_{down} fluxes from January-August 1998 against high quality ground-based radiometric measurements from several sites of the BSRN data set. For this instantaneous–footprint SW_{down} fluxes had significant biases in some sites, and random errors were much larger than acceptable values.

Gui *et al.* (2010) compared 3-hourly or hourly (when available) SW_{down} measurements for the period 2000–2002 from ISCCP-FD, GEWEX-SRB and CERES-FSW SW_{down} against 36 stations from five different ground measurement networks. Results showed that SRB met accuracy criteria in most regions, followed by FD and FSW. Both SRB and FD underestimated SW_{down} in the Tibetan Plateau and Greenland and had large biases and overestimation in Southeast Asia. In addition, FD had slight overestimation in the Amazon. FSW had low correlations, had large biases and overestimates ground measurements in the Tibetan Plateau and Southeast Asia, as well as large overestimation in North America and the Amazon. The Princeton Global Forcing data set (PGF) SW_{down} adjusts the systematic biases in NCEP-NCAR data using the GEWEX-SRB climatology and a historic cloud data set.

3. IMPLEMENTATION OF W3RA AND DATA EVALUATION AGAINST GRDC COMPOSITE RUNOFF DATA

A global version of the Australian Water Resources Assessment system Landscape model (AWRA-L) (version 0.5; Van Dijk and Renzullo, 2011) was implemented on a 1° grid cell resolution, referred to here as the "World-Wide Water Resources System" (W3RA). Bias-corrected Princeton Global Forcing (PGF) precipitation, incoming short wave radiation; minimum and maximum daily temperature and air pressure data were used as meteorological inputs. The parameters used in W3RA were derived from observations in Australia through analysis performed as part of development of AWRA-L or derived from literature. Baseflow coefficient was estimated using relationships found in a global analysis of baseflow recession (Peña-Arancibia *et al.*, 2010). This version of the model included two hydrological response units (HRUs): deep-rooted tall vegetation (forest) and shallow-rooted short vegetation (herbaceous). In each HRU, the model simulates the water balance on three soil stores (top, shallow and deep soil compartment) whereas groundwater and surface water are simulated at catchment scale. In addition, the HBV-96 snow hydrology module was included to simulate snowmelt and snow accumulation (Bergström and Singh, 1995). To represent each HRU, the 0.05° resolution vegetation continuous fields derived from MODIS reflectance data (2000–2001) (Hansen *et al.*, 2003) was aggregated to a 1° grid cell resolution land/sea mask. Other data sets used to parameterise the model included an albedo climatology derived from white-sky albedo (Moody et al., 2005) and wind speed climatology (1983–1993) from NASA. The model warm-up used the full 61 years of the PGF data (1948–2008), the model was then rerun using the states reached at the end of 2008. This was done due to the long time (around three decades) needed for deeper soil stores in arid regions to reach dynamic equilibrium.

As a preliminary evaluation of the W3RA estimates, the climatology (1950–1979) of quasi-global blended modeled runoff and river streamflow observation station network (Fekete *et al.*, 2002) was used as baseline to evaluate W3RA runoff results over the same time-period. To produce spatially distributed runoff, simulated runoff above a gauging station was scaled using correction coefficients to match river streamflow.

4. PRELIMINARY RESULTS

Figure 1a and b show the spatial distribution of W3RA and the GRDC composite mean annual log-scaled runoff for the period 1950–1979 respectively. Spatial patterns are captured particularly well in the humid tropical areas and North America, whereas W3RA produces lower runoff estimates in Europe and parts of northern Asia and higher runoff in very arid areas. Computed mean values across the latitude band 70°N–50°S show that W3RA performs better in latitudes above 0°N and overestimates runoff in lower latitudes (Fig. 1c). This overestimation may be related to a higher number of streamflow stations with better accuracy in northern latitudes (see Hong *et al.*, 2008). The landmass above 70°N was not used in comparisons since there were no GRDC composite runoff data. Mean annual runoff was 310 (±225) mm y^{-1} for W3RA and 345 (±270) mm y^{-1} for GRDC composite runoff. Correlation coefficient (R^2) and relative bias were 0.87 and -10% respectively. W3RA produces streamflow estimates that are higher than GRDC estimates for arid areas in the southern hemisphere. It is noted that the W3RA estimates should be interpreted as local catchment runoff, whereas the GRDC data are scaled to conform to river flows observed at the end of large catchments and therefore implicitly include river losses. This may explain the discrepancy for arid zones, where closed catchments are common and internal catchment losses considerable, e.g. in the Australian interior.

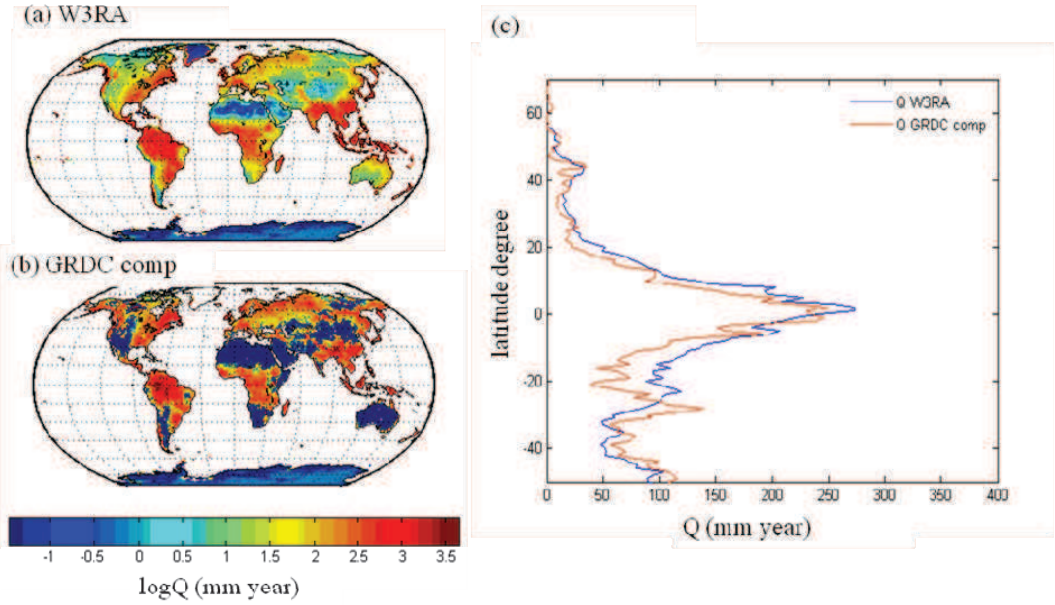

Figure 1. (a) Mean annual log-scaled runoff from W3RA for the period 1950–1979. (b) Mean annual log-scaled runoff from GRDC composite fields (1950–1979). (c) Mean latitudinal profiles comparing W3RA (blue) and GRDC (red). Means are computed by assigning a value of 0 to ocean cells in order to avoid deviations for latitude bands with few terrestrial cells.

5. SUMMARY AND FURTHER MODEL EVALUATION

We reviewed published studies of satellite-derived, reanalysis and gauge-based data with global or near-global coverage and which are routinely used in hydrological modelling. Satellite-based rainfall performed better during warm seasons and in the tropics, capturing large events better than reanalysis, although overestimating total rainfall. Daily satellite-based rainfall estimates generally missed light precipitation and the amount of false precipitation also gets exceedingly large sometimes, especially for winter. Gauge bias-corrected TRMM 3B42V6 reduced observed bias in many areas globally, however large discrepancies still exists in areas with complex topography. Reanalysis data outperformed satellite-based rainfall during winter and in higher latitudes. In this respect, a blending approach may enhance rainfall quality estimates on a global scale, using rainfall from reanalysis in higher latitudes and satellite estimates such as TRMM 3B42V6 in mid-latitudes.

Monthly, annual and climatological T_a anomalies from aggregated daily estimates had very similar values in most reanalysis data sets including both ERA reanalysis, JRA-25 and NCEP-NCAR; when compared to the observational network HadCRUT3, with both ERA and JRA-25 having a closer agreement to HadCRUT3

than NCEP-NCAR. At the daily scale, compared daily maximum and minimum T_a probability density functions from ERA-40, JRA-25 and NCEP-DOE were dissimilar with large regional differences, but overall no reanalysis showed more skill than the other two when compared against regional observational temperature data.

Surface shortwave radiation SW_{down} derived from satellite data have generally smaller biases than reanalysis because they are more constrained by observations. Of the three satellite-based incoming shortwave radiation estimates, GEWEX-SRB appeared superior to the other two. Globally, the biases in the climatology of the re-analyses are significant, more for NCEP-DOE than ERA-40.

The 60 year (1948–2008) Princeton Global Forcing (PGF) dataset with a spatial resolution of 1º and daily time step was considered an adequate compromise for trial simulations. PGF, based on the NCEP/NCAR reanalysis, used many of the data described above to constrain and reduce bias of its meteorological variables. W3RA was parameterized with the same set of parameters used in AWRA-L expect for baseflow coefficient, which was derived from a global analysis of baseflow recession. The prototype W3RA global hydrological model produced encouraging runoff estimates without substantially modifying the model structure or the parameters that were used to simulate the water balance for Australian conditions. Runoff corresponded closely to a blended data comprised of observations and modeled runoff.

Further model evaluation against streamflow will be performed using carefully quality-controlled global data sets of streamflow from small and unimpaired catchments (e.g. Peña-Arancibia *et al.*, 2010). W3RA soil moisture estimates will be evaluated against a collated international data set of in situ measurements (Dorigo *et al.*, 2011), and evapotranspiration estimates will be evaluated against a set of high quality FLUXNET site measurements covering a variety of ecosystems (cf. Miralles *et al.*, 2011).

REFERENCES

Bergström, S., Singh, V.P., (1995), The HBV model. Water Resources Publications: 443-476.

Betts, A. K., M. Zhao, P. A. Dirmeyer, and A. C. M. Beljaars (2006), Comparison of ERA40 and NCEP/DOE near-surface data sets with other ISLSCP-II data sets, *Journal of Geophysical Research-Atmospheres*, *111*(D22).

Betts, A. K., J. H. Ball, P. Viterbo, A. Dai, and J. Marengo (2005), Hydrometeorology of the Amazon in ERA-40, *Journal of Hydrometeorology*, *6*(5), 764-774.

Bosilovich, M. G., J. Y. Chen, F. R. Robertson, and R. F. Adler (2008), Evaluation of global precipitation in reanalyses, *Journal of Applied Meteorology and Climatology*, *47*(9), 2279-2299.

Dorigo, W.A., W.Wagner, R. Hohensinn, S. Hahn, C. Paulink, M. Drusch, S. Mecklenburg, P. van Oevelen, A. Robock and T. Jackson (2011), The International Soil Moisture Network: a data hosting facility for global in situ soil moisture measurements. *Hydrology and Earth System Sciences*, *15*, 1675-2011.

Ebert, E. E., J. E. Janowiak, and C. Kidd (2007), Comparison of near-real-time precipitation estimates from satellite observations and numerical models, *Bulletin of the American Meteorological Society*, *88*(1), 47.

Fekete, B. M. , Vörösmarty, C. J. & Grabs, W. (2002), High-resolution fields of global runoff combining observed river discharge and simulated water balances. *Glob. Biogeochem. Cycles* 16, 1042.

Fekete, B. M., C. J. Vorosmarty, J. O. Roads, and C. J. Willmott (2004), Uncertainties in precipitation and their impacts on runoff estimates, *Journal of Climate*, *17*(2), 294-304.

Gui, S., S. L. Liang, K. C. Wang, L. Li, and X. T. Zhang (2010), Assessment of Three Satellite-Estimated Land Surface Downwelling Shortwave Irradiance Data Sets, *IEEE Geoscience and Remote Sensing Letters*, *7*(4), 776-780.

Gupta, S. K., D. P. Kratz, A. C. Wilber, and L. C. Nguyen (2004), Validation of parameterized algorithms used to derive TRMM-CERES surface radiative fluxes, *Journal of Atmospheric and Oceanic Technology*, *21*(5), 742-752.

Hansen, M. C., R. S. DeFries, J. R. G. Townshend, M. Carroll, C. Dimiceli, and R. A. Sohlberg (2003), Global Percent Tree Cover at a Spatial Resolution of 500 Meters: First Results of the MODIS Vegetation Continuous Fields Algorithm, *Earth Interactions*, *7*.

Hong, Y., R. F. Adler, F. Hossain, S. Curtis, and G. J. Huffman (2007), A first approach to global runoff simulation using satellite rainfall estimation, *Water Resour. Res.*, *43*, W08502.

Huffman, G. J., R. F. Adler, M. M. Morrissey, D. T. Bolvin, S. Curtis, R. Joyce, B. McGavock, and J. Susskind (2001), Global precipitation at one-degree daily resolution from multisatellite observations, *Journal of Hydrometeorology*, *2*(1), 36-50.

Huffman, G. J., R. F. Adler, D. T. Bolvin, G. J. Gu, E. J. Nelkin, K. P. Bowman, Y. Hong, E. F. Stocker, and D. B. Wolff (2007), The TRMM multisatellite precipitation analysis (TMPA): Quasi-global, multiyear, combined-sensor precipitation estimates at fine scales, *Journal of Hydrometeorology*, *8*(1), 38-55.

Joyce, R. J., J. E. Janowiak, P. A. Arkin, and P. P. Xie (2004), CMORPH: A method that produces global precipitation estimates from passive microwave and infrared data at high spatial and temporal resolution, *Journal of Hydrometeorology*, *5*(3), 487-503.

Kanamitsu, M., W. Ebisuzaki, J. Woollen, S.K. Yang; J.J. Hnilo; M. Fiorino; G.L. Potter (2002), NCEP-DOE AMIP-II reanalysis (R-2). *Bulletin of the American Meteorological Society*, 83(11): 1631-1643.

Kalnay, E., et al. (1996), The NCEP/NCAR 40-year reanalysis project, *Bulletin of the American Meteorological Society*, *77*(3), 437-471.

Li, M. X., and Z. G. Ma (2010), Comparisons of Simulations of Soil Moisture Variations in the Yellow River Basin Driven by Various Atmospheric Forcing Data Sets, *Advances in Atmospheric Sciences*, *27*(6), 1289-1302.

Miralles, D. G., T. R. H. Holmes, R. A. M. d. Jeu, J. H. Gash, A. G. C. A. Meesters, and A. J. Dolman (2011), Global land-surface evaporation estimated from satellite-based observations, *Hydrology and Earth System Sciences*, *15*(2), 453-469.

Moody, E.G., King, M.D., Platnick, S., Schaaf, C.B., Feng, G., (2005), Spatially complete global spectral surface albedos: value-added datasets derived from Terra MODIS land products. *Geoscience and Remote Sensing*, IEEE Transactions on, 43(1): 144-158.

Ohmura, A., et al. (1998), Baseline Surface Radiation Network (BSRN/WCRP): New precision radiometry for climate research, *Bulletin of the American Meteorological Society*, *79*(10), 2115-2136.

Onogi, K., et al. (2007), The JRA-25 reanalysis, *Journal of the Meteorological Society of Japan*, *85*(3), 369-432.

Pan, M., H. B. Li, and E. Wood (2010), Assessing the skill of satellite-based precipitation estimates in hydrologic applications, *Water Resources Research*, *46*.

Peña-Arancibia, J. L., A. van Dijk, M. Mulligan, and L. A. Bruijnzeel (2010), The role of climatic and terrain attributes in estimating baseflow recession in tropical catchments, *Hydrology and Earth System Sciences*, *14*(11), 2193-2205.

Pitman, A. J., and S. E. Perkins (2009), Global and regional comparison of daily 2-m and 1000-hPa maximum and minimum temperatures in three global reanalyses, *Journal of Climate*, *22*(17), 4667-4681.

Sheffield, J., G. Goteti, and E. F. Wood (2006), Development of a 50-year high-resolution global dataset of meteorological forcings for land surface modeling, *Journal of Climate*, *19*(13), 3088-3111.

Simmons, A. J., P. D. Jones, V. D. Bechtold, A. C. M. Beljaars, P. W. Kallberg, S. Saarinen, S. M. Uppala, P. Viterbo, and N. Wedi (2004), Comparison of trends and low-frequency variability in CRU, ERA-40, and NCEP/NCAR analyses of surface air temperature, *Journal of Geophysical Research-Atmospheres*, *109*(D24).

Simmons, A., S. Uppala, D. Dee, and S. Kobayashi, (2007), ERA-Interim: New ECMWF reanalysis products from 1989 onwards. ECMWF Newsletter No 110, 25-35.

Sorooshian, S., K. L. Hsu, X. Gao, H. V. Gupta, B. Imam, and D. Braithwaite (2000), Evaluation of PERSIANN system satellite-based estimates of tropical rainfall, *Bulletin of the American Meteorological Society*, *81*(9), 2035-2046.

Stackhouse P.W., Gupta S.K., Cox S.J., Zhang T., Mikovitz J.C., Hinkelman L.M. (2011) 24.5-Year SRB Data Set Released. *GEWEX News, 21*(1)

Suttles J.T., and Ohring G., (1986) Surface radiation budget for climate applications. NASA 1169, 136 pp.

Tian, Y., and C. Peters-Lidard (2010), A global map of uncertainties in satellite-based precipitation measurements*Geophysical Research Letters*, *37*(L24407), 1-6

Tian, Y. D., C. D. Peters-Lidard, J. B. Eylander, R. J. Joyce, G. J. Huffman, R. F. Adler, K. L. Hsu, F. J. Turk, M. Garcia, and J. Zeng (2009), Component analysis of errors in satellite-based precipitation estimates, *Journal of Geophysical Research-Atmospheres*, *114*.

Uppala, S. M., et al. (2005), The ERA-40 re-analysis, *Quarterly Journal of the Royal Meteorological Society*, *131*(612), 2961-3012.

Van Dijk, A.I.J.M, Renzullo, L.J., (2011), Water resource monitoring systems and the role of satellite observations. *Hydrology and Earth System Sciences*, 15: 39-55.

Van Dijk, A. I. J. M., and Warren, G. (2010), The Australian Water Resources Assessment System. Technical Report 4. Landscape Model (version 0.5) Evaluation Against Observations. CSIRO: Water for a Healthy Country National Research Flagship.

Zhang, Y. C., W. B. Rossow, A. A. Lacis, V. Oinas, and M. I. Mishchenko (2004), Calculation of radiative fluxes from the surface to top of atmosphere based on ISCCP and other global data sets: Refinements of the radiative transfer model and the input data, *Journal of Geophysical Research-Atmospheres*, *109*(D19).

Appendix C - Journal article

Peña-Arancibia, J. L., A. I. J. M. van Dijk L.J. Renzullo, and M. Mulligan (2013), Evaluation of precipitation estimation accuracy in reanalyses, satellite products and an ensemble method for regions in Australia and in South and East Asia, Journal of Hydrometeorology, 14, 1323-1333.

Evaluation of Precipitation Estimation Accuracy in Reanalyses, Satellite Products, and an Ensemble Method for Regions in Australia and South and East Asia

JORGE L. PEÑA-ARANCIBIA

CSIRO Land and Water, Canberra, Australian Capital Territory, Australia, and Faculty of Earth and Life Sciences, VU University Amsterdam, Amsterdam, Netherlands, and Environmental Monitoring and Modelling Research Group, Department of Geography, King's College London, London, United Kingdom

ALBERT I. J. M. VAN DIJK* AND LUIGI J. RENZULLO

CSIRO Land and Water, Canberra, Australian Capital Territory, Australia

MARK MULLIGAN

Environmental Monitoring and Modelling Research Group, Department of Geography, King's College London, London, United Kingdom

(Manuscript received 6 September 2012, in final form 10 December 2012)

ABSTRACT

Precipitation estimates from reanalyses and satellite observations are routinely used in hydrologic applications, but their accuracy is seldom systematically evaluated. This study used high-resolution gauge-only daily precipitation analyses for Australia (SILO) and South and East Asia [Asian Precipitation—Highly-Resolved Observational Data Integration Towards Evaluation (APHRODITE)] to calculate the daily detection and accuracy metrics for three reanalyses [ECMWF Re-Analysis Interim (ERA-Interim), Japanese 25-yr Reanalysis (JRA-25), and NCEP–Department of Energy (DOE) Global Reanalysis 2] and three satellite-based precipitation products [Tropical Rainfall Measuring Mission (TRMM) 3B42V6, Climate Prediction Center morphing technique (CMORPH), and Precipitation Estimation from Remotely Sensed Imagery Using Artificial Neural Networks (PERSIANN)]. A depth-frequency-adjusted ensemble mean of the reanalyses and satellite products was also evaluated. Reanalyses precipitation from ERA-Interim in southern Australia (SAu) and northern Australasia (NAu) showed higher detection performance. JRA-25 had a better performance in South and East Asia (SEA) except for the monsoon period, in which satellite estimates from TRMM and CMORPH outperformed the reanalyses. In terms of accuracy metrics (correlation coefficient, root-mean-square difference, and a precipitation intensity proxy, which is the ratio of monthly precipitation amount to total days with precipitation) and over the three subdomains, the depth-frequency-adjusted ensemble mean generally outperformed or was nearly as good as any of the single members. The results of the ensemble show that additional information is captured from the different precipitation products. This finding suggests that, depending on precipitation regime and location, combining (re)analysis and satellite products can lead to better precipitation estimates and, thus, more accurate hydrological applications than selecting any single product.

1. Introduction

The accuracy of precipitation estimates to a great extent determines the accuracy of hydrological model outputs (Fekete et al. 2004; Fernandes et al. 2008; Voisin et al. 2008; Pan et al. 2010; Getirana et al. 2011; Van Dijk and Renzullo 2011; Yong et al. 2012). Gridded precipitation analysis based on gauging can be of dubious

* Current affiliation: Fenner School of Environment and Society, College of Medicine, Biology and Environment, Australian National University, Canberra, ACT, Australia.

Corresponding author address: Jorge L. Peña-Arancibia, CSIRO Land and Water, GPO 1666, Black Mountain, Canberra ACT 2601, Australia.
E-mail: jorge.penaarancibia@csiro.au

DOI: 10.1175/JHM-D-12-0132.1

quality in areas where gauge or radar networks do not exist or are sparse, for example, in much of the tropics. Several precipitation estimates derived from satellite data or modeled through retrospective weather forecast model analysis (reanalysis) provide estimates that are independent from gauge networks. Both types of precipitation estimates have being increasingly used in hydrological applications [e.g., for reanalysis (Dedong et al. 2007; Li et al. 2009; Yan et al. 2010; Miguez-Macho and Fan 2012) and for satellite (Shrestha et al. 2008; Behrangi et al. 2011; Khan et al. 2012; among many others)].

Previous studies evaluating reanalyses and satellite precipitation estimates in areas with dense gauge or radar coverage suggest that convective precipitation (more typical of warmer seasons and lower latitudes) is better characterized by satellite precipitation, whereas frontal system precipitation (more typical of cooler seasons and higher latitudes) is better characterized by reanalysis (e.g., Gottschalck et al. 2005; Ebert et al. 2007; Ruane and Roads 2007; Tian et al. 2009; Sapiano and Arkin 2009; Vila et al. 2010). Estimates from these products can be very different, particularly over tropical areas with high precipitation (Bosilovich et al. 2008; Tian and Peters-Lidard 2010). The incorporation of rain gauge data to correct magnitudes and frequencies can reduce total errors and bring the intensity distribution for heavy precipitation closer to the gauge data (Ebert et al. 2007). It is also noted that more recent reanalyses have improved precipitation estimates for tropical areas, although notable biases still exist (Betts et al. 2006, 2009; Bosilovich et al. 2008; Uppala et al. 2007).

The above summary suggests that reanalysis and satellite datasets can be complementary. This would be particularly relevant in areas where adjustments are difficult or impossible because of the scarcity of rain gauge networks. The aims of this paper are to 1) evaluate and compare daily satellite and reanalysis precipitation estimates routinely used in large-scale hydrologic model applications against precipitation analysis based on dense ground networks in Australia and South and East Asia and 2) evaluate and compare a depth-frequency-adjusted ensemble mean of the products (see definition in section 2 below). The performance metrics are chosen to establish which precipitation product performs best for detection (occurrence) and estimation accuracy for daily precipitation (i.e., how close to the observed magnitude and/or frequency) in three subdomains with different precipitation regimes. Section 2 introduces the reanalyses, satellite, and evaluation precipitation datasets and performance metrics. Section 3 presents results of the performance evaluation experiments. Section 4 discusses the results and draws conclusions.

2. Data and methodology

Three recent reanalysis precipitation datasets with global coverage are considered in this paper: 1) the National Centers for Environmental Prediction–Department of Energy Global Reanalysis 2 (NCEP–DOE; Kanamitsu et al. 2002), 2) the European Centre for Medium-Range Weather Forecasts (ECMWF) Re-Analysis Interim (ERA-Interim; Dee et al. 2011), and 3) the Japanese 25-yr Reanalysis (JRA-25; Onogi et al. 2007). These reanalyses build and improve on earlier reanalysis versions by improving the forecasting model physics and incorporating new satellite and other conventional data.

Also included are three quasi-global satellite-based precipitation products that combine multiple microwave and infrared sensors: 1) the bias-corrected Tropical Rainfall Measuring Mission (TRMM) Multisatellite Precipitation Analysis (Huffman et al. 2007) 3B42V6, which uses monthly gauge observations to scale precipitation estimates; 2) the Climate Prediction Center (CPC) morphing technique (CMORPH; Joyce at al. 2004); and 3) the Precipitation Estimation from Remotely Sensed Imagery using Artificial Neural Networks (PERSIANN; Sorooshian et al. 2000).

An ensemble of the six products was derived by calculating the simple mean daily precipitation and adjusting it to the depth-frequency distribution function of gauge-only daily precipitation analyses (used as evaluation data) by mapping the full spatiotemporal distribution of the ensemble estimates to that of the gauge analysis. In other words, if prob* = prob($P_{\text{ens},i}$) is the probability of the ensemble mean precipitation P_{ens} on day i, then the depth-frequency-adjusted precipitation estimate P_{adj} is $P_{\text{adj}} = P_{\text{obs}}(\text{prob}^*)$, with P_{obs} being the gauge analysis time series used. The adjustment is performed using all daily data for the grid cells selected from the gauge analysis products; consequently, the ensemble is not fully independent of the evaluation data.

The evaluation is performed at a daily temporal scale using two high-resolution gauge-only daily precipitation analyses available in Australia (SILO; Jeffrey et al. 2001) and South and East Asia [Asian Precipitation—Highly-Resolved Observational Data Integration Towards Evaluation (APHRODITE; Yatagai et al. 2012)]. All data were resampled to 1° resolution (simple averaging) as a compromise between the spatial resolutions of the different products (satellite estimate resolution data were 0.25°, whereas reanalyses ranged from 0.7° to 2.5°). Only grid cells with a density of more than one gauge per 500 km^2 were considered (see Fig. 1 for location of the grid cells). The common period for all data was 2003–07, and the time series of each precipitation product had less than 5% of days with no data. A threshold of 1 mm day^{-1}

was used to discriminate between ''rain'' and ''no rain'' in order to eliminate very light intensity ''drizzle'' that does not significantly contribute to daily precipitation but could have an undue impact on detection metrics. To account for differences in precipitation regime, the geographical domain was divided into three regions: southern Australia (SAu), mostly dominated by synoptic system precipitation during austral winter; northern Australasia (NAu), mostly dominated by convective precipitation during summer; and South and East Asia (SEA), mostly dominated by monsoon precipitation.

First, precipitation bias error estimates on annual and monthly time scales are computed following Adler et al. (2012). The standard deviation σ of the six products is used as a measure of the bias error. The dispersion among the product estimates captured in σ showcases the different physical assumptions and nature of both satellite and reanalyses precipitation retrievals. Subsequently, detection and accuracy metrics were computed for each grid cell. Every day in the estimated and gauge analysis was classified following Ebert et al. (2007) as a hit (H, observed precipitation correctly detected), miss (M, observed precipitation not detected by product), or false alarm (F, precipitation detected but none observed). The probability of detection, POD $= H/(H + M)$, gives the fraction of precipitation occurrences correctly detected (range 0–1 and a perfect score of 1). The false alarm ratio, FAR $= F/(H + F)$, gives the wrongly detected precipitation (range 0–1 and a perfect score of 0). The frequency bias, FB $= (H + F)/(H + M)$, gives the ratio of the estimated to observed precipitation frequency (range 0–∞ and a perfect score of 1). The equitable threat score (ETS), used as an overall performance metric, gives the fraction of precipitation that was correctly detected, adjusted for correct detections (H_e) that would be expected because of random chance: ETS $= (H - H_e)/(H + M + F - H_e)$, where $H_e = (H + M)(H + F)/N$ and N is the total number of estimates (range $-\frac{1}{3}$–1, a perfect score of 1 and 0 indicating no skill).

Accuracy metrics used were correlation r, root-mean-square difference (RMSD), and a precipitation intensity proxy, namely, the percentage difference of the ratio of monthly precipitation amount to the total number of days with precipitation (MPDR). Both detection and accuracy metrics were mapped for spatial patterns and examined. Results were also stratified by season to assist in interpretation. Finally, monthly and subdomain aggregated time series were plotted to detect any evidence for drifts or step changes.

3. Results

The mean annual precipitation of the six precipitation products used here is shown in Fig. 1a. The measure of the bias error, the mean annual precipitation standard deviation σ of the products, is shown in Fig. 1b. As expected, higher σ values occur in grid cells with higher precipitation, with the highest values ($>$1500 mm yr^{-1}) occurring in grid cells located in the intertropical convergence zone (ITCZ), particularly in insular Southeast Asia. The mean annual σ in SEA is 554 mm yr^{-1}, whereas it is 324 and 170 mm yr^{-1} in NAu and SAu, respectively. The months of January and July are used as an example of monthly bias. The ITCZ moves southward, and during January grid cells in northern Australia have the highest precipitation ($>$200 mm month^{-1}) and σ ($>$100 mm month^{-1}) (Figs. 1c,d). The mean January σ in SEA is 26 mm yr^{-1}, whereas it is 76 and 15 mm yr^{-1} in NAu and SAu, respectively. In July, the ITCZ shifts northward, and many grid cells in SEA are affected by the Asia–Pacific monsoon, with higher July precipitation occurring in grid cells in Japan, Nepal, southern China, and Southeast Asia ($>$400 mm month^{-1}) (Fig. 1e). Higher July σ ($>$100 mm month^{-1}) is observed not only in these grid cells, but also in southwest Australia and Tasmania (Fig. 1f).

Figure 2 shows percentage frequency of exceedance curves for the six products (for daily precipitation $>$1 mm), the simple ensemble mean, and the depth-frequency-adjusted ensemble (data are aggregated over the whole geographical domain). All satellite products have lower frequencies than the reference for mean precipitation depths $<$10 mm day^{-1}, whereas reanalyses agree reasonably well (Fig. 2a). The exceptions are NCEP–DOE, which exceeds reference depths almost across the range, and the simple ensemble mean, in which the simple averaging of all products enhances light precipitation depths (Fig. 2a). Conversely, only the bias-corrected TRMM 3B42V6 and the depth-frequency-adjusted ensemble show good agreement for mean precipitation depths $>$50 mm day^{-1} (Fig. 2b). Not surprisingly, the depth-frequency-adjusted ensemble shows this good agreement across the whole precipitation depth range.

In terms of ETS computed for the full time series, ERA-Interim performed best in SAu and parts of NAu close to SAu (Fig. 3a). NCEP–DOE performed best in parts of western and southern Australia, and JRA-25 performed best in most of Japan and South Korea. CMORPH and TRMM performed best in Southeast Asia. Results in continental Asia were mixed, with satellite products and the ensemble performing best in the tropics and reanalyses performing best in midlatitudes. From June to August (JJA), satellite data and the ensemble performed best in most of continental and southeast Asia and in areas in Japan most affected by the monsoon (Fig. 3b). JRA-25 and the ensemble generally performed best in December–February (DJF), except in

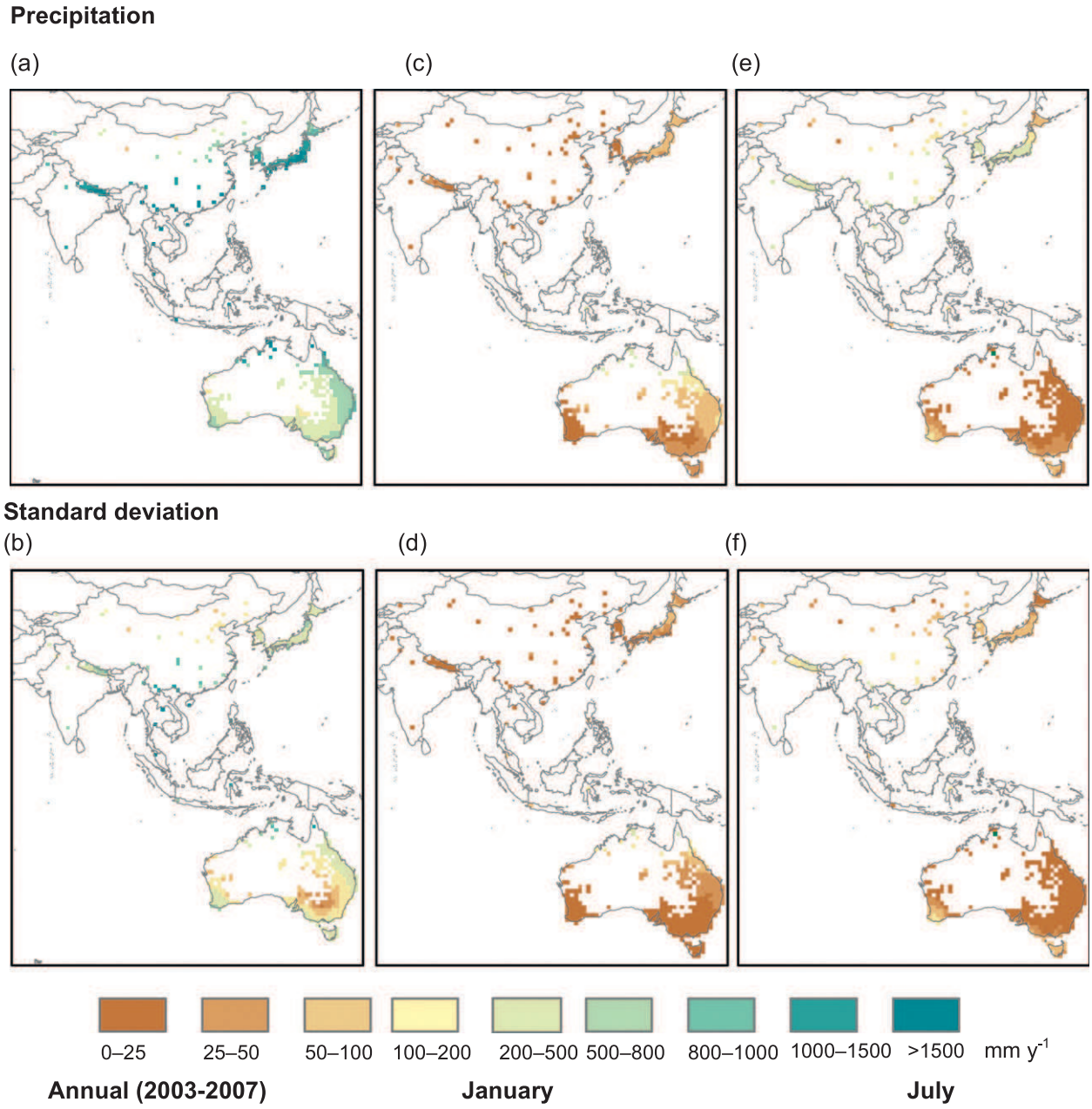

FIG. 1. (a) Mean precipitation and (b) standard deviation for the ensemble of the six precipitation products used in this study (not including the ensemble) for the years 2003–07. (c),(d) As in (a),(b) but for all January months. (e),(f) As in (a),(b), but for all July months.

insular Southeast Asia, where satellite products outperformed reanalyses and the ensemble (Fig. 3c).

Box plots in Fig. 4 highlight the superior detection performance of reanalyses for all geographical subdomains, with the exception of JJA (monsoon) in SEA (Figs. 4a–c). ERA-Interim performs better than satellite data in NAu during DJF. The ensemble shows performance somewhat intermediate to both product types. Seasonal variation in performance was not observed in SAu, but there was an improvement in CMORPH and TRMM ETS during DJF in NAu (Fig. 4b). In SEA, ETS for ERA-Interim and JRA-25 were higher than satellite, except for JJA, where CMORPH and TRMM were better (Fig. 4a).

In terms of accuracy metrics, the spatial results did not show clear seasonal variations; thus, results are presented for all months combined. For r, JRA-25 performed best in most of southeast and parts of southwest Australia,

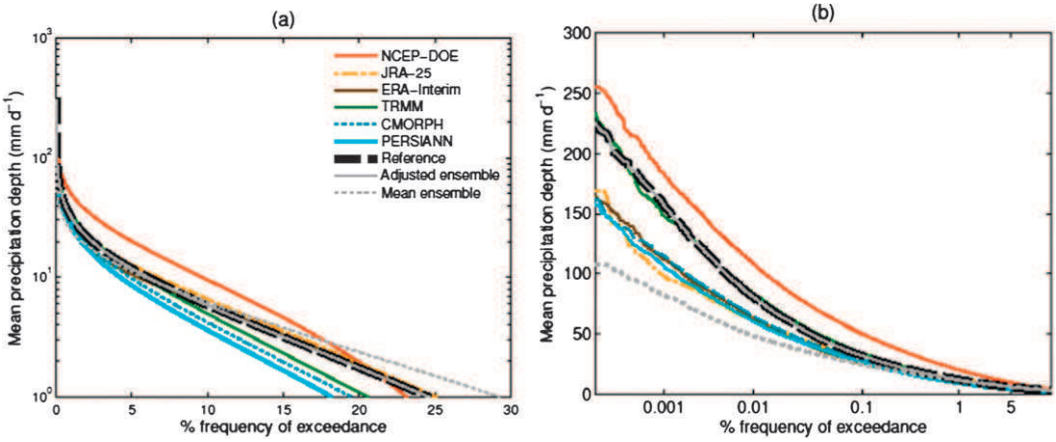

FIG. 2. (a) Percentage frequency of exceedance curves for daily precipitation (>1 mm) aggregated over the whole geographical domain. (b) As in (a), but the *x* axis is zoomed-in for higher mean precipitation depths.

whereas NCEP–DOE did so in parts of southern Australia, Tasmania, and southwest Australia (Fig. 5a).

ERA-Interim performed best in north Australia, whereas a combination of satellite and the ensemble performed best in the tropics. Box plots for all months show that *r* for ERA-Interim in both SAu and NAu were better than for satellite precipitation, with higher *r* for NAu (Fig. 6a). The ensemble performed best in Nepal, close to the coastline in China, and in part of Japan. JRA-25 and ERA-Interim had better performance in inland north China and also in some parts of Japan. For SEA, mean *r* is substantially higher (0.62) than in SAu (0.17) and NAu (0.35), with TRMM being superior and CMORPH comparable to JRA-25 and ERA-Interim (Fig. 6a). The ensemble outperformed the other products in all subdomains.

ERA-Interim had the lowest RMSD in most of SAu and NAu (Fig. 5b). In China, satellite data generally performed best close to the coastline and reanalyses in the north, the ensemble in Nepal, and JRA-25 in most of Japan and South Korea. Box plots show that RMSD was slightly lower for ERA-Interim and JRA-25 in all subdomains. Errors in NCEP–DOE were systematically higher than the other datasets, whereas the ensemble RMSD was comparable to the best results in all subdomains (Fig. 6b).

MPDR results in SAu and NAu were mixed, but overall, the best performer was JRA-25, followed by the

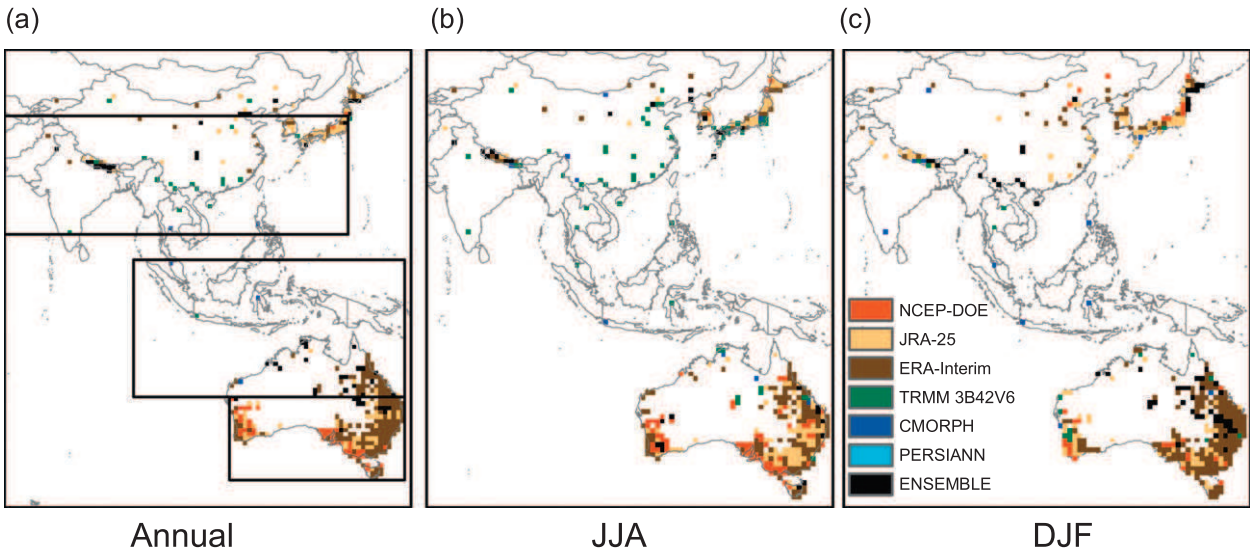

FIG. 3. Best performing product for estimating the occurrence of daily precipitation (>1 mm) in terms of the ETS for 2003–07 in each grid cell: (a) for all months, (b) for JJA, and (c) for DJF. Rectangles in (a) define the geographical extent for SAu, NAu, and SEA.

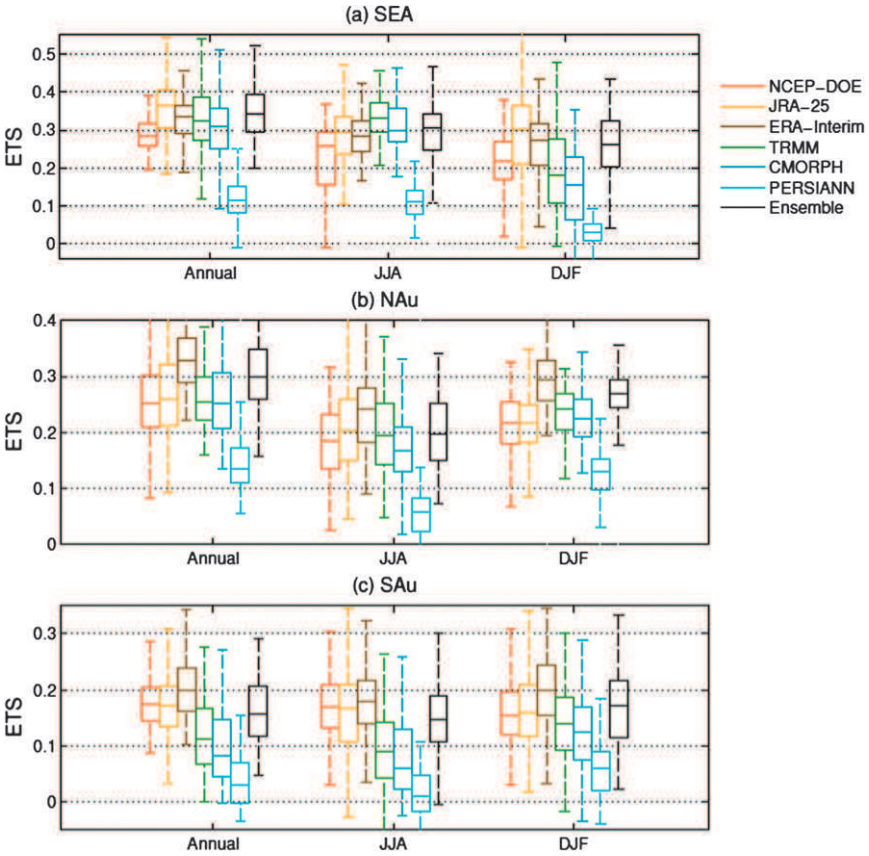

FIG. 4. Box plots showing the performance of the estimated occurrence of daily precipitation (>1 mm) in terms of ETS aggregated over three geographical subdomains for all months, JJA, and DJF: (a) SEA, (b) NAu, and (c) SAu. Tops and bottoms of each box are the 25th and 75th percentiles and whiskers are the 5th and 95th percentiles, respectively.

ensemble and ERA-Interim (Figs. 5c, 6c). Results were mixed in Japan. In China, satellite products and the ensemble generally performed best inland, whereas JRA-25 did so close to the coastline (Fig. 5c). Generally (besides NCEP–DOE), all products had less that 20% difference with observed MPDR with the exception of CMORPH and PERSIANN in SEA, which underestimated MDPR by 22% and 23%, respectively (Fig. 6c). ERA-Interim and PERSIANN systematically underestimated and TRMM and NCEP–DOE systematically overestimated MPDR (Fig. 6c).

Time series of monthly averaged ETS over the whole domain showed some seasonal variation, with an increase roughly during JJA and DJF, and a step change to reduced ETS for PERSIANN precipitation after 2005 (Fig. 7a). No clear patterns are evident for reanalysis data. The same step change in PERSIANN is present in the r time series, with again no obvious patterns for the other precipitation datasets (Fig. 7b). An analysis of PERSIANN FAR and POD over the subdomains revealed that an increase in false detections in SAu and a decrease in correct detections in SAu and SEA were the cause for the step change (not shown). This likely affected r, but only for small precipitation depths, as RMSD and MPDR appear not much affected. For all products, RMSD time series showed an increase in errors during JJA and less so during DJF, with NCEP–DOE having the largest errors (Fig. 7c). NCEP–DOE and, surprisingly, the bias-corrected TRMM produced high positive MPDR values through the analysis period; CMORPH mostly produced positive values, and the rest of the datasets mostly produced low negative MPDR values.

Table 1 shows the product ranking for detection and accuracy metrics over the whole geographical domain and for all months. The depth-frequency-adjusted ensemble mean outperformed both satellite and reanalyses for most metrics. Among individual products, JRA-25 outperformed the others in most metrics, but its high FB suggested that it tends to over predict precipitation

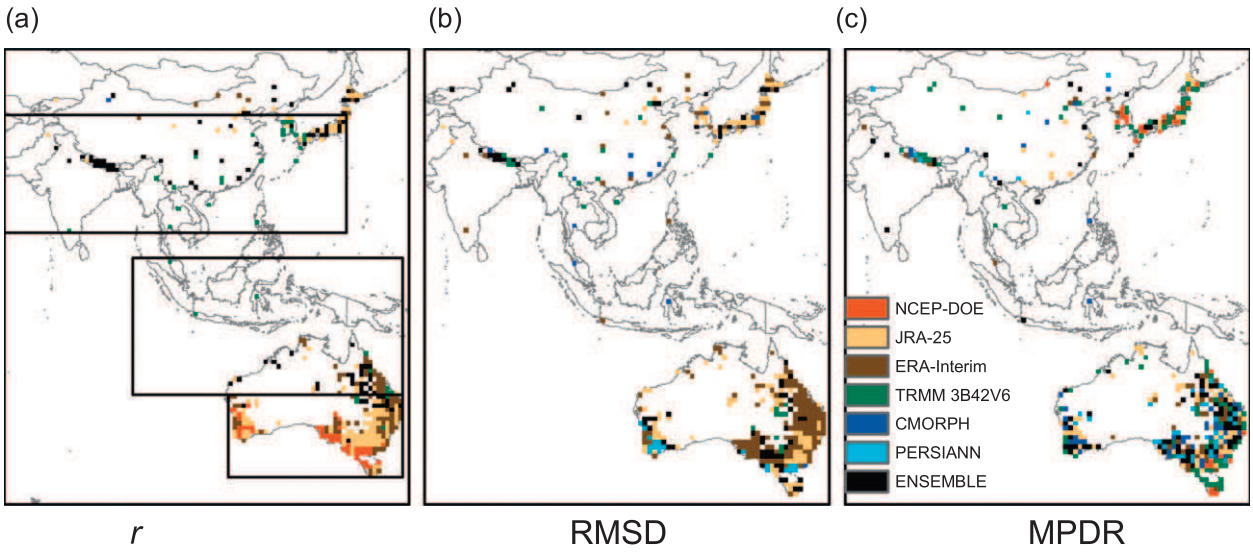

FIG. 5. Best performing product for accuracy statistics of daily precipitation (>1 mm) for 2003–07 in each grid cell: (a) correlation, (b) RMSD (mm day^{-1}), and (c) MPDR (%).

occurrence. CMORPH agreed better with observed MPDR; however, this is possibly because of compensating underprediction in SEA and overprediction in SAu and NAu (Fig. 6c).

4. Discussion and conclusions

Three reanalyses (ERA-Interim, JRA-25, and NCEP–DOE) and three satellite-based precipitation products

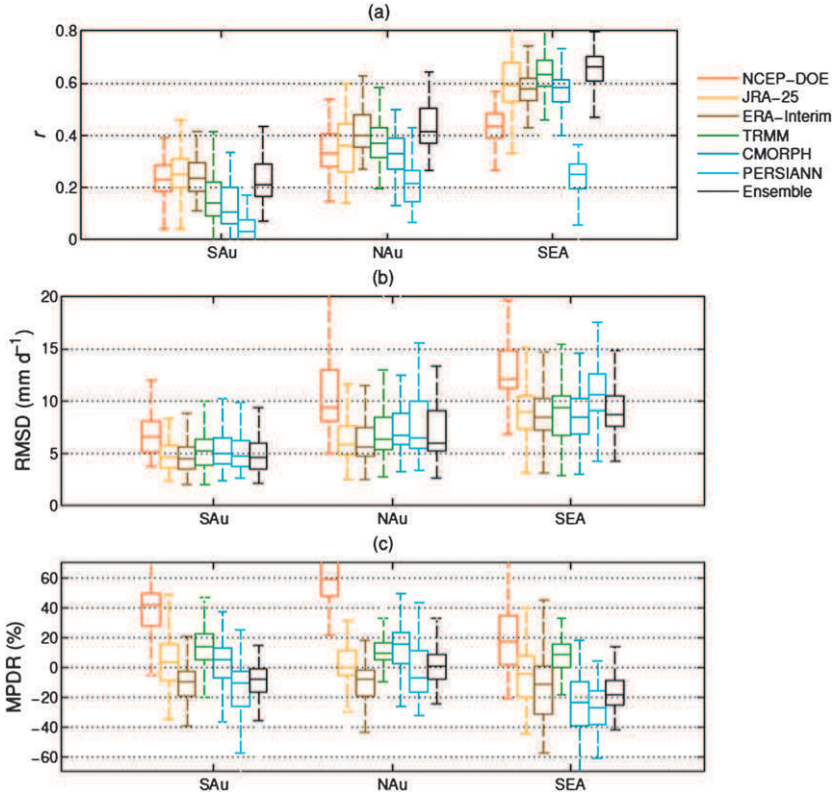

FIG. 6. Box plots showing accuracy statistics of daily precipitation (>1 mm) aggregated over three geographical subdomains: (a) *r*, (b) RMSD, and (c) MPDR. Tops and bottoms of each box are the 25th and 75th percentiles and whiskers are the 5th and 95th percentiles, respectively.

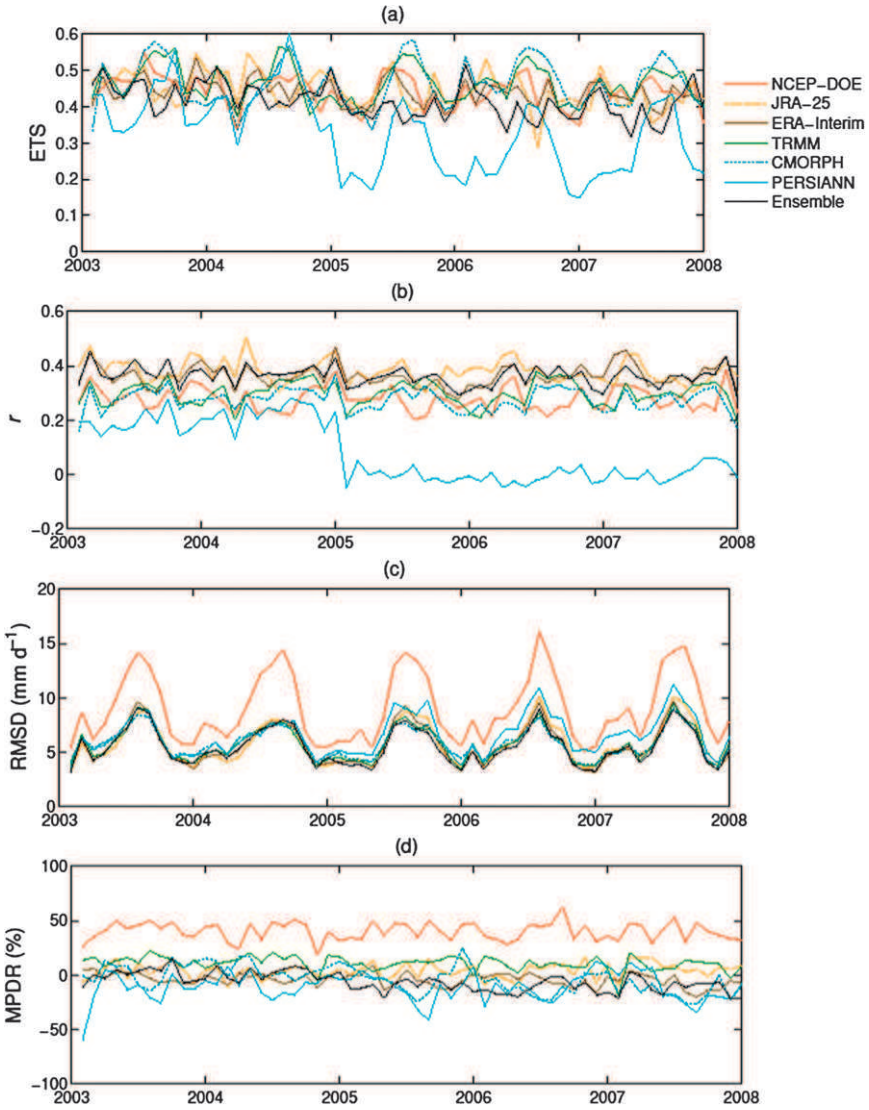

FIG. 7. Monthly time series for 2003–07 of (a) ETS, (b) *r*, (c) RMSD, and (d) MPDR averaged over the entire geographical domain.

(TRMM 3B42V6, CMORPH, and PERSIANN) were systematically evaluated, along with a depth-frequency-adjusted ensemble of the products, against analysis data in relatively well gauged areas in Australia and South and East Asia. Large bias errors (in terms of standard deviation of the products) indicated areas in which choice of precipitation estimates used in hydrologic applications should be carefully considered. Bias errors were large in some areas of high precipitation, such as the ITCZ, and also in high latitudes during winter months (southern Australia and Tasmania).

Analysis of precipitation ETS showed that reanalyses generally outperformed satellite precipitation estimates in all subdomains, except for JJA in SEA, that is, the months affected by the Asia–Pacific monsoon (Fig. 4a) (Wang and LinHo 2002). This was expected because of the better capability of satellites to detect convective precipitation. The seasonal patterns observed in SAu are consistent with those reported by Ebert et al. (2007) and are attributed to the capabilities of reanalyses to capture synoptic precipitation (Fig. 4c). Reanalysis ETS in NAu outperformed satellite on an annual basis, and surprisingly, ERA-Interim was better than satellite precipitation during DJF and JJA. Ebert et al. (2007) attributed the better performance of reanalysis in NAu during JJA to remnant frontal systems brought in from midlatitudes or orographic lifting of moist ocean air during this season. Additional cause for better reanalysis performance in JJA and DJF may be due to the many grid cells in NAu close to SAu (Fig. 3a). Similar results

TABLE 1. Performance ranking of detection and accuracy metrics of precipitation products aggregated over the geographical domain, including means and standard deviations (in parentheses) of ETS, POD, FAR, FB, *r*, RMSD, and MPDR. Refer to section 2 for the definition of the metrics.

	Rank						
	1	2	3	4	5	6	7
ETS	Ensemble	JRA-25	Era-Interim	TRMM 3B42V6	NCEP–DOE	CMORPH	PERSIANN
	0.30 (±0.05)	0.29 (±0.05)	0.29 (±0.06)	0.27 (±0.05)	0.24 (±0.04)	0.23 (±0.06)	0.13 (±0.04)
POD	Ensemble	JRA-25	ERA-Interim	NCEP–DOE	TRMM 3B42V6	CMORPH	PERSIANN
	0.62 (±0.09)	0.62 (±0.09)	0.62 (±0.08)	0.55 (±0.07)	0.52 (±0.07)	0.49 (±0.08)	0.36 (±0.07)
FAR	ERA-Interim	Ensemble	TRMM 3B42V6	JRA-25	NCEP–DOE	CMORPH	PERSIANN
	0.40 (±0.06)	0.41 (±0.07)	0.41 (±0.09)	0.42 (±0.06)	0.42 (±0.07)	0.42 (±0.10)	0.54 (±0.09)
FB	Ensemble	TRMM 3B42V6	JRA-25	NCEP–DOE	PERSIANN	CMORPH	ERA-Interim
	0.09 (±0.46)	0.09 (±0.11)	0.13 (±0.14)	0.13 (±0.17)	0.22 (±0.23)	0.23 (±0.21)	0.25 (±0.33)
r	Ensemble	JRA-25	ERA-Interim	TRMM 3B42V6	CMORPH	PERSIANN	NCEP–DOE
	0.46 (±0.09)	0.43 (±0.08)	0.42 (±0.08)	0.41 (±0.09)	0.35 (±0.10)	0.22 (±0.23)	0.33 (±0.17)
RMSD	Ensemble	TRMM 3B42V6	ERA-Interim	JRA-25	CMORPH	PERSIANN	NCEP–DOE
	6.43 (±1.3)	6.56 (±1.6)	6.60 (±1.6)	6.62 (±0.08)	6.68 (±0.10)	7.54 (±1.6)	10.7 (±2.5)
MPDR	CMORPH	ERA-Interim	Ensemble	JRA-25	PERSIANN	TRMM 3B42V6	NCEP–DOE
	−1.3 (±12.2)	−3.0 (±8.10)	−4.9 (±7.98)	5.33 (±10.90)	−7.80 (±11.8)	10.2 (±6.97)	42.8 (±13.3)

to those of ETS were observed for *r*, where the ensemble showed an equal or superior performance. Its ETS values were between both types of products because of the lower POD of satellite products especially during winter months (Tian et al. 2009). RMSD was similar for all products, with the exception of NCEP–DOE, which had a higher RMSD (particularly in NAu and SEA). NCEP–DOE also had higher positive MPDR than the other products. Large positive precipitation biases in the tropics have been reported for NCEP–DOE in other studies as well (Fekete et al. 2004; Bosilovich et al. 2008; Getirana et al. 2011). Surprisingly, although gauge-scaled, TRMM had systematically higher MPDR values in all geographical domains, and its RMSD was comparable to that of other satellite products. It has been argued that monthly scaling can propagate errors over space and time and that these may be reflected in RMSD (Gao and Liu 2012). In addition, a climatological undercatch correction is applied to TRMM (Huffman et al. 2007; Su et al. 2008), which is not present in precipitation analysis used for evaluation herein. Satellite product precipitation under or overestimation appeared to be location dependent (e.g., Ebert et al. 2007; Nesbitt et al. 2008; Romilly and Gebremichael 2011; Vernimmen et al. 2012), even for the gauge-scaled TRMM 3B42V6 product (Nair et al. 2009; Stampoulis and Anagnostou; 2012). Demaria et al. (2011) found that there was no clear gain of TRMM 3B42V6 over satellite products that are not bias corrected for precipitation exceeding 30 mm day^{-1}. They also showed that TRMM 3B42V6 would not necessarily improve estimates in areas with sparse gauges or if scaling introduces gauge data noise. Furthermore, because of data provider policies, it is not possible to know if some of the gauges used to calibrate TRMM 3B42V6 are also part of the analysis data used here (Scheel et al. 2011).

Over all months combined and over the whole geographical domain, reanalysis outperformed satellite data on detection metrics and agreement metrics. Our results did, however, confirm the strength of satellite data in detecting and estimating convective precipitation.

By combining reanalyses and satellite products in an ensemble, known strengths of both retrieval systems resulted in a reduction of system-specific and random errors (e.g., Bosilovich et al. 2009). Issues associated with simple averaging of the products, such as a large bias in precipitation area and a corresponding reduction in mean and maximum precipitation depth (Ebert 2001), were addressed using a procedure that adjusts the probability distribution of the ensemble to the observed precipitation depth frequency. Although the depth-frequency-adjusted ensemble is not fully independent of the evaluation data, our results provide strong evidence that the inclusion of gauge information is valuable by adjusting both high and low precipitation depths. The dependence was limited, since the adjustment was performed over the whole geographical domain rather than by region or even by grid cell. An adjustment by subdomain or climate type could well improve estimates even further.

Acknowledgments. The authors gratefully acknowledge funding from the National Water Commission and Microsoft Research. We are also grateful for the assistance and/or correspondence to the providers of satellite and reanalyses data. Tim Raupach from CSIRO Land and Water and Beth Ebert from the Bureau of Meteorology are also thanked for reviewing the manuscript and for

providing valuable comments and suggestions. Tim also provided formatted Australian gauge and satellite data later used in this study.

REFERENCES

Adler, R. F., G. Gu, and G. J. Huffman, 2012: Estimating Climatological bias errors for the Global Precipitation Climatology Project (GPCP). *J. Appl. Meteor. Climatol.,* **51,** 84–99.

Behrangi, A., B. Khakbaz, T. C. Jaw, A. AghaKouchak, K. Hsu, and S. Sorooshian, 2011: Hydrologic evaluation of satellite precipitation products over a mid-size basin. *J. Hydrol.,* **397,** 225–237.

Betts, A. K., M. Zhao, P. A. Dirmeyer, and A. C. M. Beljaars, 2006: Comparison of ERA40 and NCEP/DOE near-surface data sets with other ISLSCP-II data sets. *J. Geophys. Res.,* **111,** D22S04, doi:10.1029/2006JD007174.

——, M. Kohler, and Y. C. Zhang, 2009: Comparison of river basin hydrometeorology in ERA-Interim and ERA-40 reanalyses with observations. *J. Geophys. Res.,* **114,** D02101, doi:10.1029/2008JD010761.

Bosilovich, M. G., J. Y. Chen, F. R. Robertson, and R. F. Adler, 2008: Evaluation of global precipitation in reanalyses. *J. Appl. Meteor. Climatol.,* **47,** 2279–2299.

——, D. Mocko, J. O. Roads, and A. Ruane, 2009: A multimodel analysis for the Coordinated Enhanced Observing Period (CEOP). *J. Hydrometeor.,* **10,** 912–934.

Dedong, L., Y. Zhongbo, H. Zhenchun, Y. Chuanguo, and J. Qin, 2007: Groundwater simulation in the Yangtze River basin with a coupled climate-hydrologic model. *J. China Univ. Geosci.,* **18,** 155–157.

Dee, D. P., and Coauthors, 2011: The ERA-Interim reanalysis: configuration and performance of the data assimilation system. *Quart. J. Roy. Meteor. Soc.,* **137,** 553–597.

Demaria, E. M. C., D. A. Rodriguez, E. E. Ebert, P. Salio, F. Su, and J. B. Valdes, 2011: Evaluation of mesoscale convective systems in South America using multiple satellite products and an object-based approach. *J. Geophys. Res.,* **116,** D08103, doi:10.1029/2010JD015157.

Ebert, E. E., 2001: Ability of a poor man's ensemble to predict the probability and distribution of precipitation. *Mon. Wea. Rev.,* **129,** 2461–2480.

——, J. E. Janowiak, and C. Kidd, 2007: Comparison of near-real-time precipitation estimates from satellite observations and numerical models. *Bull. Amer. Meteor. Soc.,* **88,** 1–47.

Fekete, B. M., C. J. Vorosmarty, J. O. Roads, and C. J. Willmott, 2004: Uncertainties in precipitation and their impacts on runoff estimates. *J. Climate,* **17,** 294–304.

Fernandes, K., R. Fu, and A. K. Betts, 2008: How well does the ERA40 surface water budget compare to observations in the Amazon River basin? *J. Geophys. Res.,* **113,** D11117, doi:10.1029/2007JD009220.

Gao, Y. C., and M. F. Liu, 2012: Evaluation of high-resolution satellite precipitation products using rain gauge observations over Tibetan Plateau. *Hydrol. Earth Syst. Sci. Discuss.,* **9,** 9503–9532.

Getirana, A. C. V., J. C. V. Espinoza, J. Ronchail, and O. C. Rotunno Filho, 2011: Assessment of different precipitation data-sets and their impacts on the water balance of the Negro River basin. *J. Hydrol.,* **404,** 304–322.

Gottschalck, J., J. Meng, M. Rodell, and P. Houser, 2005: Analysis of multiple precipitation products and preliminary assessment of their impact on global land data assimilation system land surface states. *J. Hydrometeor.,* **6,** 573–598.

Huffman, G. J., and Coauthors, 2007: The TRMM multisatellite precipitation analysis (TMPA): Quasi-global, multiyear, combined-sensor precipitation estimates at fine scales. *J. Hydrometeor.,* **8,** 38–55.

Jeffrey, S. J., J. O. Carter, K. B. Moodie, and A. R. Beswick, 2001: Using spatial interpolation to construct a comprehensive archive of Australian climate data. *Environ. Model. Software,* **16,** 309–330.

Joyce, R. J., J. E. Janowiak, P. A. Arkin, and P. P. Xie, 2004: CMORPH: A method that produces global precipitation estimates from passive microwave and infrared data at high spatial and temporal resolution. *J. Hydrometeor.,* **5,** 487–503.

Kanamitsu, M., W. Ebisuzaki, J. Woollen, S. K. Yang, J. J. Hnilo, M. Fiorino, and G. L. Potter, 2002: NCEP-DOE AMIP-II reanalysis (R-2). *Bull. Amer. Meteor. Soc.,* **83,** 1631–1643.

Khan, S. I., and Coauthors, 2012: Microwave satellite data for hydrologic modeling in ungauged basins. *IEEE Geosci. Remote Sens. Lett.,* **9,** 663–667.

Li, J., X. Gao, and S. Sorooshian, 2008: Model performance of downscaling 1999–2004 hydrometeorological fields to the upper Rio Grande Basin using different forcing datasets. *J. Hydrometeor.,* **9,** 677–694.

Miguez-Macho, G., and Y. Fan, 2012: The role of groundwater in the Amazon water cycle: 1. Influence on seasonal streamflow, flooding and wetlands. *J. Geophys. Res.,* **117,** D15113, doi:10.1029/2012JD017539.

Nair, S., G. Srinivasan, and R. Nemani, 2009: Evaluation of multi-satellite TRMM derived rainfall estimates over a western state of India. *J. Meteor. Soc. Japan,* **87,** 927–939.

Nesbitt, S. W., D. J. Gochis, and T. J. Lang, 2008: The diurnal cycle of clouds and precipitation along the Sierra Madre Occidental observed during NAME-2004: Implications for warm season precipitation estimation in complex terrain. *J. Hydrometeor.,* **9,** 728–743.

Onogi, K., and Coauthors, 2007: The JRA-25 reanalysis. *J. Meteor. Soc. Japan,* **85,** 369–432.

Pan, M., H. B. Li, and E. Wood, 2010: Assessing the skill of satellite-based precipitation estimates in hydrologic applications. *Water Resour. Res.,* **46,** W09535.

Romilly, T. G., and M. Gebremichael, 2011: Evaluation of satellite rainfall estimates over Ethiopian river basins. *Hydrol. Earth Syst. Sci.,* **15,** 1505–1514.

Ruane, A. C., and J. O. Roads, 2007: 6-hour to 1-year variance of five global precipitation sets. *Earth Interact.,* **11.** [Available online at http://EarthInteractions.org.]

Sapiano, M. R. P., and P. A. Arkin, 2009: An intercomparison and validation of high-resolution satellite precipitation estimates with 3-hourly gauge data. *J. Hydrometeor.,* **10,** 149–166.

Scheel, M. L. M., M. Rohrer, C. Huggel, D. S. Villar, E. Silvestre, and G. J. Huffman, 2011: Evaluation of TRMM Multi-satellite Precipitation Analysis (TMPA) performance in the central Andes region and its dependency on spatial and temporal resolution. *Hydrol. Earth Syst. Sci.,* **15,** 8545–8586.

Shrestha, M. S., G. A. Artan, S. R. Bajracharya, and R. R. Sharma, 2008: Using satellite-based rainfall estimates for streamflow modelling: Bagmati Basin. *J. Flood Risk Manage.,* **1,** 89–99.

Sorooshian, S., K. L. Hsu, X. Gao, H. V. Gupta, B. Imam, and D. Braithwaite, 2000: Evaluation of PERSIANN system satellite-based estimates of tropical rainfall. *Bull. Amer. Meteor. Soc.,* **81,** 2035–2046.

Stampoulis, D., and E. N. Anagnostou, 2012: Evaluation of global satellite rainfall products over continental Europe. *J. Hydrometeor.,* **13,** 588–603.

Su, F., Y. Hong, and D. P. Lettenmaier, 2008: Evaluation of TRMM Multisatellite Precipitation Analysis (TMPA) and its utility in hydrologic prediction in the La Plata Basin. *J. Hydrometeor.,* **9,** 622–640.

Tian, Y. D., and C. D. Peters-Lidard, 2010: A global map of uncertainties in satellite-based precipitation measurements. *Geophys. Res. Lett.,* **37,** L24407, doi:10.1029/2010GL046008.

——, and Coauthors, 2009: Component analysis of errors in satellite-based precipitation estimates. *J. Geophys. Res.,* **114,** D24101, doi:10.1029/2009JD011949.

Uppala, S., A. Simmons, D. Dee, P. Kallberg, and J. N. Thepaut, 2007: Atmospheric reanalyses and climate variations. *Climate Variability and Extremes During the Past 100 Years,* S. Brönnimann et al., Eds., Advances in Global Change Research, Vol. 33, Springer, 103–117.

Van Dijk, A. I. J. M., and L. J. Renzullo, 2011: Water resource monitoring systems and the role of satellite observations. *Hydrol. Earth Syst. Sci.,* **15,** 39–55.

Vernimmen, R. R. E., A. Hooijer, E. Mamenun, Aldrian, and A. I. J. M. van Dijk, 2012: Evaluation and bias correction of satellite rainfall data for drought monitoring in Indonesia. *Hydrol. Earth Syst. Sci.,* **16,** 133–146.

Vila, D., R. Ferraro, and H. Semunegus, 2010: Improved global rainfall retrieval using the Special Sensor Microwave Imager (SSM/I). *J. Appl. Meteor. Climatol.,* **49,** 1032–1043.

Voisin, N., A. W. Wood, and D. P. Lettenmaier, 2008: Evaluation of precipitation products for global hydrological prediction. *J. Hydrometeor.,* **9,** 388–407.

Wang, B., and LinHo, 2002: Rainy season of the Asian–Pacific summer monsoon. *J. Climate,* **15,** 386–398.

Yatagai, A., K. Kamiguchi, O. Arakawa, A. Hamada, N. Yasutomi, and A. Kitoh, 2012: APHRODITE: Constructing a long-term daily gridded precipitation dataset for Asia based on a dense network of rain gauges. *Bull. Amer. Meteor. Soc.,* **93,** 1401–1415.

Yong, B., Y. Hong, L.-L. Ren, J. J. Gourley, G. J. Huffman, X. Chen, W. Wang, and S. I. Khan, 2012: Assessment of evolving TRMM-based multisatellite real-time precipitation estimation methods and their impacts on hydrologic prediction in a high latitude basin. *J. Geophys. Res.,* **117,** D09108, doi:10.1029/2011JD017069.

Appendix D - Other simulated processes in W3RA-LUM

This appendix provides a detailed description of some of the remaining processes and corresponding equations that were not included in the main body of the chapter. These were not modified as part of the implementation of W3RA-LUM and the description is taken from Van Dijk (2010a). Most of the equations used for the energy balance and to obtain potential evapotranspiration (E_0) are sourced from the published literature and are based on well-established theory and estimation methods (with few exceptions). Their inclusion here will unnecessarily extend the length of the Appendix due to the many variables, constants and intermediate equations. Appendix D1 describes the remaining components of the soil water balance. Appendix D2 details the vapour fluxes. Finally, Appendix D3 describes the vegetation phenology processes, *i.e.,* canopy changes related to water availability. The reader is referred to Van Dijk (2010a) for the description of the energy balance.

D1. Soil water balance

D1.1 Root water uptake (*U*)

Total root water uptake (U) equals total transpiration E_t (see Appendix D2.2). E_t is assumed to originate preferentially from roots that experience the lowest matrix potential difference with the surrounding soil, and is limited by the maximum root water uptake from each layer (see Appendix D2.4).

$$U_S = \min\left[S_S, \left(\frac{U_{S\max}}{U_{S\max} + U_{D\max}} \right) U \right], \qquad \text{D-1}$$

and

$$U_D = \min\left[S_D, \left(\frac{U_{D\max}}{U_{S\max} + U_{D\max}} \right) U \right], \qquad \text{D-2}$$

where S_D is deep soil water storage (mm), S_S is shallow soil water storage (mm), U is total actual root water uptake (mm d^{-1}), U_D is actual root water uptake from deep soil (mm d^{-1}), $U_{D\,max}$ is maximum root water uptake from deep soil (mm d^{-1}), U_S is actual root water uptake from shallow soil (mm d^{-1}), U_{Smax} is maximum root water uptake from shallow soil (mm d^{-1}).

D1.2 Capillary rise (*Y*)

Capillary rise accounts for upward water movement between the groundwater storage and the deep soil storage due to water extraction in the root zone. In the absence of influx from the overlying soil layer, and in the presence of a groundwater table sufficiently nearby, water extraction in the root zone will disrupt the equilibrium soil moisture profile, causing groundwater to move into the unsaturated zone to restore equilibrium. This process may be important to sustain transpiration from deep-rooted evergreen vegetation in areas with seasonal precipitation. The water exchange would depend on: depth of water uptake, depth to the groundwater table and hydraulic conductivity in the unsaturated zone between roots and groundwater table. These properties are seldom known. A simple conceptualisation describes two extreme and intermediate situations depending on the connectivity between soil and groundwater (F_{DG}). If F_{DG} is equal to unity (strong connection), water from the deep soil store is immediately replaced by groundwater. If F_{DG} is equal to zero (no connectivity) the deep soil store is only replenished by drainage form the shallow soil store. For values in between zero and unity, capillary rise occurs but does not re-establish the equilibrium profile. Capillary rise is not estimated for the HRU with shallow rooted vegetation since there is no root water uptake from the deep soil store.

$$Y = F_{DG}\left(w_{\lim D} - w_D\right)S_g\,, \qquad \text{if } w_D < w_{limD} \qquad \text{D-3}$$

$$Y = 0\,. \qquad \text{if } w_D \geq w_{limD} \qquad \text{D-4}$$

Where Y capillary rise of groundwater into deeper root zone (mm), w_D is relative deep root zone water content (dimensionless) and S_g is groundwater reservoir storage (mm).

The parameter F_{DG} interacts with the choice of maximum deep root water uptake rate (Appendix D1.1). As a default, it is assumed that the groundwater table is sufficiently close so that root water uptake from the deep soil layer can be replaced by capillary rise and therefore F_{DG} may be prescribed a value of unity.

D1.3 Streamflow (Q_{stream})

Total streamflow discharge is estimated similarly to groundwater discharge using a linear reservoir. The aims of this conceptualisation is to delay storm flow drainage normally observed in all but small and fast-responsive catchments; and provide a transient storage of surface water in the landscape subjected to open water evaporation (see Appendix D2.7).

$$Q_{stream} = [1 - \exp(-K_r)]S_r \,, \qquad \text{D-5}$$

where Q_{stream} is streamflow discharge from catchment (mm d^{-1}) and S_r is the aggregate depth of storage in freely draining surface water stores (mm).

The streamflow drainage coefficient (K_r) was estimated using streamflow from 260 Australian catchments, the average value was 0.77 and 805 of values were between 0.5 and 1.1. (Van Dijk, 2010c). It was related to potential *ET* (E_0) as follows:

$$K_r = 0.141E_0 + 0.284 \qquad \text{D-6}$$

This relationship explained 23% of the variance in K_r. The relationship suggests that storm flow in drier catchments travels faster than in wet catchments, which is related to storm flow produced via infiltration excess overland flow typical of drier catchments.

Groundwater discharge (baseflow) is routed through this store before being converted into streamflow. Therefore, groundwater discharge recession is not exactly equal to the baseflow recession; nor is streamflow recession exactly equal to storm flow recession. The numerical difference will normally be negligible, because K_g and K_r will vary an order of magnitude or more, and because the delayed drainage of one days' baseflow is compensated by the delayed drainage from the day before (Van Dijk, 2010c).

D2. Vapour fluxes

D2.1 Mass balance

Total evapotranspiration *E* is given by:

$$E = E_t + E_e = E_i + E_t + E_s + E_g + E_r \,, \qquad \text{D-7}$$

where E_t is transpiration and E_e is evaporation from all other sources, consisting of soil evaporation (E_S), groundwater evaporation (E_g, that is, evaporation from soil saturated by groundwater), open water evaporation (E_r), and rainfall interception evaporation (E_i).

Transpiration (E_t) is calculated in two steps: (1) maximum transpiration (E_{t0}; defined as the transpiration rate that would be achieved with unlimited root water supply) and maximum root water uptake (U_0) from all layers are estimated; (2) actual evapotranspiration (E_t) is estimated as the lesser of the two. In formula:

$$E_t = \min\left[E_{t0}, U_0\right] \qquad \text{D-8}$$

Consistency between the sum of E_t and E_e (minus E_i) versus maximum available energy (by potential evapotranspiration, E_0) is ensured by calculating the energy available for evaporative fluxes ($E_{0'}$) as:

$$E_{0'} = E_0 - E_t \qquad \text{D-9}$$

This formulation still allows total *E* to exceed E_0 for days with precipitation; this is deliberate (see Appendix D2.2). The equations used to estimate the constituent fluxes are explained below.

D2.2 Rainfall interception (E_i)

The approach to model rainfall interception losses is based on the Gash (1979) model, with modifications to allow applications to vegetation with sparse canopy (Gash *et al.*, 1995; Van Dijk and Bruijnzeel, 2001). An important assumption is that the ratio of wet canopy evaporation rate and rainfall intensity does not vary between storms. It is also assumed that the rate is proportional to the fraction of canopy cover.

$$E_i = f_V P_g , \qquad \text{for } P < P_{wet} \qquad \text{D-10}$$

$$E_i = f_V P_{wet} + f_{ER}\left(P - P_{wet}\right), \qquad \text{for } P \geq P_{wet} \qquad \text{D-11}$$

with

$$P_{wet} = -\ln\left(1 - \frac{f_{ER}}{f_V}\right)\frac{S_V}{f_{ER}} , \qquad \text{D-12}$$

$$S_V = s_{leaf}\Lambda \qquad \text{D-13}$$

$$f_{ER} = f_V F_{ER0} \qquad \text{D-14}$$

where f_{ER} is the ratio of average evaporation rate over average rainfall intensity during storms (dimensionless), f_V is the fraction area covered by intercepting leaves (dimensionless), P_g is gross precipitation (mm), P_{wet} is reference threshold rainfall amount at the canopy is wet (mm), S_v is canopy rainfall storage capacity (mm) and Λ is leaf area index (dimensionless).

The specific relative evaporation rate (f_{ER0}, dimensionless) can be estimated by the inversion of Gash-type models, which produce ratios of 0.05 to 0.25 with values around 0.2 being common (*e.g.* reviews by Gash *et al.*, 1995; Van Dijk and Bruijnzeel, 2001). Values for f_{ER0} of 0.05 and 0.10 are used here as defaults for shallow- and deep-rooted vegetation, as these are assumed by and large equivalent with aerodynamically smooth and rough vegetation, respectively. Values for the specific canopy rainfall storage capacity per unit leaf area parameter (s_{leaf}, in mm) can be calculated from literature and are 0.07–0.6 mm per unit LAI for most forests types, and

0.03–0.9 mm for low vegetation (*e.g.* review Van Dijk and Bruijnzeel, 2001). Most reported values are around 0.10 mm and this is therefore used as a default value for both HRUs.

D2.3 Maximum transpiration (E_{t0})

Maximum transpiration (E_0) is in accordance with a modified Penman-Monteith equation (Van Dijk, 2010a).

$$E_{t0} = f_t E_0 = E_0 \Big/ \left[1 + \left(\frac{k_\varepsilon}{1+k_\varepsilon} \right) \frac{g_a}{g_s} \right], \qquad \text{D-15}$$

with

$$f_t = \left[1 + \left(\frac{k_\varepsilon}{1+k_\varepsilon} \right) \frac{g_a}{g_s} \right]^{-1} \quad , \qquad \text{D-16}$$

and

$$g_s = f_V G_{s\max} \, . \qquad \text{D-17}$$

where E_{t0} is maximum transpiration (mm d^{-1}), E_0 potential evapotranspiration (mm d^{-1}), f_t is potential transpiration fraction (dimensionless), f_V is fraction canopy cover (dimensionless), g_a is aerodynamic conductance (m s^{-1}), g_s canopy conductance (m s^{-1}), k_ε is a coefficient that determines evaporation efficiency (dimensionless) and is Λ leaf area index (dimensionless). Aerodynamic conductance ($g_{a)}$ is estimated using the well-established approach of Thom (1975) as a function of wind speed and a roughness coefficient for use with wind measurements at 2 m inside climate stations. For a closed canopy, g_s can be thought of as a function of maximum surface conductance (G_{smax} in ms^{-1}) and a scaling factor (between zero and unity) that describes the reduction in surface conductance as a consequence of stomatal control. Various alternative formulations have been developed to describe stomatal control as a function of ambient conditions inside the vegetation, the air around the vegetation and/or the soil water status. However many of these formulations were based on interpretation of real world, small scale experiments where correlation between potential driving factors is inevitable, due to the diurnal cycles in many atmospheric and plant physiological variables; correlation between soil water

availability and atmospheric humidity; and surface-atmosphere feedback effects (*e.g.* Jarvis and McNaughton, 1986; Jones, 1998). Surface conductance g_s is estimated at 15 mm s^{-1} for a FAO-56 reference grass cover (Allen *et al.*, 1998). Other studies typically find maximum g_s values of 10 to 20 mm s^{-1}, with values of more than 30 mm s^{-1} for agricultural crops (Kelliher *et al.*, 1995; Leuning *et al.*, 2008).

The parameter G_{smax} is the only parameter that needs to be estimated. Corresponding to functional convergence theory, it has been shown that there is correlation between canopy photosynthetic capacity, surface conductance, specific leaf area and other plant physiological properties (Reich *et al.*, 1997; 2003).

A satellite-based (from MODIS) specific photosynthetic capacity index (PCI, expressed per unit canopy cover) was calculated for Australia from the Enhanced Vegetation Index (EVI, Huete *et al.*, 2002) and absorbed fraction photosynthetically active radiation (FPAR, Knyazikhin *et al.*, 1998) as an estimate of fraction canopy cover f_V (van Dijk, 2010a). This produced values of 0.5–1.0 for humid tropical vegetation and greening inland grassland areas, whereas forests typically showed a PCI of 0.30-0.45. PCI values of 0.35 and 0.65 were used as estimates in the current model version for shallow-rooted and deep-rooted HRUs respectively. Comparing these with earlier mentioned G_{smax} values suggests that it may be estimated as:

$$G_{s\max} = 0.03PCI\,. \qquad \text{D-18}$$

D2.4 Maximum root water uptake (U_0)

The formulation used for maximum root water uptake (U_0, mm d^{-1}) assumes two important limitations to root water uptake: the effect of soil water availability in different layers; and that of root presence and hydraulic properties in different layers. The description used is very similar to other approaches to estimate the impact of soil water content on root water uptake (*e.g.* Shuttleworth, 1992). The approach used here was chosen due to the high complexity of root water uptake when considering the scale of modelling, the very high spatial variability in soil properties, soil moisture availability and vegetation rooting depth, and the differences in rooting pattern and physiology between plants of different species and age. Since a unique relationship

between matrix potential and water content is always assumed (that is, any hysteresis in the soil moisture retention or 'pF' curve is ignored), one can be expressed in terms of the other and the only difference will be in the exact shape of the limitation function. Given the uncertainty in the parameters, and given that it is unlikely that robust estimates of the parameters can be derived and therefore would need to be calibrated, a formulation with a minimum number of two additional parameters was conceptualised as follows:

$$U_0 = \max\left[U_{S0}, U_{D0}\right], \qquad \text{D-19}$$

with U_{Smax} and U_{Dmax} both estimated as:

$$U_{z0} = U_{z\max} \min\left(1, \frac{w_z}{w_{z\lim}}\right), \qquad \text{D-20}$$

U_{zmax} physiological maximum root water uptake from layer *z* (mm d^{-1}), U_{z0} is maximum root water uptake rates from layer *z* under ambient conditions (mm d^{-1}) and w_z relative water content of layer *z* (subscript '*z*' is to be replaced by '*s*' and '*d*', respectively). The maximum root water uptake U_{z0} would be expected to depend on the total length of fine roots, the flow resistance from roots to leaf, and the potential difference between plant and soil. There are currently no methods to estimate maximum uptake rates, but site water use observations by flux towers suggest that maximum daily transpiration rates do not normally seem to exceed around 6 mm d^{-1} and drop to a relatively constant 1 or 2 mm d^{-1} for deep rooted vegetation after seasonal vegetation has senesced. Values adopted here for U_{S0} were 6 mm d^{-1} for both HRUs, and U_{D0} of 4 mm d^{-1}, only applicable for the deep-rooted vegetation HRU. The water content w_{zlim} at which root water uptake is affected can be assumed to be between 0.15 and 0.50 based on available pedotransfer functions (see Rawls *et al.*, 1992). It was assumed as 0.3 for both soil layers and HRUs.

D2.5 Soil evaporation (E_s)

A model comparable to the formulation of used for root water uptake using one phase of soil dry down was used here. Generally, three stages are considered to describe soil evaporation: stages (*e.g.* Ritchie, 1972; Allen *et al.,* 2005): (1) evaporation from wet soil occurs at a rate that

is approximately equal to PET; (2) once soil wetness falls below a certain threshold, evaporation is reduced and becomes increasingly reduced as soil moisture decreases further; and (3) below a certain water content soil evaporation ceases altogether. Mutziger *et al.* (2005) did a global review of published data sets and found that this approach produced realistic soil evaporation estimates. However, where litter, vegetation or other forms of non-evaporating material cover part of the soil, they will intercept radiation energy as well as increase surface roughness, and so reduce evaporation from the underlying soil. In addition, plant root systems can facilitate the transfer of deeper soil moisture to shallow soil, particularly when the top soil is very dry, through hydraulic redistribution (Burgess *et al.*, 1998; Zou *et al.*, 2005). As a consequence, top soil moisture content under living vegetation is unlikely to fall much below wilting point. The model used here combines the second and third phase of soil dry down into a single phase. This is done partly for convenience and simplicity, and partly because capillary rise and hydraulic redistribution by vegetation may well prevent this third phase from being reached. The dry down curve resulting from this approach is similar to that produced by the FAO recommended method (Allen *et al.*, 2005) if average parameters reported by Mutziger *et al.* (2005) are used (not shown). The formulation is as follows:

$$E_s = \left(1 - f_{sat} - f_{water}\right) f_{sE} \left(E_0 - E_t\right), \qquad \text{D-21}$$

with

$$f_{sE} = F_{sE\max} \min\left\{1, \frac{w_0}{w_{0\lim}}\right\}. \qquad \text{D-22}$$

where E_0 is potential ET (mm d^{-1}), E_t is actual transpiration (mm d^{-1}), f_{sat} is fraction area covered by saturated soil (dimensionless), f_{water} is fraction area covered by open water (dimensionless), f_{sE} is relative soil evaporation (dimensionless) and w_0 is relative top soil water content (dimensionless). The parameter describing relative soil evaporation when soil water supply is not limiting (F_{sEmax}, dimensionless) is commonly assumed approximately equal or slightly higher than unity when E_0 is estimated as FAO crop reference ET (Allen *et al.,* 1998). A value less than unity would be expected where there is some vegetation cover, litter or other forms of surface cover that impedes energy to, or vapour fluxes from, the wet soil. A value of F_{sEmax}=0.7 is estimated as a default, but it should be noted that this value is without much experimental

support. Where rainfall occurs infrequently (*e.g.* arid environments), the assumed value is not expected to introduce bias, as the soil will have sufficient time to dry out between storms.

The relative top soil water content at which evaporation is reduced (w_{0lim}, dimensionless) may be expected to be somewhat higher than that at which root water uptake stops. Indeed, from the five studies reviewed by Mutziger *et al.* (2005), w_{0lim} values of 0.60 to 0.89 can be calculated, with a median of 0.84. A default value of w_{0lim}=0.85 is suggested here.

D2.6 Groundwater evaporation (E_g)

The model used here is the same as that used for unsaturated soil evaporation for the condition that w=1.

$$E_g = f_{sat} F_{sE\max}\left(E_0 - E_T\right), \qquad \text{D-23}$$

where E_g is groundwater evaporation (mm d^{-1}), $E_{0\ is}$ potential ET (mm d^{-1}), is E_t actual transpiration (mm d^{-1}) and f_{sat} is the fraction of area covered by saturated soil (dimensionless). The soil evaporation scaling factor when soil water supply is not limiting evaporation (F_{sEmax}, dimensionless) has the same meaning as that used for unsaturated soil evaporation and the same default value is suggested.

D2.7 Open water evaporation (E_r)

The model formulation used is consistent with those used for the other evaporation components.

$$E_r = f_{water} F_{ow}\left(E_0 - E_T\right), \qquad \text{D-24}$$

with

$$f_{water} = \min\left(F_{bankfull}, 0.007 {S_r}^{0.75}\right), \qquad \text{D-25}$$

where E_r *is the* surface water evaporation (mm d^{-1}), E_0 is potential ET (mm d^{-1}), E_t is actual transpiration (mm d^{-1}), f_{water} is fraction of area covered by water (dimensionless) and S_r is streamflow storage (mm)

The value of f_{water} would be expected to change dynamically in response to the volume of water stored in surface water bodies. There are currently no accurate predictive models available, and it may be expected that any relationship would vary between landscapes with different drainage network morphology. Based on studies of small and large, natural and man-made reservoirs (*e.g.* Lowe *et al.*, 2005) as well as geometric considerations, the exponent of the empirical equation may be estimated to be between 0.5 and 1.0; a value of 0.75 is estimated based on the work by Lowe *et al.* (2005) for hillside farm dams and used as a default value. Based on the same study a value of 0.007 mm^{-1} was estimated for the coefficient (that is, f_{water}=0.7% of the landscape for S_r=1 mm).

The fraction of area occupied by river channels ($F_{bankfull}$) is unknown, but is estimated here as 0.5% of the landscape. The open water evaporation coefficient F_{0w} is assumed to be equal to the conversion factor between potential evaporation and pan evaporation, which is usually estimated at 0.70 and is used as default here.

D3. Vegetation phenology

The vegetation phenology model simulates canopy changes in response to water availability by calculating the vegetation cover that could be sustained given soil moisture availability. The 'equilibrium' leaf mass is estimated by considering the hypothetical leaf mass M_{eq} that corresponds with a situation in which maximum transpiration rate ($E_{t,max}$) equals maximum root water uptake (U_{max}). The vegetation moves towards this equilibrium state with a prescribed degree of inertia, representative of alternative phenological strategies.

The model can include one or more land cover types, each defined by their fractional cover and properties. Currently, two land cover types are considered: deep- and shallow-rooted vegetation. It is assumed, compared to shallow-rooted vegetation, deep-rooted vegetation has a longer leaf life span, responds less rapidly to changes in water availability, and has lower

photosynthetic capacity and stomatal conductance per unit leaf area. These expectations can be derived from functional convergence theory and agrees with observed relationships (Reich *et al.*, 1997; Wright *et al.*, 2004). Only the effects of water availability on vegetation phenology are considered in the current model version, since they will have the greatest influence on hydrological processes. However, other processes may regionally be more important in driving vegetation phenology, in particular in the humid and high elevation regions where temperature and day length are important variables driving vegetation phenology. Other factors limiting growth such as nutrient availability and salinity may impose an upper limit on the vegetation density that can be sustained.

D3.1 Mass balance

.

$$M_L(t+1) = M_L(t) + m_{Ln}(t), \qquad \text{D-26}$$

where M_L is the biomass and m_{Ln} the net biomass change of living leaves (both expressed in kg dry matter per m^2). The coupling with water balance dynamics occurs through m_{Ln}.

D3.2 Conversion equations

$$f_V = 1 - \exp\left(-\frac{\Lambda}{\Lambda_{ref}}\right), \qquad \text{D-27}$$

with

$$\Lambda = M_L C_{SLA}, \qquad \text{D-28}$$

where f_V is canopy fractional cover and Λ is leaf area index. The conversion between M_L and Λ is strictly a dimensional one. It assumes that, by good approximation, the value of the coefficient of proportionality that is specific leaf area (C_{SLA} in m^2 kg^{-1}) does not vary significantly over time for a particular vegetation type. This is a common assumption but obviously a simplification. The conversion from Λ to f_V is described by the exponential light extinction equation (Monsi and Saeki, 1953) equivalent to Beer's Law which is most commonly used for this purpose. to be consistent with notation elsewhere in the model, the so-called 'light extinction coefficient' (often

symbolised by κ) is not used but its inverse value Λ_{ref}, which represents a reference LAI at which fraction cover is 0.632. Use of the Monsi-Saeki model assumes that reference LAI (or κ) does not change over time, which is a necessary simplification. It should be noted that Λ_{ref} is a function of wavelength, leaf angle distribution and light incidence angle, or angle distribution in the case of diffuse radiation. Because f_V is primarily used to estimate light interception integrated over the day, Λ_{ref} is also best interpreted as a radiation-weighted effective value.

Globally reported values of C_{SLA} vary by two orders of magnitude, from 0.7 to 71 m^2 kg^{-1} (Wright *et al.*, 2004). Values from 1.5 to 9 m^2 kg^{-1} have been found for Australian Eucalypt species with an average value of 3 m^2 kg^{-1} (Schulze *et al.*, 2006). This value is used for the deep-rooted vegetation HRU. Grasses have thinner leaves so consequently higher C_{SLA}, an average value of 10 3 m^2 kg^{-1} was used for the shallow-rooted vegetation HRU.

Literature reported Λ_{ref} values are usually in the range of 1.3 to 2.5 (κ =0.4–0.8). Higher Λ_{ref} values correspond with more vertical leaf angles; for Eucalypt forests, values of 1.8 to 2.0 (κ=0.50–0.55) are commonly estimated, whereas values as high as 4.2–7.1 (κ=0.14-0.24) have been estimated for zenith incidence angles (Macfarlane *et al.*, 2007). Values of Λ_{ref} were derived directly from MODIS satellite LAI and FPAR products, if it is assumed that FPAR is a good approximation of canopy cover f_V. For areas with high persistent FPAR (equivalent to forest vegetation) an average Λ_{ref} value of 2.5 (κ=0.40) was calculated, whereas for areas with low persistent FPAR a Λ_{ref} =1.4 (κ=0.70) is derived. These values were used for respectively deep-rooted and shallow-rooted vegetation in the model. A caveat is that these results will be influenced, but to an unknown degree, by spurious influences from the assumptions and observations used in the derivation of the products.

D3.3 Net leaf biomass (m_{Ln})

A new formulation was developed to estimate net leaf biomass (m_{Ln}) , because literature review did not suggest a suitably simple model that predicts water-related vegetation phenology. It is based on the assumption that vegetation is able to adjusts is leaf biomass at a rate that is independent of the amount of existing leaf biomass and energy or biomass embodied in other plant organs. The approach shows good performance for dynamic, typically shallow-rooted,

vegetation in seasonally dry environments. As would be expected, its predictive performance is lesser for deep rooted vegetation, particularly in areas where temperature or radiation and not water are the most growth limiting resource.

$$m_{Ln} = \frac{M_{Leq} - M_L}{t_{grow}}, \qquad \text{if } M_{Leq} \geq M \qquad \text{D-29}$$

$$m_{Ln} = \frac{M_{Leq} - M_L}{t_{senesence}} \qquad \text{if } M_{Leq} < M \qquad \text{D-30}$$

where M_{Ln} is net leaf biomass change (kg m^{-2} d^{-1}), M_{Leq} is equilibrium dry leaf biomass given water availability and atmospheric demand (kg m^{-2}) and M_L is dry leaf biomass (kg m^{-2}). There is little information available in the literature to estimate the characteristic time scale for vegetation growth towards equilibrium ($t_{grow,}$ days) and characteristic time scale for vegetation senescence towards equilibrium ($t_{senesce}$, days) parameters. However, they can readily be calibrated to LAI patterns derived from remote sensing. Through visual estimation for around 30 sample locations across Australia, t_{growth} and $t_{senesce}$ were both estimated at 50 days for shallow-rooted vegetation, and 90 days for deep-rooted vegetation.

D3.4 Equilibrium leaf biomass (M_{Leq})

The approach adopted here is newly developed based on some simple assumptions. It follows from the principle of optimum resource use, which implies that leaf area will adjust - within the limits of plant physiology and resource availability - to bring transpiration rates in equilibrium with the capacity of the roots to draw water from the soil (U_{max}). The corresponding equilibrium fractional vegetation cover is defined by (see Appendix D2.2):

$$U_0 = f_t E_0 = \frac{E_0}{1 + \left(\frac{k_\varepsilon}{1 + k_\varepsilon}\right)\left(\frac{g_a}{f_{Veq} g_{s\max}}\right)}. \qquad \text{D-31}$$

The equilibrium dry leaf biomass given water availability and atmospheric demand is defined by:

$$M_{Leq} = -\ln\left(1 - f_{Veq}\right)\frac{\Lambda_{ref}}{C_{SLA}}, \qquad \text{D-32}$$

with

$$f_{Veq} = \frac{1}{\frac{E_0}{U_0} - 1}\left(\frac{k_\varepsilon}{1 + k_\varepsilon}\right)\frac{g_a}{G_{s\max}}, \text{ for } f_{Veq} < f_{Vmax} \qquad \text{D-33}$$

$$f_{Veq} = f_{V\max}, \qquad \text{D-34}$$

and

$$f_{V\max} = 1 - \exp\left(-\frac{\Lambda_{\max}}{\Lambda_{ref}}\right)$$

where E_0 is potential evapotranspiration (mm d^{-1}), f_V is fraction canopy cover (dimensionless), f_{Vmax} is maximum achievable canopy cover (dimensionless), g_a is aerodynamic conductance (m s^{-1}), g_s is canopy conductance (m s^{-1}), k_ε is a coefficient that determines evaporation efficiency (-dimensionless), M_{Ln} is net leaf biomass change (kg m^{-2} d^{-1}), M_{Leq} is equilibrium dry leaf biomass given water availability and atmospheric demand (kg m^{-2}) and U_0 is maximum root water uptake (mm d^{-1}).

Methods to estimate Λ_{ref} and G_{smax} are provided in Appendix D3.1 and Appendix D2.3 respectively.

The parameter Λ_{max} is introduced to replicate the limiting effect of maintenance respiration losses in the maximum leaf area that can be sustained. Maximum LAI values found in Australia generally appear to be less than 7 for eucalypt forests, although values of up to 10 have been reported for agricultural crops (Hill *et al.*, 2006). A value of Λ_{max}=8 is used as a default in the model. It is noted that this parameter will not normally have much influence on ET estimation, as water availability and growth rate will limit the LAI that can be achieved in water limited environments; whereas available energy rather than LAI will determine ET in energy-limited environments.

Appendix E - List of symbols

Roman symbols

CN	runoff curve number (-)
C_{SLA}	specific leaf area per unit dry leaf biomass (m^2 kg^{-1})
D_0	top soil water drainage (mm d^{-1})
D_d	deep soil water drainage (mm d^{-1})
D_g	ground water drainage (mm d^{-1})
D_s	shallow soil water drainage (mm d^{-1})
E_0	potential evapotranspiration (mm d^{-1})
E_e	combined evaporation (mm d^{-1})
E_g	groundwater evaporation (mm d^{-1})
E_i	interception evaporation (mm d^{-1})
E_r	surface water evaporation (mm d^{-1})
E_s	soil evaporation (mm d^{-1})
E_t	transpiration (mm d^{-1})
F_{dg}	factor describing connectivity between soil and groundwater (-)
F_{ER0}	average ratio of wet canopy evaporation rate and rainfall rate for full canopy cover (-)
$F_{loss,max}$	maximum fraction of daytime net radiation 'lost' to heat storage when there is no vegetation (-)
F_{OW}	open water evaporation scaling (-)
$F_{S,ref}$	reference soil cover fraction that determines the rate of decline in energy loss with increasing canopy cover (-)
f_{drain}	daily drainage fraction (-)
f_{ER}	estimated ratio of wet canopy evaporation rate and rainfall rate (-)
f_S	fraction uncovered surface (-)
f_{sat}	fraction area saturated (-)
f_{sE}	soil evaporation fraction (-)
f_{sEmax}	maximum soil evaporation fraction (-)
f_t	transpiration fraction (-)
f_V	vegetation canopy cover (-)
$f_{V,max}$	maximum achievable canopy cover (-)
f_{Veq}	equilibrium canopy cover (-)
f_{water}	fraction covered by water (-)
G_{smax}	maximum surface conductance for closed canopy (m s^{-1})
g_a	aerodynamic conductance (m s^{-1})
g_s	maximum surface conductance (m s^{-1})
H	catchment humidity
h	vegetation canopy height (m)
I	infiltration (mm d^{-1})
I_0	initial retention capacity (mm)
I_i	initial infiltration (mm)

I_a inital abstraction losses (mm)

K_{FC} daily drainage fraction field capacity (-)

K_g groundwater drainage coefficient (-)

K_r streamflow drainage coefficient (-)

k_ε coefficient determining the efficiency of energy use for evaporation (-)

M_L dry leaf biomass per unit area (kg m^{-2})

M_{Leq} equilibrium dry leaf biomass (kg m^{-2})

m_{Ln} net rate of change in leaf biomass per unit area (kg m^{-2} d^{-1})

P_g gross precipitation (mm d^{-1})

P_n net precipitation (mm d^{-1})

P_{wet} precipitation needed to saturate canopy (mm d^{-1})

p_{air} air pressure (Pa)

p_e vapour pressure (Pa)

p_{es} saturated vapour pressure (Pa)

Q streamflow (mm d^{-1})

Q_{CN} SCS-CN runoff (mm)

Q_R surface runoff (mm d^{-1})

R_{Lin} incoming longwave radiation (W m^{-2})

R_{loss} radiation energy 'lost' to heat storage and photosynthesis (W m^{-2})

R_{Lout} outgoing longwave radiation (W m^{-2})

R_n net radiation (W m^{-2})

R_{Sin} incoming shortwave radiation (W m^{-2})

R_{Sn} net shortwave radiation (W m^{-2})

R_{Ln} net longwave radiation (W m^{-2})

R_{Sout} outgoing shortwave radiation (W m^{-2})

S_0 top soil water storage (mm)

S_d deep soil water storage (mm)

S_{FC} soil water storage at field capacity ()

S_g groundwater storage (mm)

S_{Gref} reference groundwater storage for saturated fraction estimation (mm)

S_{max} potential soil maximum storage capacity (mm d^{-1})

S_r runoff storage (mm)

S_s shallow soil water storage (mm)

S_V canopy rainfall storage capacity (mm)

s_V canopy storage capacity per unit leaf area (mm)

S_{zFC} accessible soil water storage at field capacity of layer z (mm)

T_{a^*} effective air temperature (°C)

t_{grow} time constant determining rate of canopy increase (d)

$t_{senesce}$ time constant determining rate of canopy decrease (d)

U_0 maximum root water uptake (mm d^{-1})

U_{0z} maximum root water uptake from layer z (mm d^{-1})

U_z root water uptake from layer z (mm d^{-1})

w_{0lim} relative water content of top soil at which evaporation is reduced (-)

w_z relative wetness of layer z (-)

w_{zlim} relative water content of layer z at which root uptake is reduced (-)

$w_{\alpha,ref}$ reference value of w_0 describing the relationship between albedo and top soil wetness (-)

Y capillary rise, from groundwater to deep soil (mm d^{-1})

Greek symbols

β coefficient describing rate of hydraulic conductivity increase with water content (-)

Λ leaf area index (-)

Λ_{max} maximum achievable LAI (-)

Λ_{ref} reference LAI determining canopy cover (-)

Appendix F - Journal article

Van Dijk, A. I. J. M., **J. L. Peña-Arancibia** and L. A. Bruijnzeel (2012), Land cover and water yield: inference problems when comparing catchments with mixed land cover. Hydrology and Earth System Sciences, 16, 3461-3473.

Hydrol. Earth Syst. Sci., 16, 3461–3473, 2012
www.hydrol-earth-syst-sci.net/16/3461/2012/
doi:10.5194/hess-16-3461-2012

Hydrology and Earth System Sciences

Land cover and water yield: inference problems when comparing catchments with mixed land cover

A. I. J. M. van Dijk[1,2], **J. L. Peña-Arancibia**[2], **and L. A. (Sampurno) Bruijnzeel**[3]

[1]Fenner School for Environment & Society, Australian National University, Canberra, Australia
[2]CSIRO Land and Water, Canberra, Australia
[3]VU University, Amsterdam, The Netherlands

Correspondence to: A. I. J. M. van Dijk (albert.vandijk@anu.edu.au)

Received: 8 April 2011 – Published in Hydrol. Earth Syst. Sci. Discuss.: 26 April 2011
Revised: 10 July 2012 – Accepted: 2 September 2012 – Published: 26 September 2012

Abstract. Controlled experiments provide strong evidence that changing land cover (e.g. deforestation or afforestation) can affect mean catchment streamflow (Q). By contrast, a similarly strong influence has not been found in studies that interpret Q from multiple catchments with mixed land cover. One possible reason is that there are methodological issues with the way in which the Budyko framework was used in the latter type studies. We examined this using Q data observed in 278 Australian catchments and by making inferences from synthetic Q data simulated by a hydrological process model (the Australian Water Resources Assessment system Landscape model). The previous contrasting findings could be reproduced. In the synthetic experiment, the land cover influence was still present but not accurately detected with the Budyko- framework. Likely sources of interpretation bias demonstrated include: (i) noise in land cover, precipitation and Q data; (ii) additional catchment climate characteristics more important than land cover; and (iii) covariance between Q and catchment attributes. These methodological issues caution against the use of a Budyko framework to quantify a land cover influence in Q data from mixed land-cover catchments. Importantly, however, our findings do not rule out that there may also be physical processes that modify the influence of land cover in mixed land-cover catchments. Process model simulations suggested that lateral water redistribution between vegetation types and recirculation of intercepted rainfall may be important.

1 Introduction

1.1 Background

There is strong experimental evidence that changing land cover (e.g. deforestation or afforestation) can affect the local water balance. Such an influence has been detected at various scales, from site water balance and atmospheric water flux studies to small catchments undergoing change (see review by e.g. van Dijk and Keenan, 2007 and references therein). Controlled catchment experiments have demonstrated a change in mean catchment streamflow or (synonymously) water yield (Q) after land cover change (typically forest planting or logging; Bosch and Hewlett, 1982; Bruijnzeel, 1990, 2004; Andréassian, 2004; Brown et al., 2005; Farley et al., 2005). They appear to provide clear evidence that land cover characteristics affect Q, although this influence is moderated by a range of climate and catchment characteristics as well as vegetation attributes beyond broad land cover class alone (Andréassian, 2004; Bruijnzeel, 2004; van Dijk and Keenan, 2007). These conclusions could be corroborated by analysis of collated longer term Q estimates from multiple catchments, provided only catchments with (near complete) forest cover and herbaceous cover were selected (Holmes and Sinclair, 1986; Turner, 1991; Zhang et al., 1999, 2001). The collated data were still dominated by small experimental catchments, however, and such experiments are not without their challenges (discussed further on).

Subsequent studies have attempted to detect a similar land cover influence by statistically analysing Q from many catchments with mixed land cover. In such data sets, climate is the primary reason for variation in response and therefore

needs to be controlled for several studies do this by fitting an additive formulation of a Budyko model[1] (Budyko, 1974) that explicitly represents two (e.g. forest and herbaceous) or a small number of land cover types (Zhang et al., 2004; van Dijk et al., 2007; Oudin et al., 2008; Donohue et al., 2010; Peel et al., 2010). Such an approach has been described as a top-down analysis (sensu Klemeš, 1983; Sivapalan et al., 2003). In the following formula:

$$Q_j = \sum_i \mathrm{FC}_{i,j} f(P_j, P_j, w_i), \quad (1)$$

where Q_j, P_j, and PE_j are the long-term (e.g. > 10 yr) average Q, precipitation and potential evaporation[2] (in mm per time unit) for catchment j, $\mathrm{FC}_{i,j}$ is the fractional cover of land cover type i in catchment j, and w_i a dimensionless model parameter that characterises the hydrological behaviour of land cover class i and may be interpreted as a measure of the efficiency with which vegetation accesses and uses stored water. The influence of land cover is subsequently determined by finding the w_i values that minimise the root mean square error (RMSE) between observed and estimated Q, and interpreting the found parameter values. The cited studies performed such an analysis using collated data for 221 (Donohue et al., 2010) to 1508 (Oudin et al., 2008) catchments. They report either a much smaller land cover influence than found in controlled experiments (Zhang et al., 2004; van Dijk et al., 2007; Oudin et al., 2008; Donohue et al., 2010; Peel et al., 2010); no statistically significant influence (Zhang et al., 2004; van Dijk et al., 2007; Oudin et al., 2008; Peel et al., 2010); or even an influence opposite to that which might be anticipated – at least for some land cover classes (Oudin et al., 2008; Peel et al., 2010) or climate types (van Dijk et al., 2007; Peel et al., 2010).

It might seem surprising that land cover change would have a marked effect on the water balance of a catchment when it has homogeneous land cover, but not when it has mixed land cover. Some possible physical and methodological causes have been suggested. Physical explanations include:

1. *Catchment size.* The nature of controlled experiments puts a limit to the size of catchments that can be manipulated and the majority of experiments have been carried out on catchments smaller than 1 km^2 (see e.g. tabulated data in Andréassian, 2004; Brown et al., 2005). Conversely, data sets of real-world catchments with mixed land cover tend to have average catchment sizes in the order of hundreds to thousands km^2 (see respective studies listed earlier). A known issue with small catchments is the risk of ungauged subterranean transfers (e.g. Bruijnzeel, 1990), which could lead to overestimation of the influence of land cover change on Q. Conversely, while land surface-atmosphere feedbacks perhaps can safely be ignored for small catchments, that may not be the case for large catchments, where land cover certainly influences overall evaporative energy and may even modulate precipitation (for discussion see Donohue et al., 2007; van Dijk and Keenan, 2007).

2. *Catchment hydrological processes.* As catchment experiments require small and well defined watersheds, they may be expected to have greater relief in comparison to larger catchments. Greater relief may mean shallower soils, less infiltration and therefore more storm flow, a more efficient surface drainage network, and lesser evaporation losses from streams, wetlands and groundwater-using vegetation (van Dijk et al., 2007).

3. *Land cover characteristics*. Experimental catchments may be expected to have a more idealised and homogenous vegetation cover and fewer activities and structures designed to reduce storm runoff. In afforestation studies, the selection of suitable catchments may have created a bias towards low-complexity land cover, whereas land cover after clearing is unlikely to be representative of established agricultural landscapes. Large mixed land-cover catchments may include surface runoff intercepting features (e.g. hillside farm dams, tree belts) and unaccounted surface water or groundwater use (Calder, 2007; van Dijk et al., 2007). In addition, forest clearing in experimental studies may be associated with soil disturbance, which may enhance Q generation for reasons that are not directly attributable to land cover per se (Bruijnzeel, 2004). The consequence may be that the contrast in hydrological response between forest and herbaceous vegetation may be greater in experimental catchments than in non-experimental catchments. Finally, depending on the configuration of vegetation types within a catchment, forests may intercept and use lateral flows of water from herbaceous vegetation (further discussed in Sect. 4.2)

There are also some potential methodological issues:

4. *Other overriding climate and terrain factors.* Several studies have reported difficulty in detecting changes in the streamflow response of individual catchments as they undergo land use or land cover change, in large part because of the influence of climate variability (e.g. Beven et al., 2008; Peña-Arancibia et al., 2012). Confident detection and attribution of land cover influence requires that other factors are considered and controlled for Budyko theory controls for the two most important determinants of the long-term water balance, P and PE. One might question whether the Budyko framework is sufficiently powerful to evaluate effects in addition to P and PE alone, and if so, whether indeed land

[1] Defined here as any rational function that embodies the same conceptual model as the original (see various examples in e.g. Oudin et al., 2008).

[2] In evaporation we include all evaporation and transpiration fluxes.

cover is the next most important variable. Additional factors potentially equally or more important than land cover include the phase difference between seasonal P and PE patterns (Budyko, 1974; Milly, 1994) and other aspects of their temporal behaviour (e.g. rainfall intensity). Depending on their covariance with land cover, these attributes may attenuate or enhance any land cover influence on Q.

5. *Covariance between land cover and climate*. Covariance between land cover and climate is commonly present in collated catchment data sets due to the correlation between natural biomes and climate, and because of the role of landscape and climate in land use and land cover change decisions. For example, catchments with considerable remnant and plantation forests will usually be found more commonly in regions with greater relief, usually associated with greater P and lower PE than their lowland counterparts. Applying an additive response model to a data set with covariance between candidate predictors makes erroneous results more likely. Van Dijk et al. (2007) attempted to control for this effect and demonstrated that it influenced the results, but was probably not the only cause for the counterintuitive results they obtained.

6. *Measurement error*. Studies analysing data from small catchments have not been able to detect a significant change in stream flow when land cover is changed in less than 15–20 % of a catchment (Bosch and Hewlett, 1982; but see Trimble et al., 1987; Stednick, 1996). Arguably, this can be attributed to the influence of measurement noise on the analysis. Statistically, therefore it might be expected that it is harder to detect a land cover influence in large catchments with land cover mixtures than it is for catchments with homogeneous land cover. Using additive Budyko models requires estimates not only of Q, but also of catchment average P, PE and fractional cover (FC) of the land cover classes of interest. Errors will occur in each of these and may affect the analysis results, even more so if errors are not random. For example, Oudin et al. (2008) speculated that systematic precipitation measurement errors affected their analysis.

1.2 Objective

In this study, we aim to test the hypothesis that methodological issues with the use of a Budyko framework to interpret collated data from multiple mixed land-cover catchments may explain why a land cover influence has not been detected. To test this, we used Q observations from 278 non-experimental Australian catchments, the Zhang formulation of the Budyko model (Zhang et al., 2001), and a bottom-up dynamic hydrological process model with explicit representation of vegetation characteristics (AWRA-L). Synthetic experiments were performed in which the Budyko model was used to analyse process model simulations for the 278 catchments. To paraphrase, we use the more complex model (AWRA-L) to create a virtual laboratory. We then perform a virtual experiment and use the Budyko model as an analytical tool to interpret the results. If our experiment can reproduce both a land cover influence for individual catchments as well as the lack of influence found in the type of multi-catchment studies described in the introduction, then this would support our hypothesis.

It is emphasised that we do not aim to prove that the methodological issues described are the single most important cause for the discrepancies arising from the discussed application of the Budyko model. Their presence certainly does not rule out the plausibility and presence of additional methodological or physical explanations. Several such explanations were mentioned and are further explored in the discussion (Sect. 4.2).

Strictly speaking, we are only able to test our hypothesis for the specified combination of catchment data, Budyko model formulation and process model. Moreover, we use models in our synthetic experiment as a plausible but not necessarily highly accurate representation of reality. This type of synthetic study is not unique but somewhat uncommon in the hydrological literature, and therefore we briefly discuss some caveats as to what are *not* our objectives.

Firstly, we do not aim to validate or falsify the dynamic process model (AWRA-L) we used in this experiment. We also do not aim to prove that the model structure and parameter values used here are the best possible description of reality, or better than any other model(s). Any model can only ever be a flawed and simplified abstraction of reality (e.g., Oreskes et al., 1994). Here we use the AWRA-L model because it is comparatively simple, because we understand it sufficiently well to interpret its behaviour and, most importantly, because it is able to reproduce two key features also observed in real data sets, as discussed in further detail below. Any other model able to meet this criterion should have been suitable for the experiment.

Secondly, we do not propose that we can use the more complex process model to prove a land cover influence; rather we show that it can reproduce such an influence in conditions were it has been observed as well as reproduce its absence in conditions were it has not. Proving the existence of a land cover influence is neither necessary (we refer to the empirical evidence discussed) nor possible (a model fundamentally cannot provide proof of a real-world phenomenon, at best only a plausible explanation). We will discuss this point in more detail further on.

Finally, we do not seek to falsify Budyko type models as a useful and predictive theory, or question the usefulness of top-down analysis as a paradigm. We focus here on only one very specific application: whether analysing collated data from mixed land-cover catchments by fitting a

Fig. 1. Location of the 278 Australian catchments for which streamflow data were used in the analysis.

form of the Budyko model is able to accurately detect land cover influence.

2 Methods

2.1 Data

The Q data used here were identical to the data used by van Dijk and Warren (2010), which is a subset of 278 out of around 326 records used in previous studies (Guerschman et al., 2008, 2009; van Dijk, 2010a, c) and very similar in composition to Australian catchment data used in other studies (e.g. Zhang et al., 2004; Peel et al., 2010). Catchment boundaries were derived from a 9″ resolution digital elevation model (Fig. 1) and catchments with major water regulation infrastructure were excluded. The 278 catchments that were selected had data for at least five (not necessarily consecutive) years between 1990 and 2006 (median 16 yr). The woody vegetation cover fraction was mapped on the basis of Landsat Thematic Mapper imagery for 2004 and daily precipitation and Priestley-Taylor PE was interpolated at 0.05° resolution from station data (Jeffrey et al., 2001). Catchment areas varied from 23–1937 (median 278) km^2, tree cover from 0–90 % (median 25 %), P from 404–3138 (median 836) mm yr^{-1}, PE from 766–2096 (median 1265) mm yr^{-1}, and Q_{obs} from 4–1937 (median 114) mm yr^{-1}.

2.2 Budyko model

Oudin et al. (2008) tested five different Budyko model formulations and found little difference in their explanatory power, and all formulations have a very similar functional form. We chose the model of Zhang et al. (2001) because it was used successfully in previous studies to detect land cover influence in a global Q data set of (mostly small) catchments with homogeneous land cover. For a single land cover class, the model can be written as

$$Q = \frac{P}{1 + \frac{P}{\mathrm{PE}} + w\left(\frac{\mathrm{PE}}{P}\right)^2}. \quad (2)$$

For a catchment with a two land cover classes, forest and herbaceous vegetation, Eq. (2) can be rewritten as (cf. Eq. 1)

$$Q = \mathrm{FC\ (forest)}\frac{P}{1 + \frac{P}{\mathrm{PE}} + w(\mathrm{forest})\left(\frac{\mathrm{PE}}{P}\right)^2} + \mathrm{FC\ (herbaceous)}\frac{P}{1 + \frac{P}{\mathrm{PE}} + w(\mathrm{herbaceous})\left(\frac{\mathrm{PE}}{P}\right)^2}. \quad (3)$$

2.3 Dynamic model

The dynamical model used is the Australian Water Resources Assessment system Landscape hydrology (AWRA-L) model (version 0.5; van Dijk, 2010b; van Dijk and Renzullo, 2011; van Dijk et al., 2012). AWRA-L can be considered a hybrid between a simplified grid-based land surface model and a non-spatial catchment model applied to individual grid cells. Where possible process equations were selected from literature and selected through comparison against observations. Prior estimates of all parameters were derived from literature and analyses carried out as part of model development. Full technical details on the model can be found in van Dijk (2010b) but some salient aspects are summarised here. The configuration used here considers two hydrological response units (HRUs): deep-rooted tall vegetation (forest) and shallow-rooted short vegetation (herbaceous). The water balance of a top soil, shallow soil and deep soil compartment are simulated for each HRU individually and have 30, 200 and 1000 mm plant available water storage, respectively. Groundwater and surface water dynamics are simulated at catchment scale. Minimum meteorological inputs are gridded daily total precipitation and incoming short-wave radiation, and daytime temperature. Maximum evaporation and transpiration given atmosphere and vegetation conditions are estimated using the Penman-Monteith model (Monteith, 1965). Actual transpiration is calculated as the lesser of maximum transpiration and maximum root water uptake given soil water availability. Rainfall interception is estimated separately using a variable canopy density version of the event-based Gash model (Gash, 1979; van Dijk et al., 2001a, b) to account for observed high rainfall evaporation rates (for discussion see e.g. van Dijk and Keenan, 2007). The influence of vegetation on the water balance occurs in a number of ways: compared to short vegetation, forest vegetation is parameterised to have lower albedo, greater aerodynamic conductance, greater wet canopy evaporation rates, lower maximum stomatal conductance, thicker leaves, access to deep soil and ground water, and adjust less rapidly to changes in water availability.

Van Dijk and Warren (2010) evaluated AWRA-L with the configuration and parameterisation used here against a range of in situ and satellite observations of water balance components and vegetation dynamics. This included evaluation against Q_{obs} from the catchments used in this analysis, as well as flux tower latent heat flux observations at four sites across Australia, including both forest and herbaceous sites (van Dijk and Warren, 2010). Latent heat flux patterns for dry canopy conditions were reproduced well. Comparison of total latent heat flux was difficult due to the large uncertainty in rainfall interception evaporation estimated from the flux tower measurements. Streamflow records were reproduced well, that is, with an accuracy that was commensurate to that achieved by other rainfall-runoff models with a similar calibration approach.

2.4 Experiments

2.4.1 Can previous contrasting findings be reproduced and reconciled with the process model?

We did two tests to see whether we could reproduce the contrasting findings of published analyses of Q from homogenous experimental and from multiple non-experimental mixed land-cover catchments, respectively. First, we fitted the two parameter Zhang model (Eq. 3) by minimising the standard error of estimate (SEE) against Q_{obs} from the 278 catchments (using Solver in Microsoft Excel^{TM}). We interpreted the derived w(forest) and w(herbaceous) parameter values and implied land cover to assess whether we obtained the same contrasting findings as previous studies.

Next, we investigated whether the AWRA-L could reconcile these contrasting findings, which means meeting two conditions. First, the model needed to reproduce the observed Q from the 278 catchments as well as, or better than, the calibrated two-parameter Zhang model, as judged by several measures of agreement (Table 1). Second, the model needed to be in agreement with the results of experimental catchment studies of land cover change impacts on Q. One test of this would be to reproduce Q changes observed in an actual paired catchment experiment, but unfortunately we did not have access to daily streamflow and meteorological data for a number of such experiments, and one example would have a very limited statistical significance. Instead, we used AWRA-L to simulate Q from the 278 catchments under conditions of full forest and full herbaceous cover, respectively. We compared the resulting water balance estimates with the empirical relationships for the respective land cover type reported by Zhang et al. (2001), who propose two alternative models to estimate Q. The first method (Zhang-A) is to use Eq. (3) with values of w(forest) = 2.0 and w(herbaceous) = 0.5, with PE estimated using the Priestley–Taylor formula and a standard land cover with assumed albedo and aerodynamic conductance. The second method (Zhang-B) is to use the same approach, but substitute PE by values of 1410 and 1100 mm yr^{-1} for forest and herbaceous cover, respectively. The latter reduces the physical realism of the model, but provides a convenient alternative to where PE estimates are not readily available, and has been shown to agree well with other empirical relationships (Holmes and Sinclair, 1986; Turner, 1991) and data from catchments with homogeneous land cover (Zhang et al., 2001; Brown et al., 2005). These so-called Zhang curves have been widely used to estimate the impact of conversion between forest and non-forest cover on Q in scenario studies and policy reports (e.g. Austin et al., 2010; Brown et al., 2007; Dawes et al., 2004; Sun et al., 2006; van Dijk et al., 2006), and as such were considered a relevant point of reference. The vast majority of such reports assume that land cover impact is linearly proportional to the area of land cover change.

The prominent use of the Zhang curves in policy development puts further onus on understanding the apparent discrepancies between the results from the two experimental designs discussed. We emphasise that our objective does not require that the process model explains more variation than the Zhang models in one or both cases; equal or similar performance would be sufficient. The critical difference is that fitting the Zhang models typically leads to two substantially different parameter sets, essentially producing two mutually contradictory models in the respective applications. By contrast, the process model uses one parameter set only for both cases and therefore by definition produces internally consistent results. The process model parameters were estimated a priori rather than optimised, which is not essential but arguably preferable.

In summary, if the tests described above would be successful, we would be able to conclude that previous contrastive findings can be reproduced, and appear to be at least partly due to methodological problems. To put it differently: if the same process model with identical parameters can reproduce both (1) the land cover influence expected for individual catchments, and (2) the observed Q from mixed catchments, then the fact that two different parameter sets are required in the case of the Zhang model suggests a methodological problem with that particular inference approach.

The subsequent analyses were designed to try and analyse three potential methodological problems, viz. measurement errors, an overriding influence of other environmental factors, and covariance between land cover and climate.

2.4.2 Are measurement errors responsible?

One feasible explanation for the reduced or absent land cover impact inferred from catchments with mixed land cover is the possible impact of data error: P, PE, Q and forest cover fraction (FC) are all prone to measurement and estimation error. This could affect values for the two Zhang model parameters that were optimised. To test for this, we performed a synthetic experiment in which noise was added to the Q estimates produced by the process model (Q_{sim}), for the case

with actual, mixed land cover (we did not use the actually observed Q as this already contains measurement noise, with unknown characteristics). First, a simulated measurement error with an absolute average of 10 % was added to all 278 original values of FC and mean P, PE and Q_{sim}. The errors were drawn independently for each variable and each catchment. For FC an error was added that was drawn from a normal (Gaussian) distribution with mean of zero and standard deviation of 0.1; the result was limited within the range 0 to 1. The values of P, PE and Q_{sim} were multiplied with a factor drawn from a normal distribution with mean of one and standard deviation of 0.1. Next, the two Zhang model parameters were optimised to the resulting noisy FC, P, PE and Q_{sim} values for all 278 catchments combined. This experiment was repeated 3000 times, each time with a sample of 278 catchments. The resulting 3000 pairs of w values were compared to those fitted to the original FC, P, PE and Q_{sim} values (i.e. without noise added), to assess whether the simulated measurement noise led to parameter values suggestive of a smaller than predicted land cover influence.

2.4.3 Are additional environmental factors responsible?

The premise of the Budyko framework is that mean $P$and PE are the main determinants of Q. Beyond this, however, other climate factors or terrain factors may be more important than land cover category. To investigate this possibility, we used the Zhang model to analyse the AWRA-L simulations for the forest and herbaceous scenarios. For each catchment, we calculated the model parameter (w) value corresponding to the Q simulated for each land cover scenario (i.e. full forest or full herbaceous cover) using the following inverted model form (cf. Eq. 2):

$$\frac{\frac{P}{Q_{\mathrm{sim}}(\mathrm{scenario})} - \frac{P}{\mathrm{PE}} - 1}{\left(\frac{\mathrm{PE}}{P}\right)^2}. \quad (4)$$

For each land cover category, we attempted to find catchment attributes that could explain the variance in inferred w values. We used the same step-wise regression approach used in earlier analyses of the same Q data (van Dijk, 2010a, c). In summary, candidate predictors were selected from a range of catchment attributes based on the parametric and non-parametric (ranked) correlation coefficients (r and r^*, respectively). Linear, logarithmic, exponential and power regression equations were calculated for all potential predictors, and the most powerful one was selected. The residual variance was calculated and the same procedure was repeated. The catchment attribute data available included measures of catchment morphology (catchment size, mean slope, flatness); soil characteristics (saturated hydraulic conductivity, dominant texture class value, plant available water content, clay content, solum thickness); climate indices (mean P, mean PE, humidity index P/PE, remotely sensed actual evapotranspiration, average monthly excess precipitation); and land cover characteristics (fraction woody vegetation, fractions non-agricultural land, grazing land, horticulture, and broad acre cropping, remotely sensed vegetation greenness). Full details on data sources and catchment climate, terrain and land cover attributes can be found in van Dijk (2010a, c).

2.5 Is covariance between land cover and climate responsible?

Our catchment data set shows modest covariance between forest cover (FC) and P/PE ($r = 0.44$). Earlier analyses showed that this type of covariance can affect the ability to accurately determine land cover influence (see van Dijk et al., 2007, for a detailed example). We performed a further synthetic experiment using the AWRA-L model to test the magnitude of this problem:

1. Each of the 278 catchments was assigned a new virtual land cover by randomly drawing a new value for FC from a normal distribution with the same mean and standard deviation as the observed FC values (0.284 and $\pm$0.224, respectively). Values were truncated to remain within the range 0 and 1.

2. For each catchment, the AWRA-L model was run with the new FC values and the original meteorological inputs.

3. The two Zhang model parameters were fitted to the resulting 278 Q_{sim} values.

The experiment was repeated 3000 times (each time with all 278 catchments), and the results were analysed to determine whether there was a relationship between any (randomly introduced) covariance between the FC and P/PE values on the one hand, and the inferred land cover influence on the other.

3 Results

3.1 Previous contrasting findings can be reproduced and reconciled by the process model

Indicators of the agreement between Q observed in the 278 catchments and values estimated by the optimised two-parameter Zhang model (Eq. 3) and the AWRA-L model are listed in Table 1. For comparison, the performance of the originally proposed Zhang-A and Zhang-B models and an optimised Zhang model (Eq. 2) are also shown. This comparison is important, as these two models incorporate the response of Q to land cover change as inferred from experimental catchment studies and widely used in scenario analysis.

Calibrating the Zhang model parameters led to an improvement in model performance and reduction in bias, when

Table 1. Performance indicators of the original Zhang et al. (2001) models (Zhang-A and Zhang-B; see text for explanation), the Zhang model with one and two calibrated parameters, respectively, and the AWRA-L with prior parameter estimates. Al metrics relate to the agreement between modelled and observed mean annual streamflow (Q, mm per year) for all catchments ($N = 278$). SEE = standard error of estimate, MAE = mean absolute error, and Bias = mean bias (all in mm yr^{-1}); Rel. Bias = mean of absolute values of percentage bias and FOM=fraction of values overestimated by model (in %).

	SEE	MAE	Bias	Rel. Bias	FOM
Zhang-A	119	97	79	44 %	91 %
Zhang-B	136	114	86	47 %	86 %
Zhang – 2 parameter	84	54	4	2 %	62 %
Zhang – 1 parameter	84	54	4	2 %	62 %
AWRA-L	78	50	1	1 %	54 %

compared to the original models. However, reducing the Zhang model to a one-parameter model (that is, making the model insensitive to land cover), did not degrade model performance (optimised values were w(forest) = 1.91 and w(herbaceous) = 1.98 versus $w = 1.95$, respectively). These results support previously published result that fitting a Budyko model to observations from non-experimental catchments does not show the predicted land cover influence, in contrast with results based on experimental catchments. In other words, we were able to reproduce previous contrasting findings and reconcile them.

Table 1 also shows that, despite the lack of parameter optimisation, AWRA-L performs slightly better than the calibrated Zhang models. The AWRA-L predictions of Q for the same 278 catchments, but this time for a hypothetical scenario of full forest and herbaceous cover, are compared to the original Zhang-A and Zhang-B model in Fig. 2. AWRA-L is able to reproduce the approximate differences between forest and herbaceous catchments predicted by the original Zhang models, although the forest scenario predictions agree better with the Zhang-B model than with the Zhang-A model (Fig. 2). It follows that the process model (1) can predict Q from the 278 catchments with mixed land cover as well as (in fact, slightly better than) a fitted Zhang model, and (2) suggests a land cover influence of similar magnitude as that predicted by the original Zhang curves. Therefore, the process model can reconcile the contrasting conclusions drawn from experimental and mixed catchment Q data that the Zhang model cannot reconcile.

Further supporting this conclusion, the same results could also be reproduced when process model Q estimates were interpreted using the Zhang model. If a one-parameter Zhang model was fitted to the modelled Q_{sim} with hypothetical full forest or herbaceous cover, w values 3.6 and 1.0 where found, respectively – producing curves quite similar to the original Zhang-A and Zhang-B models. However, when the two-parameter Zhang model was fitted to the Q_{sim} obtained

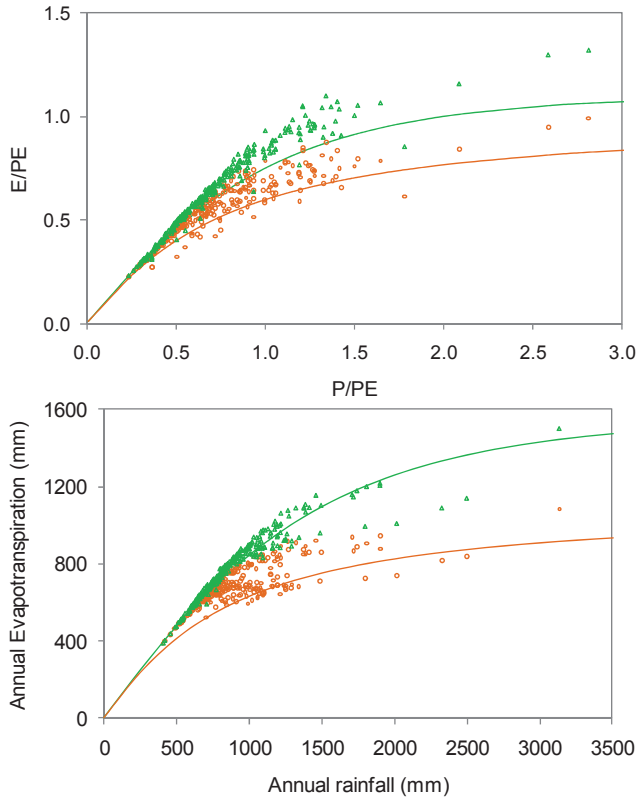

Fig. 2. Comparison of AWRA-L simulated mean streamflow for the 278 catchments for scenarios of forest cover (green triangles) and herbaceous cover (orange circles) shown in two different ways. Also shown are the two models proposed by Zhang et al. (2001): (top panel) Zhang-A and (bottom panel) Zhang-B.

with actual FC values, the resulting values were much closer, at 2.22 and 1.79, respectively, predicting only a very small land cover influence (average forest water use is only 2 % greater than herbaceous water use). This shows that previous contrasting findings can also be reproduced with the synthetic Q data.

3.2 Measurement errors are at least partly responsible

The introduction of noise in the data led to higher average optimised w values than for the experiment without noise added: 2.7 (range 0.6–9.4) for forest and 2.3 (1.3–9.2) for herbaceous cover. Importantly, for 39 % of the 3000 replicates, the optimised w value for forest was actually lower than for herbaceous cover. It follows that random errors in the observations reduce the likelihood that land cover influence is detected, let alone accurately quantified.

3.3 Underlying climate factors may be responsible

The distribution of w values calculated from simulated Q for individual catchments appeared approximately log-normally distributed and therefore all values were log-transformed

before step-wise regression analysis. The ratio P/PE itself did not explain significant variance in either land cover scenario ($r^2 < 0.04$).

Somewhat unexpectedly, the most powerful predictor of variation in w values varied between the forest and herbaceous cover scenarios. In the full forest cover scenario, PE itself explained 45 % (r^2) of the variance in log-transformed w values (see Fig. 3a). Other predictors did not explain any of the residual variance. In the full herbaceous cover scenario, depth-weighted average event precipitation (DWAEP, calculated as the sum of squared daily rainfall totals divided by total rainfall) explained 33 % of the variation (Fig. 3b). Alternatively, mean event precipitation (total rainfall divided by the number of rain days) explained 27 % of variation (instead of, not in addition to the variation explained by DWAEP). Both are indicators of the irregularity of rainfall distribution (see van Dijk, 2010c for definitions). Other predictors did not explain any of the residual variance.

It is concluded that other climate factors than only the ratio P/PE may have considerable influence on Q and hence affect fitted w values. We speculate that the explicit consideration of temporal climate patterns may also be the main reason why the (uncalibrated) process model was slightly more skillful at reproducing observed Q from the 278 catchments than the (calibrated) Zhang model.

3.4 There is structure in the data set that is at least partly responsible

Using simulated Q for randomly generated hypothetical forest cover fractions ($N = 3000$), Zhang model parameter values of 3.4 ± 0.7 (range 1.9–6.1) and 1.1 ± 0.1 (0.9–1.4) were fitted for forest and herbaceous cover, respectively. These average values are relatively close to the w values of 3.6 and 1.0 fitted for the full forest and herbaceous cover scenarios (experiment 1). In some experiments the optimised Zhang parameters were similar to the full cover ones, whereas in other experiments they were very close to each other (Fig. 4a) (it is noted that w(herbaceous) never exceeded w(forest), unlike in the measurement error experiment). It would be tempting to conclude that the covariance between FC and P/PE in the original data set ($r = 0.44$) was the main cause for the underestimation of land cover influence. However, no relationship was found between the fitted parameter pair and the covariance between forest cover and P/PE that was introduced into the data set (Fig. 4a). Nonetheless, our manipulation of the data must have introduced another form of hidden structure in the data that affected the optimised parameter values.

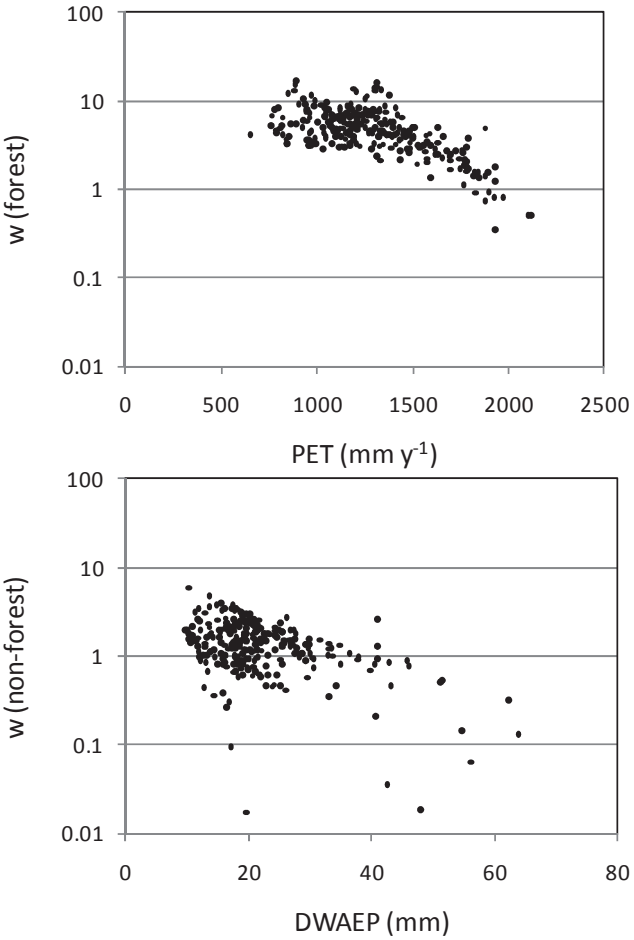

Fig. 3. Relationship between the catchment variable that explained most of the variance in (log-transformed) Zhang model parameter (w) values inferred from the synthetic land cover experiment, (top panel) potential evaporation (PE) for forest catchments and (bottom panel) depth-weighted average event precipitation (DWAEP) for herbaceous catchments.

4 Discussion

4.1 Methodological problems can explain previous contrasting findings

Despite their simplicity, Budyko models have shown impressive skill in predicting Q from P and PE alone, when compared to more complex dynamic catchment models. Indeed in comparison with the more complex AWRA-L model, the Zhang model could achieve very similar performance in explaining the observed Q, albeit after parameter fitting. It was this same fitting, however, that produced land cover parameter values that could not be reconciled with the results of experimental catchment studies, thus reproducing previous contrasting findings. We showed that the dynamic hydrological process model could resolve this inconsistency, and therefore, that there appear to be methodological problems with

the use of Budyko models as a detection method in this particular application.

The synthetic experiments demonstrated that all methodological issues tested (measurement errors, the presence of other important uncontrolled factors, structure in the catchment data set) were plausible and can contribute to a failure to accurately quantify land cover influence with the Budyko model that was used. In all cases, underestimation of the land cover influence was the most likely result. Desirable aspects of Budyko models are their conceptual simplicity and the minimal number of parameters. However, in qualifying the principle of Occam's Razor, Albert Einstein (1934) proposed that "the supreme goal of all theory is to make the irreducible basic elements as simple and as few as possible without having to surrender the adequate representation of a single datum of experience". On the basis of our results we conclude that, for the purpose at hand, Budyko models fail at the second part of this statement; that is, they are too simple to adequately quantify the influence of land cover in collated Q data from catchments with mixed land cover.

Although we only tested one particular Budyko model, previous studies suggest that conclusions would likely have been very similar if any other Budyko model had been used, due to the identical conceptual structure and similar function form (see e.g. Oudin et al., 2008). Moreover, we argue that the methodological issues with heterogeneous data sets such as the one we analysed are probably not limited to Budyko models but likely to extend to similarly simple top down inference methods.

There have been attempts to increase the predictive performance of the Budyko models by including additional variables, often within a stochastic framework (e.g. Porporato et al., 2004). Those not related to land cover include absolute PE values (Peel et al., 2010), solar radiation, phase differences between the seasonal P and PE patterns (Donohue et al., 2010), and the daily distribution of precipitation (see review in Gerrits et al., 2009). Our results suggest that some of these factors may indeed exert a similarly large or larger influence on catchment response than land cover. However, trying to control for these additional factors introduces further parameters and observed or estimated attributes with associated uncertainty. Ultimately such an approach must fall prey to the very issue that top-down approaches aim to avoid, that is, an underdetermined (or undetermined) problem in which competing hypotheses create similar outcomes and therefore cannot be tested conclusively.

This is obviously certainly not avoided by the use of dynamic process models. An advantage of such models, however, is that process assumptions can be made more explicit and individually tested against different types of observations with different spatial and temporal characteristics. In light of this, we question whether it is advisable to fit a simplified hydrological model to collated heterogeneous Q data such as the data analysed here. Arguably, it is more pertinent to demonstrate that the observations can be explained satisfactorily by a (more, but not unnecessarily complex) theory and therefore are not falsified by experimental knowledge. In this context, the Budyko framework may be a valuable benchmark test, whose predictive power should be matched or exceeded by any competing theory (cf. van Dijk and Warren, 2010). It is however perhaps less advisable as inference method to detect second order drivers in heterogeneous data sets.

Strictly speaking, our results are only valid for one particular data set. However, all factors we investigated negatively affected accurate quantification of the land cover influence. We consider it inevitable that at least some of these problems will be encountered in any Q data set from large catchments with mixed land cover. Zhang et al. (2001) showed that this need not prevent detection of land cover impacts in data from catchments that represent extreme scenarios and in controlled experiments. Paired catchment experiments in particular are much more likely to adequately control for climate and terrain factors and thereby allow accurate quantification of the land cover influence. Apart from experimental issues associated with such necessarily small-scale experiments (e.g. subterranean leakage), a critical issue in the extrapolation of the results from such experiments will be the degree to which hydrological processes and land cover characteristics are representative for those in larger, non-experimental catchments (see van Dijk and Keenan, 2007 for a discussion). More elaborate process models may have a role to play here, as the influence of such representational errors can be investigated in model experiments.

4.2 Potential physical causes for reduced land cover influence in catchments with mixed land cover

We did not set out to explore possible physical rather than methodological causes for the inability to adequately detect a land cover influence in previous Budyko model applications in multiple mixed land-cover catchments. They can certainly play a role. The AWRA-L model was not suitable to explore all potential processes in-depth; for example, it cannot simulate land surface-atmosphere feedbacks, and observations were not available to parameterise the impacts of human interferences (e.g. farm dams, roads and soil management) and lateral water redistribution within hill slopes and in the river system. Streamflow routing per se (that is, the accumulation and propagation of streamflow through the river network) has no influence on long-term average Q, but the spatial redistribution of water in the landscape does create a potential for Q to be reduced, e.g. by greater evaporation from streams and riparian areas and the lateral redistribution and subsequent evapotranspiration of surface and sub-surface water at hill slope level. A simple model experiment was performed to assess the possible magnitude of these processes by (i) changing the AWRA-L model code to reroute all lateral flows (surface, soil and groundwater) from the herbaceous to the forest landscape component; (ii) running the

model across all catchments, varying the catchment fraction of forest from 0–100 %; and (iii) comparing the resultant Q estimates to those obtained in the case without redistribution as a reference. The experiment is similar to that reported on by Vertessy et al. (2002), and can be interpreted as a case in which forest is preferentially located in the catchment valleys, maximising its potential streamflow impact by intercepting and lateral flows from upslope areas with herbaceous vegetation. The reference case (i.e. that used in all previous experiments) can be interpreted as a case where any of the hill slopes within a catchment are either fully with or without forest, in which case the forest impact scales linearly with the area under the forest. The results (Fig. 5) show that, according to the model, a considerable departure from the reference case is plausible, in line with previous modelling results reported by Vertessy et al. (2002, their Fig. 3). Climate humidity was a strong determinant of the relative influence of lateral interactions; the strongest non-linear response was predicted for the driest catchments (top curve in Fig. 5), whereas the wettest catchments showed an approximately linear response (bottom curve). Importantly, the results predict that a small fraction of forest can cause a disproportionate reduction in Q, which can indeed lead to an underestimation of land cover influence from analysing mixed land-cover catchments. It is noted that this model experiment likely overestimates the importance of land cover configuration. Firstly, the scenario tested is extreme and in contrast with actual land cover distribution in the catchments, which tend to have most of the forested area on the less accessible and less productive hill slopes and tops. Secondly, we are not able to validate the magnitude of the model-predicted fluxes against experimental data. Indeed, the potential effectiveness of deep-rooted vegetation in intercepting lateral flows from upslope has been speculated on and predicted with models several times (e.g. Stirzaker et al., 2002) but so far rarely observed in reality (e.g. McJannet et al., 2000; van Dijk et al., 2007).

An examination of the main model-predicted causes of Q change associated with land cover change may provide some further insight into reasons why large catchments with mixed land cover might behave differently from small, homogenous (experimental) ones. The model predicts that the main cause of the different hydrological response is the greater rainfall interception loss from forest vegetation (Fig. 6). The difference represents around 10–15 % of rainfall; consistent with the majority of published experiments (e.g. Roberts, 1999; although much greater differences can occur under maritime conditions, e.g. Schellekens et al., 1999; McJannet et al., 2007). A priori it would seem plausible that that the associated rapid return of moisture to the atmosphere may influence rainfall generation downwind (cf. D'Almeida et al., 2007; Pielke et al., 2007; van Dijk and Keenan, 2007). If this is indeed the case, then accurate prediction of the influence of land cover change on the water balance of large catchments may depend on the spatial distribution of precipitation and how it is measured and represented in models. In other words, in sufficiently large catchments the rainfall interception effect might be mitigated by rainfall recirculation.

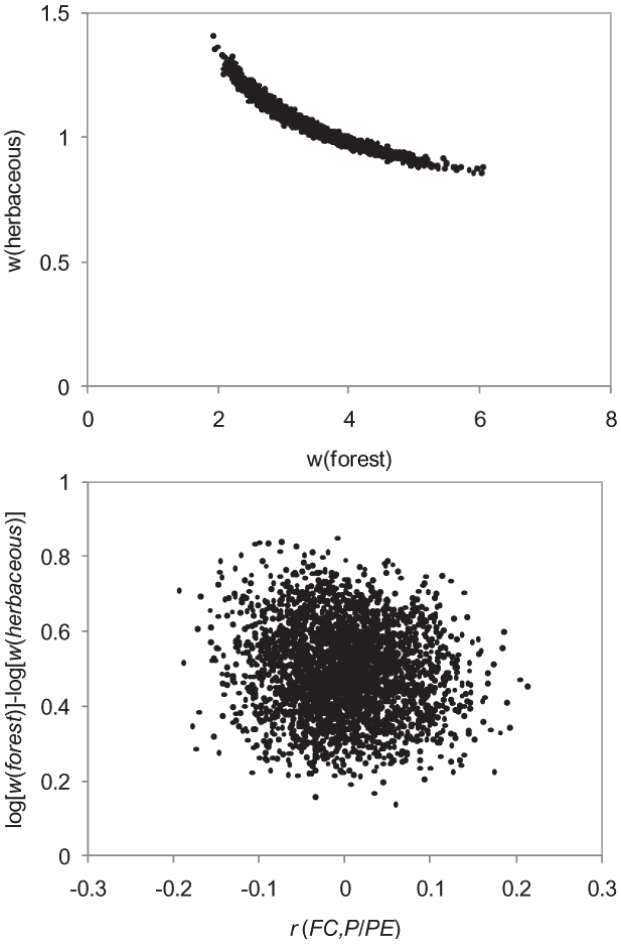

Fig. 4. Zhang model parameter values fitted to synthetic mean streamflow estimates for 278 catchments produced by AWRA-L with random forest cover fractions assigned to each of the catchments. Data points represent the results of 3000 replicate experiments. (Top panel) Zhang model parameter data pairs fitted in each experiment showing a well-defined relationship; (bottom panel) the difference between log-transformed parameter values versus the correlation between synthetic forest cover fraction (FC) and catchment humidity (P/PE) introduced in the experiment, showing no relationship ($r = 0.11$).

Finally, it is emphasised that the interpretation of our model results, and particularly those presented in this section, are contingent on the algorithms, assumptions and parameterisations of the process model we used here. We believe it very likely that the methodological problems with the inference method investigated here would be confirmed if other realistic process model structures or parameter sets were used. However, the predicted magnitude of the influence of lateral interactions and the relative importance of rainfall interception loss are likely to be more sensitive to model structure and assumptions, and therefore more speculative.

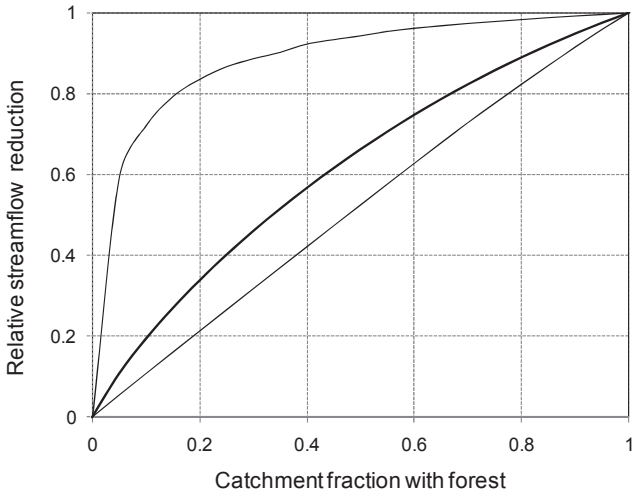

Fig. 5. The theoretical maximum influence of lateral water redistribution, from herbaceous to forest areas, on mean streamflow (Q) as predicted by the AWRA-L model for 278 Australian catchments. The middle bold and two outer lines represent the catchments with the median and most extreme responses, respectively. Q reduction is shown relative to the difference between the 0 and 100 % forest cover cases (in the absence of redistribution a linearly proportional influence would be predicted).

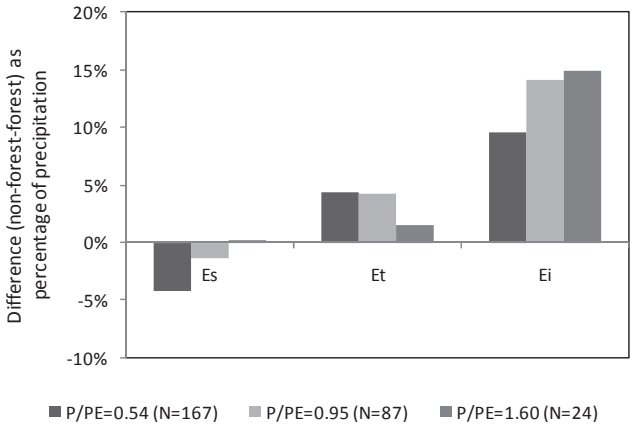

Fig. 6. Contribution of different evaporation terms to the increase of mean streamflow after forest removal estimated by the AWRA-L model, expressed as a percentage of rainfall. Values represent fluxes averaged over three groups of catchments, intended to represent (from left to right) water-limited (P/PE < 0.75), transitional, and energy-limited (P/PE > 1.25) environments. Es = soil and open water evaporation; Et = transpiration; Ei = rainfall interception losses.

5 Conclusions

Controlled experiments provide strong evidence that changing land cover (e.g. deforestation or afforestation) can affect mean catchment streamflow (Q). By contrast, a similarly strong influence has not been found in studies that interpret Q from multiple catchments with mixed land cover. One possible reason is that there are methodological issues with the way in which the Budyko framework was used in the latter type studies. We examined this using Q data observed in 278 Australian catchments and by making inferences from synthetic Q data simulated by a hydrological process model (the Australian Water Resources Assessment system Landscape model). We draw the following conclusions:

1. Carrying out synthetic experiments with the process model, we could reproduce the absence of a detectable influence in mixed land-cover catchments as well as the presence of such an influence in individual catchments. In other words, previous contrasting findings could be reconciled.

2. Several potential methodological problems with the Budyko framework based inference approach applied in previous studies were investigated. The apparent absence of a detectable influence when comparing mixed land-cover catchments could, at least partially, be explained by the three factors investigated, viz. (i) noise in land cover, precipitation and Q data; (ii) additional catchments climate characteristics more important than land cover; and (iii) covariance between Q and catchment attributes. Such methodological issues are likely to be found in any heterogeneous streamflow data set.

3. In addition to these methodological issues, there are also plausible physical causes for the failure to adequately detect a land cover influence in catchments with mixed land cover. This includes the lateral redistribution of water from herbaceous to forest areas, and potential recirculation of rainfall intercepted by the forest canopy.

Acknowledgements. This work is part of the water information research and development alliance between the Bureau of Meteorology and CSIRO's Water for a Healthy Country Flagship. Comments from Lu Zhang and Randall Donohue helped improve earlier versions of this paper, as did reviews by N. McIntyre, the editor, and two anonymous referees.

Edited by: R. Merz

References

Andréassian, V.: Waters and forests: from historical controversy to scientific debate, J. Hydrol., 291, 1–27, 2004.

Austin, J., Zhang, L., Jones, R. N., Durack, P., Dawes, W., and Hairsine, P.: Climate change impact on water and salt balances: an assessment of the impact of climate change on catchment salt and water balances in the Murray-Darling Basin, Australia, Climatic Change, 100, 607–631, 2010.

Beven, K., Young, P., Romanowicz, R., O'Connell, E., Ewen, J., O'Donnell, G. M., Holman I., Posthumus, H., Morris, J., Hollis, J., Rose, S., Lamb, R., and Archer, D.: Analysis of historical data sets to look for impacts of land use and management

change on flood generation, R&D Technical Report FD2120/TR, UK Department for Environment, Food and Rural Affairs, London, 84 pp., 2008.
Bosch, J. R. and Hewlett, J. D.: A review of catchment experiments to determine the effect of vegetation change on water yield and evapotranspiration, J. Hydrol., 55, 3–22, 1982.
Brown, A. E., Zhang, L., McMahon, T., Western, A., and Vertessy, R.: A review of paired catchment studies for determining changes in water yield resulting from alterations in vegetation, J. Hydrol., 310, 28–61, 2005.
Brown, A. E., Podger, G. M., Davidson, A. J., Dowling, T. I., and Zhang, L.: Predicting the impact of plantation forestry on water users at local and regional scales An example for the Murrumbidgee River Basin, Australia, Forest Ecol. Manage. 251, 82–93, 2007
Bruijnzeel, L.: Hydrology of moist tropical forests and effects of conversion: a state of knowledge review, International Hydrological Programme of UNESCO, Paris/Vrije Universiteit, Amsterdam, 224 pp., 1990.
Bruijnzeel, L.: Hydrological functions of tropical forests: not seeing the soil for the trees?, Agric., Ecos. Env., 104, 185–228, 2004.
Budyko, M. I.: Climate and Life Academic Press, New York, 508 pp., 1974.
Calder, I. R.: Forests andWater – Ensuring benefits outweigh water costs, For. Ecol. Man., 251, 110–120, 2007.
D'Almeida, C., Vörösmarty, C. J., Hurtt, G. C., Marengo, J. A., Dingman, S. L., and Keim, B. D.: The effects of deforestation on the hydrological cycle in Amazonia: a review on scale and resolution, Int. J. Clim., 27, 633–647, doi:10.1002/joc.1475, 2007.
Dawes, W. R., Gilfedder, M., Walker, G. R., and Evans, W. R.: Biophysical modelling of catchment-scale surface water and groundwater response to land-use change, Math. Comput. Simulat. 64, 3–12, 2004.
Donohue, R. J., Roderick, M. L., and McVicar, T. R.: On the importance of including vegetation dynamics in Budyko's hydrological model, Hydrol. Earth Syst. Sci., 11, 983–995, doi:10.5194/hess-11-983-2007, 2007.
Donohue, R. J., Roderick, M. L., and McVicar, T. R.: Can dynamic vegetation information improve the accuracy of Budyko's hydrological model?, J. Hydrol., 390, 23–34, 2010.
Einstein, A.: On the method of theoretical physics, Philos. Sci., 1, 163–169, 1934.
Farley, K., Jobbágy, E., and Jackson, R.: Effects of afforestation on water yield: a global synthesis with implications for policy, Glob. Ch. Biol., 11, 1565–1576, 2005.
Gash, J. H. C.: An analytical model of rainfall interception by forests, Q. J. Roy. Meteorol. Soc., 105, 43–55, 1979.
Gerrits, A. M. J., Savenije, H. H. G., Veling, E. J. M., and Pfister, L.: Analytical derivation of the Budyko curve based on rainfall characteristics and a simple evaporation model, Water Resour. Res., 45, W04403, doi:10.1029/2008wr007308, 2009.
Guerschman, J.-P., van Dijk, A. I. J. M., McVicar, T. R., Van Niel, T.G., Li, L., Liu, Y., and Peña-Arancibia, J.: Water balance estimates from satellite observations over the Murray-Darling Basin, CSIRO, Canberra, Australia, 93, 2008.
Guerschman, J. P., van Dijk, A., Mattersdorf, G., Beringer, J., Hutley, L. B., Leuning, R., Pipunic, R. C., and Sherman, B. S.: Scaling of potential evapotranspiration with MODIS data reproduces flux observations and catchment water balance observations across Australia, J. Hydrol., 369, 107–119, 2009.
Holmes, J. W. and Sinclair, J. A.: Water yield from some afforested catchments in Victoria, in: 17th Hydrology and Water Resources Symposium, Brisbane, Institution of Engineers, Australia, Barton, ACT, Australia, 1986.
Jeffrey, S. J., Carter, J. O., Moodie, K. B., and Beswick, A. R.: Using spatial interpolation to construct a comprehensive archive of Australian climate data, Environ. Modell. Softw., 16, 309–330, 2001.
Klemeš, V.: Conceptualization and scale in hydrology, J. Hydrol., 65, 1–23, 1983.
McJannet, D. L., Vertessy, R. A., and Clifton, C. A.: Observations of evapotranspiration in a break of slope plantation susceptible to periodic drought stress, Tree Physiol., 20, 169–177, 2000.
McJannet, D., Wallace, J., Fitch, P., Disher, M., and Reddell, P.: Water balance of tropical rainforest canopies in north Queensland, Australia, Hydrol. Process., 21, 3473–3484, 2007.
Milly, P.: Climate, soil water storage, and the average annual water balance, Water Resour. Res., 30, 2143–2156, 1994.
Monteith, J. L.: Evaporation and environment, Symposia of the Society for Experimental Biology, 19, 205–224, 1965.
Oreskes, N., Shrader-Frechette, K., and Belitz, K.: Verification, validation, and confirmation of numerical models in the earth sciences, Science, 263, 641–646, 1994.
Oudin, L., Andréassian, V., Lerat, J., and Michel, C.: Has land cover a significant impact on mean annual streamflow? An international assessment using 1508 catchments, J. Hydrol., 357, 303–316, 2008.
Peña-Arancibia, J. L., van Dijk, A. I. J. M., Guerschman, J. P., Mulligan, M., Bruijnzeel, L. A. S., and McVicar, T. R.: Detecting changes in streamflow after partial woodland clearing in two large catchments in the seasonal tropics, J. Hydrol., 416, 60–71, 2012.
Peel, M., McMahon, T., and Finlayson, B.: Vegetation impact on mean annual evapotranspiration at a global catchment scale, Water Resour. Res., 46, W09508, doi:10.1029/2009WR008233, 2010.
Pielke, R. A., Adegoke, J., Beltrán-Przekurat, A., Hiemstra, C. A., Lin, J., Nair, U. S., Niyogi, D., and Nobis, T. E.: An overview of regional land-use and land-cover impacts on rainfall, Tellus B, 59, 587–601, doi:10.1111/j.1600-0889.2007.00251.x, 2007.
Porporato, A., Daly, E., and Rodriguez-Iturbe, I.: Soil water balance and ecosystem response to climate change, Am. Nat., 164, 625–632, 2004.
Roberts, J.: Plants and water in forests and woodlands, in: Ecohydrology, Routledge, London, UK, 1999.
Schellekens, J., Scatena, F. N., Bruijnzeel, L. A., and Wickel, A. J.: Modelling rainfall interception by a lowland tropical rain forest in northeastern Puerto Rico, J. Hydrol., 225, 168–184, 1999.
Sivapalan, M., Blöschl, G., Zhang, L., and Vertessy, R.: Downward approach to hydrological prediction, Hydrol. Process., 17, 2101–2111, 2003.
Stednick, J. D.: Monitoring the effects of timber harvest on annual water yield, J. Hydrol., 176, 79–95, 1996.
Stirzaker, R., Vertessy, R. A., and Sarre, A. (Eds.): Trees, water and salt: An Australian guide to using trees for healthy catchments and productive farms, Joint Venture Agroforestry Program, Canberra, 159, 2002.

Sun, G., Zhou, G., Zhang, Z., Wei, X., McNulty, S. G. and Vose, J. M.: Potential water yield reduction due to forestation across China, J. Hydrol., 328, 548–558, 2006.

Trimble, S. W., Weirich, F. H., and Hoag, B. L.: Reforestation and the reduction of water yield on the Southern Piedmont since circa 1940, Water Resour. Res. 23, 425–437, 1987.

Turner, K. M.: Annual evapotranspiration of native vegetation in a Mediterranean-type climate, J. Am Water Resour. Assoc., 27, 1–6, 1991.

van Dijk, A. I. J. M.: Selection of an appropriately simple storm runoff model, Hydrol. Earth Syst. Sci., 14, 447–458, doi:10.5194/hess-14-447-2010, 2010a.

van Dijk, A. I. J. M.: AWRA Technical Report 3, Landscape Model (version 0.5) Technical Description, WIRADA/CSIRO Water for a Healthy Country Flagship, http://www.clw.csiro.au/publications/waterforahealthycountry/2010/wfhc-aus-water-resources-assessment-system.pdf, (last access: 8 March 2011), Canberra, 2010b.

van Dijk, A. I. J. M.: Climate and terrain factors explaining streamflow response and recession in Australian catchments, Hydrol. Earth Syst. Sci., 14, 159–169, doi:10.5194/hess-14-159-2010, 2010c.

van Dijk, A. I. J. M. and Bruijnzeel, L. A.: Modelling rainfall interception by vegetation of variable density using an adapted analytical model. Part 1. Model description, J. Hydrol., 247, 230–238, 2001a.

van Dijk, A. I. J. M. and Bruijnzeel, L. A.: Modelling rainfall interception by vegetation of variable density using an adapted analytical model. Part 2. Model validation for a tropical upland mixed cropping system, J. Hydrol., 247, 239–262, 2001b.

van Dijk, A. I. J. M. and Keenan, R. J.: Planted forests and water in perspective, Forest Ecol. Manage., 251, 1–9, doi:10.1016/j.foreco.2007.06.010, 2007.

van Dijk, A. I. J. M. and Renzullo, L. J.: Water resource monitoring systems and the role of satellite observations, Hydrol. Earth Syst. Sci., 15, 39–55, doi:10.5194/hess-15-39-2011, 2011.

van Dijk, A. I. J. M. and Warren, G.: AWRA Technical Report 4, Evaluation Against Observations, WIRADA/CSIRO Water for a Healthy Country Flagship, http://www.clw.csiro.au/publications/waterforahealthycountry/2010/wfhc-aus-water-resources-assessment-system.pdf, (last access: 8 March 2011), Canberra, 2010.

van Dijk, A. I. J. M., Evans, R., Hairsine, P. B., Khan, S., Nathan, R., Paydar, Z., Viney, N., and Zhang, L.: A Systems View of Water in the Murray-Darling Basin. 2. Risks to Our Shared Water Resources, CSIRO/Murray-Darling Basin Commission, Canberra, 2006.

van Dijk, A. I. J. M., Hairsine, P. B., Arancibia, J. P., and Dowling, T. I.: Reforestation, water availability and stream salinity: A multi-scale analysis in the Murray-Darling Basin, Australia, Forest. Ecol. Manage., 251, 94–109, 2007.

van Dijk, A. I. J. M., Bacon, D., Barratt, D., Crosbie, R., Daamen, C., Fitch, P., Frost, A., Guerschman, J. P., Henderson, B., King, E. A., McVicar, T., Renzullo, L. J., Stenson, M. P., and Viney, N.: Design and development of the Australian Water Resources Assessment system. In: Proceedings, Water Information Research and Development Alliance Science Symposium, August 2011, Melbourne, 2012.

Vertessy, R. A., Zhang, L., and Dawes, W. R.: Plantations, river flows and river salinity, Australian Forestry, 66, 55–61, 2002.

Zhang, L., Dawes, W. R., and Walker, G. R.: Predicting the effect of vegetation changes on catchment average water balance. Technical Report 99/12, Cooperative Research Centre for Catchment Hydrology, Canberra, 1999.

Zhang, L., Dawes, W. R., and Walker, G. R.: Response of mean annual evapotranspiration to vegetation changes at catchment scale, Water Resour. Res., 37, 701–708, 2001.

Zhang, L., Hickel, K., Dawes, W. R., Chiew, F. H. S., Western, A. W., and Briggs, P. R.: A rational function approach for estimating mean annual evapotranspiration, Water Resour. Res., 40, W02502, doi:10.1029/2003WR002710, 2004.

Appendix G - Errata

Chapter 2 Identifying hydrological impact of LUCC on streamflow data at the regional scale

Regretfully, minor errors in a figure and text in the original manuscript published in the Journal of Hydrology escaped detection at the proof stage.

Peña-Arancibia, J. L., A. I. J. M. van Dijk, J. P. Guerschman, M. Mulligan, L. A. Bruijnzeel, and T. R. McVicar (2012), Detecting changes in streamflow after partial woodland clearing in two large catchments in the seasonal tropics, Journal of Hydrology, 416/417, 60-71. The following errata correct these errors.

1. Page 64, Figure 3. The two lower quadrants of the figure describe 'increase in excess energy' whereas the vertical axis indicates an increase in evaporative demand, thus an increase in excess energy. The correct figure should read:

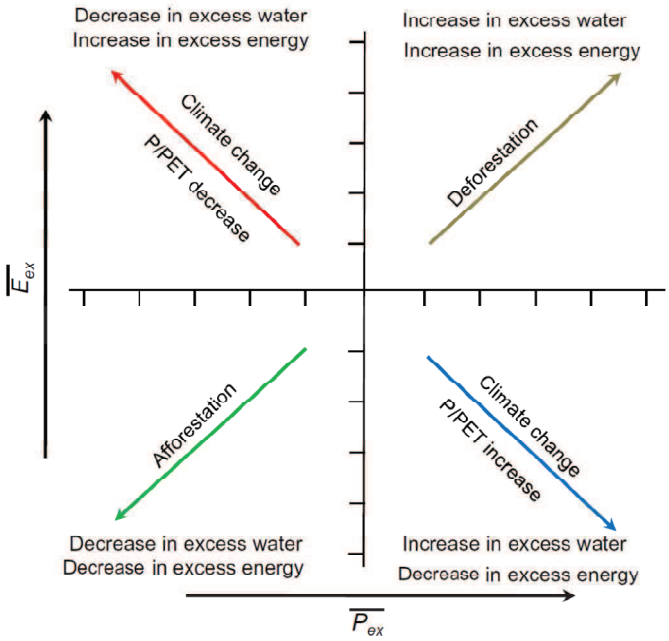

Fig. 3. Conceptual model based on the long-term coupled water–energy budget at interannual scales associated with changes in climate and land use (adapted from Tomer and Schilling, 2009). *P* refers to rainfall, areal *PET* to potential evapotranspiration, $\overline{P_{ex}}$ and $\overline{E_{ex}}$ refer to excess amounts of water and energy respectively. Other types of land management which increase (e.g. conservation tillage, removal of perennials) or decrease *ET* (e.g. conservation cover, increased forages) are encompassed by deforestation or afforestation, respectively (Tomer and Schilling, 2009).

2. Page 64, 3rd paragraph of Section 3.2 should read $\overline{P_{ex}}$ instead of *overline*P_{ex}.

The results and conclusions of the related work are not affected by these errors.

Appendix C Journal article - Peña Arancibia *et al.* (2013, Journal of Hydrometeorology)

A significant digit needed to be included in Table 1 of Appendix C in order to clarify the ranking of the precipitation products. The amended table is reproduced below.

Table 1. Performance ranking of detection and accuracy metrics of precipitation products aggregated over the geographical domain, including means and standard deviations (in brackets) of: equitable threat score (ETS), probability of detection (POD), False Alarm Ratio (FAR), frequency bias (FB), correlation (r), root mean square difference (RMSD), and percentage difference in the ratio of monthly precipitation amount to total days with precipitation (MPDR). Refer to Section 2 for the definition of the metrics.

	Rank						
	1	2	3	4	5	6	7
ETS	**Ensemble** 0.302 (±0.051)	JRA-25 0.293 (±0.054)	ERA-Interim 0.290 (±0.065)	TRMM 3B42 V6 0.271 (±0.049)	NCEP-DOE 0.245 (±0.037)	CMORPH 0.231 (±0.067)	PERSIANN 0.130 (±0.043)
POD	**Ensemble** 0.625 (±0.090)	JRA-25 0.622 (±0.094)	ERA-Interim 0.620 (±0.083)	NCEP-DOE 0.557 (±0.078)	TRMM 3B42 V6 0.524 (±0.079)	CMORPH 0.497 (±0.080)	PERSIANN 0.368 (±0.071)
FAR	ERA-Interim 0.400 (±0.06)	**Ensemble** 0.412 (±0.078)	TRMM 3B42 V6 0.412 (±0.091)	JRA-25 0.415 (±0.056)	NCEP-DOE 0.417 (±0.070)	CMORPH 0.423 (±0.103)	PERSIANN 0.54 (±0.087)
BIAS	**Ensemble** 0.09 (±0.46)	TRMM 3B42 V6 0.09 (±0.11)	JRA-25 0.13 (±0.14)	NCEP-DOE 0.13 (±0.17)	PERSIANN 0.22 (±0.23)	CMORPH 0.23 (±0.21)	ERA-Interim 0.25 (±0.33)
r	**Ensemble** 0.46 (±0.09)	JRA-25 0.43 (±0.08)	ERA-Interim 0.42 (±0.08)	TRMM 3B42 V6 0.41 (±0.09)	CMORPH 0.35 (±0.10)	PERSIANN 0.22 (±0.23)	NCEP-DOE 0.33 (±0.17)
RMSD	**Ensemble** 6.43 (±1.32)	TRMM 3B42 V6 6.56 (±1.58)	ERA-Interim 6.60 (±1.55)	JRA-25 6.62 (±0.08)	CMORPH 6.68 (±0.10)	PERSIANN 7.54 (±1.63)	NCEP-DOE 10.7 (±2.47)
MPDR	CMORPH -1.30 (±12.24)	ERA-Interim -3.00 (±8.10)	**Ensemble** -4.85 (±7.98)	JRA-25 5.33 (±10.93)	PERSIANN -7.79 (±11.77)	TRMM 3B42 V6 10.21 (±6.97)	NCEP-DOE 42.80 (±13.35)